



Poznan University of Technology

Faculty of Chemical Technology

Institute of Chemistry and Technical Electrochemistry
Division of Applied Electrochemistry



DOCTORAL DISSERTATION

Mathematical analysis of processes and phenomena in electrochemical energy storage and conversion systems

*Analiza matematyczna procesów i zjawisk
w elektrochemicznych systemach do magazynowania i konwersji energii*

Przemysław Galek

Field of study: Chemical Technology

Scientific Supervisor:

Krzysztof Fic

Poznan, 2022



European Research Council
Established by the European Commission

The **European Research Council** is acknowledged for the financial support within the Starting Grant project (GA 759603) '***If immortality unveil...'***– ***development of the novel types of energy storage systems with excellent long-term performance'*** under the Horizon 2020 Research and Innovation Programme of the European Union.

Principal Investigator: Krzysztof Fic

*“I’m a great believer in luck,
and I find the harder I work,
the more I have of it.*

Thomas Jefferson

Acknowledgments

This thesis could be created only with the help of people who appeared in my life in recent years and with the participation of those who have always been with me...

First of all, I would like to express my gratitude to my **Promoter – Krzysztof Fic**. During our first joint meeting regarding the master's thesis, I already knew that I wanted to start my adventure with science. Thank you for providing theoretical and practical knowledge, for many hours spent together in the laboratory, for meetings such as *'I have one question'* which used to turn into an hour-long discussion, and for the opportunity to share my results at many conferences and participate in courses.

'If you love your work, you'll be out there every day trying to do it the best you possibly can, and pretty soon everybody around will catch the passion from you – like a fever.'

Sam Walton

I would also like to acknowledge the **Head of Group – Prof. Elżbieta Frąckowiak** for giving me the opportunity to work in challenging *'Power Sources Group'*. The work with you and being the coauthor of publications was a great pleasure. The experience I gained here changed me a lot, opened my mind in many areas, and allowed me to meet many great people around the world.

'My mentor said, 'Let's go do it,' not 'You go do it.'
How powerful when someone says, 'Let's!'

Jim Rohn

Moreover, I would like to thank my office mates and coauthors: **Jakub, Paulina, Adam M., Justyna, Anetta, Adam Ś., Sylwia and Maciej**. You were part of my daily life and I am very happy that we still keep in touch. Here, we could have very good times with a lot of joy, funny moments, and scientific discussions. Together we shared the sorrow of failures and the joy of success. Thanks are also due to **Dr. Maciej Staszak**, without whom the calculations necessary for the implementation of this dissertation would take ages.

'If everyone is moving forward together, then success takes care of itself.'

Henry Ford

I would like to dedicate this thesis to my parents, **Barbara** and **Sławomir**. Through these years you have been supporting me at each stage of my life and always forcing me to a continuous development. Many times you have shown that by acting properly, I did not have to worry about anything. You motivate me, inspire me, and share your point of view with me – all of these make me who I am, right here, right now.

*'First your parents, they give you your life,
but then they try to give you their life.'*

Chuck Palahniuk

Last but not least, I cannot go around without mentioning my dearest friend **Maksymilian**. We were unmatched when we worked on one task during our studies. You were the mastermind of the group, I was the coordinator. You have always been the basis for passing on all my projects. Our acquaintance was not limited only to the time spent at university, but to every single moment.

*'Don't walk behind me; I may not lead. Don't walk in front of me;
I may not follow. Just walk beside me and be my friend.'*

Albert Camus



Table of contents

Acknowledgments	7
Abstract	13
The purpose and scope of the thesis	17
Abbreviations, patterns, symbols.....	19
Literature review.....	23
1. Motivation and context of the research	23
2. Electrochemical energy storage and conversion systems.....	25
3. Electrochemical capacitors – state of art.....	28
3.1. Definition.....	28
3.2. Construction	28
3.3. Principle of operation	28
3.4. Nominal parameters.....	31
3.5. Electrode materials	33
3.6. Electrolytes.....	40
3.7. Composition and production	45
4. Electrochemical research techniques.....	46
5. Summary	53
Experimental part.....	55
6. Article A1	55
7. Article A2	66
8. Article A3	81
9. Article A4	94
10. Article A5	103
11. Computer software.....	120
12. Summary	125





13. Articles not included in the dissertation topic.....	126
List of figures and tables.....	131
Scientific accomplishments	132
1. Publications.....	132
2. Chapter.....	133
3. Patents and patents applications	133
4. Reports.....	134
5. Scientific conferences.....	134
5.1. Oral presentations.....	134
5.2. Poster presentations.....	137
6. Awards	139
7. Research project.....	140
8. Memberships in scientific organizations and other functions/trainings .	140
Literature	142
Co-authorship statements	153

Abstract

The first part of the dissertation is devoted to a review of the literature on electrochemical energy storage and conversion systems. The theoretical background begins with a general introduction to energy sources, global approach to the need to search for alternative energy sources, and division of energy storage systems. The next part compares the most popular electrochemical systems, lists their advantages, disadvantages, and applications. Particular attention was paid to the main subject of research – electrochemical capacitors. This part of the work provides their definition, construction description, and explains the operation principle, including the nominal parameters in their characterization. The division and discussion of electrolytes and electrode materials, with particular emphasis on carbon materials, were taken into account. The final part includes information on the electrode composition, devices production, and basic electrochemical techniques used in the experimental part. The summary describes the economic aspect in terms of the global market and the prospects in the coming years, including the research challenges that formed the research in this dissertation.

In the experimental part, the research results that fit into the topic of the doctoral dissertation have been compiled. These are three published manuscripts (**Article A2, A3, A4**), two unpublished (**Article A1, A5**) and a description of the created computer program (**Chapter 12**). Motivation is presented before each article for taking up a given topic, and the importance of obtained results is emphasized. **Article A1** refers to the electrode composition. The rheological properties of the electrode slurry were related to the geometry of the final product. **Articles A2, A3** refer to the electrolyte. The first article (**A2**) describes the concept of a highly concentrated conductive medium called in the literature ‘*water in salt*’ type electrolyte. The second article (**A3**) explains the influence of the electrolyte viscosity on the performance of the electrochemical capacitor. The other two manuscripts are devoted to the phenomena at the electrode/electrolyte interface – the charge accumulation mechanism (**A4**) and the effect of pH on the ion fluxes (**A5**).



In the dissertation, computer software ('*SPECSfit*'), which was used to improve the calculations of the collected experimental results and helped in the extensive interpretation of data related to the accumulation of ions in the pores of electrode material, is also briefly discussed. The obtained results from five topics were the basis for formulating the conclusions.

The final part presents abstracts of articles that do not belong to the topic of the dissertation, but are a valuable part of the scientific output. The list of figures and tables, scientific achievements, as well as the literature, which formed the basis of the considerations.

Streszczenie

Pierwsza część dysertacji poświęcona jest przeglądowi literatury dotyczącej elektrochemicznych systemów do magazynowania i konwersji energii. Przegląd rozpoczyna się od ogólnego wprowadzenia związanego z podziałem źródeł energii oraz globalnego podejścia w kontekście konieczności poszukiwania alternatywnych jej źródeł. W dalszej części porównano najpopularniejsze systemy elektrochemiczne, wymieniono ich zalety, wady oraz zastosowania. Szczególną uwagę poświęcono głównemu przedmiotowi badań pracy – kondensatorom elektrochemicznym. W tej części pracy przedstawiono ich definicję, opis budowy oraz wyjaśniono zasadę działania w tym nominalne parametry stosowane przy ich charakterystyce. Podział oraz omówienie stosowanych elektrolitów oraz materiałów elektrodowych ze szczególnym uwzględnieniem materiałów węglowych wzięto pod uwagę. Na końcową część składają się informacje dotyczące składu elektrod, produkcji urządzeń oraz podstawowych technik elektrochemicznych wykorzystanych w części eksperymentalnej. Podsumowanie stanowi aspekt ekonomiczny w ujęciu globalnego rynku oraz perspektywy na najbliższe lata, w tym wyzwania badawcze, które stanowiły podstawę badań w niniejszej rozprawie.

W części eksperymentalnej zestawiono wyniki badań wpisujące się w temat pracy doktorskiej. Są to trzy opublikowane manuskrypty (**Artykuł A2, A3, A4**), dwa nieopublikowane (**Artykuł A1, A5**) oraz opis opracowanego programu komputerowego (**Rozdział 12**). Przed każdym z artykułów przedstawiono motywację decydującą o podjęciu danego tematu oraz podkreślono znaczenie uzyskanych wyników. **Artykuł A1** odnosi się do składu elektrody. Właściwości reologiczne produktu pośredniego elektrody, tzw. gęstwy elektrodowej, odniesiono do geometrii finalnego produktu. **Artykuły A2, A3** dotyczą elektrolitu. W pierwszym z nich (**A2**) opisano koncepcję wysoko stężonego medium przewodzącego zwanego w literaturze elektrolitem typu „woda w soli”. Drugi artykuł (**A3**) z kolei precyzuje wpływ lepkości elektrolitu na finalną sprawność kondensatora elektrochemicznego. Dwa pozostałe manuskrypty poświęcone są zjawiskom na interfejsie elektroda/elektrolit – mechanizmowi



gromadzenia ładunku (**A4**) oraz wpływu pH na strumienie jonów (**A5**). W dysertacji opisano pokrótce powstały w trakcie doktoratu program komputerowy („*SPECSfit*”), który posłużył do usprawnienia obliczeń zebranych wyników eksperymentalnych i pomógł w rozbudowanej interpretacji danych związanych z akumulacją jonów w porach materiału elektrodowego. Uzyskane wyniki z pięciu tematów stanowiły podstawę do sformułowania wniosków.

W końcowej części przedstawiono streszczenia artykułów, które nie zaliczają się do tematu dysertacji, jednak stanowią wartościowy element dorobku naukowego. Spis rysunków oraz tabel, zestawienie dorobku naukowego doktoranta, a także literatura, która stanowiła podstawę przeprowadzonych rozważań kończy pracę.

The purpose and scope of the thesis

The aim of the doctoral dissertation is to use a mathematical analysis to describe the electrochemical capacitor electrode production process and to better understand the phenomena in the electrolyte bulk and at the electrode/electrolyte interface. The analysis should involve the heart of the system, the electrodes and the electrolyte. Finally, the conducted research should contribute to increasing the efficiency of the devices for future applications. The first topic (**Article A1**) concerning the electrode component should describe the rheological properties of the electrode slurry. Moreover, these properties can be linked with the final performance of the electrode. In addition, the research should provide the optimal slurry composition (the ratio between the components) ensuring even coverage of the current collector. On the basis of collected experimental data, appropriate calculations are to lead to a mathematical formula linking the electrode geometry with viscosity and electrode slurry composition. The electrolyte section aims to define the performance of the electrochemical capacitor based on the new concept of a highly concentrated and saturated aqueous electrolyte (**Article A2**). Impact of water concentration reduction in an electrolyte on the potential window, self-discharge, capacitance, cycle life, etc. device should be considered. Moreover, the advantages and disadvantages resulting from their implementation in electrochemical capacitors must be taken into account. Issues related to the physicochemical properties, such as viscosity, of the conductive medium are open to discussion (**Article A3**). The currently available literature does not explicitly define the effect of an increase in electrolyte viscosity. So far, no universal method for determining the charge accumulation mechanism at the porous electrode/electrolyte interface has been proposed. And it is possible by combining two complementary electrochemical techniques, step potential electrochemical spectroscopy and electrochemical dilatometry (**Article A4**). The proposed solution should give the possibility to describe the influence of pH on ions fluxes in the bulk electrode (**Article A5**). Experimental data processing collected by the step potential electrochemical spectroscopy



technique takes a long time. Therefore, it is necessary to develop a computer program to solve this problem (**Chapter 12**). The program should reduce the time spent on calculations from hours to minutes and provide honest results about resistance, capacitance, ions diffusion, and side reactions.

Abbreviations, patterns, symbols

Abbreviation	Description
AC	– activated carbon
AES	– alternative energy sources
AN	– acetonitrile
ARTIL	– aprotic room temperature ionic liquid
CB	– carbon black
CCVD	– catalyst chemical vapour deposition
CDC	– carbide-derived carbon
CE	– counter electrode
CF	– carbon nanofoam
CNF	– carbon nanofiber
CNH	– carbon nanohorn
CNO	– carbon nanoonion
CNT	– carbon nanotube
CO	– carbon onion
CV	– cyclic voltammetry
CVD	– chemical vapour deposition
DEC	– diethyl carbonate
DMC	– dimethyl carbonate
DWNT	– double wall carbon nanotube
EB	– ethyl butyrate
EC	– electrochemical capacitor
EC	– ethylene carbonate
EDL	– electrical double-layer
EDLC	– electrical double-layer capacitor
EES	– electrical energy storage system
EIS	– electrochemical impedance spectroscopy
EMC	– ethylmethyl carbonate
ESR	– equivalent series resistance
GCD	– galvanostatic charge-discharge

GCPL	– galvanostatic cycling with potential limitation
GITT	– galvanostatic intermittent titration technique
GO	– graphene oxide
GPE	– gel polymer electrolyte
IL	– ionic liquid
KERS	– kinetic energy recovery system
LSV	– linear sweep voltammetry
MB	– methyl butyrate
MWCNT	– multiwall carbon nanotube
NMP	– N-Methyl-2-pyrrolidone
OLC	– onion like carbon
PC	– propylene carbonate
PTFE	– poly(tetrafluoroethylene)
PVDF	– poly(vinylidene fluoride)
RC	– redox capacitor
RE	– reference electrode
SPE	– solid polymer electrolyte
SWCNH	– single wall carbon nanohorn
SWCNT	– single wall carbon nanotube
TDC	– template derived carbon
WE	– working electrode

Pattern

Description

Ag	– silver
Ar	– argon
CO ₂	– carbon dioxide
CsF	– caesium fluoride
Cu	– copper
Fe	– iron
H ₂ SO ₄	– sulfuric acid
H ₃ PO ₄	– phosphoric acid
K	– potassium
KCl	– potassium chloride

KOH	– potassium hydroxide
Li ₂ SO ₄	– lithium sulfate
Mn	– manganese
MnO ₂	– manganese oxide
Mo ₂ C	– molybdenum carbide
N ₂	– nitrogen
Na	– sodium
Na ₂ SO ₄	– sodium sulfate
NaCl	– sodium chloride
Ru	– rubidium
RuO ₂	– ruthenium oxide
SiC	– silicon carbide
TiC	– titanium carbide
V	– vanadium
VC	– vanadium carbide
Zn	– zinc
ZnCl ₂	– zinc chloride

Symbol	Description	Unit
A	– electrode surface area	m ²
B	– constant proportional to the capacitance of the diffusion limited processes	A s ^{0.5}
C^-	– negative electrode capacitance	F
C	– concentration of the species at the electrode surface	mol m ³
C_d	– differential EDL capacitance	F
C^+	– capacitance of positive electrode	F
C_{DYF}	– diffusion layer capacitance	F
C_e	– electrode capacitance ($C_e=C^++C^-$)	F
C_s	– rigid Stern capacitance	F
D	– diffusion coefficient of the species	m ² s
d	– EDL thickness	m
C_{EDL}	– EDL capacitance	F
E	– energy	Wh

E	– potential	V
F	– Faraday’s constant (96496.7)	C mol ⁻¹
I	– current	A
I_C	– current related with EDL formation or capacitive charging processes	A
I_G	– current (calculated from SPECS technique) corresponding to EDL formation on easily accessible electrode surface for electrolyte (geometric component)	A
I_P	– current (calculated from SPECS technique) corresponding to EDL formation in electrode bulk (porous component)	A
I_D	– current (calculated from SPECS technique) corresponding diffusion-limited processes (diffusion component)	A
ImZ	– imaginary part of complex impedance	Ω
I_R	– current (calculated from SPECS technique) corresponding to side reactions (residual component)	A
I_T	– current registered at given potential step in SPECS technique	A
n	– the number of electrons involved in an electrode reaction	-
P	– power	W
Q	– electric charge	C
R	– series resistance	Ω
R_A	– the bulk electrolyte resistance	Ω
R_{AB}	– charge transfer resistance	Ω
R_B	– internal resistance ($R_B=R_A+R_{AB}$)	Ω
R_{BC}	– equivalent distribution resistance	Ω
R_C	– internal resistance	Ω
ReZ	– real part of complex impedance	Ω
t	– time in SPECS technique	s
U	– voltage	V
ΔE	– potential step in SPECS technique	V
ε	– relative electrolyte permittivity	F m ⁻¹
ε_0	– vacuum permittivity	F m ⁻¹

Literature review

1. Motivation and context of the research

Reliable and sustainable energy extraction is essential for the present and future society. The demand for energy has steadily increased, especially in the last few decades. The reason for such a situation is human population growth and more and more wide spreading application of electronics [1]. According to **Fig. 1**, the technologies for energy generation can be divided into several groups, i.e., electrical, chemical, thermal, and mechanical ones.

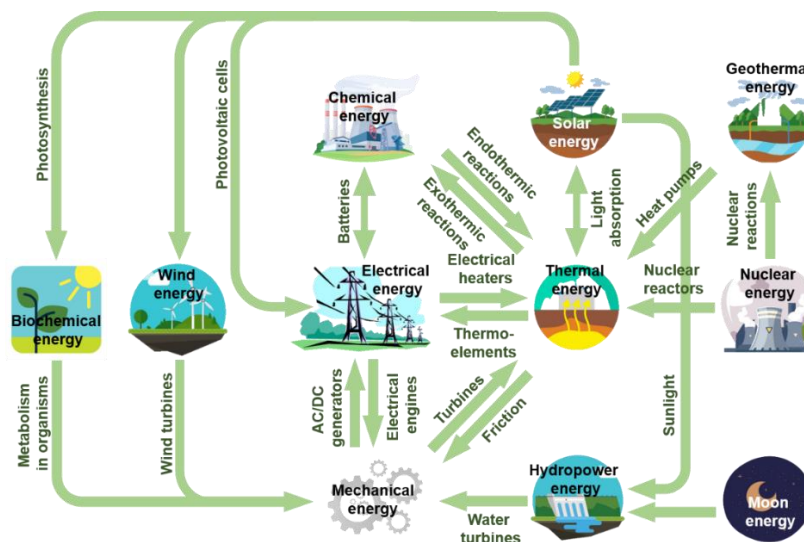


Fig. 1. Energy sources and methods of its conversion [2].

There are specific relations between different groups related to different ways of energy conversion. Since the beginning of the industrial revolution, the dominant form of energy is chemical energy derived from fossils – coal, crude oil and natural gas. However, because of the intensive exploitation of these sources, their reserves are currently limited. Furthermore, the extraction of energy from fossil fuels is neither sustainable nor ecological. Global climate warming is also a serious problem, which is mainly caused by greenhouse gases emitted during the combustion of chemical energy sources [3]. This forces the search for alternative (renewable) energy sources (AESs). AES should not only be obtained in an environmentally friendly manner but also provide

the possibility of providing energy when unexpectedly required. However, despite the fact that AESs have been used in many areas and significantly reduce the consumption of fossil fuels, they cannot be completely replaced in the near future. They do not always provide the right amount of energy and currently only support conventional sources [4].

AESs use energy from solar, wind, geothermal, or hydrothermal energy, which is converted most often into electricity. This kind of energy is the simplest form of transferred energy. By definition, it is the energy of the ordered movement of electric charges. Integrating AESs into the electrical grid presents many challenges in terms of grid stability and supply security. Therefore, it is important to be supported by electricity storage systems (EESs), which perfectly fit the power/energy imbalance between its generation and demand. EESs allow energy to be stored during the surplus of its production and the possibility of giving it back during increased demand [5-7].

2. Electrochemical energy storage and conversion systems

Energy conversion/storage devices are becoming a broad group of electrochemical technologies that can convert, store, and deliver energy on demand. Currently, there are several ways to distinguish between the different types of devices. Fuel cells, batteries, and capacitors are common categories of energy storage and conversion systems [8-11]. The Ragone plot presented in **Fig. 2** shows the correlation of the gravimetric or volumetric energy density versus the power density for different energy storage systems.

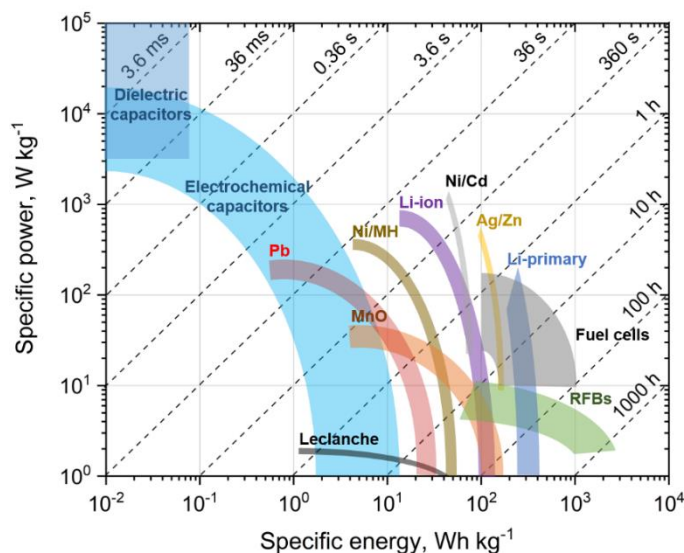





Fig. 2. Ragone plot for electrochemical energy storage systems [12, 13].

However, not only energy and power play a role in dictating the devices applicability. Other features such as cyclability, cost effectiveness, safety and environmental considerations should be taken into account [12, 14, 15]. Fuel cells are characterized by relatively high energy efficiency (1000 Wh kg^{-1}) with moderate or even low power characteristics (100 W kg^{-1}) [13]. Their main advantage over the fuel engine is the production of clean energy. Water (vapour) is the main product of a chemical reaction [16]. In such systems, a constant supply of fuel in the form of hydrogen, methanol, or other chemical substance should be provided [17]. However, the fuel network is currently unable to support such electrochemical systems globally. Fuel storage technology is also a problem



because hydrogen is considered a hazardous gas [18]. Capacitors are located in the high-power area (up to 20 kW kg⁻¹ for electrochemical capacitors and to 10 MW kg⁻¹ for dielectric capacitors) and low-energy (up to 15 Wh kg⁻¹ for electrochemical capacitors) [12]. The detailed characteristics of these devices are discussed in **Chapter 3**. In turn, batteries are placed between fuel cells and capacitors. Their energy reaches 300 Wh kg⁻¹, and the power is 2 kW kg⁻¹ [19]. This type of energy storage system is the most commonly used and, in many cases, irreplaceable. The principle of their operation is based on the use of scarce materials, such as lithium. Currently, there is a search for innovative and advanced materials to replace Li⁺ with more available materials, for example, Na⁺ [20] or K⁺ [21].

The appropriate energy storage system should be selected depending on the customer's needs, i.e., for a specific application (**Tab. 1**), taking into account the advantages and disadvantages of individual technologies (**Tab. 2**). Even if the characteristics of energy storage devices are now well known and the number of articles on the subject is increasing, there is still a space for improvement.

Tab. 1. Application of electrochemical energy storage systems (fuel cells, batteries, capacitors) [8-10].

 Fuel cells	 Batteries	 Capacitors
<ul style="list-style-type: none"> – portable systems (< 0.5 kW_e): laptops, cell phones, cameras – stationary applications (1 – 10 kW_e): laundries, backup power generation, traffic lights – transport (50 – 100 kW_e and higher): scooters, bicycles, cars, buses, trains, planes, rockets, unmanned aerial vehicles, boats, submarines – municipal applications (10 – 200 kW_e and higher): schools, hospitals, police stations, industrial buildings, data centers, air terminals, waste management, small power plants, military facilities – stationary systems (> 1 MW): power plants, industrial plants 	<ul style="list-style-type: none"> – portable systems (100 mWh – 2 Wh): watches, calculators, implanted medical devices, (2 Wh – 100 Wh): toys, power tools, mobile phones, flashlights, power tools, portable radio and TV, camcorders, lap-top computers, memory refresh, instruments, cordless devices, wireless peripherals – start lighting and ignition (100-600 Wh): cars, trucks, buses, lawn mowers, wheel chairs, robots, emergency beacons – vehicle traction systems (20 -630 kWh): EVs, HEVs, PHEVs, forklift trucks, milk floats, locomotives – stationary applications (250 Wh-5 MWh): emergency power, local energy storage, remote relay stations, communication base stations, uninterruptible power supplies (UPS) – military and aerospace (wide range): satellites, munitions, robots, emergency power, communications – special purpose (3 MWh): submarines, aircraft systems – load levelling applications (5-100 MWh): spinning reserve, peak shaving, load levelling – standby power resources – emergency no-fail systems 	<ul style="list-style-type: none"> – renewable sources: wind farms (pitch control) and feathering of blades) – robotics – automotive and transportation: electric vehicles, kinetic energy recovery systems (KERSs), cold start aids, start-stop systems, power steering, electric heating, power supplies when parked, catalytic converters preheating, emergency door opening in airplanes and trains, forklifts, seaport cranes and elevators (energy recovery, particularly in gantry cranes for improved emissions and fuel economy) – guaranteed power supply systems (UPS), grid power buffers – consumer electronics: laptop computers, PDAs, GPS, portable media players, hand-held devices, photovoltaic systems, photographic flashes in digital cameras, LED flashlights, speakers, computer memories, electric toothbrushes, memory backups, AC filterings, turning on the batteries, electric screwdrivers – medical, military and space industry

Tab. 2. Advantages and disadvantages of electrochemical energy storage systems (fuel cells, batteries, capacitors) [8-10].

Advantages 	Disadvantages 
Fuel cells	Fuel cells
<ol style="list-style-type: none"> 1) relative simplicity and modular construction 2) high specific energy (1000 Wh kg⁻¹) 3) high efficiency (~80%) 4) low noise level 5) possibility of very high temporary overloads 6) nonpolluting 7) very good regulatability 8) possibility of continuous work 9) size reduction 10) fast and easy refueling process 11) low maintenance 12) efficient energy conversion 	<ol style="list-style-type: none"> 1) expensive 2) moderate specific power (100 W kg⁻¹) 3) lack of supplying infrastructure 4) a lot of fuel cells are in the prototype stage 5) high costs of hydrogen 6) limited access to hydrogen 7) problems with hydrogen storage 8) complex to operate 9) impurities in gas stream and pulse demands shorten life 10) low durability 11) limited availability
Batteries	Batteries
<ol style="list-style-type: none"> 1) low self-discharge 2) high specific energy (300 Wh kg⁻¹) 3) wide range of types and sizes 4) operate over a wide temperature range 5) operate in any orientation 6) do not require pumps, filters, etc. 7) can deliver high current pulses 	<ol style="list-style-type: none"> 1) short cyclic life 2) high toxicity 3) long charging time 4) low specific power (2 kW kg⁻¹) 5) high production cost 6) poor charge retention 7) explosion possibility
Capacitors	Capacitors
<ol style="list-style-type: none"> 1) short charge/discharge time (~1 s) 2) long cycle life (>500 000) 3) high specific power (20 kW kg⁻¹) 4) high efficiency (75 – 95%) 5) low components degradation 6) low toxicity 7) wide operating temperature range 8) low cost per unit of capacity 9) no maintenance requirements 10) low operating costs 11) possibility of complete discharge 	<ol style="list-style-type: none"> 1) low specific energy (15 Wh kg⁻¹) 2) variable voltage at the terminals 3) low permissible operating voltage 4) high self-discharge

3. Electrochemical capacitors – state of art

The purpose of this chapter is to present basic information on electrochemical capacitors, their classification, construction, principles of operation, and nominal values.

3.1. Definition

A traditional capacitor device (using dielectric technology) has a very low energy density, which limits its use [22]. In 1957, a new group of capacitors, called electrochemical capacitors (ECs), was proposed. Unlike dielectric capacitors, they use electrodes with a highly developed surface to increase energy while maintaining their power characteristics [23]. ECs are known for their advantages presented in **Tab. 2**. An electric double-layer, pseudocapacitance, redox, and hybrid capacitors belong to ECs.

3.2. Construction

The EC consists of two porous electrodes (**Chapter 3.5**) coated on the current collectors, separated by an insulator and immersed in the electrolyte (**Chapter 3.6**). One of the electrodes is called positive (+), polarized positively. The latter electrode is called negative (-) and is negatively polarized. An insulator (porous membrane) prevents both electrodes from short circuit (**Fig. 3a**) [24].

3.3. Principle of operation

An electric double-layer capacitor (EDLC) is a basic type of EC (**Fig. 3a**). The electrolyte is ions carrier; these an ion are capable of adsorbing/desorbing at the electrode/electrolyte interface. Ions are in the electrolyte volume, which fills the space between the electrodes and penetrates the electrode porosity. Positively charged ions (cations) are adsorbed on the (-) electrode surface, while negatively charged ions (anions) are adsorbed on the (+) electrode surface. Physical adsorption (electrostatic attraction) occurs at the electrode/electrolyte interface, which ensures a rapid reorganization of the ions in the electrode

and the electrolyte volume. At the electrode/electrolyte interface, the so-called electrical double-layer (EDL) is formed (**Fig. 3b**) [24]. EDL is formed from charges on the electrode and ions of the opposite sign immediately adjacent to the electrode surface. The prototype of the EDL model was proposed by Helmholtz in 1857 [25]. The ordering (adsorption) of a single ionic layer on the polarized electrode surface was taken into account by him. In 1910 Gouy-Chapman proposed the blurring effect of a layer due to thermal ion movement. In this case, the counterions are adsorbed, and the co-ions are repelled from the surface. This phenomenon includes the potential (E ; V) gradient as it moves away from the electrode surface and the presence of solvent molecules as a result of an ion concentration gradient following the Boltzmann distribution. This leads to the treatment of the capacitance as a non-constant parameter because it depends on both the applied potential and the ion concentration. Under this assumption, the potential decreases exponentially towards the electrolyte volume according to the Maxwell-Boltzmann statistical model. In 1927 Stern combined these previously mentioned models [26]. He took into account the limitations of ions, which led to the so-called Stern layer. In this layer, the decrease in potential follows a linear trend and not an exponential trend, as in the diffusion layer. As a result, the theory claims that there are two capacitors connected in series: a rigid Stern layer capacitor with capacitance (C_S ; F) and a diffusion layer capacitor with capacitance (C_{DYF} ; F). The total capacitance of the EDL (C_{EDL} ; F) EDL capacitance is given by the equation: $C_{EDL}^{-1} = C_S^{-1} + C_{DYF}^{-1}$. It follows that the ordering of charges at the point of contact of two electrically conductive phases leads to the generation of a capacitor. Taking into account the presence of solvent dipoles, Graham's (1947) model is the most developed (**Fig. 3b inset**) [27]. Grahame proposed two concepts: the inner Helmholtz plane (IHP), which covers the extent of the Stern layer, and the outer Helmholtz plane (OHP), which is close to the boundary potential of the diffusion layer. Grahame then pointed out that IHP might consist of uncharged individuals (such as solvent molecules) or coions due to some specific ion-electrode surface interactions. During the discharge, the ions desorb and pass into the electrolyte volume.

The electrical current flows through the external wiring and enables the electrical device to be powered. For these types of system, there is a linear relationship of the stored charge (capacitance) with a variable potentials.

A pseudocapacitance capacitor (PC) has the signature of a capacitive electrode (as in the case of EDLC). However, a charge storage mechanism, in addition to EDL formation, is also based on various oxidation-reduction (redox, faradaic) reactions of the electroactive electrode material (**Fig. 3b**). The pseudocapacitance term is used when a device has a constant slope of charge/discharge curve by using a constant current – so it functions as a non-Faradaic process. The pseudocapacitance mechanisms include the pseudo-redox capacitance found in metal oxides (e.g. RuO_2 or MnO_2) and the pseudocapacitance intercalation (e.g. Li^+ is introduced into the parent material) [28].

A redox capacitor (RC), apart from the EDL capacitance, is characterized by an additional capacitance resulting from the redox reaction of the compounds included in the electrolyte (**Fig. 3b**). In this case, the registered capacitance is not constant in the investigated potential range. RC has additional capacitance (visible as capacitance peaks) resulting from the transformation of the oxidation-reduction of the electrolyte compound/compounds [29].

Electrochemical capacitor hybrids (HEC) combined previously mentioned solutions into one system. This involves, for example, the incorporation of heteroatoms and/or metal oxides (pseudocapacitance materials) into the activated carbon structure (EDL materials). In HECs, the electrodes do not work symmetrically, and one of them has a battery mechanism (pseudocapacitance). The latter electrode corresponds to the capacitance characteristic of EDL formation [30].

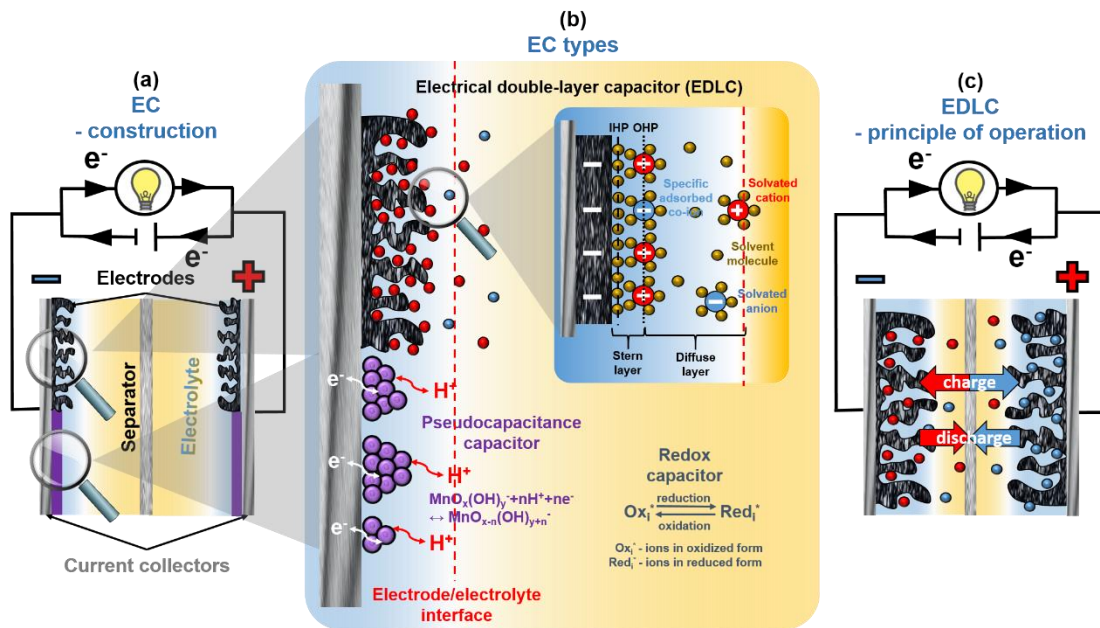


Fig. 3. Electrochemical capacitor: (a) construction, (b) types, and (c) principle of operation.

3.4. Nominal parameters

An electric charge (Q ; C) is a fundamental property of matter that manifests itself in the electromagnetic interaction of bodies endowed with this charge. They have the ability to generate and interact with an electromagnetic field. The interaction of the charge with the electromagnetic field is determined by the Lorentz force and is one of the fundamental forces. The electric charge can be positive or negative. Two charges of one sign repel each other, whereas charges of the opposite sign attract each other. Electric charges are quantized. The electron has an elementary negative charge, while the proton has a positive charge. The orderly movement of electric charges is called an electric current [24].

By definition, a system capacitance (C_T ; F) is the ability of the body to store an electric charge. The EDL capacitance given by **Eq. 1** represents the electric charge at the electrode/electrolyte interface and is constant over a given voltage (U ; V) [24].

$$C_T = \frac{\Delta Q}{\Delta U} \quad (1)$$

The C_{EDL} depends on the surface density of the electrostatically (i.e., non-faradaic) accumulated charges on the phase surfaces of both electrodes. According to **Eq. 2**, the more developed the specific surface area (S_{BET}) of the electrode (A ; m^2), the more charge can accumulate (higher capacitance). Furthermore, the enhancement of capacitance can be achieved by selecting an electrolyte that will be characterized by high relative permittivity (ϵ ; $F\ m^{-1}$) or by reducing the thickness of the EDL layer (d ; m) (ϵ_0 ; $F\ m^{-1}$ – vacuum permittivity) [24].

$$C_{EDL} = \frac{A\epsilon\epsilon_0}{d} \quad (2)$$

Since the capacitor consists of two electrodes (C^+ ; F – positive electrode capacitance, C^- ; F – negative electrode capacitance) connected in series, its C_T can be calculated from **Eq. 3** [24].

$$\frac{1}{C_T} = \frac{1}{C^+} + \frac{1}{C^-} \quad (3)$$

When considering the symmetrical system (composed of the same materials on the positive and negative sides), it can be assumed that $C^+ = C^-$. Thus, C_T is half of electrode capacitance (C_e ; F) (**Eq. 4**) [31].

$$C_T = \frac{C_e}{2} \quad (4)$$

The EC energy (E ; Wh) is proportional to C_T and voltage (**Eq. 5**) [24].

$$E = \frac{C_T U^2}{2} \quad (5)$$

As previously mentioned (**Eq. 2**), the impact on capacitance has one of the three parameters. Moreover, this can be realized by implementing active redox species into the electrode (pseudocapacitance) or electrolyte (redox capacitance). The type of electrolyte decides mainly on the maximum voltage. The electrolyte properties determine the voltage at which it decomposes and are not suitable for further use [24].

The power of device (P ; W) depends on the voltage and system series resistance (R ; Ω) (**Eq. 6**). Resistance can be reduced by providing high electrolyte conductivity [24].

$$P = \frac{U^2}{4R} \quad (6)$$

3.5. Electrode materials

According to the type of charge accumulation mechanism, the active materials in ECs are divided into two main groups: porous carbons and pseudocapacitance materials. Additionally, there is a group of composites that combine the properties of both mentioned groups (**Fig. 4**).

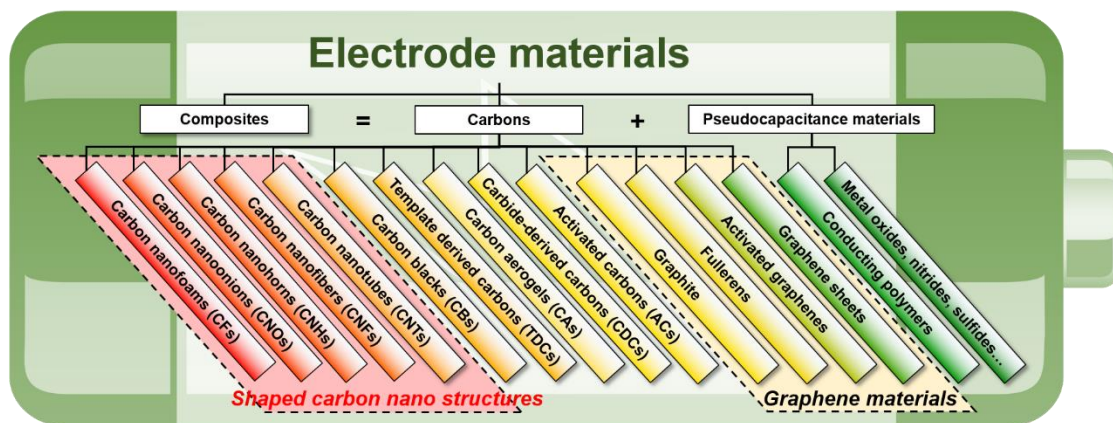


Fig. 4. Electrode materials for electrochemical capacitors.

The electrolyte with the electrode material plays a crucial role in the maximum voltage achieved by EC. Moreover, according to **Eq. 2**, materials with a high specific surface area are needed to obtain high capacitance values. The energy that can be stored in the three-dimensional (3D) structure of the electrode material is higher than the energy stored in the two-dimensional (2D) structure. The specific surface area (S_{BET}) of porous materials can be determined by adsorption of various gases (the most commonly N_2 at 77 K and CO_2 at 273 K). In addition (not taken into account by the equation), the electrode material should have pores of an appropriate size, capable of adsorbing electrolyte ions of the given dimensions. Basically, it is mainly

the micropores (2 nm) that contribute to the phenomenon of charge storage in the ECs. A share of micropores is dominant in electrode materials, ensuring their high surface area. However, the tortuous nature of the micropores does not provide sufficient ionic diffusion. Mesopores (2 – 50 nm) provide tunnels that facilitate the transport of ions to the interior of the bulk material, especially when relatively large cations are used (e.g., ionic liquids). Their presence improves the availability of micropores. Macropores (>50 nm) presence serves as an ion buffer reservoir; they provide a short diffusion distance for the ions. Existing excessive mesopores and macropores usually sacrifice the high specific surface area. Therefore, it is vital to balance a micro-/meso-/macropores ratio to a given ions dimension in electrolytes.

As a result of their unique chemical and physical properties, carbon materials are the most widely used electrode material in energy storage technologies (**Fig. 5**). It comes in several allotropic forms, such as fullerenes, graphite, and nanotubes, with dimensions ranging from 0 to 3D [24].

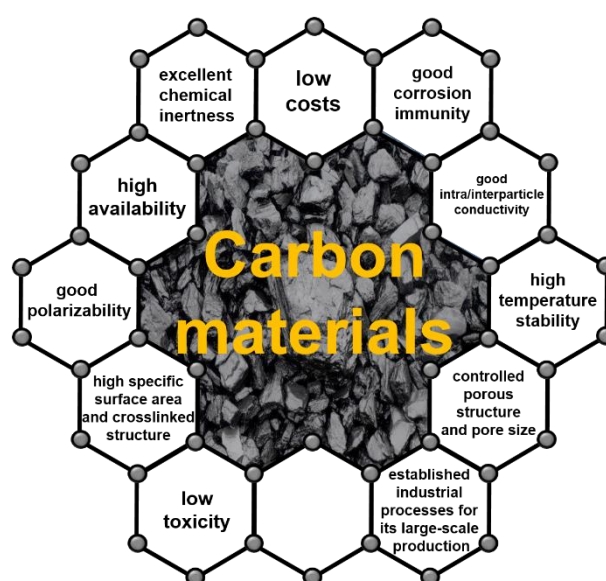


Fig. 5. The advantages of carbon materials [32-34].

Activated carbons

The uniqueness of activated carbon (AC) as an electrode material is due to the possibility of obtaining high capacitance $100 - 200 \text{ F g}^{-1}$, with an energy density $1 - 2 \text{ Wh kg}^{-1}$, power densities to 10^4 W kg^{-1} and with minimal performance fade for over 10^5 cycles [14, 35-38]. AC is a form of carbon with a network of micropores produced from synthetic or natural precursors by a carbonization process (heat treatment in an inert gas atmosphere) [39]. Carbon is then activated through physical activation (named thermal, by CO_2 /steam) [40] or chemical activation [41]. As a result of the activation, a material with small pores, small volume, high degree of microporosity, and a surface area exceeding $1000 \text{ m}^2 \text{ g}^{-1}$ is obtained. In physical activation, carbon is activated at $400 - 1000^\circ\text{C}$ with a constant flow of CO_2 . In chemical activation, carbon is treated at lower temperatures in the range $400 - 700^\circ\text{C}$ in the presence of an activating/dehydrating agent (H_3PO_4 [42], H_2SO_4 [43], ZnCl_2 [44], KOH [45]). The surface area, pore size, and distribution can be controlled by varying various parameters, such as temperature, firing time, and type of activating agent, during carbon treatment. There are natural and synthetic activated carbons [46]. The commercially available carbons are rather physically activated. Chemical activation is simply too costly for industrial applications.

Natural precursors include cotton [47], rice [48], peanut husk [49], coconut [50], bamboo [51], wood [52] and seaweed [53], plant stems [54], fruit seeds [55] and many more. This group includes active carbon fibers obtained mainly by electrospinning of natural materials, such as pitch or by the use of polymer solutions. The process of activated carbon producing fibers from electro-spun precursors begins with oxidative stabilization in an oxygen-containing environment in the temperature range of $180 - 300^\circ\text{C}$. The next step is carbonization in an inert atmosphere, followed by graphitization with further heating of the fiber to 3000°C . The final step is activation in an oxidizing environment in the temperature range of $700 - 1200^\circ\text{C}$ [56].

Polymer-based carbons are a type of synthetic carbon materials produced by the carbonization of polymer gels (high temperature heat treatment up to 800°C in an inert environment such as Ar or N_2). One of the main

advantages of these carbons is the better control of their porous structure during the synthesis of polymeric gel precursors prior to the carbonization process. Due to the cross-linked structure of the initial gel, which can be controlled during the polycondensation step of the gelling process, these carbons have a 3D structure with very high conductivity. Further control of the porosity of these carbons can be achieved by producing activated carbons in the activation process [57, 58].

Carbide-derived carbons

Carbon derivatives (carbide-derived carbons, CDC) are a group of carbons obtained by removing metal atoms or metalloids from ceramic precursors such as SiC [59], TiC [60], Mo₂C [60] and VC [61], by using physical processes (thermal decomposition, thermochemical process or as a result of chemical transformations, e.g., halogenation). The disadvantages of these materials are high production costs and environmental problems.

Template derived carbons

Template derived carbons (TDCs) are a group of carbons synthesized by using an inorganic matrix (ordered silica [62] or zeolite [63]) and a carbon precursor (sucrose solution [64], polyfurfuryl alcohol [65], propylene [66] or pitch [67]). The preparation of TDC involves three steps including the synthesis of the template itself, the infiltration of the carbon precursor and the removal of the backbone template.

Graphene

Graphene is a 2D carbon structure composed of monolayers of carbon atoms arranged in a honeycomb structure with six-membered rings. Graphene materials come in the following forms: graphene sheets, activated graphenes, fullerenes, and graphite [68]. Preparation methods include mechanical exfoliation of bulk graphite [69], silicon sublimation from silicon carbide (SiC) [71], synthesis of multilayer graphene arc discharge [70] and epitaxial growth by chemical vapor deposition (CVD) of hydrocarbons on metal substrates [71]. Graphite oxidation to graphite oxide, thermal or mechanochemical exfoliation of graphite oxide to graphene oxide (GO), and then reduction of GO sheets to graphene

are the most commonly used methods, thanks to which graphene is obtained with higher efficiency. Graphene and its derivatives cannot be used for high current applications because their capacitance dramatically decreases with increasing current density [72].

Shaped carbon nanostructures

These materials have a specially designed structure, obtained mainly through complex synthetic pathways. Carbon nanotubes, carbon nanofibers, carbon nanorods, carbon nanocubs and carbon nanofoams belong to this category of carbons [56].

Carbon nanotubes

Carbon nanotubes (CNTs) are coiled graphite sheets that form a tubular shape (parallel to the cylindrical axis). Both ends are usually closed with a fullerene-like structure (diameters ranging from 1 to 30 nm) [73]. CNTs can be synthesized by arc discharge [74], laser ablation [75] and chemical catalyst vapor deposition (CCVD) methods [76]. CCVD is the most widely used technique for large-scale production. The addition of graphite sheets around the core of single-walled carbon nanotubes (SWCNTs) [77] produces double-walled carbon nanotubes (DWCNTs) [78] or multi-walled carbon nanotubes (MWCNTs) [79]. SWCNTs show a much larger surface area at more expensive production costs compared to DWCNTs and MWCNTs. ECs fabricated only with CNTs have a rather small capacitance compared to ACs as electrode materials [80]. CNTs are effective spacers between the graphene sheets (and its derivatives). They suppress an irreversible agglomeration caused by the strong van der Waals interactions. The access of ions to the graphene layers is facilitated, which leads to a capacitance improvement. Therefore, CNTs are often used as an electrode material in the form of AC composites or pseudocapacitance materials such as conductive polymers [81]. The cost of energy storage is approximately 2 – 300 \$ Wh⁻¹ with AC as electrode material, while the cost increases significantly to 5200 – 8300 \$ Wh⁻¹ with SWCNT [82]. CNTs have reduced their resistance. The main disadvantages of these materials are high production costs and complex synthesis pathways.

Carbon nanofibers

Carbon nanofibers (CNFs) have cylindrical nanostructures produced by using synthetic methods similar to those used to make CNTs. The carbon precursor is heated in the presence of a catalyst. The change in experimental conditions, such as the type of precursor or catalyst, determines whether CNT or CNF must be produced [83]. Electrospinning is one of the most commonly used CNF synthesis methods with a controlled fiber diameter. CNFs consist of carbon nanochips with diameters in the 50 – 200 nm range stacked on top of them to form the fiber shape [84].

Carbon nanohorns

Carbon nanohorns (CNHs) were first produced by CO₂ laser ablation without a catalyst [85]. The structure of CNHs is closely related to CNTs, consisting of a single tubular structure with a conical end, 2 – 5 nm in diameter, assembled into a dahlia flower-shaped aggregate with an average diameter of 80 nm [86]. Asymmetric CNHs are proposed as active materials for high performance soft electronics and energy storage applications (in flexible solid-state ECs) [87]. As-grown single-wall CNHs (SWCNHs) do not have high surface area and pore volume due to their closed structure. Therefore, various attempts have been made to develop the porosity of SWNHs [88, 89]. Oxidation of SWNHs in O₂ gas could create 'nanowindows' in closed SWCNHs, and thus the porosity of SWCNHs is dramatically developed [89]. After opening, the internal spaces are accessible to various guest molecules through the nanowindows [90]. SWCNHs with asymmetric hollow structure exhibit high capacitance, excellent mechanical strength with a little irreversible agglomeration [91]. However, the use of SWCNHs in ECs is not widely used, mainly due to the specialized nature of their synthesis [92, 93].

Carbon nano-onions

Carbon nano-onions (CNOs) also called carbon onions (Cos) or onion like carbons (OLCs) consist of concentric layers of spherical closed carbon shells that form an onion-like structure. The most common method of CNO producing is annealing temperature 1400 – 2000°C in a vacuum or in inert gases [94]. CNO can be synthesized in greater amounts under atmospheric pressure with reduced complexity and cost by the arc discharge method. However, this process produces other nanostructured carbons such as CNTs, polyaromatic, and amorphous carbons as impurities [95]. Other techniques including laser excitation [96], ion implantation [97] and CVD [98] are also used to produce CNO. The S_{BET} of CNO ranges from 400 to 600 $\text{m}^2 \text{g}^{-1}$, where the nonporous outer coating contributes to a very high energy efficiency. As a result of their inaccessible inner surface, these materials exhibit a low energy density. CNOs are still among the least studied nanocarbon structures due to the difficulties and costs associated with producing them on a commercial scale [99].

Carbon composites

The aim of composites is to improve an overall electrode behaviour through synergistic interaction between the components [56, 100, 101]. The carbon materials (AC, CNT and graphene) capacitance can be improved by introducing pseudocapacitance mechanism by doping them with pseudocapacitance materials (oxides of transition metals such as Mn [102], Ru [103], V [104], Fe [105], Ag [106], Cu [107] and Zn [108] at various oxidation states) or heteroatoms (oxygen [109], nitrogen [110] or boron [111]). In addition to the capacitance, they also improve the wettability of the electrode. Nitrogen functional groups with five valence electrons exhibit electron donor characteristics and alkaline pH [112]. Nitrogen can be introduced to the surface and/or into the structure of the carbon by chemical material treatment with reagents such as urea [113], nitric acid [114], pyrrole [115], potassium hydroxide [116] and ammonia [117] or by carbonization of various precursors containing nitrogen such as urea polymer [118], polyaniline [119], melamine [120], organic gel based on melamine [121]







and biomass containing nitrogen [122-124]. The source of pseudocapacitance is pyridinic [125] and pyrrolic nitrogen [126], while quaternary [127] and pyridine-N-oxides [128] improve the operation of the EC at high current density. The nitrogen content should not exceed 8% by mass [129]. Carbon-nitrogen composites can be used with aqueous and organic electrolytes [130].

Both acidic (electron acceptor inducing properties) and alkaline oxygen functional groups can be present in carbon. Acid groups (mainly present) can be introduced by elevated temperatures of carbon activation (in air and HNO_3) and electrochemical oxidation [131]. Alkaline groups are present in the carbon network when carbon is treated at high temperatures under inert conditions, followed by cooling and exposure to an oxygen atmosphere. Due to the irreversible reaction of functional groups containing oxygen with organic electrolytes, the use of functional oxygen carbons is limited only to ECs based on aqueous electrolytes [130]. Oxygen surface functionality (e.g., quinone/hydroquinone) can increase carbon wettability and EC capacitance (especially in acidic environment), but usually at the expense of power density and cycle life [132]. Furthermore, higher rates of self-discharge are recorded for oxygen-rich carbons due to the redox shuttle effect [133]. Composites allow for an energy density similar to that of a battery, extending the EC cycle life, increasing its efficiency, power density, and capacitance.

3.6. Electrolytes

The interaction of ions-electrodes in all electrochemical processes has a significant impact on the state of the electrode-electrolyte interface and the internal structure of active materials. The most general division of electrolytes concerns their physical state. They can be in the liquid or solid state. The use of electrolytes in the liquid phase appears to be very important, as they ensure high mobility and/or ions activity. The group of liquid-phase electrolytes includes aqueous and non-aqueous (organic or ionic liquids) solutions. A detailed breakdown of the advantages and disadvantages of each group is presented in **Tab. 3**.

Tab. 3. Advantages and disadvantages of the electrolytes used in EC [56].

Advantages 	Electrolytes	Disadvantages 
Aqueous		
<ol style="list-style-type: none"> 1) low price 2) environment friendly 3) high ionic conductivity (850 mS cm⁻¹ for 5 mol L⁻¹ KOH in 50 °C) 4) no need to use an inert atmosphere during production 5) a simple way to clean and dry electrode materials during the manufacturing process 6) high compatibility 7) good availability 8) low viscosity 		<ol style="list-style-type: none"> 1) low energy 2) low electrochemical stability (~1.6 V) 3) corrosive environment 4) electrolyte leakage possibility 
Organic		
<ol style="list-style-type: none"> 1) average electrochemical stability (~2.6 V) 2) low freezing temperature 		<ol style="list-style-type: none"> 1) low ionic conductivity 2) high volatility 3) high flammability 4) high viscosity 5) decomposition on AC surface increases ESR and the ECs ageing (blockage of pores with decomposition product) 6) dependent on temperature variations 7) inert atmosphere requirements 8) high price 9) low power 10) toxic and harmful to the environment 
Room temperature ionic liquids		
<ol style="list-style-type: none"> 1) high electrochemical stability (>3 V) 2) high security 3) high chemical and thermal stability 4) hydrophobicity 5) negligible vapor pressure (non-flammable and low risk of explosion) 		<ol style="list-style-type: none"> 1) high viscosity 2) lower ionic conductivity than for organic electrolytes 3) inert atmosphere requirements 4) poor ECs power performance 
Solid-state		
<ol style="list-style-type: none"> 1) good ionic conductivity 2) no leakage of electrolyte 3) simplicity of packaging 4) mechanical durability 5) high processability 6) good electrochemical stability 7) flexibility 8) high security 9) barrier properties for O₂ i CO₂ 10) biodegradability 11) chemical and thermal stability 		<ol style="list-style-type: none"> 1) high viscosity 2) the possibility of salt crystallization at low temperature 3) low conductivity (only solid polymer electrolytes SPE) 4) low mechanical stability (only gel polymer electrolytes GPE) 

Aqueous electrolytes

Aqueous electrolytes are mainly divided into acidic, alkaline and natural solutions; the most common are KOH [134], NaCl [135], KCl [136], H₂SO₄ [137] and Na₂SO₄ [138] solutions. This type of electrolyte is used in applications that require higher power outputs. The main goal of research on this type

of electrolytes is to increase the electrochemical window stability. The decomposition of water occurs with the release of oxygen at the positive electrode and hydrogen at the negatively polarized electrode [139].

A new concept of aqueous media is highly concentrated electrolytes called '*water in salt*' electrolytes. The main purpose of the applicability of such electrolytes in ECs is to improve the energy density in the device by increasing the electrochemical stability. It is assumed that reducing the water in such a medium, by increasing the concentration of dissolved salt, may lead to an increase in the solvation power of water molecules with ions. Both the volume and weight of the dissolved salt should be greater than of the water [140]. Reports in the literature show that it is possible to obtain 2.4 V (comparable to the voltage of organic electrolytes), while in conventional water-based devices it is difficult to exceed 1.6 V (theoretically 1.23 V). Capacitance is also improved in such systems. The energy density is up to three times that of conventional water devices and is on the same order of magnitude as that of redox-enhanced ECs. The performance of ECs using the '*water in salt*' electrolyte is a trade-off between high concentration (to extend the potential window and energy density) and good ionic conductivity (to maintain an acceptable power density) [141]. In order to reduce the viscosity and increase the conductivity of such an electrolyte, a cosolvent (e.g., acetonitrile) was added. This additive also has a positive effect on extending the temperature range in which the concentrated electrolyte retains its unique properties [142].

Redox-mediated electrolytes (cationic, anionic, and neutral) belong to the aqueous group of electrolytes [143]. The main disadvantage of EC systems based on redox-mediated aqueous electrolytes is poor cycle performance [144, 145]. This is mainly due to a strong redox reaction at the electrode/electrolyte interface, which will affect the electroactive site to some extent [144]. The energy density based on multiple redox additives is higher than that of a single redox additive [146, 147]. In mixed electrolytes, their ratio is a key factor for ECs performance. There are three types in this group: cationic, anionic, and neutral aqueous redox electrolytes. Depending on the redox pair selection, one of the electrodes has battery-like behaviour, and the other one is based on purely

capacitance performance. However, the kinetics of such reactions is generally limited, deteriorating the output power of the device. Moreover, the reversibility of redox processes is often limited by changing the environment within the electrochemical cell. Potential variation causes the separation of ions in the electrolyte bulk, while the separation of ions causes a concentration gradient and local pH changes. The inclusion of micro- and even ultramicropores in the electrode material acts as small, multiple chemical reactors in which pressure variations affect the equilibrium of species.

Organic electrolytes

Most commercial ECs are based on organic electrolytes due to their wide electrochemical windows and long cycle life [148]. Organic electrolytes consist of aprotic organic solvents, both pure and mixed. Acetonitrile (AN) [149], linear carbonates including ethylene carbonate (EC), propylene carbonate (PC) [150], dimethyl carbonate (DMC) [151], diethyl carbonate (DEC) [152], ethyl methyl carbonate (EMC) [152], methyl butyrate (MB) [153] and ethyl butyrate (EB) [154] are the most commonly used organic conductive mediums. For some electrolytes (e.g., ethylene carbonate) whose melting point varies slightly above the ambient temperature, DMC, DEC, EMC, MB or EB are added to decrease the viscosity and melting point and to improve the temperature electrolyte stability [155-157].

Aprotic room temperature ionic liquids

Aprotic room temperature ionic liquids (ARTILs) are low-temperature molten salts and are considered '*environmentally friendly*' solvent-free electrolytes consisting only of ions capable of forming efficient EDL. ILs are characterized by weak interactions, due to the combination of a bulky, unsymmetrical organic cation and a weakly coordinating inorganic/organic (charge-delocalized) anion [158]. Chemical and physical properties depend strongly on the water content. Relatively small amounts of water can dramatically affect the ionic conductivity, viscosity, and electrochemical stability. ILs with water content lower than 10-20 ppm are needed [159]. So far, mainly two families of IL have been considered, based, respectively, on the imidazolium cation (lower electrochemical stability window 3.0 – 3.2 V, higher ionic conductivity, lower

viscosity) [158, 160-163] and the pyrrolidinium cation (higher electrochemical stability window 3.5 – 3.7 V, higher energy density, lower power density and ionic conductivity, higher viscosity) cation [164-170]. Because of the relatively high viscosity of ILs and the high equivalent series resistance (ESR), power is often poor at or below room temperature. To overcome this limitation, mixtures of two different ILs have been proposed. An important advantage related to the use of such mixtures is the possibility of decreasing the melting point [160] and, consequently, extending the temperature range of EC [163, 166, 170-172]. Yet, such mixtures require essentially mesoporous carbons which are obviously not optimal for high-volumetric ECs performance.

Solid and quasi-solid-state electrolytes

The solid-state electrolytes developed for ECs have been based on polymers. They are especially appreciated in flexible electronic devices. Polymer electrolytes are classified into three groups: solid polymers (SPEs), gel polymers (GPEs), and polyelectrolytes. The use of SPEs is very limited because of their low conductivity. GPEs are called hydrogel or quasi-solid electrolytes due to the presence of a liquid phase (as a plasticizer). The liquid phase in GPEs results in the highest ionic conductivity among solid electrolytes [173]. GPEs consist of a polymer host (e.g. poly(acrylic acid) (PAA) [174], poly(vinyl alcohol) (PVA) [175], poly(ethylene oxide) (PEO) [176], potassium polyacrylate (PAAK) [177], poly(ether ketone) (PEEK) [178], poly-(methylmethacrylate) (PMMA) [179], poly(vinylidene fluoride-co-hexafluoropropylene) (PVDF-HFP) [180], poly(acrylonitrile)-*block*-poly(ethylene glycol)-*block*-poly(acrylonitrile) (PAN-*b*-PEG-*b*-PAN) [181] and conducting salt dissolved in a solvent (e.g., KOH, H₂SO₄, K₂SO₄ etc. dissolved in water or in organic EC, DMF, PC and their mixtures PC-EC and PC-EC-DMC [182]). However, gel polymer electrolytes may also suffer from a narrow operating temperature due to the presence of water and relatively poor mechanical strength [173].

3.7. Composition and production

The selection of the appropriate electrode material must be coupled with a selected electrolyte to improve the performance of the system in terms of its energy and power density (gravimetric and/or volumetric), self-discharge, electrochemical stability and cycle life [183, 184]. As a consequence, research is carried out on various levels: electrode design, electrolyte composition, separator selection, and device packaging. Typically, an EC electrode consists of several components. The basis is the active material (one of those listed in **Section 3.5**), which is responsible for storage of electric charges. The addition of a polymer, most often poly(tetrafluoroethylene) PTFE or poly(vinylidene fluoride) PVDF [185], acts as a binder connecting the individual electrode components (active material and additives) in a uniform form on the current collector surface. Additives such as carbon black (CB), CNT, and OLC are responsible for increasing the conductivity. The share of individual components in the electrode structure is shown in **Fig. 6**.

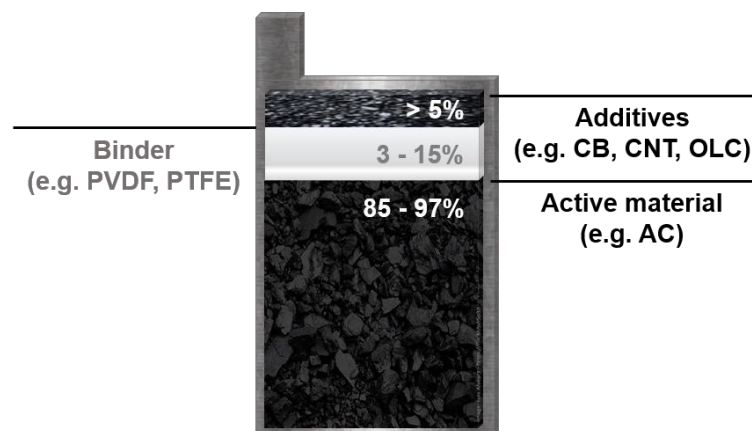


Fig. 6. Composition of electrode in electrochemical capacitor.

It should be mentioned that in the EC production process, aluminum foil is most often used as a current collector, which shows good chemical and mechanical stability. It is inexpensive and suitable for a commonly used organic medium. Stainless steel is the most promising material for current collectors in an aqueous environment. Therefore, it is not recommended to use noble metal foil or other unstable materials in an aqueous solution because

they are sensitive to corrosion.

The EC electrodes production includes:

- 1) Electrode slurry preparation – it is a homogeneous electrode material suspension consisting of materials in the solid state (active material, binder, additives) and solvent (most often N-methyl-2-pyrrolidone, NMP). The components are mixed before being weighted in advance.
- 2) Covering the current collector with the electrode layer – the liquid form of the electrode material allows the current collector to be evenly covered in the form of a thin film. For this purpose, spray nozzles or a device called a doctor blade are used.
- 3) Solvent evaporation – in a drying and solvent recovery zone the current collector covered with a thin layer of electrode slurry is heated to evaporate the solvent.
- 4) Electrodes shaping – electrodes are cut to the appropriate length, rolled with the opposite electrode and the moistened separator by electrolyte. In this form, electrodes are packaged into the EC package.

4. Electrochemical research techniques

Before discussing the individual electrochemical techniques used in the dissertation, it is necessary to mention a possible electrode configuration in which the experiments can be performed. An EC measurement can be carried out in a 2- or 3-electrode system. The 3-electrode connection is common in fundamental research where one electrode is tested in isolation – without the complications coming from the electrochemistry of other electrodes. The 3-electrode system consists of the working electrode WE (the test electrode), the reference electrode RE (the electrode with a constant electrochemical potential) and the counter electrode CE (usually the neutral electrode present in the cell that closes the circuit). Testing packaged/commercial capacitors requires a 2-electrode connection.

The following electrochemical techniques were used in the research that made up this dissertation. cyclic voltammetry, galvanostatic cycling with potential limitation, galvanostatic intermittent titration technique,

potentiostatic electrochemical impedance spectroscopy, linear sweep voltammetry, and step potential electrochemical spectroscopy. A more detailed description of each of them can be found below.

Cyclic voltammetry

Cyclic voltammetry (CV) at the beginning of an ECs development provides basic information about the voltage, capacitance, and cycle life. In addition, it allows one to gain knowledge about redox processes. In the voltammogram, the X-axis represents a parameter that is superimposed on the system, here applied voltage in a 2-electrode or potential in a 3-electrode system. The system response – current (I) is recorded on the Y axis. CV primarily provides qualitative information about the system under study. On the basis of the collected data, it is also possible to calculate the capacitance, but a galvanostatic cycling with potential limitation technique is recommended for this. Voltammograms, in particular for ECs storing charge primarily through EDL formation, are expected to be ‘*box-like*’ and approach that of an ideal capacitor. The reason for this behaviour is the delocalized charge at the electrode-electrolyte interface. Deviations from the ideal ‘*box-like*’ shape may be caused by various electrode processes. The rise in voltammetry response (peaks) is generated by electrode site oxidation/reduction (presence of redox-active moieties) at a specific potential (localized charge storage). The peaks breadth and potentials where they occur may be dependent on characteristics such as solvent reorganization or redox kinetics. The peak shift can be caused when the redox processes at this electrode site are limited by mass transport (not necessarily the case for an interfacial process). Another possibility is electrode/electrolyte instability (decomposition particularly at the extreme potentials) or the resistivity of processes. Higher resistivity leads to greater curvature and deviation from ideality of voltammogram just after its sweep reversal. Electrode (ohmic) resistivity is due to limited active material and electrolyte conductivity, poor electronic conductor mixing in the electrode, and resistive electrode-substrate interfaces [186].

Galvanostatic charge-discharge

The efficiency is determined as a function of its electric charge and the charge/discharge conditions for which the rate and the potential range are given. While the CV provides basic information (stability window, capacitance, etc.), the galvanostatic charge-discharge (GCD) is used to determine the energy response. Therefore, among the available techniques, CVs and GCDs are considered to provide qualitative and quantitative information, respectively. The determination of the boundary ECs conditions, possible perturbation phenomena, the stability of the electrode material, and the entire system is based on galvanostatic cycling with potential limitation (GCPL). Users expect that the devices will work for over several hundred thousand cycles. Considering that cycle life studies are very time-consuming, the duration is generally limited to only tens of thousands of cycles. Therefore, the appropriate aging protocol is known as a floating test (periodically holding the maximum voltage) and, in some cases, higher than the ambient temperature of the experiments conducted [187-189]. More specifically, the floating protocol consists of several GCD cycles that occur immediately and consecutively, followed by a period of time maintaining the maximum operating voltage of the device. The purpose of several consecutive GCD cycles is to assess the capacitance and ESR, and to restore the system to its initial state after a period of high voltage (what favors the packaging of ions in pores). For both GCPL and floating results, the capacitance and ESR are plotted against time. The EC is usually considered as losing its properties when the capacitance reaches 80% of the initial value or the ESR is increased by 100%. Floating sequences are repeated until at least one of the end-of-life criteria is reached. Typically, a series of 60 sequences (total cumulative floating time of 120 hours) is sufficient to distinguish between major failures that may occur during EC operation with AC as electrode material in an aqueous electrolyte. In addition to the increase in the ECR and loss of capacitance, collector corrosion, carbon oxidation, and electrolyte decomposition also indicate system degradation. In addition, by using the basic GCD it is possible to determine the charge/discharge efficiency, self-discharge time, leakage current, and the determination of energy

and power values (Ragone diagram).

Galvanostatic intermittent titration technique

Galvanostatic intermittent titration technique (GITT) enables the determination of equilibrium potentials of the electrodes. A low magnitude constant current (titrated) is applied to the system to reach the potential plateau. After the plateau is maintained, the current is terminated (open-circuit conditions) and the electrode tends to reach its equilibrium potential. The process is repeated until the desired electrode potential (or the total charge titrated) is reached. The maximum theoretical capacitor voltage was estimated by the offset of the resting potential during hydrogen sorption on the negative electrode and carbon oxidation on the positive electrode [190].

Electrochemical impedance spectroscopy

Electrochemical impedance spectroscopy (EIS) consists of imposing a time harmonic oscillating electric potential of small oscillation amplitude around a time-independent '*DC potential*' at the electrode and measuring the resulting harmonic current density. The Nyquist plot presents the imaginary negative part of the impedance $-ImZ$ (axis Y) compared with the real part ReZ (axis X). The EIS provides both qualitative and quantitative information. The first point ($R_A; \Omega$, for the highest frequency) in the Nyquist plot was attributed to the bulk electrolyte resistance. Furthermore, a final value ($R_B=R_A+R_{AB}; \Omega$) ending semicircle region can be interpreted as the internal resistance of the system, that is, the sum of the bulk electrolyte resistance ($R_A; \Omega$) and the so-called charge transfer resistance ($R_{AB}; \Omega$, sum of the electrolyte resistances in the porous electrode structure, the electrode resistance and the contact resistance). The nonvertical BC segment (ended with R_{BC} equivalent distribution resistance) recorded at intermediate frequencies is assigned to ion transport limitation in the electrolyte in porous electrode structures, ion transport limitation in the bulk electrolyte, or nonuniform pathway for ion transport from the bulk electrolyte to the porous electrode surface caused by a nonuniform electrode pore size and electrode roughness. The vertical line at low frequencies (above R_{BC} resistance) has been attributed to the dominant EDL capacitance behaviour. The intersection between

the vertical line and the ReZ axis is called the internal resistance (R_C ; Ω), equivalent series resistance (ESR) or the total resistance of an electrode/device [191].

Linear sweep voltammetry

Linear sweep voltammetry (LSV) is a technique similar to CV, but rather than a linearly cycling over the potential range in both directions, it involves only a single linear sweep from the lower to the upper potential limit (one-segment CV). WE potential is swept linearly between an initial and final value; the current is measured as a function of time (voltammogram). This shows the electrochemical response (oxidation or reduction). LSV can be used to determine the stability of the electrolyte window and provides qualitative and quantitative information. LSV is often used to study the kinetics of electron transfer reactions and the fundamental physical mechanics of electron transfer reactions, such as reversibility, formal potential, and diffusion coefficient determination.

Step potential electrochemical spectroscopy

The description of the step potential electrochemical spectroscopy (SPECS) technique is more detailed than other techniques due to the essential contribution to the recording of data necessary to reach the conclusions presented in the experimental part of the dissertation.

SPECS was developed to characterize the behaviour of electrochemical capacitor electrodes. Conventional electrochemical analysis methods, such as CV and GCD, provide only limited data on the electrode under test. However, SPECS has been shown to characterize the electrochemical response more fully. The basis of SPECS is the separation of charge storage input from faradaic processes (*'capacitor-like'*) and non-faradaic processes (*'battery-like'*) [192].

SPECS is based on a series of steps of equal magnitude potential with the rest time throughout an applied potential window [192-194]. In the rest time the current equilibrium (i - t transient) is established for each potential step. This slow sweep rate enables one to approach its maximum charge storage capabilities. By results obtained from the SPECS technique it is possible

to characterise the kinetics of ion fluxes, the stability of the electrode material, the equivalent series resistance, the existence of the residual current such as leakage and self-discharge current, and the effectiveness of device engineering. The SPECS current (I_T ; A) registered at the given potential step is a result of the current related with EDL formation, or capacitive charging process (I_{EDL} ; A) and the diffusion-limited processes (I_D ; A and I_R ; A). SPECS allows for separate of both charge storage mechanisms. The current related to the first mechanism is given by **Eq. 7**, where: ΔE ; V – potential step, t , s – time (independent of the previous step), R ; Ω – series resistance, C_d ; F – differential EDL capacitance.

$$I_{EDL} = \frac{\Delta E}{R} \exp\left(-\frac{t}{RC_d}\right) \quad (7)$$

EDL can be formed at the surface of the pores in the bulk of the electrode (I_P ; A) as well as in easily accessible for electrolyte the so-called geometric electrode surface area (I_G ; A). In this case **Eq. 7** can be divided into two components given by **Eq. 8**.

$$I_{EDL} = I_P + I_G = \frac{\Delta E}{R_P} \exp\left(-\frac{t}{R_P C_{dP}}\right) + \frac{\Delta E}{R_G} \exp\left(-\frac{t}{R_G C_{dG}}\right) \quad (8)$$

Diffusion-limited processes are much slower than EDL formation because of continuous redox reactions. Therefore, the diffusional current decreases slowly over the equilibration time. This current (I_D ; A) can be modeled by using the Cottrell **Eq. 9** for semi-infinite planar diffusion, where: n ; - – the number of electrons involved in an electrode reaction, F ; C mol⁻¹ – Faraday's constant (96496.7), A ; m² – electrode surface area, C ; mol m³ – concentration of the species at the electrode surface, D ; m² s – diffusion coefficient of the species, B ; A s^{0.5} – constant proportional to the capacitance of the diffusion limited process.

$$I_D = nFAC \left(\frac{D}{\pi t}\right)^{0.5} = \frac{B}{t^{0.5}} \quad (9)$$

I_T does not reach zero at the end of the equilibration time. This does not happen because of the existence of residual processes, along with EDL and diffusion-limited processes. The residual processes occur due to slow diffusional processes (side reactions) in a given equilibration time. Hence, the residual current (I_R ; A) is another term that needs to be added to the SPECS model to account for the I_T . Thus, the I_T current of the SPECS data can be given by **Eq. 10**.

$$I_T = I_P + I_G + I_D + I_R \quad (10)$$

The current data from each potential step (i-t transient) can be used to calculate representative voltammograms at different scan rates by averaging the output current for a specified time after the potential step change. The voltammograms highlight the most important factors that affect the overall EC performance at various scan rates. Charge storage in EDL form (I_P , I_G), dominates at high scan rates (fast kinetics), leading to 'box-like' voltammograms and electrode-like capacitor behaviour. Although diffuse energy storage – redox (I_D , I_R) dominates at lower scan rates (slow kinetics) and is characterized by the battery response of the electrode [192].

Recently, the basic methodology for separating the individual I_T components has been refined. The previous protocol assumed that each i-t transient step was independent of the former one. The basic protocol provides excellent relative information, but cannot reproduce the actual CV data. The revised methodology provides results much closer to that of the CV. It takes into account the interactions between the i-t transients in the next potential stages. The revised methodology emphasizes the independence of the EDL charge-storage processes compared to faradic processes. For the latter mechanism, the i-t transients depend on the previous [195].

5. Summary

Nowadays, ECs occupy a limited electrochemical energy storage devices market niche. The low energy and high cost per Wh are the main reasons why they are not the preferred technology, and enhancing its value is the main challenge facing ECs developers. However, due to their irreplaceable properties, ECs create new possibilities for themselves and have the opportunity to enter the market more widely. This is already evident in emergency power areas and on a larger scale in hybrid capacitor systems development for electric vehicle power. The electrolyte has been recognized as one of the most important elements influencing EC performance. The main factors are conductivity, temperature range, and electrochemical/thermal stability. While significant progress has been made, there are various challenges that make it difficult to exploit the potential of certain solutions for commercial applications. Both the energy and the power density are directly dependent on the voltage. However, a higher voltage often degrades other electrolyte properties. Non-aqueous electrolytes (ionic and organic liquids) are suitable candidates for an energy density improvement. Unfortunately, they are characterized by lower conductivity, and their use in EC leads to lower capacitance and higher resistance in comparison to that in aqueous electrolyte-based systems. Still, the charge storage mechanism systems based on ionic liquids, solid electrolytes, and redox activity have not been fully explained. Other strategies that have been proposed to improve ECs performance include pseudocapacitance electrode materials, where charge storage is realized via pseudocapacitance redox reactions at the electrode surface. Furthermore, a compatibility of the electrolyte/electrode material is essential. Material research directions typically focus on novel, optimized structures and morphologies, and their contact with electrolytes ultimately maximize the amount of charge storage. Some in situ experimental advances and significant theoretical research have been achieved, but there is still some controversy regarding the phenomena at the electrode/electrolyte interface, the effect of organic solvent addition on the EDL formation, and the temperature effect. There is also a lack of a complete



understanding of the dynamics of ions in more complex electrode structures (e.g., hybrid nanostructures). Moreover, compared to basic research on EDL charge storage mechanisms, theoretical modeling of pseudocapacitance and hybrid devices with specific electrolytes is still very limited. There is an urgent need to establish standardized methods to characterize the performance of new systems. It is also not easy to select and compare the appropriate electrolyte/electrode material systems for a given application, as performance indicators are typically obtained under different conditions. From a practical point of view, optimizing individual stages of electrode production is also of key importance, leading to a reduction in financial outlays. The selection of the correct electrode manufacturing conditions should increase the efficiency of the ECs. Additionally, the energy, power density, and gravimetric capacitance given are based on the weight of the active electrode materials. However, an electrolyte and separator also make up a large content of the total mass, which should not be underestimated. The challenges presented in this section must be met while reducing costs, without sacrificing the long cycle life and extremely high efficiency that make ECs so different from batteries [196-198].

Experimental part

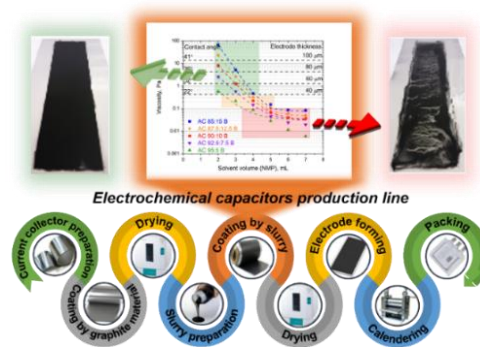
6. Article A1

Title: ***Toward better porous carbon-based electrodes by investigation of the viscoelastic properties of carbon suspension***

Authors: Przemysław Galek, Krzysztof Fic

Journal: unpublished, restricted access until 29.09.2022

DOI: -



Motivation

If the processing of electrode materials is improperly performed, the potential of electrochemical energy storage devices will not be fully used [199]. The subject of electrode suspension rheology, known as electrode slurry, is rarely discussed and this forms the basis for further research on this topic. The rheology of the electrode slurry combines all variables that ultimately affect the mechanical and electrochemical properties of the electrode [200]. To increase ECs efficiency, it is necessary to specify optimal manufacturing conditions, bearing in mind the cost of their production. The manufacturing optimization process leads to cheaper electrode production with improved properties such as efficiency, lifetime, safety, and production costs. Slurry processing and electrode production are some of the most important stages. These stages ensure high quality, reliability, performance, and safety of the assembled devices. The interactions between active and inactive electrochemical materials have an important impact on suspension stability, mixing efficiency, coating process, and final electrode properties.

Summary

In **Article A1** – ‘*Toward better porous carbon-based electrodes by investigation of the viscoelastic properties of carbon suspension*’ electrode slurry based on AC was assigned to the Newtonian fluid group. Only at very low shear rates does the material belong to non-Newtonian (shear-thinning) fluids. The research applicability comes when specifying the viscosity window of the electrode slurry, which provides even coverage of the current collector and finally ensures high EC efficiency. The viscosity limit is 0.3 Pa·s. Below this value, the slurry spreads on the collector surface and, while the viscosity decreases, the level of the uncovered surface increases after a drying process. Above 14 Pa·s the material is characterized by solid response and does not allow it to spread as a film. On the basis of the delivered equation, it is possible to predict geometric dimensions of an electrode based on the slurry viscosity and its composition. Moreover, the developed economic analysis predicts the price of substrates necessary to produce electrode slurry at the given electrode end parameters. It can be concluded that the price of the electrode material does not change linearly with the AC content. The mixing process has a major influence on suspension stability. The positive impact of the ULTRA-TURAX type mixer has been confirmed experimentally. This type of mixing results in chaotic circulation of the suspension throughout the volume. AC particles are evenly spaced from each other, and their mutual interactions are limited. The suspension remains stable after the shear forces have stopped. The aggregation is limited despite the long storage time of the sample. The presence of microstructure was confirmed in the final part of the research. Suspension has some energy storage capacity and should be able to return to some extent to its original configuration before applying some force. The slurry behaves as a flexible solid (although not an ideal one). The non-ideality comes from mechanical energy dissipating. The binder forms bridges between the AC particles. These bonds are destroyed under the influence of sufficiently high shear forces. The carbon-polymer-carbon bridges may be partially restored after shear forces have ceased.

Toward better porous carbon-based electrodes by investigation of the viscoelastic properties of carbon suspension

Przemyslaw Galek, Krzysztof Fic*

Poznan University of Technology, Institute of Chemistry and Technical Electrochemistry, Berdychowo 4, 60965, Poland

*Corresponding author: krzysztof.fic@put.poznan.pl

Keywords

Electrochemical capacitors; Electrode slurry; Rheological properties; Mixing; Modelling

Abstract

In the article, we assign an electrode slurry based on activated carbon to a given group of rheological fluids. We explain the interactions between the slurry components and their impact on the flow nature. The effect of the microstructure formed after slurry preparation is also discussed. We provide a universal mathematical model that correlates the electrode thickness, the viscosity, and composition of slurry (mass of solid materials, solvent volume, and ratio between components). The viscosity window and optimal ratio between components, which are necessary to form the right coating on the stainless-steel foil as a current collector, have been specified. Moreover, the phenomena accompanying the selected mixing technique are discussed. Finally, the paper provides an economic analysis of electrode slurry production.

1. Introduction

Rapid progress in the development of energy storage and conversion systems is motivated by the huge energy demand from society [1]. Electricity is the kind of energy that can be relatively easily transported and converted, without significant losses. Transfer of the electric energy must be realized with the help of various tools and devices for its storage. The literature widely explains electric charge storage phenomena and addresses the issues of improving the device production processes. In addition to many conventional energy storage systems such as batteries, electrochemical capacitors (ECs) are relatively new and effective tools for energy storage. Research on new electrode materials is a continuous trend in the development of ECs [2, 3]. However, the application potential of the most promising materials will not be fully exploited if the processing of these materials is not performed in a right way. In this context, the aspect of the electrode material suspension (so-called electrode slurry) is rarely discussed. To increase the efficiency of ECs, it is necessary to specify optimal manufacturing conditions, bearing in mind the cost of their production. The manufacturing optimization process leads to cheaper electrode production with improved properties such as efficiency, lifetime, safety, and production costs.

ECs consists of three main components: a positive and negative electrode, a separator, and an electrolyte. Electrodes are de facto responsible for charge storage, the separator prevents short circuiting, and the electrolyte is a charge carrier [4]. Electrodes are formed in the first stage of the production chain

by coating the current collector with electrode slurry. The coating should be characterized by a continuous, homogeneous, and smooth structure. Slurry processing and electrode production are some of the most important stages. These stages ensure ECs high quality, reliability, performance, and safety of the assembled devices [5]. However, the charge/discharge efficiency depends on the active and inactive electrochemical materials. Their interactions have an important impact on suspension stability, mixing efficiency, coating process, and final electrode properties. Electrode suspensions usually contain electrochemically active material such as activated carbon (AC) and inactive components such as additives, a polymeric binder (B) dissolved in a solvent [6]. The rheological properties of the slurry depend both on the ratio and type of components. Each electrode production stage subjects the slurry to various stresses and requires detailed controlling of rheological properties. The second area of ECs manufacturing concerns the design, evaluation, and new assembly processes optimization. The last step of the production chain deals with scrap reduction and quality assurance.

The industrial process of EC production starts with the preparation of the current collector for the coating process (Fig. 1).



Fig. 1. Block diagram of the electrochemical capacitor production line.

The current collector surface must be cleaned with surfactants and is followed by a thorough degreasing. Incorrect surface cleaning may result in future problems with peeling off of graphite glue and slurry layers, performed in subsequent production stages. In the next stage, adhesive glue (often based on graphite) is distributed in the form of a thin film on the collector surface. This component is responsible for improving the adhesion of the electrode material to the collector surface. Moreover, it increases the electrode conductivity and decreases the resistance. The covered collector is then subjected to drying. The electrode slurry is prepared on the next production stage. The suspension consists of solid materials (AC, B, and additives) suspended in a (fluid) solvent. Electrode material in liquid form is necessary for its distribution on the current collector surface. Polymer-based materials in the formulation play the role of binder. Binder keeps the active material particles together on the collector surface and ensures electrode flexibility. Binder content is usually adjusted between 3 and 15% of the electrode mass (counted for dry and solid materials). Polyvinylidene fluoride (PVdF) is the most commonly used binder. The literature proposed several alternatives such as water-suspended binders such as styrene-butadiene rubber (SBR) or PTFE [5]. More recent scientific reports give an example of volatile poly(propylene carbonate) (PPC) in batteries. PPC easily evaporates during drying, and it is observed that it might also reduce the negative impact of the binder on electrode resistance [7]. Activated carbon (AC) is the predominant slurry component in ECs. The AC content ranges between 85 and 97% of the final mass of the electrode.

Finally, all materials are mixed to obtain a homogeneous suspension. Therefore, the correct selection of mixing type is an important step towards further production of good quality electrodes. Furthermore, the suspension coats the collector surface previously covered by conductive agents. A covered collector is subjected to drying. Temperature and drying time depend on the amount and type of solvent. The coating must form the layer with very uniform thickness and density distribution, as any heterogeneity in the layer can cause future electrode instability. Drying can take a long time, even up to 24 hours at 120 °C under deep vacuum, and is one of the most expensive steps in the electrode manufacturing process [8, 9]. Solvent recovery systems are usually used in commercial manufacturing, due to the high cost of solvents and to prevent pollution of the environment [10]. Cheaper and more environmentally friendly solvents, such as water-based suspensions, do not require a recovery system and, in this context, seem to be an interesting alternative for organic formulations [11, 12].

Non-conventional methods include an electrostatic coating. This method is based on adding high voltage to the spray nozzle and grounding the current collector. Sprayed material is thus attracted

to the collector surface. Although this method allows for coating various collectors, it still requires solvent re-use and the drying step cannot be eliminated. Interestingly, for battery electrode production, so-called dry powder coating processes are used; hence, the thermal activation time has been significantly shortened and the costs remarkably reduced. In this process, the solvent evaporation step was completely eliminated and replaced by so-called hot rolling [13]. Dry-coated electrodes demonstrate good flexibility and coatability on large surfaces. Based on the cost analysis, dry painting reduces costs by up to 15% [13]. This includes the elimination of solvent recovery systems. In addition, it eliminates the time-consuming and energy-intensive drying step.

Although significant progress has been made over the past twenty years in EC and Li-ion (LIB) electrode technology, solutions for higher energy and power densities are still being sought. A conventional strategy to improve these parameters is to increase the density of the electrode [14]. However, increasing the packing density is not always desired. Increasing the electrode thickness seems to be an alternative strategy. However, this approach limits ion transport and results in poor energy efficiency and inefficient use of electrode material. Another solution may be the arrangement of well-organized electrode particles. Most electrodes are produced by randomly arranging particles. Free-distributed particles easily agglomerate and can also become an isolated group in the electrode network. This isolated group does not play its basic role, but hinders ion transport instead. A well-organized structure provides better responses and performance compared to randomly distributed particles [14]. An efficient method for the production of 3D electrode with organized structures exploits the electric field. This technique is easy to implement and provides the effect of long-range electrostatic interactions between particles [15, 16]. It has been found that with these forces one can effectively manipulate the particles in colloidal suspension.

Once the drying step is completed, the coated collector is subjected to calendaring to increase its density. Afterwards, the electrodes are cut to the desired size, depending on the purpose: tablets or pouch cells, pocket electronic, and rolls for industrial or automotive applications. The mechanical cutting process is the most used method for electrode formation. The main disadvantages of this method are the microshape change and bending of the electrode edges; these can affect local changes in the cell volume in larger systems. In contrast, laser cutting is a non-contact process – free from wear, providing fast, flexible adjustment of cutting geometry and increased cut speed, compared to conventional technologies.

Viscosity, concentration, dispersibility, and the ability to thicken the slurry affect its stability and susceptibility to sedimentation. Finally, the viscoelastic properties of the electrode slurry affect

the coating quality including coating speed, film thickness, and edge profiles (Fig. 2).

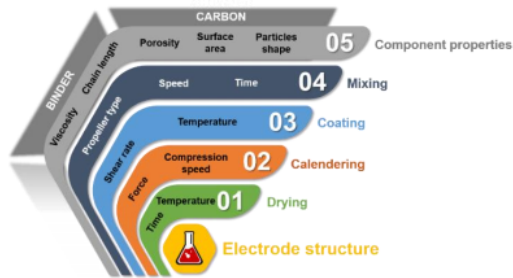


Fig. 2. Production parameters affecting the electrode structure.

The aim is to achieve a constant thickness not only at the electrode center but also at its edges. Incorrect viscoelastic properties of the slurry may generate so-called "heavy edges", originating from increased material volume in this area. This leads to a non-homogeneous pressure distribution during calendaring, which further results in an inhomogeneous structure of the electrode. Uneven edges must be removed to ensure a constant amount of active material per unit of area. However, it is associated with the loss of valuable material and generating wastes that cannot be included for reuse. The production of rolled electrodes with a longer length increases the cantering of the spread material and causes undesirable electrode folds [17]. It is possible to produce layers with better coating properties by increasing the viscosity of the slurry at low shear rates [18]. It results in sharper edge contours and reduces the amount of waste. However, the high viscosity determines the coating problems and poor dispersibility (low film homogeneity) [19]. The uniform layer thickness and density are crucial to guarantee a long lifetime and ensure efficient ion transport. Adjusting the thickness using calendaring leads to smaller, more compact ECs [20]. Thickness can also be controlled by selecting components, their proportion, physical properties (shape of molecules, size) and mutual interactions. For example, the viscosity of the polymeric binder solution can be adjusted by varying the concentration of the polymer in solution or changing the properties of the polymer [21]. The binder type affects the porous structure availability for the attracted ions, which translates into the final capacitance value. It has been proven that the presence of large numbers of irregularly shaped particles results in an increase in suspension viscosity. This is due to the increased impact of particle friction and blocking, but also to the extra energy of flow needed to bypass molecules through the fluid. The shape and distribution of the particles also affect the density of the packing. Uneven particles pack more efficiently than ball-shaped particles. Another model is based on the suspension polydispersity (with different particle size), which ensures a more efficient packing compared to the monodisperse sample at the same concentration. The increased

surface area of particles in a volume unit increases the dispersion viscosity. This phenomenon enhances the interaction between particles and particles/liquid. The viscoelastic properties are also directly affected by the method of processing the electrode material, the type of homogenization, the mixing time and the applied shear rate [22, 23].

Electrode slurry demonstrates shear-thinning properties, regardless its composition [6]. However, the viscosity decreases with increasing shear rate and may vary significantly, depending on the composition of the material and preparation. At low shear rates, the carbon-black-free slurry prepared without intense mixing behaves similarly to Newtonian fluids (plateau with a very small gradient). The active particles slide against one another, and the viscosity is largely a function of the properties of the continuous phase, the binder solution and solvent. The behavior of shear-thinning at higher shear rates can be attributed to the orientation and extension of the binding molecules. The carbon black suspensions exhibit a yield point characterized by a decrease in viscosity at low shear rates. This suspension is more stable and shows greater resistance to sedimentation. Materials with carbon black, which are subjected to intensive mixing, do not show a yield point, but exhibit behavior similar to that of graphite formulas. Intensive carbon black deagglomeration clearly affects the properties of the slurry. The lower deformation energy indicates the difficulty to compress the stiffer structure. The sample with highly agglomerated CB shows yield stress, compressing more easily than with the CB dispersed. The shear-thinning effect is beneficial during slurry manufacture [24]. Viscosity at low shear rates can vary over a wide range without changing the concentration of the polymeric agents. It is possible by using capillary forces created by adding a second nonimmiscible liquid [18]. This generates a network that connects the components (Van der Waals forces) [25, 26]. Such a suspension provides stability (slow sedimentation) and no sharp edges. This reduces waste and increases the density of active ingredients, thereby improving cost-effectiveness. The viscosity at high shear rates remains unchanged, so that slurries can be processed and coated using fixed apparatus and process parameters. The adhesion and electrochemical properties are similar to those of conventional suspensions. The added liquid evaporates during coating and does not remain in the dry electrode layer. The capillary suspension concept aims to reduce organic additives, such as rheological additives and binders. It enables a higher active material density and enhances electrical conductivity.

2. Experimental

2.1. Materials

Carbon electrodes based on six types of AC (Kuraray® YP-50F and YP-80F, Norit® DLC Super 30 and 50, Norit® DLC Supra 30 and 50) were prepared by the coating method. Polymer polyvinylidene fluoride (PVDF) played the role of binder and N-Methyl-2-pyrrolidone (NMP) (Sigma Aldrich®, USA, $\rho=1.024 \text{ g cm}^{-3}$) as solvent. The conductive graphite glue was abandoned to eliminate changes in the regional electrode thickness. The slurry samples were prepared in 10 mL beakers (AC + 5wt% PVDF in NMP + free NMP). 5wt% PVDF in NMP solution was mixed by magnetic stirrer for 24 h at 23°C. A constant mass (1 g) of solid materials (AC and PVDF) was used with different ratios 85:15%, 90:10%, 95:5% and solvent volumes (3, 4, 5 and 7 mL). After that, the samples were subjected to mixing with a high-speed IKA® ULTRA-TURRAX® disperser for 90 seconds. The IKA® RCT basic magnetic stirrer was used for studies of mixing influence (AC 85:15 PVDF + 4 mL of NMP for 12 h at 600 rpm). All measurements and coating processes were carried out immediately after the preparation of the samples to eliminate the sedimentation effect. 316L stainless-steel foil was applied as the current collector (5 x 10 x 0.01 cm). The collector surface was cleaned with surfactants and degreased with acetone. After that, the collectors were dried for 12 h at 70°C. A DOCTOR BLADE (model 4340) made by Elcometer ensured a uniform distribution of the slurry film on the collector surface. The device ensures that the film bends by vacuum mechanism during coating. The knife gap was 200 μm and the blade speed $5.7 \cdot 10^{-3} \text{ m s}^{-1}$. The coatings thus prepared were allowed to pre-evaporate the NMP (for 30 min.) and then transported to a dryer for 24 h at 70°C to fully evaporate the solvent.

2.2 Measurements

Rheological measurements were carried out with BROOKFIELD plate-cone viscometer (model DV2T). The shear stress and viscosity range included the torque above 10% recommended by the producer. The cone and rheometer plate were cleaned with distilled water and acetone and then thoroughly dried. Electrode slurries samples were applied to the rheometer plate using a 1 mL volume syringe. A cone CPA-51Z (2.4 – 47990 mPa s) designed for highly viscous liquids was used. For each sample, more than 6 values (representing an average of 3 repetitions) shear stress and viscosity were obtained throughout the possible shear rate. The contact angle experiment was performed on a DataPhysics goniometer equipped with an optical contact angle (OCA 15Pro) analysis system. Liquid droplet analysis was performed using the SCA 20 module software, which allowed the measurement of the static contact angle on a flat surface by automatically detecting baselines and tangents.

The accuracy of the contact angle measurement was considered $\pm 0.1^\circ$. The injection sample volume was 5 μL and the speed $1.5 \mu\text{L s}^{-1}$. The electronic screw micrometer from ELECTRONIC DIGITAL was used to measure the thickness of the thickness of the electrode material on the collector surface.

3. Results and discussion

The viscosity data for the studied electrode slurries are presented in Fig. 3 (for AC Kuraray® YP-50F).

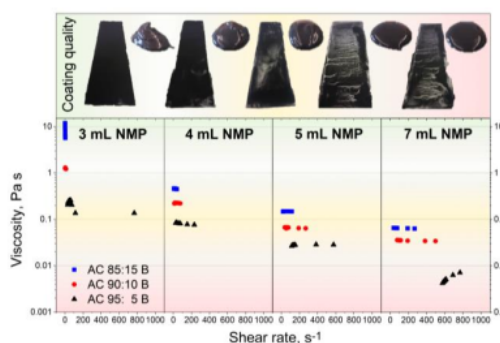


Fig. 3. Viscosity data for electrode slurries based on activated carbon (Kuraray® YP-50F), binder (polyvinylidene fluoride PVDF) and solvent (N-Methyl-2-pyrrolidone NMP).

The shear rate range (for which the measurement is possible to realize) decreases as the viscosity of the slurry increases. This range is wider as the binder fraction decreases (from 15 to 5% of the solid materials content) and the solvent volume increases (from 3 to 7 mL per 1 g of solid materials). The suspension with 15% binder and 3 mL of NMP is characterized by the highest viscosity. The suspension with 5% binder and 7 mL of NMP has the lowest viscosity. It can be seen that the slurry can be classified as Newtonian fluid. The curves are characterized by constant viscosity in a wide shear rate range. The suspension behaves like a non-Newtonian fluid (strong shear-thinning phenomenon) only at a very slow shear rate ($<200 \text{ s}^{-1}$). This is especially true for slurries with ratio of 3:1 (NMP:solid materials). Due to the shear-thinning region, power trend lines were used to describe the course of the recorded points. The only exception is for AC 95:5 B + 7 mL of NMP. Here the trend line is described by SI Eq. 1.

To compare the viscosity for all samples (SI Fig. 1) the viscosity value for one shear rate (384 s^{-1} , 100 RPM) was selected. Given viscosities were determined on the basis of equations describing particular trend lines for viscosity curves. To determine the viscosity for intermediate points (e.g., for 6 mL NMP), trend lines for materials with different compositions and different solvent volumes were again appointed. Eq. 1 describes the course of the viscosity curve versus NMP volume (for 384 s^{-1} , where: μ – dynamic viscosity [mPa s], a, b, c – constant values [-], V – solvent volume [mL]).

$$\mu = a \cdot e^{-b \cdot V} + c \quad (1)$$

SI Fig. 2 presents the viscosity of the slurry vs. the AC:B ratio for different solvent volumes. The viscosities for the intermediate composition (e.g., 86:14) were determined based on **Eq. 2** (where: no. – ordinal number corresponding to the composition of the suspension: 1 – 85:15, 2 – 90:10, 3 – 95:5 [-]).

Eq. 2 allows one to calculate the viscosity for a given AC share in the solid material in the range (0.85 – 0.95).

$$\mu = a \cdot e^{-b \cdot \text{no.}} + c \quad (2)$$

For the curves shown in **SI Fig. 3** in the range of AC 0.85 – 0.95 (with 0.01 AC content step) in the solid material, for this purpose the models describing them were based on **Eq. 3**.

$$\mu = a \cdot e^{-b \cdot V} + c \quad (3)$$

To find the universal equation for the viscosity of the slurry, it is necessary to find the equation that describes the *a*, *b*, and *c* constants. **SI Fig. 4** presents the constant the constant *a*, *b*, and *c* versus the AC content in the slurry. The given constants are described as different trend lines (*y(a)* – power trend line, *y(b)* – polynomial trend line of the order of 6, *y(c)* – polynomial trend line of the order of 6).

$$y(a) = 0.5 \cdot u^{-61.73} \quad (4)$$

$$y(b) = -3641262.68 \cdot u^6 + 19527777.34 \cdot u^5 - 43595,531.9 \cdot u^4 + 51860176.02 \cdot u^3 - 34670208.16 \cdot u^2 + 12350606.05 \cdot u - 1,831555.76 \quad (5)$$

$$y(c) = -351485.37 \cdot u^6 + 1883678.1 \cdot u^5 - 4204860.23 \cdot u^4 + 5004390.05 \cdot u^3 - 3349095.26 \cdot u^2 + 1194961.26 \cdot u - 177588.82 \quad (6)$$

These equations were substituted for the **Eq. 7**.

$$y = a \cdot e^{-b \cdot x} + c \quad (7)$$

Finally, a **Eq. 8** (where: *y(a)*, *y(b)*, *y(c)* – constants depending on the AC share in the solid material [-], *m* – mass of solid materials in the slurry [g]) was obtained for the viscosity, depending on its composition – AC share in solid material [0.85 – 0.95], solid material mass [g] and solvent volume [mL].

$$\mu = y(a) \cdot e^{-y(b) \cdot \frac{V}{m}} + y(c) \quad (8)$$

The coatings were necessary to link viscosity with the thickness of the electrode material on the collector surface (**SI Fig. 5**). The thickness

of the electrode material was measured on the collector surface after the drying process. **Eq. 9** (where: *d* – the thickness of the electrode material on the collector surface [μm]) present electrode thickness based on the viscosity of the slurry. **Eq. 9** can be used during planning the amount of electrode slurry and the proportion between its components to cover a given current collector area.

$$d = 17.01 \ln(\mu) + 56.63 \quad (9)$$

Controlling electrode thickness is also carried out by selecting the height of the knife gap. However, this procedure will not be used effectively when the viscosity and density of the slurry will be lower than the values that allow the obtainment of a greater electrode thickness. In this case, the electrode material will dissolve on the coated surface and the knife will not limit the final thickness. It is possible, based on **Eq. 10** to predict the composition to obtain the intended material thickness on the collector. The contact angle of the collector was also determined (**SI Fig. 6**).

Further research aimed at determining the viscosity window that allows for uniform coating of the stainless-steel foil by electrode material. Individual viscosity ranges and the appearance of the collector surface covered by electrode slurry for a given range are shown in **Fig. 4**. The thickness of the electrode material and the contact angle are shown in the same plot.

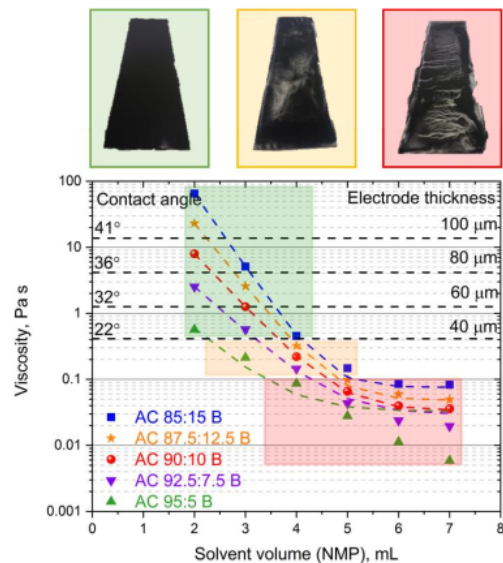


Fig. 4. Viscosity ranges of electrode slurry for current collector coating.

It appears that the viscosity limit is 0.3 Pa s. Below this value, the slurry spreads on the collector surface and along with the decrease in viscosity, the level of the uncovered surface increases after the drying

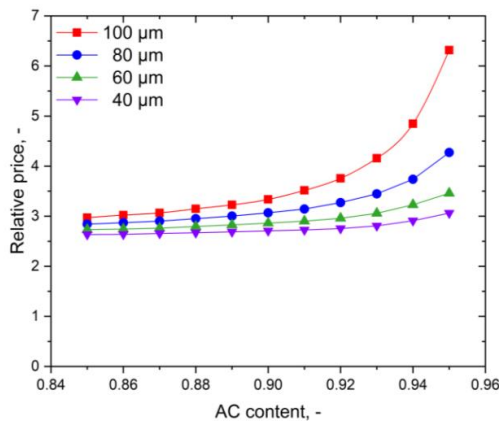


Fig. 5. The relative price for electrode slurry with a given AC content and the final electrode thickness.

It can be concluded that the electrode material price does not change linearly with the AC content. For materials with a composition corresponding to 40 μm electrode material thickness, the price increases slightly after crossing 0.93 AC content. For materials intended for getting thicker electrodes, a significant increase in price occurs above 0.92, 0.91, 0.9 for 60, 80 and 100 μm respectively. **Fig. 6** presents the percentage price increase in relation to the slurry price with an earlier ratio AC : B.

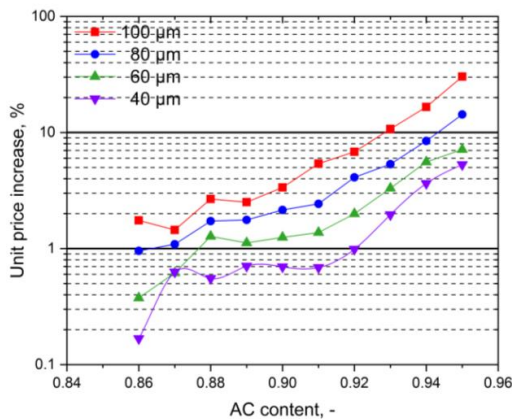


Fig. 6. The percentage increase in price of electrode slurry related to the price of the material with the previous composition.

The slurry price was calculated based on the equation (10) (where: C_{total} , C_{AC} , C_B , C_S – total price, price for AC, binder and solvent respectively; $C_{unit AC}$, $C_{unit B}$, $C_{unit S}$ – unit price for AC, B and solvent; m_{solid} – mass of solid materials; u_{AC} , u_B – share of AC and B in solid materials; V_S – solvent volume, ρ_S – solvent density).

$$C_{total} = C_{AC} + C_B + C_S = (C_{unit AC} \cdot m_{solid} \cdot u_{AC}) + (C_{unit B} \cdot m_{solid} \cdot u_B) + (C_{unit S} \cdot V_S \cdot \rho_S) \quad (10)$$

The research plan also included the mixing technique influence on the homogenization degree of solid materials in the NMP. After selecting a composition for a uniform collectors coverage the slurry was subjected to mixing by two techniques. The fluid movement in the vessel and a phenomena related to the mixing method are shown in **Fig. 7**.

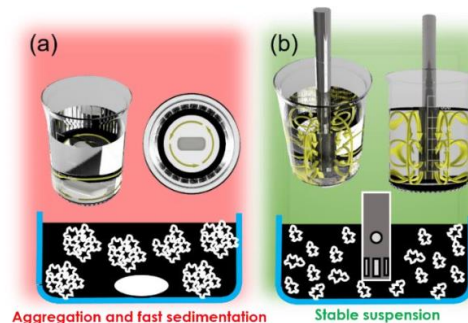


Fig. 7. Activated carbon particles movement depending on mixing technique: (a) magnetic, (b) type ULTRA-TURRAX with high-speed.

A magnetic stirrer mixing does not allow obtaining a homogeneous suspension. A fluid circulation takes place only horizontally, at the vessel bottom. The liquid only circulates, which results in a lack of mixing of adjacent slurry layers. The AC aggregates are formed over time after the shear forces cease and quickly sediment at the vessel bottom. The positive impact of the ULTRA-TURRAX type mixer has been confirmed experimentally. This mixing type results in a chaotic circulation of the suspension on the whole volume. The AC particles are spaced evenly from each other, and their mutual interactions are limited. The suspension remains stable after the shear forces cease. The aggregation is limited despite the long storage time of the sample.

In further studies, the microstructure presence has been searched for. A microstructure appears in macroscopic terms as a homogeneous structure, in micro terms as a system with clear phase boundaries between the individual components. Such a material should also have some forces connecting the components included in the whole volume. In the studied materials, the presence of such a structure is confirmed. A schematic explanation and data confirming the assumptions are presented in **Fig. 8**.

and quickly sediment at the bottom of the vessel. The positive impact of the ULTRA-TURAX type mixer has been confirmed experimentally. This type of mixing results in chaotic circulation of the suspension across the whole volume. The AC particles are spaced evenly from each other, and their mutual interactions are limited. The suspension remains stable after the shear forces cease. Aggregation is limited despite the long storage time of the sample.

In further studies, the presence of microstructure was searched for. Microstructure appears in macroscopic terms as a homogeneous structure, in micro terms as a system with clear phase boundaries between the individual components. This material should also have some forces that connect the components included in the whole volume. In the materials studied, the presence of such a structure is confirmed. The schematic explanation and data confirming the assumptions are presented in Fig. 8.

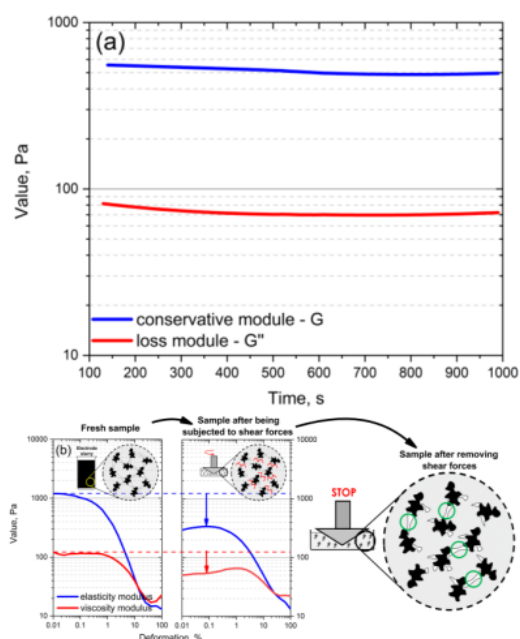


Fig. 8 (a) Conservative (G) and loss (G'') modulus in slurry with schematic representation of the microstructure behavior under the influence of shear forces. (b) Impact of shear forces on the elasticity and the viscosity modulus.

The conservative and loss modulus plot was created to verify the presence of microstructure in the studied material. To break the microstructure force greater than that which occurs between the particles must be applied. When the applied force is weaker than the molecular forces (G is greater than G''), the material has a certain energy preservation capacity and should be able to return to some extent to its original configuration before applying the force. The material behaves like a flexible solid (although not ideal). The non-ideality comes from mechanical energy

dissipating. However, when the applied force is higher, the microstructure is filled and the mechanical energy fed to the material is dispersed. It means the flow of material (G becomes greater than G''). In the fluid under consideration, the first state is present. The binder forms bridges between AC particles. These bonds are destroyed under the influence of sufficiently high shear forces. The viscous and elastic modulus decreases with respect to the fresh sample. The carbon-polymer-carbon bridges may be partially restored after the shear forces have ceased. However, this hypothesis requires further confirmation.

Conclusions

The viscoelastic features of the electrode slurry combine all of the variables that ultimately affect mechanical and electrochemical electrode properties. Precise knowledge of the behavior of the slurry flow led to the finding of optimal conditions for its preparation, ensuring high capacitor efficiency. Research specifies the electrode slurry composition (ratio between its components). The composition received the viscosity window in which it is possible to uniformly coat the current collector. Derived equations linked the viscosity of the slurry, its composition, and the geometric dimensions of the electrode. The developed economic analysis predicts the price of substrates necessary to produce electrode slurry at the given electrode end parameters.

Acknowledgments

The authors acknowledge the funding received from the European Research Council within the Starting Grant project (StG-2017, GA 759603) under European Unions' Horizon 2020 research and innovation programme.

References

- [1] D. Larcher, J.M. Tarascon, Towards greener and more sustainable batteries for electrical energy storage, 2015, pp. 19-29.
- [2] P. Simon, Y. Gogotsi, Materials for electrochemical capacitors, Nature materials 7(11) (2008) 845-854.
- [3] J.R. Miller, P. Simon, Materials science: Electrochemical capacitors for energy management, 2008, pp. 651-652.
- [4] M. Winter, R.J. Brodd, What are batteries, fuel cells, and supercapacitors?, Chemical Reviews 104(10) (2004) 4245-4269.
- [5] M.R. Kronthaler, F. Schloegl, J. Kurfer, R. Wiedenmann, M.F. Zaeh, G. Reinhart, Laser Cutting in the Production of Lithium Ion Cells, Physics Procedia 39(C) (2012) 213-224.
- [6] D. Dr. John, Optimal Rheology, Better Electrodes: Understanding the Links Between Battery Slurry Properties and Electrode Performance, 2017.
- [7] K.L. Van Aken, C.R. Pérez, Y. Oh, M. Beidaghi, Y. Joo Jeong, M.F. Islam, Y. Gogotsi, High rate capacitive performance of single-walled carbon nanotube aerogels, Nano Energy 15 (2015) 662-669.
- [8] T. Cetinkaya, A. Akbulut, M.O. Guler, H. Akbulut, A different method for producing a flexible LiMn2O4/MWCNT composite electrode for lithium ion batteries, Journal of Applied Electrochemistry 44(2) (2014) 209-214.

- [9] A. Guerfi, M. Kaneko, M. Petitclerc, M. Mori, K. Zaghbi, LiFePO₄ water-soluble binder electrode for Li-ion batteries, *Journal of Power Sources* 163(2) (2007) 1047-1052.
- [10] Nmp distilling apparatus, (2010).
- [11] J. Li, C. Rulison, J. Kiggans, C. Daniel, D.L. Wood III, Superior Performance of Aqueous LiFePO₄ Cathodes Dispersions via Corona Treatment and Surface Energy Optimization, *Journal of the Electrochemical Society* 159(8) (2012).
- [12] C.-C. Li, Y.-W. Wang, Importance of binder compositions to the dispersion and electrochemical properties of water-based LiCoO₂ cathodes, *Journal of Power Sources* 227 (2013) 204-210.
- [13] B. Ludwig, Z. Zheng, W. Shou, Y. Wang, H. Pan, Solvent-Free Manufacturing of Electrodes for Lithium-ion Batteries, *Scientific Reports* 6(1) (2016) 23150-23150.
- [14] J. Li, X. Liang, F. Liou, J. Park, Macro-/Micro-Controlled 3D Lithium-ion Batteries via Additive Manufacturing and Electric Field Processing, *Sci Rep* 8(1) (2018) 1846-1846.
- [15] L. Bouffier, V. Ravaine, N. Sojic, A. Kuhn, Electric fields for generating unconventional motion of small objects, *Current Opinion in Colloid & Interface Science* 21 (2016) 57-64.
- [16] J.S. Park, D. Saintillan, Electric-field-induced ordering and pattern formation in colloidal suspensions, *Physical review. E, Statistical, nonlinear, and soft matter physics* 83(4 Pt 1) (2011) 041409.
- [17] M. Schmitt, P. Scharfer, W. Schabel, Slot die coating of lithium-ion battery electrodes: investigations on edge effect issues for stripe and pattern coatings, *Journal of Coatings Technology and Research* 11(1) (2014) 57-63.
- [18] B. Bitsch, J. Dittmann, M. Schmitt, P. Scharfer, W. Schabel, N. Willenbacher, A novel slurry concept for the fabrication of lithium-ion battery electrodes with beneficial properties, *Journal of Power Sources* 265(C) (2014) 81-90.
- [19] A.A. Tractor, *Coatings technology handbook*, Taylor & Francis 2005.
- [20] H. Zheng, L. Tan, G. Liu, X. Song, V.S. Battaglia, Calendering effects on the physical and electrochemical properties of Li[Ni_{1/3}Mn_{1/3}Co_{1/3}]O₂ cathode, *Journal of Power Sources* 208 (2012) 52-57.
- [21] Q. Abbas, D. Pajak, E. Frąckowiak, F. Béguin, Effect of binder on the performance of carbon/carbon symmetric capacitors in salt aqueous electrolyte, *Electrochimica Acta* 140 (2014) 132-138.
- [22] K.M. Kim, W.S. Jeon, I.J. Chung, S.H. Chang, Effect of mixing sequences on the electrode characteristics of lithium-ion rechargeable batteries, *Journal of Power Sources* 83(1) (1999) 108-113.
- [23] G.-W. Lee, J.H. Ryu, W. Han, K.H. Ahn, S.M. Oh, Effect of slurry preparation process on electrochemical performances of LiCoO₂ composite electrode, *Journal of Power Sources* 195(18) (2010) 6049-6054.
- [24] H. Bockholt, M. Indrikova, A. Netz, F. Golks, A. Kwade, The interaction of consecutive process steps in the manufacturing of lithium-ion battery electrodes with regard to structural and electrochemical properties, *Journal of Power Sources* 325 (2016) 140-151.
- [25] E. Koos, J. Johannsmeier, L. Schwebler, N. Willenbacher, Tuning suspension rheology using capillary forces, *Soft Matter* 8(24) (2012) 6620-6628.
- [26] E. Koos, N. Willenbacher, Particle configurations and gelation in capillary suspensions, *Soft Matter* 8(14) (2012) 3988-3994.

Supplementary information

$$\mu = a \cdot e^{-b\dot{\gamma}} + c \quad (\text{SI 1})$$

where: μ – dynamic viscosity [Pa s], a, b, c – constants values, respectively: a =14867.68, b=1.05, c=5115.87 [-], $\dot{\gamma}$ – shear rate [s⁻¹]).

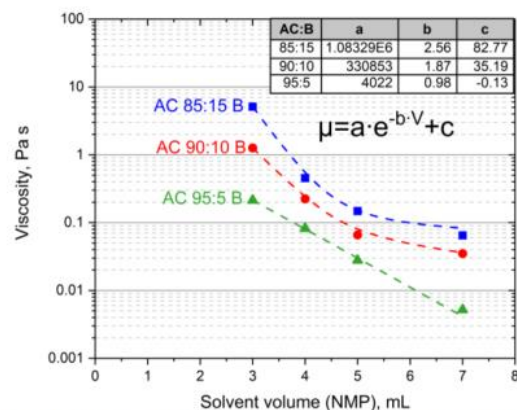


Fig. S1. Electrode slurry viscosity (for shear rate 384 s⁻¹, 100 RPM) vs. solvent volume (NMP) for different activated carbon : binder ratio.

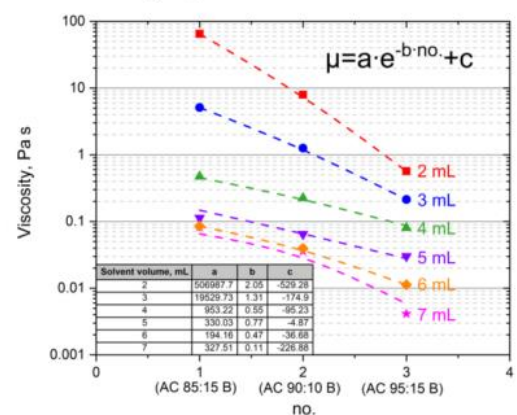


Fig. S2. Electrode slurry viscosity vs. activated carbon : binder ratio for a given solvent volume (NMP).

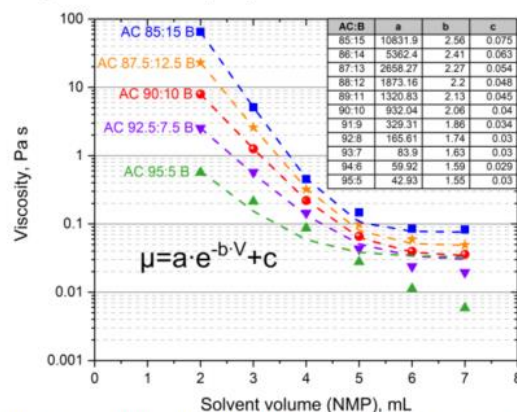


Fig. S3. Calculated electrode slurry viscosity vs. solvent volume in 85 – 95% range of activated carbon content.

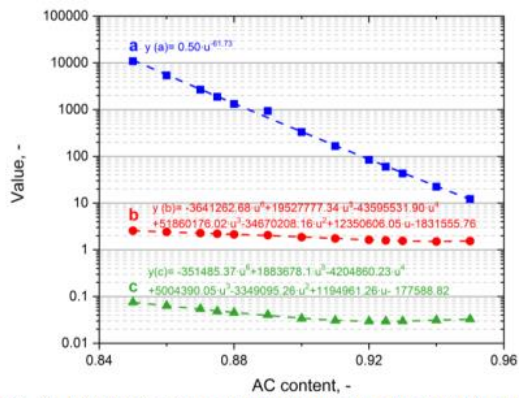


Fig. S4. Calculated a, b, c constants in equations for slurry viscosity vs. activated carbon content.

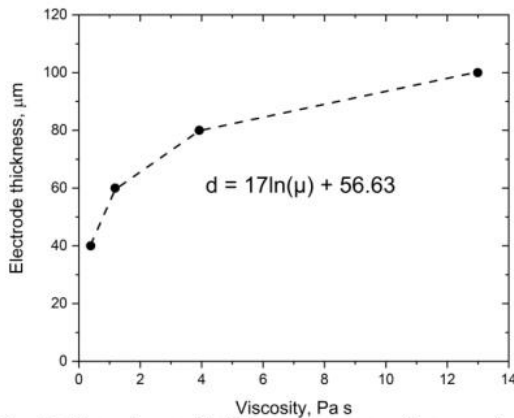


Fig. S5. Electrode material thickness on current collector vs. slurry viscosity.

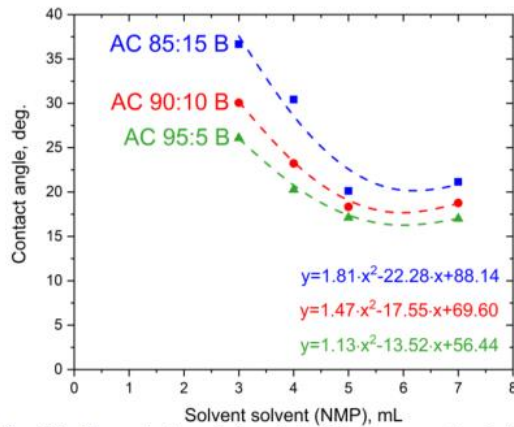


Fig. S6. The contact angle for steel foil as a current collector by electrode slurry vs. solvent volume (NMP).

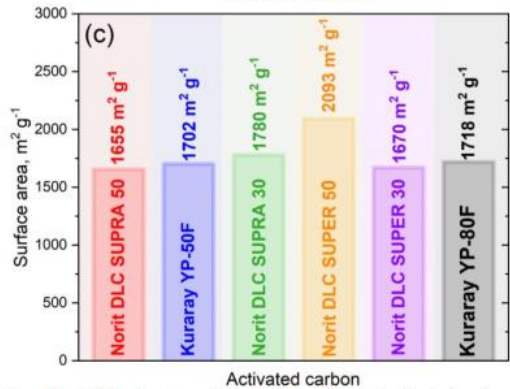
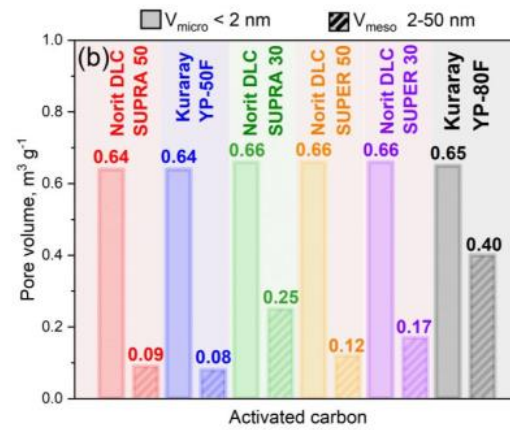
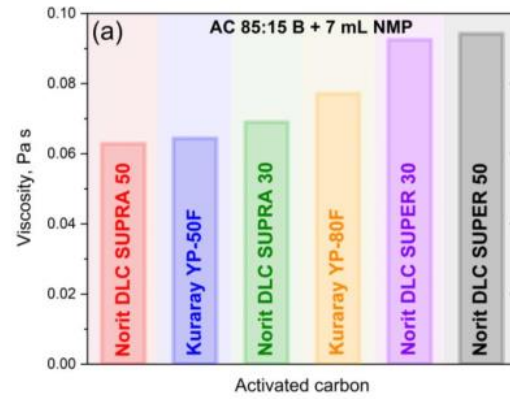


Fig. S7. (a) Slurries viscosity based on different activated carbons characterized by wide range of surface area (b) and pore distribution (c) (for AC 85 : 15 B ratio with 7 mL NMP per 1 g of solid materials).

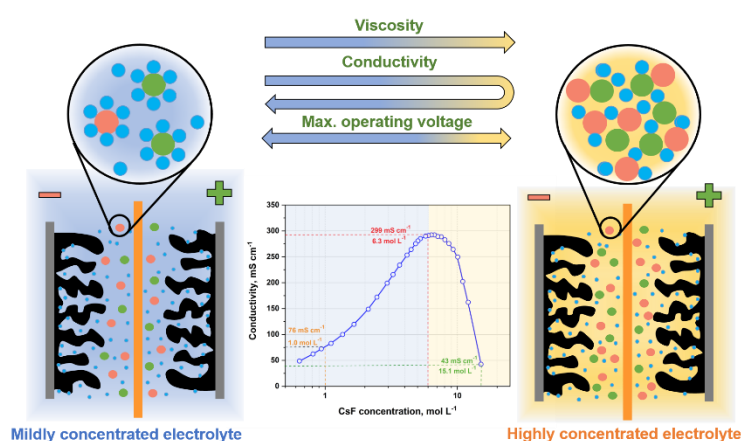
7. Article A2

Title: ***Interfacial aspects induced by saturated aqueous electrolytes in electrochemical capacitor applications***

Authors: Przemysław Galek, Elżbieta Frąckowiak, Krzysztof Fic

Journal: *Electrochimica Acta*, 2020, vol. 334, 135572-1 - 135572-12

DOI: 10.1016/j.electacta.2019.135572



Motivation

The main purpose of the applicability of ‘water-in-salt’ electrolytes in ECs is to improve the energy density by increasing voltage. It is assumed that reducing the water in such a medium, by increasing the concentration of dissolved salt, may lead to an increase in the solvation power of water molecules with ions. Both the volume and weight of the dissolved salt should be greater than those of the water. The literature shows that it is possible to obtain 2.4 V (comparable to the voltage of organic electrolytes), while in conventional water-based devices it is difficult to exceed 1.6 V. The limited voltage results from the low value of the water decomposition voltage reaching theoretically up to 1.23 V. The capacitance is improved in proposed concept systems. The energy density is up to three times that of conventional water-based devices and is on the same order of magnitude as redox-enhanced ECs. EC performance is obviously a trade-off between high concentration (to extend the potential window and energy density) and good ionic conductivity (to maintain an acceptable power density) [141].

Summary

The **Article A2** – ‘*Interfacial aspects induced by saturated aqueous electrolytes in electrochemical capacitor applications*’ describes the concept of highly concentrated “*water in salt*” type electrolyte in the EC. The CsF was chosen for the research – a highly soluble inorganic ionic salt. In the research course, the optimal electrode material with the proposed electrolyte was selected. Furthermore, the exact electrochemical characteristics were determined for the three characteristic electrolyte concentrations (1 mol L⁻¹ – reference, 6.3 mol L⁻¹ – with maximum conductivity and 15.1 mol L⁻¹ – saturated). Basic physicochemical properties (conductivity, viscosity, and pH) were determined for the entire concentration range. With the use of saturated CsF, a positive effect on self-discharge and charge-discharge efficiency is observed. The concentrated electrolyte of increased viscosity suppresses the leakage current and the amount of gas generated during EC work. The disadvantage is that the capacitance decreases faster during the cyclic charge/discharge compared to that solution. It has been observed that the electrolytic solution with the highest conductivity does not necessarily provide the highest system capacitance. Moreover, concentrated solutions are characterized by a poor wettability of the carbon electrodes and exhibit high surface tension. The correlation between the microtexture properties of carbon, the viscoelastic properties of the electrolyte, and the capacitance is still unclear. The increase in voltage and energy is small. This is most likely due to a slight improvement in the solvation strength for the selected salt (the heavier the ion, the weaker the solvation strength). The interactions between ions and water molecules are still too weak to shift the water decomposition potential toward higher values. The concept of ‘*water in salt*’ has enormous application potential and is currently at the forefront of research on water electrolytes. However, this is a ground new topic and requires a more in-depth explanation of the phenomenon related to the solvation shell formation and the ions transport in the porous structure of the electrode material.



ELSEVIER

Contents lists available at ScienceDirect

Electrochimica Acta

journal homepage: www.elsevier.com/locate/electacta



Interfacial aspects induced by saturated aqueous electrolytes in electrochemical capacitor applications



Przemyslaw Galek, Elzbieta Frackowiak, Krzysztof Fic*

Poznan University of Technology, Berdychowo 4, 60965, Poznan, PL, Poland

ARTICLE INFO

Article history:

Received 6 September 2019
Received in revised form
17 December 2019
Accepted 23 December 2019
Available online 28 December 2019

Keywords:

Saturated electrolyte
Aqueous electrolyte
Electrochemical capacitors
Carbon electrodes
Energy storage

ABSTRACT

This paper reports on the “water-in-salt” electrolyte concept, applying CsF as an ionic compound in a symmetric electrochemical capacitor. CsF has been selected as a highly soluble inorganic salt that allows the amount of free water in the electrolyte to be significantly reduced. Several activated carbons with various microtextural parameters have been investigated to identify the most suitable electrode material. A wide range of electrolyte concentrations have been investigated in terms of conductivity, pH and viscosity. The electrochemical characteristics have been determined for three electrolyte concentrations and indicate critical changes in the electrolyte physicochemical properties. It seems that ion-solvent interactions, residual water content, electrolyte viscosity and charging/discharging conditions remarkably affect the electrochemical performance of capacitors with elevated concentrations of electrolyte. In addition to the capacitance increase, a positive impact on the self-discharge and charge/discharge efficiency has been observed for higher CsF concentrations.

© 2019 The Authors. Published by Elsevier Ltd. This is an open access article under the CC BY-NC-ND license (<http://creativecommons.org/licenses/by-nc-nd/4.0/>).

1. Introduction

Energy-related issues are currently an emerging topic among researchers, policy makers and legal authorities, especially in countries with developed economies. The world demand for energy is currently very high and undoubtedly will continue to grow. For these reasons, new, alternative and highly efficient sources of electric power are sought [1]. However, harvesting of energy is directly connected with the necessity for further storage. For this purpose, a great variety of energy storage systems have been proposed. In addition to well-known batteries (such as Li-ion, Ni-MH, etc.) normally used for high-energy-density applications, electrochemical capacitors (ECs) should be noted. ECs are also known by different names, such as supercapacitors (SCs) or electric double-layer capacitors (EDLCs). The major differences between these devices result from the method of electric charge storage, the operating mode and the kinds of components (e.g., electrodes) [2]. ECs can be distinguished from other energy storage devices by their high specific power (above 10 kW kg^{-1}) [3–5] which results from a purely electrostatic charge storage mechanism. However, in comparison with conventional batteries, ECs are characterized by a

moderate specific energy, usually 3–30 times lower (up to $10 \text{ Wh} \cdot \text{kg}^{-1}$); in fact, in batteries, the entire electrode mass participates in redox reactions [6–8]. The involvement of the entire electrode volume in the charge storage process leads to a high energy density but limits the charge/discharge kinetics. Furthermore, the cycle life (a few thousands of charge/discharge cycles) is still a serious drawback, but it has to be noted that it strongly depends on the charging/discharging current rate applied and the operating voltage used. In contrast, ECs can be fully charged and discharged for up to a million cycles, as there are no chemical changes in the electrode structure (at least in principle). Thus, the excellent cyclability and short charging/discharging time of ECs allow their use in so-called hybrid (complementary) systems with batteries or as stand-alone devices [9].

Current research seeks to find a solution that gives an energy similar to that of batteries while maintaining the fast kinetics typical of ECs. The specific energy E_d ($\text{Wh} \cdot \text{kg}^{-1}$) depends on the specific capacitance of a device C_{spe} (F g^{-1}) and its operating voltage U (V) according to the formula $E_d = 0.5 \cdot C_{spe} \cdot U^2$.

Extensive research on the optimization of EC performance in the last few years has mainly focused on the development of new electrode materials and electrolytes with designed properties. Particular attention has been given to carbon-based materials [5,10]. Activated carbons (ACs) are distinguished within this group due to their well-developed specific surface area (reaching

* Corresponding author.

E-mail address: krzysztof.fic@put.poznan.pl (K. Fic).

<https://doi.org/10.1016/j.electacta.2019.135572>

0013-4686/© 2019 The Authors. Published by Elsevier Ltd. This is an open access article under the CC BY-NC-ND license (<http://creativecommons.org/licenses/by-nc-nd/4.0/>).

2000 m² g⁻¹) and adjustable porosity. The highly developed surface area allows for reversible accumulation of charge by means of electrostatic interactions [11]. The capacitances of the various materials used depend on their specific surface area and size and distribution of pores. Commercial ACs have a specific capacitance of approx. 100–150 F g⁻¹ (depending on the electrolyte in the system).

Another solution is to replace carbon materials with metal oxides (MnO₂, RuO₂ or FeWO₄), resulting in a device that can behave like a capacitor [12–14]. Due to the different mechanisms responsible for charge storage (redox and adsorption), devices made of transition metal oxides were formerly called “pseudocapacitors”; as a consequence of the dramatically increasing number of papers reporting very high and misleading capacitance values for redox-type materials, it is now recommended to use the term “pseudocapacitance” at the electrode level only [15–17]. The main problem arising from the incorporation of redox-based processes is the remarkably reduced power density, as the redox processes involved in these devices cannot cope with high charge/discharge rates [18]. Hybrid systems, which consist of a faradaic electrode and a capacitive electrode, have also been proposed. In fact, hybrid systems are a promising approach to mitigate the problem of low energy while maintaining reasonable power [19–22]. For instance, Omar et al. investigated a prototype of lithium-ion capacitor with an energy density of 14 Wh·kg⁻¹ and power up to 10 kW kg⁻¹ [23]. Besides, passive cascade systems based on hybrid systems (Ni-MH battery 192 V/ultracapacitors 48 V, 80 F) are used in hybrid electric vehicles (HEVs). These systems demonstrate the specific energy of 35 Wh·kg⁻¹ and specific power of 750 W kg⁻¹ [24]. However, it has to be noted that hybrid technologies are still under development and the long-time performance is still limited.

Other solutions propose hybrid capacitors that can exploit the full range of the operating potential for individual electrodes. As a result, the voltage, specific capacity and energy density are improved. The systems using various active materials such as: AC//MnO₂, AC//Li₂Mn₄O₉, AC//LiTi₂(PO₄)₂, AC//Li₄Ti₅O₁₂ with water electrolytes have been proposed [25].

In addition to electrode materials, several electrolytes have been proposed [26]. Among electrolytes, the most common are aqueous solutions, which are characterized by high conductivity (resulting in high EC power) and the lack of flammable or toxic solvents. ECs based on this type of electrolyte are attractive due to their relatively high capacitance, excellent power rate, low cost and negligible environmental impact. An important aspect is also the lack of a need for an inert atmosphere during production. The main disadvantage of aqueous electrolytes, especially those based on acidic or alkaline solutions, is their modest voltage window, which is limited by the thermodynamic stability of water and reaches a theoretical value of only 1.23 V [27]. In practice, the obtained voltage is slightly higher; this higher voltage is achieved by adjusting the physico-chemical properties of the electrolyte (pH or conductivity) and/or by modifying the surface chemistry of carbon electrodes [28]. In some cases, it is possible to reach a voltage of up to 2 V [29], but only for pH-neutral electrolytes.

Exceeding the theoretical value results in the appearance of OH⁻ anions, derived from the decomposition of water at the negative electrode [30]. The reduction of water in the range of negative potentials generates molecular hydrogen, according to equation (1), which is then adsorbed by porous carbon electrodes in the place of its formation (*in situ nascendi*).



Recent results have indicated that the main factor contributing to the deterioration of carbon/carbon cell performance in aqueous

electrolytes is (excessive) hydrogen (H₂) production at the negative electrode, oxidation of the positive carbon electrode and corrosion of the current collector [31–38]. Excessive gas production obviously leads to an increase in internal pressure and cell damage [39]. Although hydrogen electrosorption is claimed to be a pseudocapacitive phenomenon, the adsorption and desorption of hydrogen inside a porous carbon electrode is never fully reversible. The irreversibility of this process varies with the applied voltage and contributes to reduced energy efficiency in the system. To improve the charging efficiency, ions must be quickly transported to/from the carbon/electrolyte interface with the minimum amount of free water. This process contributes to the effective redistribution of ions and their separation via the so-called sieving effect [40].

Organic electrolytes (based on acetonitrile or carbonates) are characterized by a wide range of thermal stability from -40 °C to 60 °C and an electrochemical stability reaching 3.0 V [41]. Their disadvantages include high volatility, flammability and the need for an inert atmosphere during cell production. This is related to their high sensitivity to moisture and oxygen from the air. Furthermore, acetonitrile-based electrolytes are much more toxic than aqueous-based solutions as acetonitrile might be easily converted to the lethal cyanide form. Another serious disadvantage is their low conductivity [42,43].

The last kinds of electrolytes are ionic liquids (ILs), i.e., electrolytes composed entirely of ions. A high voltage (up to 4.0 V), lack of flammable solvent and negligible impact on the environment are their main advantages [44]. Furthermore, their “adjustable” properties make ILs suitable for a wide range of specific applications [45,46]. However, this type of electrolyte is still too expensive for EC mass production. Considering the most important factor (i.e., cost) when evaluating the practical application of a certain type of electrolyte in the mass production of ECs, aqueous electrolytes appear to be the most reasonable choice. However, the low operating voltage slightly increases the cost per unit energy stored.

As already mentioned, the energy stored in a capacitor strongly depends on the operating voltage of the system. In the case of aqueous electrolytes, the voltage can be increased by local pH changes at the electrode or by using so-called “water-in-salt” electrolyte. The idea of “water-in-salt” electrolyte is to limit the amount of “free” water to a minimum, which is determined by the salt solubility [47]. Taking into account the concentration gradient, this concept should also have a positive effect on local pH changes and the water decomposition reaction rate, as it depends on the amount of water available near the electrode surface [48]. The term “water-in-salt” electrolyte refers to the high concentration of salt dissolved in water (solvent), with mass (m_{salt}:m_{water}) and volume (V_{salt}:V_{water}) ratios greater than 1 [49]. The critical feature that determines the electrochemical properties of these electrolytes is the solvation process, which is completely different here than in classic water electrolytes. The number of water molecules surrounding the ions is significantly reduced and depends on the salt concentration. As a consequence, the structure of the interface area changes; for a suitably designed electrolyte, it is possible to strongly reduce or even completely suppress water decomposition.

So far, mainly pH-neutral electrolytes, such as aqueous solutions of Li₂SO₄, Na₂SO₄ and K₂SO₄, have been applied in ECs [31]. However, these salts are characterized by low solubility in water, which furthermore decreases with increasing cation size. Due to their low solubility, these salts cannot be considered in the proposed concept. It is also well known that EC performance also depends on the ionic mobility. Therefore, the introduction of highly conductive neutral electrolytes is essential for high power retention. An example of such salts for aqueous electrolytes may be alkali-metal nitrates. These salts are interesting candidates due to their high solubility, low cost and lack of harmful impact on the environment

[50]. Sodium nitrate (NaNO_3) offers very high solubility in water (up to 10 mol L^{-1} at 25°C). It has been demonstrated that by using 8 mol L^{-1} NaNO_3 solution, hydrogen adsorption and desorption are suppressed [51]. Recently, there has been substantial interest in super-concentrated electrolytes in lithium-ion batteries [7,52–59] and electrochemical capacitors [47,60,61]. It thus appears that LiTFSI is one of the most often investigated compounds. However, the problems of poor wettability and low conductivity at elevated concentrations affect the capacitance at high power rates. Thus, the energy is improved, but the power decreases [62]. However, most of the “free” water molecules are “blocked” or surrounded by TFSI⁻ anions. For instance, LiTFSI-based electrolytes at concentrations of 2.5 and 5.0 mol L^{-1} have been proposed as promising solutions [63]. The capacitor operating voltages achieved were 2.0 and 2.4 V, respectively, with good stability over ten thousand cycles reported. In this case, it was found that the “water-in-salt” electrolyte did not affect the capacity of the carbon electrode ($100\text{--}150 \text{ F g}^{-1}$) [5]. This result is a typical value observed for carbon electrodes operating in water-based electrolytes.

Another effective strategy accompanying the concept of “water-in-salt” electrolytes is the selection of suitable electrodes that can suppress the decomposition of water. It is known that the potential stability window is determined both by the electrochemical stability of the electrolyte and by the electrocatalytic activity of the electrodes. For instance, it has been reported that birnessite (MnO_2) has a high specific capacitance and excellent stability in various electrolytes [64]. This material has a high specific capacity and low electrocatalytic activity towards OER (oxygen evolution reaction) in a “water-in-salt” electrolyte applied in a hybrid system (Li/polymer electrolyte/ $\text{Li}_{1+x+y}\text{Ti}_{2-x}\text{Al}_x\text{Si}_y\text{P}_{3-y}\text{O}_{12}$ (LTAP) solid electrolyte/“water-in-salt” electrolyte/ MnO_2). A voltage of 4.4 V was achieved. However, the high cost of LTAP and the formation of lithium dendrites make this concept somewhat problematic for large-scale applications [65–67].

Of course, the final performance of capacitors operating with “water-in-salt” electrolytes must be a compromise among high concentration, voltage, energy density and ionic conductivity. In this paper, we do not use LiTFSI salt and instead report on the performance of systems based on highly concentrated aqueous CsF solutions. The study was performed using a wide range of salt concentrations to determine the effect of the water content in the electrolyte on the final electrochemical capacitor performance. The electrochemical results are correlated with the physicochemical and viscoelastic properties of the solution. The impact of the pore size and specific surface area of the carbon electrode is also considered.

2. Experimental

2.1. Electrode preparation and characterization

To select the most suitable carbon material and considering the viscous character of the electrolytic solutions applied, several materials were investigated. If not stated otherwise, the term activated carbon electrode describes a self-standing electrode made of activated carbon cloth (ACC), Kynol® 507-20, and annealed at 500°C for 3 h prior to the experiment to eliminate oxygen-based surface functional groups. For comparative purposes, Cabot® Black Pearl 2000 (BP 2000), Norit® SX2 activated (N SX2-A) and non-activated (N SX2-nA) and Kuraray YP-80F (YP-80 F) powders were also investigated after being subjected to the following formulation procedure: 5 wt% poly(tetrafluoroethylene) (PTFE) binder (60% suspension in water, Sigma-Aldrich®) was added to the pristine powders to obtain the composite electrodes. The binder was diluted in water, and then the solution was gradually added

dropwise to a beaker containing the carbon material and isopropanol (under magnetic stirring). This procedure allowed for the even distribution of the polymer in the entire suspension volume. Then, the prepared material was stirred for 24 h until the solvent and water were evaporated completely. In the next step, the electrode material was roll-pressed to a final thickness of $200 \mu\text{m}$ and dried in this form at 70°C for 12 h. Then, electrodes with a diameter of 10 mm were cut from the dried materials and the carbon cloth.

The microtextural characteristics of the materials were determined by using the Brunauer-Emmett-Teller (BET) isotherm method (77 K) with N_2 as an adsorbate (ASAP 2460, Micromeritics, USA). Before the adsorption/desorption steps, samples were flushed at 350°C for 12 h under continuous He flow and further degassed at 25°C for 5 h (vacuum).

2.2. Electrolyte characterization

Caesium fluoride (CsF) (Sigma-Aldrich, 99.9%) was directly diluted in deionized water at various concentrations to determine the conductivity, viscosity and electrochemical stability of the electrolyte with respect to concentration. Solid CsF is generally classified as a hazardous substance. It belongs to hygroscopic compounds and readily absorbs the moisture from the air. The toxicological properties of this material have not been fully investigated. As all of the compounds containing fluorine, it may cause respiratory and digestive tract irritations. For obvious reasons, direct contact with acid should be avoided, due to possible HF formation.

However, one should keep in mind that these data relate to pure, crystalline form of CsF; once dissolved in the electrolytic solution, its physicochemical properties and also its toxicity are changed and most likely diminished. However, its dangerous nature should not be neglected, in particular, in highly concentrated solutions.

The viscosity measurements were made using a Brookfield plate-cone rheometer (model DV2T).

The conductivity and pH were measured using a Mettler-Toledo conductivity- and pH-meter.

2.3. Electrochemical measurements

The operating voltage, capacitance and other capacitor metrics were determined by the galvanostatic charge/discharge technique at different current densities within the voltage range of 1.0–2.0 V.

Cyclic voltammetry (CV) and linear sweep voltammetry (LSV) were applied to determine the electrolyte stability in two- and three-electrode cells. LSV was performed in a 5 mL cell with a reference electrode of $\text{Hg|Hg}_2\text{SO}_4$ in 0.5 mol L^{-1} K_2SO_4 .

Symmetric 2- and 3-electrode systems (with a single electrode mass of approx. 9.1 mg) were assembled in Swagelok® type cells. Platinum wire was used as a pseudo-reference electrode in three-electrode measurements in order to prevent the transfer of ions between the reference electrode compartment and highly concentrated electrolyte, caused by the concentration gradient or osmotic pressure. It has been assumed that the application of saturated calomel electrode (SCE) or Ag/AgCl electrode in such an environment can result in ion exchange (electrolyte/electrode) and changes in pH of electrolyte in the reference electrode.

The electrochemical investigations were performed on a VMP-3 and SP-200 BioLogic® potentiostat/galvanostat.

It should be highlighted that all capacitance values and current densities are referenced to the mass of one electrode.

3. Results and discussion

The microtextural properties of the investigated carbons are

presented in Fig. 1.

The selected carbons demonstrated different microtextural properties claimed to be essential for efficient capacitive charge storage, such as specific surface area, pore size distribution and micro-to-mesopore volume ratio. The highest surface area value ($2113 \text{ m}^2 \text{ g}^{-1}$) was recorded for the KOH-activated carbon powder Norit® SX-2 (Norit®, Netherlands). The non-activated form of this material demonstrated the lowest specific surface area ($843 \text{ m}^2 \text{ g}^{-1}$). Similar values have been recorded for Kuraray YP-80F powder (Kuraray®, Japan) and Kynol® ACC 507-20 tissue. For all activated carbons, the micropore volume dominated over the mesopore volume; this property and the moderate specific surface area ($1500 \text{ m}^2 \text{ g}^{-1}$) usually ensure excellent charge propagation. This aspect, however, will be discussed later in the manuscript.

Regarding the electrolytic solution, caesium fluoride (CsF) was selected as this compound demonstrates high solubility in water, reaching up to 600 g CsF per 100 mL (ca. 100 g) of H_2O in 25°C

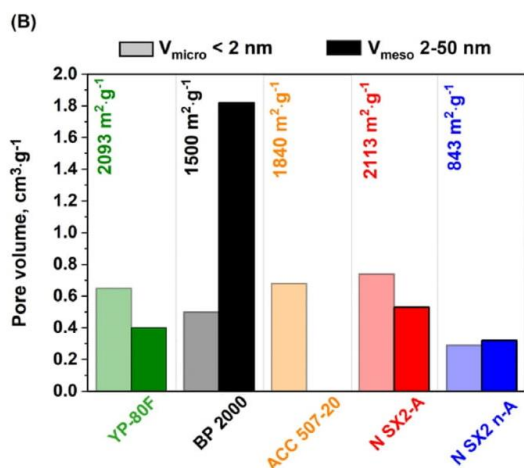
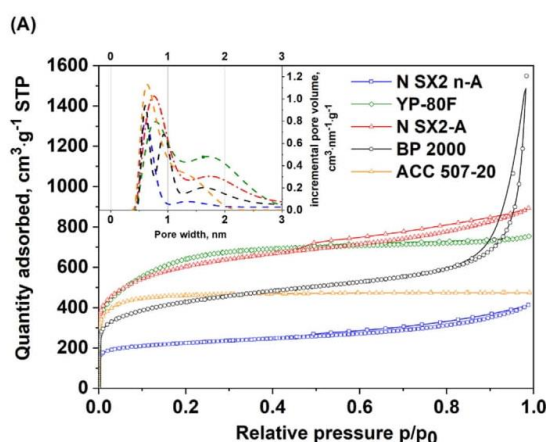


Fig. 1. N_2 adsorption isotherms (77 K) (A) and microtextural properties of the carbon materials used (B).

(molarity: $\sim 18 \text{ mol L}^{-1}$, molality: $\sim 39.5 \text{ mol} \cdot 1 \text{ kg H}_2\text{O}^{-1}$). This means that from a mass ratio perspective, the criterion for a “water-in-salt” electrolyte is fulfilled. In comparison to other frequently applied compounds, CsF displays one of the highest solubilities among popular salts, even comparable to that of LiTFSI. For comparative purposes, the molality values of saturated solutions are presented in Fig. 2.

For a given concentration, the molality (M) of CsF ($M = 37 \text{ mol kg}^{-1}$) exceeds the value for LiTFSI by almost two-fold. Thus, CsF appears to be an interesting ionic specimen for highly concentrated “water-in-salt” electrolytes. The pH, conductivity and viscosity of aqueous solutions were measured for selected CsF concentrations within the $0.2\text{--}15.1 \text{ mol L}^{-1}$ range. The results are presented in Fig. 3A–C.

The conductivity (Fig. 3A) of diluted (up to 1.0 mol L^{-1}) CsF solutions is moderate ($< 76 \text{ mS} \cdot \text{cm}^{-1}$); at elevated concentrations, the profile displays a maximum point at 6.3 mol L^{-1} . Then, the conductivity drops dramatically. It is assumed that this conductivity decay originates from the high viscosity and reduced ionic mobility at CsF concentrations higher than 6.3 mol L^{-1} (Fig. 3B).

The viscosity of the electrolyte is an important factor and presents the same trend as that observed in the conductivity vs. CsF concentration profile. Interestingly, the viscosity remains almost constant at $2 \text{ mPa} \cdot \text{s}$ up to a CsF concentration of 6.3 mol L^{-1} . At higher concentrations, the viscosity increases rapidly, reaching $35 \text{ mPa} \cdot \text{s}$ at a concentration of 15.1 mol L^{-1} . This viscosity increase might explain the dramatic drop in electrolyte conductivity.

The pH value (Fig. 3C) of diluted and low-concentrated solutions (up to 1.0 mol L^{-1}) is close to neutral (pH 6.9). However, the pH value increases with the CsF concentration and reaches 11.8 (alkaline) for a CsF concentration of 15.1 mol L^{-1} .

Considering specific points along the conductivity and viscosity profiles, three concentrations were selected for analysis of further electrochemical characteristics: 1.0 , 6.3 and 15.1 mol L^{-1} . However, based on the conditions that $m_{\text{salt}}:m_{\text{water}} > 1$ and $V_{\text{salt}}:V_{\text{water}} > 1$, the term “water-in-salt” is applicable for 15.1 mol L^{-1} CsF solution, as in this case $m_{\text{salt}}:m_{\text{water}}$ equals 5.49, and $V_{\text{salt}}:V_{\text{water}}$ equals 1.33. For 6.3 mol L^{-1} , these values are 1.19 and 0.29, respectively. In this case, the second condition is not met, so a CsF concentration of 6.3 mol L^{-1} does not qualify as a “water-in-salt” electrolyte.

The selection of a suitable carbon material for the CsF-based electrolyte was the next step of the investigation. The maximum

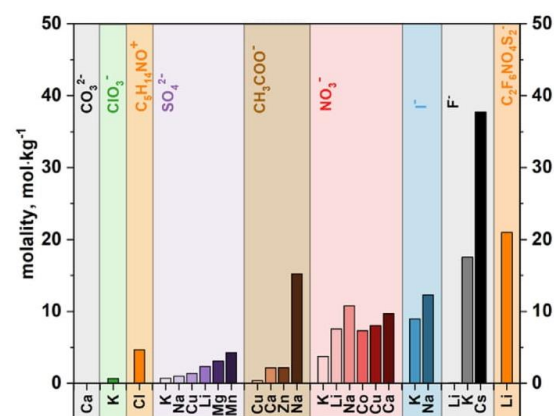


Fig. 2. The molality of saturated aqueous solutions of the compounds most often applied in electrolyte formulations (standard conditions).

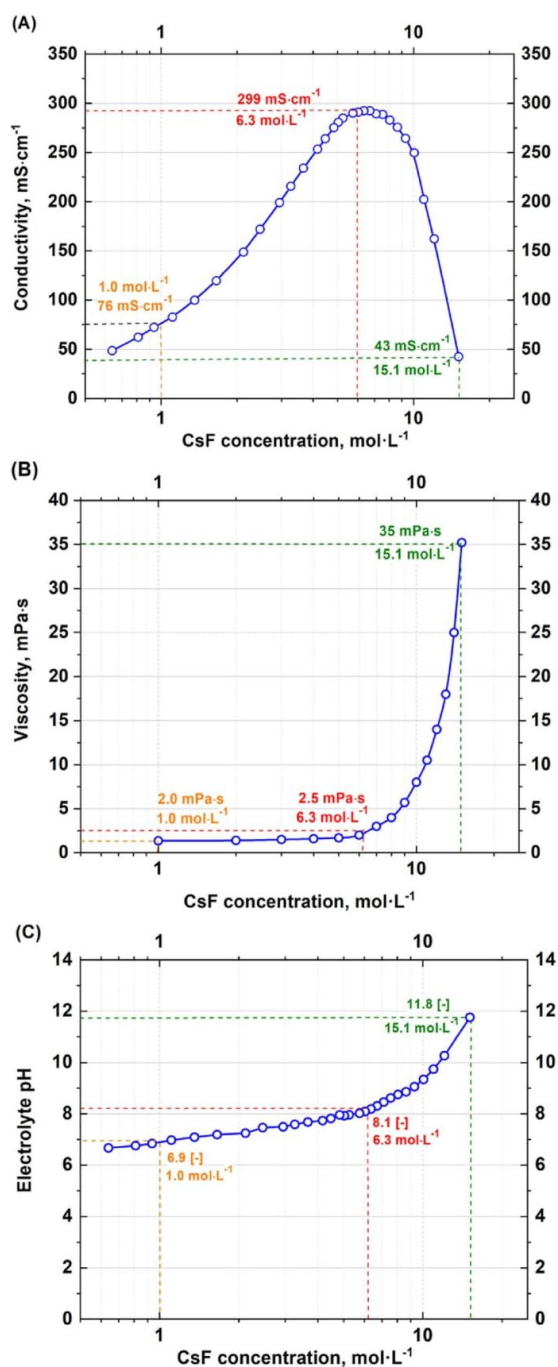


Fig. 3. The conductivity (A), viscosity (B) and pH (C) of CsF-based solutions at various concentrations at 25 °C.

CsF concentration (15.1 mol L⁻¹) was used, as the “worst-case scenario” was assumed for this highly concentrated electrolyte. It was expected that a high concentration would result in the lowest wettability, which was confirmed by observations during cell assembly.

To determine the capacitive properties of different carbons operating in highly concentrated electrolytes, cyclic voltammetry (5 mV s⁻¹) was carried out in two electrode cells. The vertex voltage of 1.8 V was established as a safe value in three-electrode experiments. During the CV experiment, the voltage was gradually increased from 1.0 V with a step of 0.2 V, and 3 full cycles were recorded for each voltage.

The highest capacitance values were obtained for the capacitor operating with ACC 507-20 (134 F g⁻¹) electrodes. A remarkably high capacitance value was also obtained for the capacitor based on the KOH-activated Norit® SX2 material (99 F g⁻¹). Surprisingly, the system with Kuraray® YP-80F demonstrated low specific capacitance; Cabot BP 2000 and non-activated Norit® SX did not demonstrate any significant capacitive response; it is assumed that poor wettability was the cause of this result. Although several attempts have been made to develop these systems, this has not resulted in higher capacitance.

To confirm the data from CV, galvanostatic charge/discharge profiles were recorded at a current density of 1 A g⁻¹ (Fig. 4B). The results confirmed that the most promising operating conditions are ensured by using ACC 507-20 electrodes (denoted further as ACC).

During the tests, it was also noticed that the cut-off voltage is an important factor for effective electrolyte absorption. For a capacitor based on ACC electrodes, the capacitance was negligible if the device was charged up to 1.4 V. Capacitor voltages above 1.6 V led to effective electrolyte absorption into the porous electrode structure. Cycling (in a potentiodynamic protocol) at lower voltages allowed the capacitance to be improved; however, this occurred after the 50th cycle.

In addition to the tests concerning the applied voltage, the “conditioning” time was investigated. In this experiment, a voltage of 1.4 V was applied to evaluate whether the electrolyte will penetrate the electrode bulk under such conditions. The measurement consisted of charging the system with a current density of 0.5 A g⁻¹ to a capacitor voltage of 1.4 V; then, the voltage was maintained for 1, 10, 100, 1 000, 10 000 and 100 000 s (at that time, the leakage current was also measured). After the leakage current measurement, the CV profile was recorded. The final results are summarized in Fig. 5.

It turns out that the time for which the voltage is maintained plays a significant role. Increasing the conditioning time improves the capacitance during the following discharge and diminishes the leakage current. As expected, the highest capacitance is obtained at 100 000 s, while at 1 s, the CV profile seriously deviates from a rectangular shape. The leakage current follows this tendency: at a voltage holding time of 1 s, the leakage current reaches 420 mA g⁻¹, while at 100 000 s, the value is only 3 mA g⁻¹.

After selecting a suitable electrode material, cyclic voltammetry at 5 mV s⁻¹ was performed for capacitors operating with the selected electrolytes (Fig. 6).

The highest capacitance value was recorded for the capacitor operating with the highest CsF concentration. However, one cannot neglect the remarkable current peak for the capacitor operating with the 15.1 mol L⁻¹ electrolyte, which was most likely due to the residual water decomposition. Nevertheless, a current peak at a voltage of 2.0 V is also observed for the capacitor operating with a CsF concentration of 6.3 mol L⁻¹.

To verify the CV results, the capacitance values were also determined by the constant current technique at various current regimes (0.2, 0.5, 1.0, 2.0, 5.0, 10.0 and 20 A g⁻¹) (Fig. 6B). In this

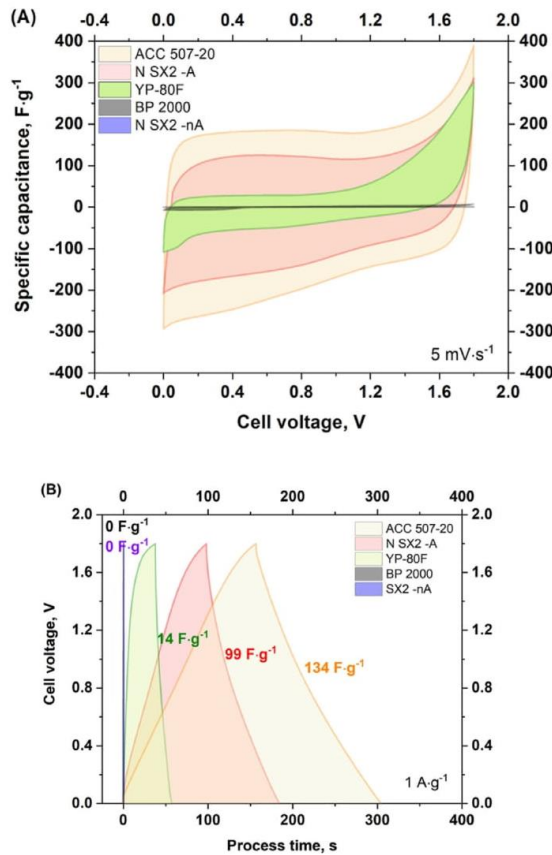


Fig. 4. (A) Cyclic voltammetry and (B) galvanostatic charge/discharge profiles of systems based on 15.1 mol L⁻¹ CsF with different ACs as a component of the electrode material.

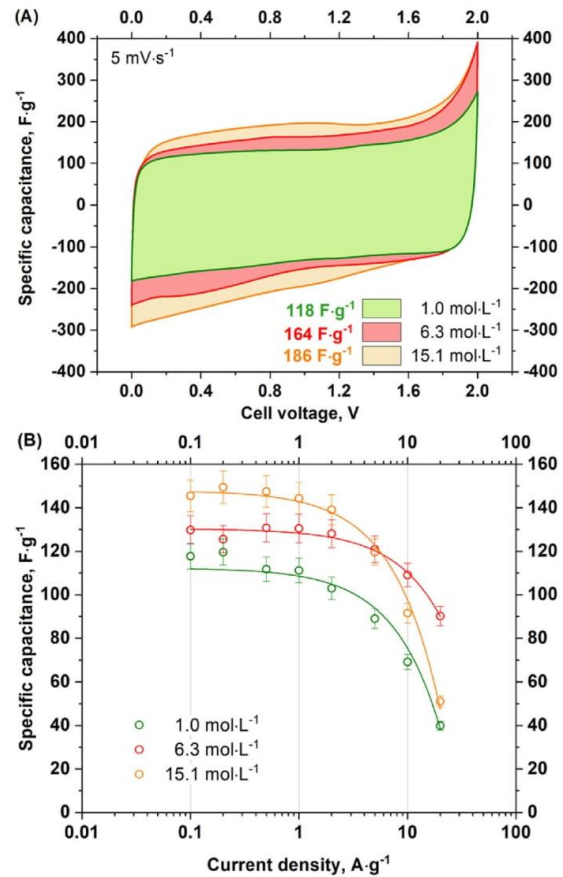


Fig. 6. (A) Cyclic voltammetry profiles and (B) capacitance vs. current loads for systems operating with selected CsF-based electrolytes.

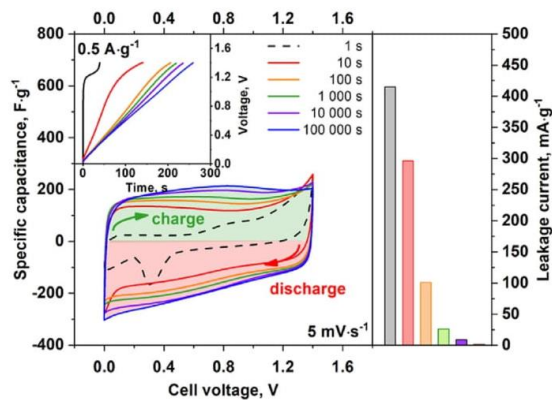


Fig. 5. Cell conditioning at a capacitor voltage of 1.4 V with various times of max. voltage holding. CV profiles after different conditioning times and the corresponding leakage currents measured during voltage holding. Inset: charging profile after different voltage holding periods.

case, as in the CV analysis, the capacitance of the capacitor is higher at higher electrolyte concentrations.

Interestingly, for the system operating with 15.1 mol L⁻¹ electrolyte, there is a limit value for the applicable current density, i.e., 5 A g⁻¹; for higher current loads, the capacitance recorded is lower than that for the system with 6.3 mol L⁻¹ electrolyte. This effect most likely results from the current regime, which does not allow the rapid redistribution of ions in the pore structure of the electrode material and comes from the high viscosity and reduced mobility.

More in-depth information about the system performance was obtained during investigations made in three-electrode configuration. During this experiment, the cell voltage was imposed and monitored by treating the system as a regular two-electrode cell. As the cell was equipped with a third, pseudo-reference electrode (Pt wire), it was possible to record the performance of each electrode separately.

Pt wire was used to avoid the dilution of highly concentrated electrolyte by the reference electrode body.

The terminal potentials of the capacitor electrodes were also monitored during the galvanostatic charge/discharge experiment, which was performed at various cut-off voltages (Fig. 7).

As shown in Fig. 7, the differences in terminal potential are negligible for all electrolyte concentrations. The only difference is a variation in rest potential $E(0)$ for the capacitor operating with 15.1 mol L⁻¹ CsF solution. The difference in $E(0)$ values at capacitor max. voltages of 1.0 V and 2.0 V is ca. 300 mV, which is a significant difference when compared to the $E(0)$ values for the 1.0 mol L⁻¹ and 6.3 mol L⁻¹ electrolytes.

To investigate the capacitive performance of the individual electrodes, cyclic voltammety profiles were recorded within designated potential ranges (Fig. 8).

At first glance, the only difference is the limited potential range of the negative electrode (i.e., 0.7 V, from -0.50 to -1.20 V vs. Pt) compared to the potential range of the positive electrode, (i.e., 1.05 V, from -0.50 to 0.55 V vs. Pt) for the system operating with 6.3 mol L⁻¹ CsF.

Given this result, it is clear that the voltage window does not increase linearly with the increase in electrolyte salt concentration, as was initially expected. In the case of the systems with electrolytes at concentrations of 1.0 and 15.1 mol L⁻¹, the positive electrode reaches the limiting potential (OEP) faster for the same capacitor voltage.

Consequently, the effect of an increased concentration of salt in the electrolyte on the voltage ($U = 1.8$ V), and thus on the energy of the system, was negligible, as presented in Fig. 9.

Definitely, the ECs are to find widespread use in sustainable transport based on hybrid electric vehicles (HEVs) [22,68,69]. The ECs as stand-alone devices do not fulfil energy requirements for power support in HEV. For instance, electrochemical energy storage systems stated by the U.S. Advanced Battery Consortium (USABC) and the U.S. Department of Energy (DOE) are expected to provide 620 W kg⁻¹ of power for 10 s for over 3×10^5 shallow cycles and 7.5 Wh·kg⁻¹ of total available energy. These requirements should concern the device operating in the range -30 °C - 60 °C. It has to be stated that Li-ion batteries fulfil given requirements, however, there are still serious concerns regarding their reliability and safety. The main disadvantage is their low tolerance to such aggressive conditions as overcharging and exposure to high temperatures. EDLC have a much higher safety level. Their efficiency is also much higher (>90%). The specific energy for commercially available ECs reaches only 0.1–5 Wh·kg⁻¹ for mild current regimes (i.e. at low power densities) and at temperatures near 25 °C and for some systems exploiting pseudocapacitive effects it might even reach

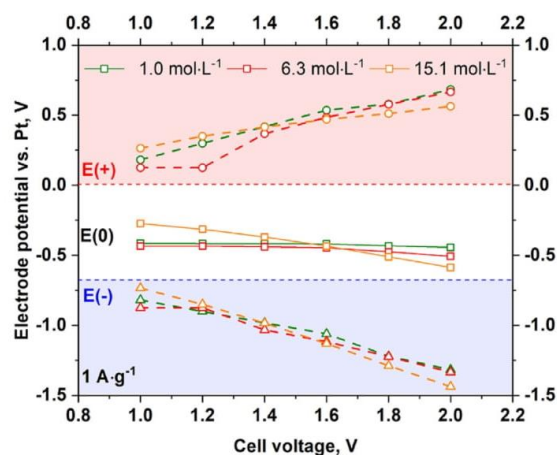


Fig. 7. Dependence of the electrode terminal potential on the applied voltage.

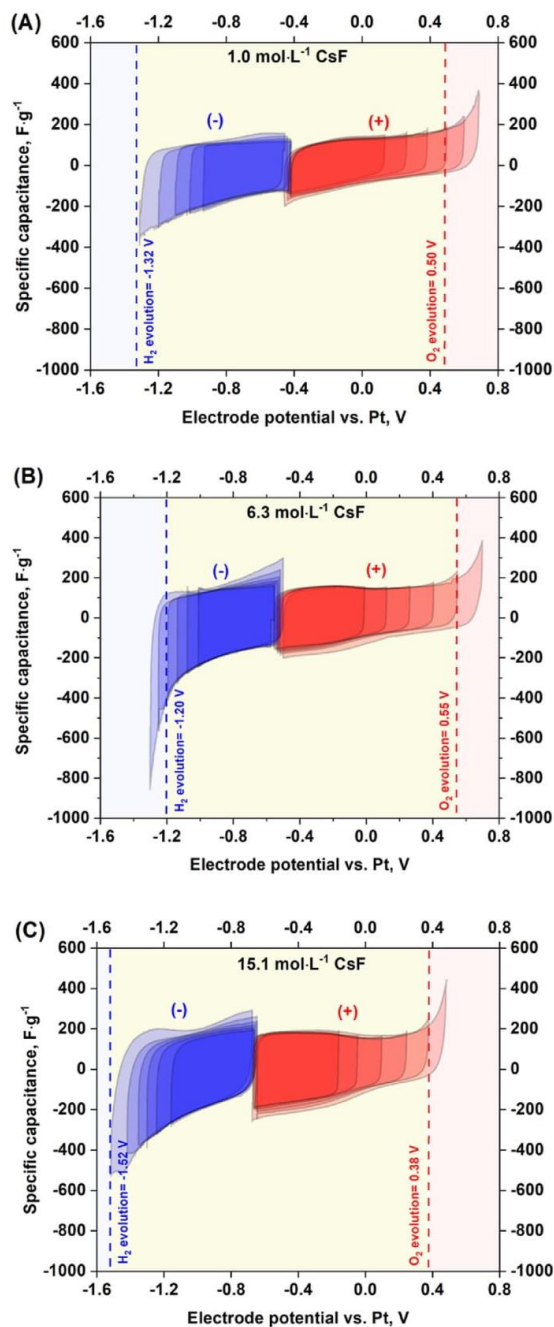


Fig. 8. Cyclic voltammety profiles for individual electrodes of capacitors operating with different concentrations of CsF.

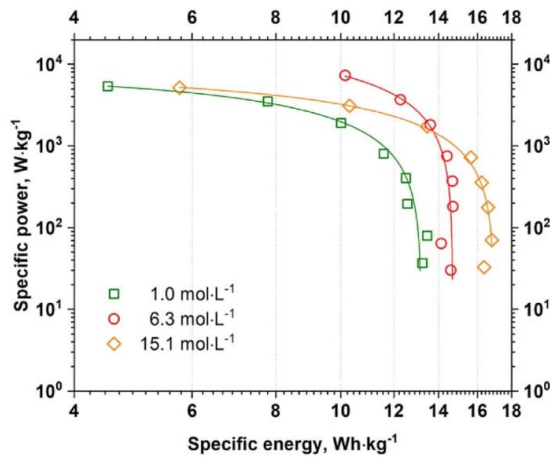


Fig. 9. Ragone plot for electrochemical capacitors operating with 1.0, 6.2 and 15 mol L⁻¹ CsF electrolyte.

18 Wh·kg⁻¹ at similar power. Of course, at moderate and high power rates, the specific energy decreases rapidly, essentially above 1 kW kg⁻¹. It must be also said again here that the commercial capacitors normally operate with organic (aprotic) electrolytes that allows the operating voltage of 2.85 V to be reached. Higher voltages might be achieved for hybrid systems, like Li-ion capacitors (LiC), demonstrating specific energy at the level of 50 Wh·kg⁻¹ at the specific power up to 1 kW kg⁻¹. Detailed metrics might be found at the websites of the respective manufacturers.

The solution proposed in the manuscript belongs to the category of ECs with water-based solvent, thus, of limited specific energy. Nonetheless, the systems presented maintain a specific energy above 10 Wh·kg⁻¹ at a specific power of up to 1 kW kg⁻¹. As might be expected, the difference in specific energy values is rather minimal for different electrolyte concentrations.

Although the energy and power of the investigated systems were not improved remarkably, other aspects of electrochemical capacitor operation were also investigated.

First, the self-discharge process was monitored. For this purpose, the capacitors were charged with a current density of 1 A g⁻¹, and then the system was maintained at a certain voltage for 2 h. After this time, the circuit was opened, and the system was subjected to self-discharge for 6 h (Fig. 10).

The slowest self-discharge is demonstrated by the system with 15.1 mol L⁻¹ CsF. For a capacitor cut-off voltage of 1.0 V, this profile is comparable with that of the cell containing electrolyte at a concentration of 6.3 mol L⁻¹. The fastest self-discharge at all cut-off voltages is observed for the cell operating with 1.0 mol L⁻¹ CsF. The cell with an electrolyte concentration of 6.3 mol L⁻¹ has a self-discharge profile very similar to that of the cell with 1.0 mol L⁻¹ electrolyte at voltages exceeding 1.2 V. Furthermore, the self-discharge rate is the fastest during the first 2 h of the measurement, and the initial rate increases with the applied voltage.

It is assumed that the limited self-discharge for highly concentrated electrolytes originates from the high viscosity of the electrolyte and reduced ion mobility, which prevent ion re-distribution and self-driven migration to the electrolyte bulk.

A positive effect of increased electrolyte concentrations was noted in the charging discharging efficiency (called here "charge imbalance"). The charge considered "lost" could have been used, for instance, for the decomposition of residual water. To determine the differences in the charge and discharge processes, cyclic voltammetry and constant current techniques were used (Fig. 11). The

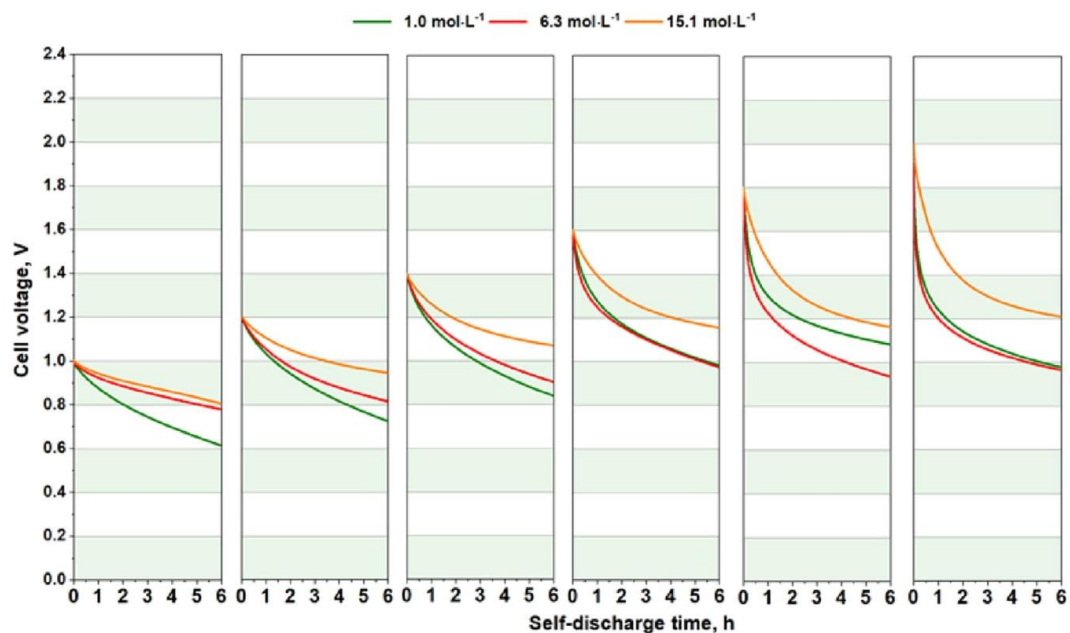


Fig. 10. Voltage drop during the self-discharge process of an electrochemical capacitor operating with 1.0, 6.3 and 15.1 mol L⁻¹ CsF electrolyte.

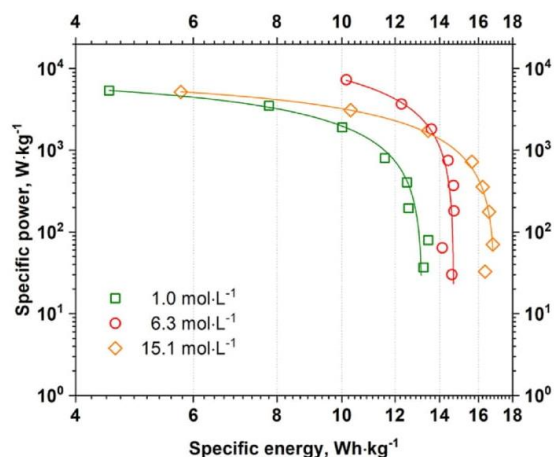


Fig. 9. Ragone plot for electrochemical capacitors operating with 1.0, 6.2 and 15 mol L⁻¹ CsF electrolyte.

18 Wh·kg⁻¹ at similar power. Of course, at moderate and high power rates, the specific energy decreases rapidly, essentially above 1 kW kg⁻¹. It must be also said again here that the commercial capacitors normally operate with organic (aprotic) electrolytes that allows the operating voltage of 2.85 V to be reached. Higher voltages might be achieved for hybrid systems, like Li-ion capacitors (LiC), demonstrating specific energy at the level of 50 Wh·kg⁻¹ at the specific power up to 1 kW kg⁻¹. Detailed metrics might be found at the websites of the respective manufacturers.

The solution proposed in the manuscript belongs to the category of ECs with water-based solvent, thus, of limited specific energy. Nonetheless, the systems presented maintain a specific energy above 10 Wh·kg⁻¹ at a specific power of up to 1 kW kg⁻¹. As might be expected, the difference in specific energy values is rather minimal for different electrolyte concentrations.

Although the energy and power of the investigated systems were not improved remarkably, other aspects of electrochemical capacitor operation were also investigated.

First, the self-discharge process was monitored. For this purpose, the capacitors were charged with a current density of 1 A g⁻¹, and then the system was maintained at a certain voltage for 2 h. After this time, the circuit was opened, and the system was subjected to self-discharge for 6 h (Fig. 10).

The slowest self-discharge is demonstrated by the system with 15.1 mol L⁻¹ CsF. For a capacitor cut-off voltage of 1.0 V, this profile is comparable with that of the cell containing electrolyte at a concentration of 6.3 mol L⁻¹. The fastest self-discharge at all cut-off voltages is observed for the cell operating with 1.0 mol L⁻¹ CsF. The cell with an electrolyte concentration of 6.3 mol L⁻¹ has a self-discharge profile very similar to that of the cell with 1.0 mol L⁻¹ electrolyte at voltages exceeding 1.2 V. Furthermore, the self-discharge rate is the fastest during the first 2 h of the measurement, and the initial rate increases with the applied voltage.

It is assumed that the limited self-discharge for highly concentrated electrolytes originates from the high viscosity of the electrolyte and reduced ion mobility, which prevent ion re-distribution and self-driven migration to the electrolyte bulk.

A positive effect of increased electrolyte concentrations was noted in the charging discharging efficiency (called here “charge imbalance”). The charge considered “lost” could have been used, for instance, for the decomposition of residual water. To determine the differences in the charge and discharge processes, cyclic voltammetry and constant current techniques were used (Fig. 11). The

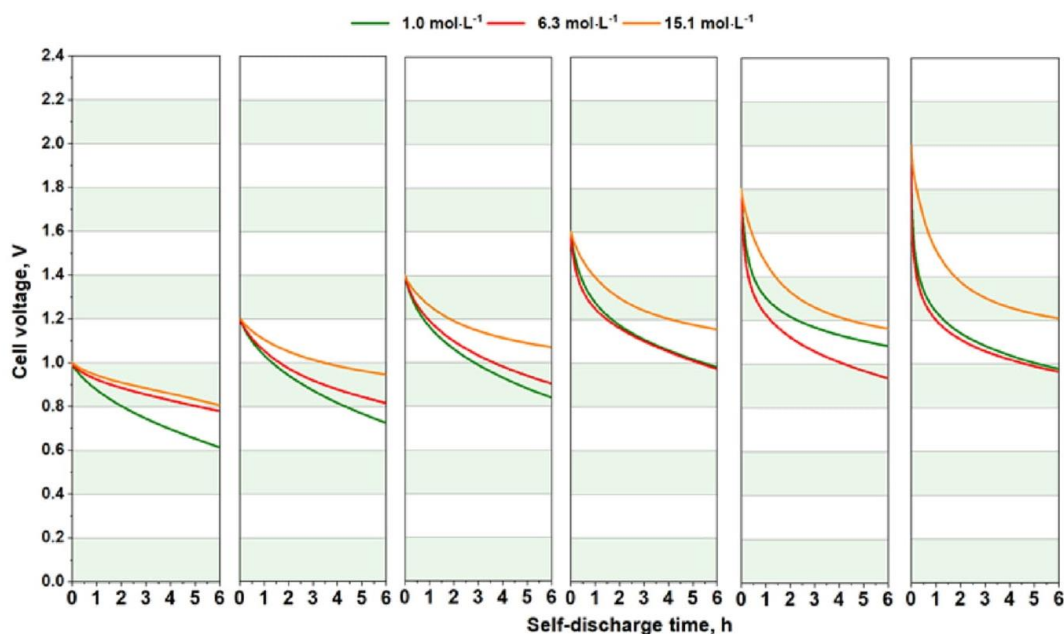


Fig. 10. Voltage drop during the self-discharge process of an electrochemical capacitor operating with 1.0, 6.3 and 15.1 mol L⁻¹ CsF electrolyte.

differences in the obtained absolute values result from the different current regimes used during the tests.

Both techniques reflect a decrease in the loss of charge with increasing electrolyte concentration. For the constant current technique, there is a remarkable difference between the performance of the cells with 1.0 mol L⁻¹ electrolyte and other concentrations. In the case of 1.0 V, the difference is 90%; at a capacitor voltage of 2.0 V, the difference is still 75%. The coulombic loss (considered as the difference in the charge provided/received) values for 6.3 and 15.1 mol L⁻¹ are similar in the whole voltage range.

Since it has been claimed that highly concentrated electrolytes should prevent either hydrogen or oxygen evolution, some quantitative insight might be necessary in order to determine the charge necessary to decompose water in each cell. The corresponding values are summarized in Table 1.

The calculations are based on the 1st Faraday law, and water electrolysis is assumed to be described by the following equation:



Thus, the theoretical charges needed to decompose all water in the cell are 2088 C, 1721 C and 895 C for CsF concentrations of 1.0, 6.3 and 15.1 mol L⁻¹, respectively. Taking into account the total charge accumulated in the cells (Fig. 12), these values are simply enormous.

The calculations performed for the “worst-case scenario” do not include the solvation effect, and all water molecules are assumed to be decomposed. Most likely, this is not the case, as several ion-solvent, ion-ion and solvent-solvent interactions must be taken into account. For a more accurate approximation, the hydration numbers for Cs and F were considered. Based on the literature data, it was assumed that the hydration clusters for Cs⁺ and F⁻ include 4 water molecules per single ion: Cs(OH₂)₄⁺ and F(OH₂)₄⁻ [70–75]. Of course, these numbers will most likely change with salt concentration (it has been claimed that the values might be as high as 8), but it is assumed that they will not be lower than 4.

In this case, the amount of free residual water changes dramatically. For 1 mol·L⁻¹ CsF, 1779 C is still necessary to decompose the water in the cell. However, for higher concentrations, it seems that all of the water is “trapped” by the ions. This will result either in a high overpotential for water decomposition or at least high concentration-related polarization above the water decomposition voltage. Taking into account the galvanostatic profiles, the latter option seems to be the case.

One could remark that the hydration effect (even if the numbers assumed are over-/underestimated) has a remarkable impact on the electrolyte conductivity and viscosity (Fig. 3A and B). Once the concentration of “free” water approaches 0, the conductivity decreases, and the viscosity increases. From the rough calculations presented above, it might be concluded that the water is fully consumed for hydration at a CsF concentration of 5.5 mol L⁻¹, if the assumed hydration numbers are correct. Taking into account the inflection points on the viscosity and conductivity vs. CsF concentration profiles, these values might not be far from the real ones.

To verify the character of the charge storage mechanisms at elevated voltages during quasi-steady state conditions, a potentiodynamic protocol resembling the step potential electrochemical spectroscopy (SPES) technique was applied [76]. The test was performed for the cell with concentrated CsF electrolyte (15.1 mol L⁻¹). The imposed voltage step was 0.01 V, and the voltage holding time was 30 s. The results are shown in Fig. 13. During the voltage holding step, the leakage current was measured, and the results were then integrated for charge calculation.

The charge profile in Fig. 13 suggests that the charging process occurs via several steps. Initially (until a cell voltage of 0.85 V), the charge consumed is small, which suggests that the capacitance is not high and that the electrode is not well soaked with the viscous electrolyte. Then, the profile changes (capacitance increases) and remains almost linear until the maximum capacitor voltage is reached. However, a small profile change was identified numerically (derivative) at a capacitor voltage of 1.5 V. This suggests that the mechanism is changed but capacitive storage still dominates. After the voltage is reached and the polarization changes, the profile is substantially different, suggesting that the charging process causes ions to penetrate the pores; during discharge, a number of ions are most likely trapped in the electrode pores and cannot be recovered. Additionally, some of the charge above 1.5 V is consumed for residual water decomposition. Of course, carbon oxidation and overall surface redox activity cannot be neglected.

Finally, the capacitor lifetime was evaluated using the galvanostatic cycling protocol at a current density of 1 A g⁻¹. The experimental cut-off value was 80% of the initial capacitance. The initial capacitance (100%) was calculated after 500 initial cycles, which

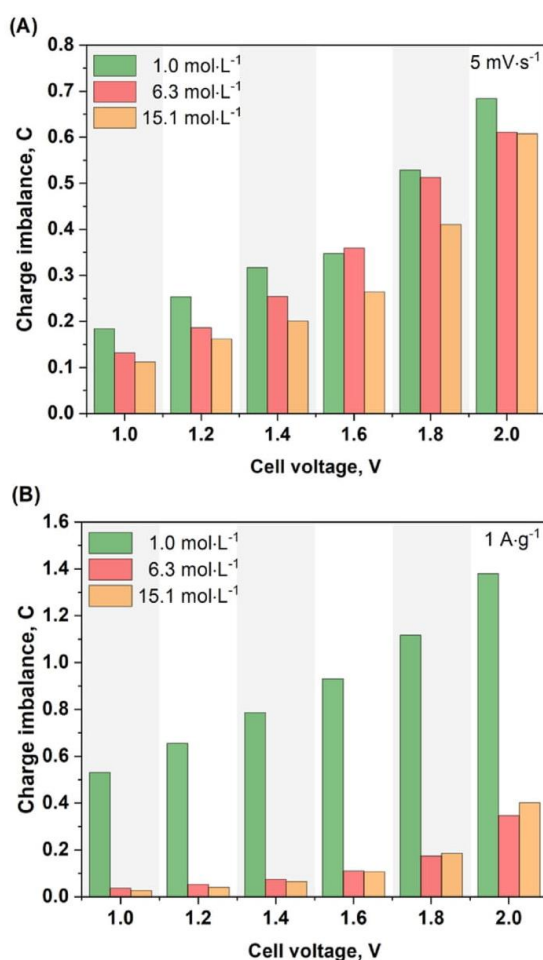


Fig. 11. Charge imbalance between charging and discharge determined using cyclic voltammetry (A) and constant current load (B) techniques.

Table 1
Data necessary to determine the charge required for water decomposition in the cells.

Molar concentration of the electrolyte, mol L ⁻¹	1.0	6.3	15.1
Density of solution, g L ⁻¹	1125	1759	2711
Mass of CsF in 1000 cm ³ of solution, g	151	957	2293
Mass of water in 1000 cm ³ of solution, g	973	802	417
Volume of electrolyte in the cell, μ L	200		
Mass of electrolyte in the cell, g	0.225	0.352	0.542
Mass of water in 200 μ L of electrolyte, g	0.195	0.161	0.084
No. of electrons exchanged	4		
Molar mass of water, g mol ⁻¹	18		
Molar mass of CsF, g mol ⁻¹	152		
Faraday constant, C mol ⁻¹	96 500		
Mass of working electrode, mg	9.1		
Mole fraction of water in solution	0.982	0.876	0.605
Mass fraction of water in solution	0.865	0.456	0.154
Charge needed to decompose water, C	2088	1721	895
Re-calculations for hydrated CsF structures, Cs(OH₂)₄⁺ and F(OH₂)₄⁻			
Water molar concentration, mol·L ⁻¹	54	44	23
Water molecules for CsF hydration, mol·L ⁻¹	8	50	120
Residual water in 200 μ L of electrolyte, g	0.166	0 (-0.023)	0 (-0.349)
Charge needed to decompose water, C	1779	0	0

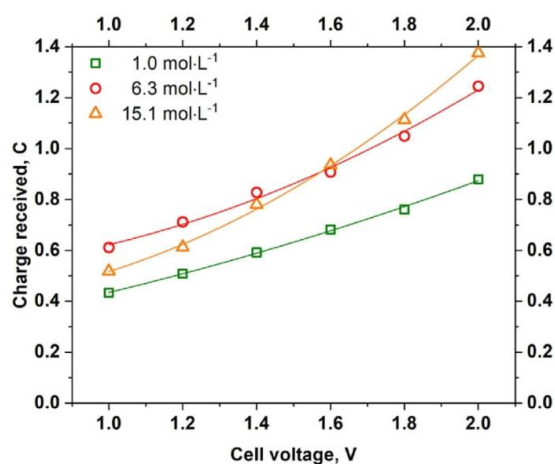


Fig. 12. Charge accumulated in cells operating with various concentrations of CsF salt.

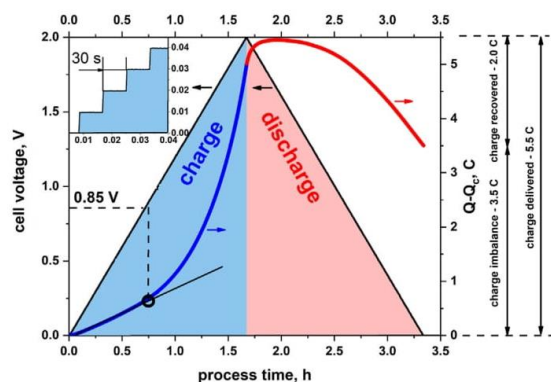


Fig. 13. Staircase potentiostatic chronoamperometry profile for the cell with 15.1 mol L⁻¹ CsF aqueous solution.

were performed for system conditioning.

Based on the obtained results, one can conclude that poor cycle life might be a disadvantage of capacitors operating with highly concentrated electrolytes (Fig. 14). The cell with 1.0 mol L⁻¹ electrolyte, despite the relatively high voltage rating (as for an aqueous electrolyte), allows more than 10 000 charge/discharge cycles to be performed.

Unfortunately, the situation is less optimistic for the cells with higher electrolyte concentrations. The cells with electrolyte concentrations of 6.3 and 15.1 mol L⁻¹ reach a critical capacitance value after 6000 cycles. Both systems demonstrate a similar profile of capacitance drop with cycle number.

4. Conclusions

It has been observed that highly concentrated electrolytes are characterized by poor wettability towards carbon electrodes and

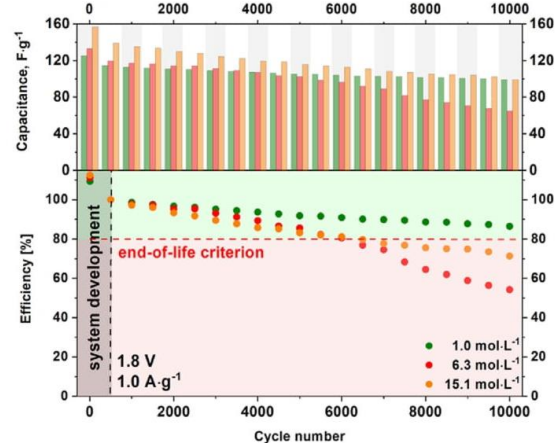


Fig. 14. Efficiency and capacitance of capacitors operating with 1.0, 6.3 and 15.1 mol L⁻¹ CsF electrolyte with respect to the charge/discharge cycle number.

demonstrate high surface tension. Thus, the selection of a suitable carbon material seems to be crucial in order to benefit from their properties. However, the correlation between the microtextural properties of the carbon, electrolyte viscoelastic properties and capacitor performance remains unclear.

The application of highly concentrated CsF solutions allows competitive capacitance values to be obtained. However, the maximum voltage and energy improvements are rather negligible. It has been observed that the electrolytic solution with the highest conductivity not necessarily ensures the highest system capacitance. The literature mainly reports on the electrolytes based on LiTFSI salt; it seems to be a reasonable choice as the limited amount of available water most likely impacts the solvation energy. However, for salts such as CsF, this might not be the case. This is most likely related to the interactions between solvated ions and water dipoles. In CsF based electrolyte, a decrease in water concentration does not translate directly into an increase in solvation energy.

The positive effect of increased salt concentration in this study is envisaged in reduced self-discharge. Limiting the water content improved also charge/discharge efficiency at higher capacitor voltages. The capacitance decay during cycling is much faster for concentrated solutions.

Finally, the concept of “water-in-salt” electrolytes in capacitor applications seems to be a promising approach. It turns out that in the case of CsF, the interactions between the ions and surrounding water are still too weak to shift the potential of water decomposition towards higher values. However, this feature does not exclude “water-in-salt” or highly concentrated electrolytes from applications due to the other positive aspects they provide – reduced self-discharge, higher capacitance values and improved charge discharge efficiency. Furthermore, it seems that an increased viscosity of the electrolyte suppresses the leakage current and the amount of gas generated during the operation of electrochemical capacitors.

Acknowledgements

This work was financially supported by European Research Council within the Starting Grant project (GA 759603) under the European Union’s Horizon 2020 research and innovation programme.

References

- [1] Y. Gogotsi, 2D carbides and carbonitrides: a new family of materials for electrochemical energy storage, *Abstr. Pap. Am. Chem. Soc.* (2014) 247.
- [2] B.E. Conway, Transition from “supercapacitor” to “battery” behavior in electrochemical energy storage, *J. Electrochem. Soc.* 138 (1991), 1539–1539.
- [3] P. Simon, Y. Gogotsi, Materials for electrochemical capacitors, *Nat. Mater.* 7 (2008) 845–854.
- [4] R. Kötz, M. Carlen, Principles and applications of electrochemical capacitors, *Electrochim. Acta* 45 (2000) 2483–2498.
- [5] E. Frackowiak, F. Béguin, Carbon materials for the electrochemical storage of energy in capacitors, *Carbon* 39 (2001) 937–950.
- [6] Z. Lin, E. Goikolea, A. Balducci, K. Naoi, P.L. Taberna, M. Salanne, G. Yushin, P. Simon, Materials for supercapacitors: when Li-ion battery power is not enough, *Mater. Today* 21 (2018) 419–436.
- [7] Y. Yamada, Developing new functionalities of superconcentrated electrolytes for lithium-ion batteries, *Electrochemistry* 85 (2017) 559–565.
- [8] M.A. Danzer, V. Liebau, F. Maglia, Aging of Lithium-Ion Batteries for Electric Vehicles, 2015.
- [9] B.E. Conway, W.G. Pell, Double-layer and pseudocapacitance types of electrochemical capacitors and their applications to the development of hybrid devices, *J. Solid State Electrochem.* 7 (2003) 637–644.
- [10] K. Fic, A. Platek, J. Piwek, E. Frackowiak, Sustainable materials for electrochemical capacitors, *Mater. Today* 21 (2018) 437–454.
- [11] H. Marsh, F. Rodríguez-Reinoso, *Activated Carbon (Origins)*, 2006, pp. 13–86.
- [12] G. Wang, Z. Lei, Z. Jiujuan, A review of electrode materials for electrochemical supercapacitors, *ChemsocChem* 5 (2012), 797–797.
- [13] J. Jiang, Y. Li, J. Liu, X. Huang, C. Yuan, X.W.D. Lou, Recent advances in metal oxide-based electrode architecture design for electrochemical energy storage,

Adv. Mater. 24 (2012) 5166–5180.

- [14] X. Lang, A. Hirata, T. Fujita, M. Chen, Nanoporous metal/oxide hybrid electrodes for electrochemical supercapacitors, *Nat. Nanotechnol.* 6 (2011) 232–236.
- [15] Q. Abbas, P. Ratajczak, P. Babuchowska, A. Le Comte, D. Belanger, T. Brousse, F. Béguin, Strategies to improve the performance of carbon/carbon capacitors in salt aqueous electrolytes, *J. Electrochem. Soc.* 162 (2015) A5148–A5157.
- [16] T. Brousse, D. Bélanger, J.W. Long, To Be or not to Be pseudocapacitive? *J. Electrochem. Soc.* 162 (2015) A5185–A5189.
- [17] A. Balducci, D. Belanger, T. Brousse, J.W. Long, W. Sugimoto, A guideline for reporting performance metrics with electrochemical capacitors: from electrode materials to full devices, *J. Electrochem. Soc.* 164 (2017) A1487–A1488.
- [18] P. Lannelongue, R. Bouchal, E. Mourad, C. Bodin, M. Olarte, S. le Vot, F. Favier, O. Fontaine, “Water-in-Salt” for supercapacitors: a compromise between voltage, power density, energy density and stability, *J. Electrochem. Soc.* 165 (2018) A657–A663.
- [19] P. Simon, Y. Gogotsi, B. Dunn, Where Do Batteries End and Supercapacitors Begin?, 2014, pp. 1210–1211.
- [20] K. Naoi, P. Simon, New materials and new configurations for advanced electrochemical capacitors, *Electrochem. Soc. Interface* 17 (2008) 34–37.
- [21] Z. Chang, Y. Yang, M. Li, X. Wang, Y. Wu, Green energy storage chemistries based on neutral aqueous electrolytes, *J. Mater. Chem. A* 2 (2014) 10739–10755.
- [22] V. Ruiz, A. Pfrang, A. Kriston, N. Omar, P. Van den Bossche, L. Boon-Brett, A review of international abuse testing standards and regulations for lithium ion batteries in electric and hybrid electric vehicles, *Renew. Sustain. Energy Rev.* 81 (2018) 1427–1452.
- [23] Y. Firouz, N. Omar, J.M. Timmermans, P. Van den Bossche, J. Van Mierlo, Lithium-ion capacitor – characterization and development of new electrical model, *Energy* 83 (2015) 597–613.
- [24] A. Khaligh, Z. Li, Battery, ultracapacitor, fuel cell, and hybrid energy storage systems for electric, hybrid electric, fuel cell, and plug-in hybrid electric vehicles: state of the art, *IEEE Trans. Veh. Technol.* 59 (2010) 2806–2814.
- [25] D.P. Dubal, O. Ayyad, V. Ruiz, P. Gomez-Romero, Hybrid energy storage: the merging of battery and supercapacitor chemistries, *Chem. Soc. Rev.* 44 (2015) 1777–1790.
- [26] E. Frackowiak, F. Béguin, Electrochemical storage of energy in carbon nanotubes and nanostructured carbons, *Carbon* 40 (2002) 1775–1787.
- [27] E. Frackowiak, Q. Abbas, Carbon/carbon supercapacitors, *J. Energy Chem.* 22 (2013) 226–240.
- [28] K. Fic, M. Meller, E. Frackowiak, Strategies for enhancing the performance of carbon/carbon supercapacitors in aqueous electrolytes, *Electrochim. Acta* 128 (2014) 210–217.
- [29] V. Khomenko, E. Raymundo-Piñero, E. Frackowiak, F. Béguin, High-voltage asymmetric supercapacitors operating in aqueous electrolyte, *Appl. Phys. Mater. Sci. Process* 82 (2006) 567–573.
- [30] S.-E. Chun, J.F. Whitacre, Investigating the role of electrolyte acidity on hydrogen uptake in mesoporous activated carbons, *J. Power Sources* 242 (2013) 137–140.
- [31] M. He, K. Fic, E. Frackowiak, P. Novák, E.J. Berg, Ageing phenomena in high-voltage aqueous supercapacitors investigated by in situ gas analysis, *Energy Environ. Sci.* 9 (2016) 623–633.
- [32] M. He, K. Fic, E. Frackowiak, P. Novák, E.J. Berg, Towards more durable electrochemical capacitors by elucidating the ageing mechanisms under different testing procedures, *Chemelectrochem* 6 (2019) 566–573.
- [33] A. Platek, J. Piwek, K. Fic, E. Frackowiak, Ageing mechanisms in electrochemical capacitors with aqueous redox-active electrolytes, *Electrochim. Acta* 311 (2019) 211–220.
- [34] Q. Abbas, F. Béguin, High voltage AC/AC electrochemical capacitor operating at low temperature in salt aqueous electrolyte, *J. Power Sources* 318 (2016) 235–241.
- [35] P. Ratajczak, K. Jurewicz, P. Skowron, Q. Abbas, F. Béguin, Effect of accelerated ageing on the performance of high voltage carbon/carbon electrochemical capacitors in salt aqueous electrolyte, *Electrochim. Acta* 130 (2014) 344–350.
- [36] P. Azais, L. Duclaux, P. Florian, D. Massiot, M.-A. Lillo-Rodenas, A. Linares-Solano, J.-P. Peres, C. Jehoulet, F. Béguin, Causes of supercapacitors ageing in organic electrolyte, *J. Power Sources* 171 (2007) 1046–1053.
- [37] S.A. Kazaryan, S.V. Litvinenko, G.G. Kharisov, Self-discharge of heterogeneous electrochemical supercapacitor of PbO[sub 2]|H[sub 2]SO[sub 4]|C related to manganese and titanium ions, *J. Electrochem. Soc.* 155 (2008), A464–A464.
- [38] S.A. Kazaryan, G.G. Kharisov, S.V. Litvinenko, V.I. Kogan, Self-discharge related to iron ions and its effect on the parameters of HES PbO[sub 2]|H[sub 2]SO[sub 4]|C systems, *J. Electrochem. Soc.* 154 (2007), A751–A751.
- [39] T. Brousse, M. Toupin, D. Bélanger, A hybrid activated carbon-manganese dioxide capacitor using a mild aqueous electrolyte, *J. Electrochem. Soc.* 151 (2004), A614–A614.
- [40] C. Merlet, B. Rotenberg, P.A. Madden, P.-L. Taberna, P. Simon, Y. Gogotsi, M. Salanne, On the molecular origin of supercapacitance in nanoporous carbon electrodes, *Nat. Mater.* 11 (2012) 306–310.
- [41] F. Béguin, V. Presser, A. Balducci, E. Frackowiak, Carbons and electrolytes for advanced supercapacitors, *Adv. Mater.* 26 (2014) 2219–2251.
- [42] P. Azais, L. Duclaux, P. Florian, D. Massiot, M.A. Lillo-Rodenas, A. Linares-Solano, J.P. Peres, C. Jehoulet, F. Béguin, Causes of supercapacitors ageing in organic electrolyte, *J. Power Sources* 171 (2007) 1046–1053.
- [43] P. Kurzweil, M. Chwistek, Electrochemical stability of organic electrolytes in

- supercapacitors: spectroscopy and gas analysis of decomposition products, *J. Power Sources* 176 (2008) 555–567.
- [44] M.P.S. Mousavi, B.E. Wilson, S. Kashefolgheta, E.L. Anderson, S. He, P. Bühlmann, A. Stein, Ionic liquids as electrolytes for electrochemical double-layer capacitors: structures that optimize specific energy, *ACS Appl. Mater. Interfaces* 8 (2016) 3396–3406.
- [45] A. Balducci, U. Bardi, S. Caporali, M. Mastragostino, F. Soavi, Ionic liquids for hybrid supercapacitors, *Electrochem. Commun.* 6 (2004) 566–570.
- [46] W.-Y. Tsai, R. Lin, S. Murali, L. Li Zhang, J.K. McDonough, R.S. Ruoff, P.-L. Taberna, Y. Gogotsi, P. Simon, Outstanding performance of activated graphene based supercapacitors in ionic liquid electrolyte from –50 to 80 °C, *Nano Energy* 2 (2013) 403–411.
- [47] L. Coustan, G. Shul, D. Belanger, Electrochemical behavior of platinum, gold and glassy carbon electrodes in water-in-salt electrolyte, *Electrochem. Commun.* 77 (2017) 89–92.
- [48] L. Demarconnay, E. Raymundo-Piñero, F. Béguin, A symmetric carbon/carbon supercapacitor operating at 1.6 V by using a neutral aqueous solution, *Electrochem. Commun.* 12 (2010) 1275–1278.
- [49] L. Suo, O. Borodin, T. Gao, M. Olguin, J. Ho, X. Fan, C. Luo, C. Wang, K. Xu, "Water-in-salt" electrolyte enables high-voltage aqueous lithium-ion chemistries, *Science* 350 (2015) 938–943.
- [50] K. Fic, M. He, E.J. Berg, P. Novák, E. Frackowiak, Comparative operando study of degradation mechanisms in carbon-based electrochemical capacitors with Li₂SO₄ and LiNO₃ electrolytes, *Carbon* 120 (2017) 281–293.
- [51] Q. Abbas, B. Gollas, V. Presser, Reduced Faradaic Contributions and Fast Charging of Nanoporous Carbon Electrodes in a Concentrated Sodium Nitrate Aqueous Electrolyte for Supercapacitors, *Energy Technology*, 2019, 1900430-1900430.
- [52] Y. Yamada, M. Yaegashi, T. Abe, A. Yamada, A superconcentrated ether electrolyte for fast-charging Li-ion batteries, *Chem. Commun.* 49 (2013) 11194–11196.
- [53] Y. Yamada, K. Usui, C.H. Chiang, K. Kikuchi, K. Furukawa, A. Yamada, General observation of lithium intercalation into graphite in ethylene-carbonate-free superconcentrated electrolytes, *ACS Appl. Mater. Interfaces* 6 (2014) 10892–10899.
- [54] S. Okuoka, Y. Ogasawara, Y. Suga, M. Hibino, T. Kudo, H. Ono, K. Yonehara, Y. Sumida, Y. Yamada, A. Yamada, M. Oshima, E. Tochigi, N. Shibata, Y. Ikuhara, N. Mizuno, A new sealed lithium-peroxide battery with a co-doped Li₂O cathode in a superconcentrated lithium bis(fluorosulfonyl)amide electrolyte, *Sci. Rep.* 4 (2014) 5684.
- [55] Y. Yamada, K. Furukawa, K. Sodeyama, K. Kikuchi, M. Yaegashi, Y. Tateyama, A. Yamada, Unusual stability of acetonitrile-based superconcentrated electrolytes for fast-charging lithium-ion batteries, *J. Am. Chem. Soc.* 136 (2014) 5039–5046.
- [56] Y. Yamada, C.H. Chiang, K. Sodeyama, J.H. Wang, Y. Tateyama, A. Yamada, Corrosion prevention mechanism of aluminum metal in superconcentrated electrolytes, *ChemElectrochem* 2 (2015) 1687–1694.
- [57] Y. Yamada, A. Yamada, Review-Superconcentrated electrolytes for lithium batteries, *J. Electrochem. Soc.* 162 (2015) A2406–A2423.
- [58] J. Wang, Y. Yamada, K. Sodeyama, C.H. Chiang, Y. Tateyama, A. Yamada, Superconcentrated electrolytes for a high-voltage lithium-ion battery, *Nat. Commun.* 7 (2016) 12032.
- [59] Y. Yamada, A. Yamada, Superconcentrated electrolytes to create new interfacial chemistry in non-aqueous and aqueous rechargeable batteries, *Chem. Lett.* 46 (2017) 1056–1064.
- [60] L. Coustan, K. Zaghbi, D. Belanger, New insight in the electrochemical behaviour of stainless steel electrode in water-in-salt electrolyte, *J. Power Sources* 399 (2018) 299–303.
- [61] A. Gambou-Bosca, D. Belanger, Electrochemical characterization of MnO₂-based composite in the presence of salt-in-water and water-in-salt electrolytes as electrode for electrochemical capacitors, *J. Power Sources* 326 (2016) 595–603.
- [62] A. Gambou-Bosca, D. Bélanger, Electrochemical characterization of MnO₂-based composite in the presence of salt-in-water and water-in-salt electrolytes as electrode for electrochemical capacitors, *J. Power Sources* 326 (2016) 595–603.
- [63] G. Hasegawa, K. Kanamori, T. Kiyomura, H. Kurata, T. Abe, K. Nakanishi, Hierarchically porous carbon monoliths comprising ordered mesoporous nanorod assemblies for high-voltage aqueous supercapacitors, *Chem. Mater.* 28 (2016) 3944–3950.
- [64] M. Huang, F. Li, F. Dong, Y.X. Zhang, L.L. Zhang, MnO₂-based nanostructures for high-performance supercapacitors, *J. Mater. Chem.* 3 (2015) 21380–21423.
- [65] M. Zhang, S. Makino, D. Mochizuki, W. Sugimoto, High-performance hybrid supercapacitors enabled by protected lithium negative electrode and "water-in-salt" electrolyte, *J. Power Sources* 396 (2018) 498–505.
- [66] M. Zhang, K. Takahashi, N. Imanishi, Y. Takeda, O. Yamamoto, B. Chi, J. Pu, J. Li, Preparation and electrochemical properties of Li_{1-x}Al_xGe_{2-x}(PO₄)₃ synthesized by a sol-gel method, *J. Electrochem. Soc.* 159 (2012) A1114–A1119.
- [67] M. Zhang, Z. Huang, Z. Shen, Y. Gong, B. Chi, J. Pu, J. Li, High-performance aqueous rechargeable Li-Ni battery based on Ni(OH)₂/NiOOH redox couple with high voltage, *Adv. Energy Mater.* 7 (2017), 1700155-1700155.
- [68] L. Jin, X. Guo, R. Gong, J. Zheng, Z. Xiang, C. Zhang, J.P. Zheng, Target-oriented Electrode Constructions toward Ultra-fast and Ultra-stable All-Graphene Lithium Ion Capacitors, *Energy Storage Materials*, 2019.
- [69] A. Barré, B. Deguilhem, S. Grolleau, M. Gérard, F. Suard, D. Riu, A Review on Lithium-Ion Battery Ageing Mechanisms and Estimations for Automotive Applications, 2013, pp. 680–689.
- [70] S. Odde, C. Pak, H.M. Lee, K.S. Kim, B.J. Min, Aqua dissociation nature of cesium hydroxide, *J. Chem. Phys.* 121 (2004) 204–208.
- [71] R. Goldberg, L. Chai, S. Perkin, N. Kampf, J. Klein, Breakdown of hydration repulsion between charged surfaces in aqueous Cs⁺ solutions, *Phys. Chem. Chem. Phys.* 10 (2008) 4939–4945.
- [72] H.J. Feng, J. Zhou, X.H. Lu, K.A. Fichtorn, Communication: molecular dynamics simulations of the interfacial structure of alkali metal fluoride solutions, *J. Chem. Phys.* 133 (2010).
- [73] M.D. Levi, S. Sigalov, G. Salitra, R. Elazari, D. Aurbach, Assessing the solvation numbers of electrolytic ions confined in carbon nanopores under dynamic charging conditions, *J. Phys. Chem. Lett.* 2 (2011) 120–124.
- [74] J.I. Partanen, A.K. Covington, Re-evaluation of the thermodynamic activity quantities in aqueous solutions of uni-univalent alkali metal salts of aliphatic carboxylic acids and thallium acetate at 25 degrees C, *J. Chem. Eng. Data* 56 (2011) 4524–4543.
- [75] J. Mahler, I. Persson, A study of the hydration of the alkali metal ions in aqueous solution, *Inorg. Chem.* 51 (2012) 425–438.
- [76] M.F. Dupont, S.W. Donne, Separating faradaic and non-faradaic charge storage contributions in activated carbon electrochemical capacitors using electrochemical methods I. Step potential electrochemical spectroscopy, *J. Electrochem. Soc.* 162 (2015) A1246–A1254.

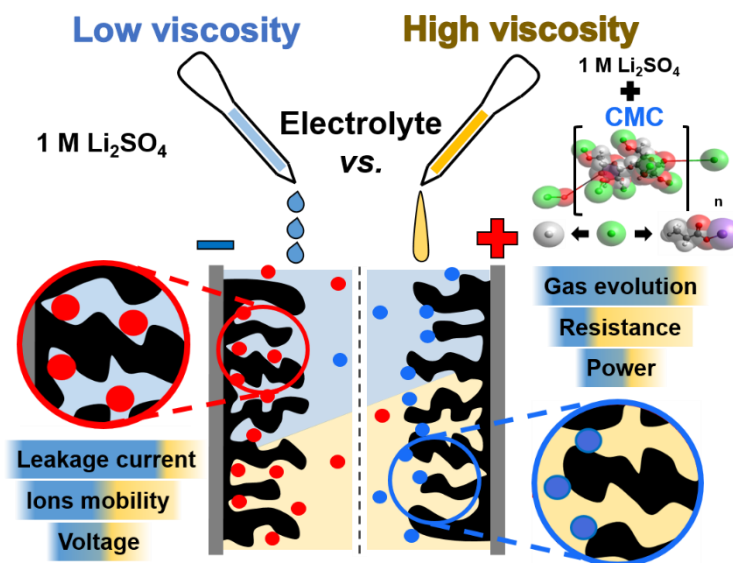
8. Article A3

Title: ***Peculiar role of the electrolyte viscosity in the electrochemical capacitor performance***

Authors: Przemysław Galek, Adam Ślesiński, Krzysztof Fic, Jakub Menzel

Journal: Journal of Materials Chemistry A, 2021, vol. 9, iss. 13, 8644 – 8654

DOI: 10.1039/D0TA11230E



Motivation

The literature reports that the increase in electrolyte viscosity usually reduces the overall EC efficiency (energy, capacitance, increase resistance) [201]. It is mainly assigned to hindered mobility of ions in a conductive medium, which is associated with low conductivity [162, 166, 202-204]. The formation of an EDL at the electrode/electrolyte interface, is not fast enough during repeated charging/discharging processes. The literature is lacking reliable data that confirm the reflection of the behaviour in aqueous electrolytes. Each time the authors emphasize the negative effect of increased viscosity, whereas the positive aspects of such electrolytes are usually omitted. Our work aims to verify this popular approach in terms of the use of highly viscous electrolytes in ECs.

Summary

In **Article A3** – ‘*Peculiar role of the electrolyte viscosity in the electrochemical capacitor performance*’ the influence of increased aqueous electrolyte viscosity on EC performance was determined. Sodium carboxymethylcellulose (CMC) was added 1 mol L⁻¹ lithium sulfate to increase its viscosity. One of the main conclusions to be highlighted is that the electrolyte viscosity itself does not significantly limit the mobility of ions (conductivity). However, the exchange of ions in viscous electrolytes in porous materials can be difficult. This may be related to insufficient pore penetration and deterioration in EC performance. Therefore, a system conditioning is recommended. This solution should increase the electrode wettability and device efficiency. Electrowetting depends on the polarization magnitude. Viscosity does not necessarily reduce energy and power. The effect of viscosity has been found to be complex. It depends greatly on the texture/structure of the carbon electrode properties and the availability of pores. Moreover, the viscosity does not affect the long-term stability, regardless of the porosity of the electrode material. Viscosity has a marginal effect on the potential window and does not affect the efficiency of the hydrogen sorption/desorption process. The self-discharge limitation in microporous materials is slight. In mesoporous materials, a significant reduction in self-discharge has been observed by limiting the delocalization of the charge in the EDL. The application of viscous electrolytes has been found to be beneficial in reducing leakage current and internal gas evolution. The results obtained may be of interest not only for aqueous electrolytes but also for ILs. Finally, these results give rise to being more sceptical of the general statement that viscosity itself is not a limiting factor for EC performance.



Cite this: *J. Mater. Chem. A*, 2021, 9, 8644

Received 17th November 2020
Accepted 31st January 2021

DOI: 10.1039/d0ta11230e

rsc.li/materials-a

Peculiar role of the electrolyte viscosity in the electrochemical capacitor performance

Przemysław Galek, Adam Slesinski, Krzysztof Fic* and Jakub Menzel*

This paper reports on the electrochemical performance of symmetric carbon/carbon electrochemical capacitors operating in an aqueous electrolyte (1 mol L⁻¹ Li₂SO₄ solution) whose viscosity is modified by various amounts of carboxymethyl cellulose additive. The literature states that increased electrolyte viscosity usually decreases the overall capacitor performance. However, it has been found that the influence of this parameter is complex and depends significantly on the carbon electrode texture/structure properties. Fortunately, the application of viscous electrolytes is found to be beneficial in terms of reduced leakage current and internal gas evolution (by approximately 50%). Furthermore, the examination of differently structured carbons showed that in materials with well-designed micro-/mesoporous interconnectivity, it is possible to retain high power and energy performance even for devices with 104-fold increased viscosity.

1. Introduction

Energy generation and consumption are currently among the most important economic and social considerations, especially in highly developed countries. The demand for energy is increasing continuously, which requires the search for new, alternative and highly efficient energy sources.¹ The generated energy is also inherently associated with the necessity of storage. Energy storage devices can have the form of bulky, large, stationary units but can also be a component of small, portable devices for everyday use, such as laptops, mobile phones, and cameras.

The solutions currently proposed for high-energy-storage devices such as electrochemical cells, fuel cells, and redox flow batteries suffer from limited power output, resulting mostly from sluggish redox reaction kinetics. To overcome this limitation, one can consider electrochemical capacitors (EC), which are characterized by high power performance and long lifetimes, originating from their double-layer charge storage mechanisms.^{2–5} One way to benefit from both types of these devices is to merge them in the form of a hybrid system to incorporate both energy and power properties. However, such an approach significantly increases the cost of the final energy storage station. The other approach is to develop capacitors with energy approaching that of batteries while maintaining fast charge/discharge kinetics. To reach this goal, much work has been devoted to the development of the two primary EC components, namely, the electrode materials and electrolytes.

In recent years, research on electrode materials has been focused on the development of new materials with high surface porosity. In particular, most of the research has been devoted to the study of porous and layered materials such as activated carbons,^{2,4,6,7} graphene,⁸ carbon nanotubes,^{9,10} carbon nanofibers,^{11,12} and recently, MXenes as electrode materials.^{13,14} Nevertheless, activated carbons are still most widely used in commercial devices due to their well-developed specific surfaces, reaching 2500 m² g⁻¹; high accessibility; and low production costs.¹⁵

Simultaneously, a considerable amount of research has focused on electrolyte development, as their properties ultimately determine the maximum operating voltage of ECs.^{16–19} Currently, in commercial devices, organic-based electrolytes are the most widely used. They are characterized by wide electrochemical stability up to 3 V and the ability to operate within a broad temperature range of -40 °C to 60 °C. However, their main disadvantages are high volatility and flammability, high cost, sensitivity to moisture, and low conductivity.^{12,13}

In recent years, the increase in environmental protection awareness has forced researchers to seek new electrolyte compositions. To meet the environmental friendliness demands, two types of electrolytes are of interest: water-based formulations and ionic liquids. Due to good electrochemical properties, excellent power ratings, and low cost, interest in aqueous-based solutions is still increasing. The main disadvantage of aqueous ECs, especially those based on acidic or alkaline electrolytes, is a narrow operating voltage window limited by thermodynamic water stability (in principle, 1.23 V).²⁰ However, the practical maximum voltage of the devices based on this type of electrolyte can be increased by adjusting the physicochemical properties. Modification of the

Institute of Chemistry and Technical Electrochemistry, Poznań University of Technology, Berdychowo 4, 60-965 Poznań, Poland. E-mail: jakub.menzel@put.poznan.pl; krzysztof.fic@put.poznan.pl

electrolyte (pH or conductivity) and/or surface chemistry of activated carbons (AC) is a way to affect the evolution potential of di-hydrogen and/or oxidation of the electrode. It results in increased voltage.²¹ In some cases, it is possible to achieve a voltage of up to 1.8 V.^{22–24} However, the latest research on “water-in-salt” electrolytes shows that even more than 2 V can be achieved for very concentrated electrolytes.^{25,26}

The third group of electrolytes is ionic liquids; their advantages include the possibility of reaching high voltages, up to 4 V;^{27–31} non-flammability; and environmental friendliness. However, their high production cost and poor conductivity limit their application ability in high-power devices.

According to many authors, the ideal electrolyte should be characterized by a wide potential window, low resistance, low viscosity, non-flammability, high electrochemical stability, and environmental friendliness.⁷ In the literature, one can find that high viscosity hinders the mobility of ions in a conductive medium, which is associated with low conductivity.^{32–37} The diffusion of ions through an electrolyte, leading to the formation of an electric double layer at the electrode/electrolyte interface, is not fast enough during repeated charging/discharging processes, which reduces the EC power and, ultimately, the efficiency. Thus, the transport properties of the electrolyte, such as low ion conductivity and high viscosity, negatively affect the device performance.³⁸ The authors also report reduced device power and increased resistance while using such an electrolyte. Among the disadvantages, there is also poor wettability of the electrodes and poor pore penetration ability of the strongly developed electrode surface. Poor wettability reduces the effective use of the highly developed specific surface area of the carbon material. It has been shown that the low viscosity of water electrolytes enables easy diffusion of ions into pores with diameters less than 1 nm. Additionally, the presence of oxygen/nitrogen functional groups on the surface of the carbon in combination with the aqueous electrolyte increases the capacitive performance of the device by modifying the electronic structure of the carbon electrode.³⁹

The viscosity of electrolytes of organic origin is similar to or even lower than that of aqueous electrolytes. However, their conductivity is limited, e.g., 1 mol L⁻¹ TEA⁻BF₄ in acetonitrile 56 mS cm⁻¹, 1 mol L⁻¹ LiPF₆ in acetonitrile, 50 mS cm⁻¹, 1 mol L⁻¹ LiTFSI in acetonitrile 36 mS cm⁻¹,⁴⁰ 1 mol L⁻¹, and LiPF₆ in EC : DMC 10 mS cm⁻¹.

For some solvents, such as ethylene carbonate (EC), where the melting point is slightly above ambient temperature (35 and 38 °C), dimethyl carbonate (DMC), ethyl methyl carbonate (EMC), methyl butyrate (MB), or ethyl butyrate (EB) is added to decrease the viscosity, which simultaneously improves the melting temperature and electrolyte temperature stability. However, due to the increase in the equivalent cell series resistance (ESR), the power density deteriorates.^{41,42} It has been shown that the range of EC working temperatures can be expanded without sacrificing conductivity and viscosity when using the eutectic IL mixture.^{43,44}

Self-discharge is an unavoidable problem for ECs that causes loss of voltage and stored energy.^{45,46} Due to self-discharge, the widespread use of electrochemical capacitors as long-term

backup energy devices is severely limited. It is accepted that charged ECs are in a high energy state and that the Gibbs free energy is a driving force that induces (mostly) self-discharge. There are three main processes responsible for self-discharge: spontaneous charge diffusion and its redistribution,^{47–49} faradaic reactions^{50,51} and so-called ohmic leakage.⁴⁷ Charge redistribution is caused by the movement or loss of charged ions adsorbed on the electrode due to their concentration gradient.⁵² Faradaic reactions concern the oxidation or reduction of redox species on the surface of the electrode. Ohmic leakage occurs due to the internal ohmic leakage pathways between electrodes. All these processes will lead to a reduction in voltage and a loss of stored energy of the charged device. Several solutions to this problem have been proposed, including the formation of an insulating layer on the electrode by depositing a thin film of poly(*p*-phenylene oxide).⁵³ Another method is to use an ion-exchange membrane for active redox⁵⁴ or addition of surfactants to the electrolyte.⁵⁵ Due to the long alkyl chain, surfactants adsorbed on the surface of the electrode should serve as a micro-insulator and hinder the flow of discharge current. The method proposed by Xia M. *et al.* turned out to be a very effective solution.⁵² They proposed the use of increased electrolyte viscosity in the electrode vicinity. The nematic phase of the 4-*N*-pentyl-4'-cyanobiphenyl liquid crystal was used for this purpose as an addition to the primary electrolyte. When the EC is charged, the electric field in the double layer near the surfaces of the electrodes induces alignment of the additive particles, resulting in a significantly increased viscosity of the fluid by means of an electrorheological effect. As a result, the diffusion of ions and redox compounds in the electrolyte may be hindered; however, the rate of self-discharge may be reduced. The simulation results confirmed the reduced contribution of both ion diffusion and faradaic reaction to self-discharge. With this solution, the charge efficiency which was obtained was much higher than that of the electric double-layer capacitor (EDLC) without additive.

The authors each time stress the negative effect of increased viscosity, but the positive aspects of such electrolytes are usually neglected.

Our work aims to verify this popular approach in terms of the use of highly viscous electrolytes in electrochemical capacitors. For this purpose, the aqueous 1 mol L⁻¹ Li₂SO₄ electrolyte was modified by the addition of the carboxymethyl cellulose (CMC) additive, which allows strict control of the solution viscosity. The obtained result provides new insights into the problem of electrolyte viscosity and shows that viscosity itself is not the limiting parameter.

2. Experimental section

2.1 Electrolytes

An aqueous solution of 1 mol L⁻¹ Li₂SO₄ was prepared by dissolving the appropriate mass of Li₂SO₄ salt (purity – 99%, Sigma-Aldrich®) in deionized water. Sodium carboxymethyl-cellulose (CMC) (substitution degree, 1.2; Sigma-Aldrich®) and guar gum (GG) (Sigma-Aldrich®) were selected as viscosity-adjusting agents. The modified electrolytes were prepared by

dissolving the relevant mass of CMC (1, 3, 5, and 7 wt%) and GG (1, 2, 3 wt%) in 1 mol L⁻¹ Li₂SO₄ prepared before. The additives were intended to increase the viscosity only, not to become a source of additional redox activity in the system. Conductivity measurements were performed using a conductometer (Mettler Toledo®), and the final conductivity was the average of three measurements. The viscosity of the electrolytes was examined by a Brookfield® DV2T viscometer.

2.2 Electrodes

Carbon electrodes were prepared by the wet method. Three types of carbon materials were used in the research as electrode materials: pristine mesoporous Norit® SX2 (SX2n-A) (897 m² g⁻¹), microporous AC Kuraray® YP-80F (YP-80F) (1717 m² g⁻¹) and KOH-activated Norit® SX2 (SX2A) (1833 m² g⁻¹). The electrodes were prepared by 24 h of mechanical mixing of the AC powders with a 60% polytetrafluoroethylene (PTFE) solution in a ratio of 95 : 5 (AC : PTFE) immersed in isopropanol until homogeneity was achieved. The homogenized material was formed into rectangular sheets, calendered to produce a 200 μm thick film and dried for 12 h at 70 °C. The specific surface area, pore volume and pore distribution of individual carbonaceous materials were determined by nitrogen adsorption at 77 K with an ASAP 2460 sorptometer (Micromeritics®, USA). For comparative purposes, the physio-chemical properties of microporous YP-50F were measured and are presented.

2.3 Electrochemical investigation

Electrochemical measurements were performed in a symmetric, two-electrode Swagelok® cell and verified in a three-electrode setup. Two types of three-electrode cells were used: an SVC-3 Biologic® volume cell with two glassy carbon electrodes serving as the working and counter electrodes and a custom-made three-electrode cell with a platinum mesh serving as the counter electrode. In both cases, the Hg/Hg₂SO₄ reference electrode was used to monitor the potential of the electrodes. The electrodes were immersed in electrolyte for 1 h prior to the measurement and separated by a Whatman GF/A porous membrane. Long-term cycling tests were performed with application of galvanostatic charge/discharge technique at current density of 1 A g⁻¹ for 10 000 cycles. The 12-hour self-discharge measurement was performed after system has been charged to the voltages of 1 V, 1.2 V, 1.4 V and 1.6 V, followed by the voltage hold for 2 hours. All current and capacitance values are expressed per mass of one electrode. All measurements were conducted with a computer-controlled multichannel potentiostat/galvanostat (VMP3, Biologic®, France).

2.4 Internal pressure measurements

The gas generation rate was measured for a symmetric carbon/carbon system in a customized cell connected to the pressure sensor (Keller®, Switzerland). To maintain controlled conditions, the cell was placed in a thermostatic chamber at 30 °C and stabilized for 6 h before the experiment. The internal pressure build-up was measured during 2 h of constant voltage at cell voltages of 1.0 V, 1.2 V, 1.4 V, 1.6 V, and 1.8 V.

2.5 Electrowetting/contact angle

The electrowetting measurements were performed with a computer-controlled goniometer (Dataphysics® OCA). The carbon samples in the form of pellets (diameter 10 mm) serving as working electrodes were placed horizontally in front of the contact angle camera and the platinum wire (counter electrode). The circuit between the electrodes was closed by placing a 3 μL electrolyte drop on the surface of the electrode material. During the measurement, the subsequent electrodes were then polarized for 6 minutes at a constant voltage. The electrochemical characteristics were carried out with a computer-controlled potentiostat/galvanostat SP-200 Biologic®, France.

3. Results and discussion

Fig. 1 presents the nitrogen adsorption isotherms and pore size distributions of selected carbon materials: pristine SX2n-A, SX2A, and YP-80F.

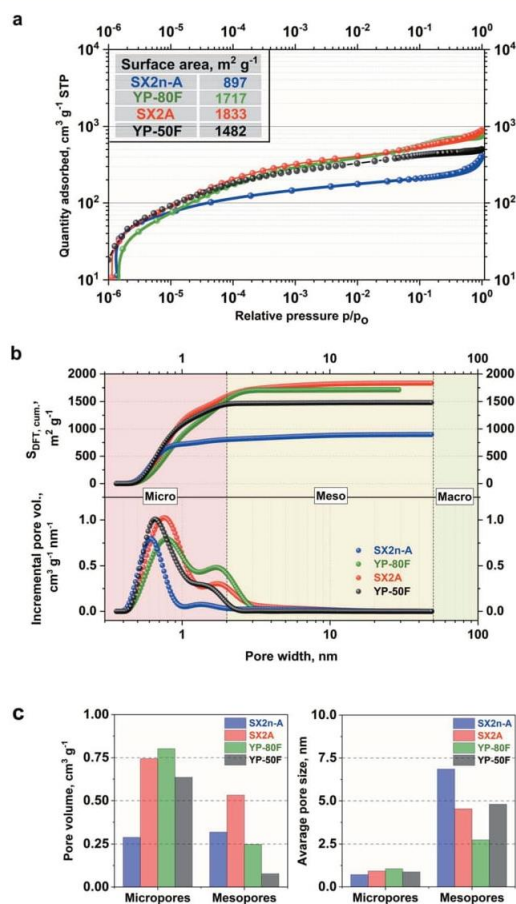


Fig. 1 (a) Nitrogen adsorption/desorption isotherms at 77 K; (b) cumulative surface area calculated with NL-DFT method and corresponding pore size distributions; (c) pore volume and average pore size ratio of micro- to mesoporosity for selected carbon materials.

All of the examined materials are represented by type I adsorption/desorption isotherms, which are characteristic of microporous AC. However, for the SX2n-A and SX2A materials, a clearly defined hysteresis loop characteristic for mesoporous materials as well as an upward trend of adsorption is observed. This might be explained by condensation of desorbed nitrogen in the bulk of the mesopores. The shapes of both isotherms are very similar; the only change is in the absolute nitrogen adsorption volume, which is the result of a higher specific surface area, *i.e.*, 1833 m² g⁻¹ in the case of SX2A and 897 m² g⁻¹ for SX2n-A. The YP-80F and YP-50F isotherm are typical of microporous materials with an insignificant adsorption/desorption hysteresis loop, and less pronounced upward trend at higher relative pressures. These materials display a high specific surface area of 1717 m² g⁻¹ and 1482 m², respectively. The comparison of cumulative surface area and pore size distribution in Fig. 1b also confirm the different porous character of selected carbons. One may observe that for all materials the highest contribution to the total surface area comes from micropores (<2 nm). Quick stabilization of the curve, thus, no further surface increase is observed for microporous carbons YP-80F and YP-50F even up to 3 nm pore width. In the case of micro-mesoporous carbons, an additional increase of the surface area is observed across the whole mesopores (2–50 nm) region. As shown by other authors, the difference in pore distribution has a significant impact on the mass transfer inside the electrode and final electrochemical capacitor performance.⁵⁶ Hence, in this work, the importance of internal mesoporous channels on the performance of electrochemical capacitors in terms of viscous electrolytes will be discussed. The presented PSD plots confirm the microporous character of selected AC; moreover, the micropore/mesopore volume ratio shows that SX2A and YP-80F and especially YP-50F carbons are mostly microporous carbons. However, in SX2n-A, most of the volume is the contribution of the mesopores. Nonetheless, the comparison of average pore size shows that the SX2n-A carbon is characterized by the smallest micropores size (0.7 nm) while in the case of other carbons it is ~1 nm. The YP-50F was used only as a comparison material to expose the differences between microporous and micro-mesoporous materials. In further work, we focus on the comparison between YP-80F and SX2A, because of similar surface area (considering both BET and DFT calculations).

To confirm the negligible impact of viscosity on the conductivity of electrolytes, two gelling agents were used, CMC and guar gum. The maximum polymer content in the electrolyte was limited by the polymer solubility. The conductivity to viscosity relation of the prepared electrolytes is presented in Fig. 2.

It can be observed that even a small amount of gelling agents has a significant influence on the electrolyte viscosity. The addition of 7% CMC or 3% guar gum increases the viscosity by 100 000 times. However, even though such a notable change in viscosity has a marginal effect on the conductivity of the electrolyte, the loss is at a maximum of approximately 10%. Due to the strong impact of even small amounts of GG on the electrolyte viscosity, only CMC was applied as an additive for further

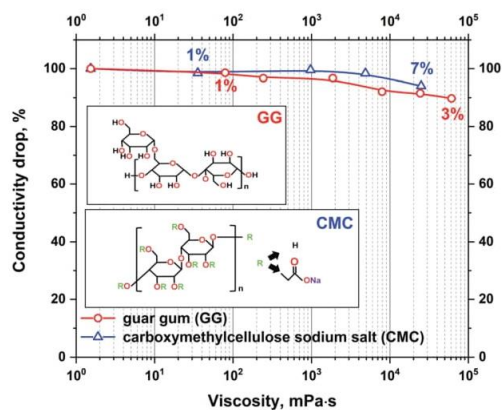


Fig. 2 The absolute change in conductivity with increasing viscosity of the 1 mol L⁻¹ Li₂SO₄ electrolyte with guar gum and CMC additives.

research. Small addition enables better control of solution properties.

The measured conductivity drop with increasing viscosity might also be interesting for research on ionic liquid applications in EDLCs. In the research presented in the literature it is frequently stated that viscosity is the limiting parameter of such electrolytes. It has been shown that even slight changes in ionic liquid viscosity have a significant impact on conductivity.^{57,58} However, the analysis of ionic liquid conductivity and viscosity dependency is always shown as a function of temperature. To avoid the influence of temperature on conductivity in the present research, the temperature of the electrolyte is fixed, and the change in viscosity is determined by the addition of low conducting gelling agents.

Moreover, there is no clear dependence between the high viscosity of specific ionic liquids and their low conductivity. One may find that two different ionic liquids with different viscosities, *e.g.*, *N*-methyl-*N*-propylpyrrolidinium dicyanamide (Pyr13DCA) (27 mPa s) and 1-ethyl-3-methylimidazolium bis(fluorosulfonyl)imide (EMIFS1) (17.9 mPa s), are characterized by very similar conductivities of 15.7 and 15.5 mS cm⁻¹, respectively.^{58,59} This might show that the viscosity is not the only parameter influencing the electrolyte conductivity. The observation of the interaction between the electrode and electrolyte under polarization was performed by the electrowetting experiment with the use of a contact angle apparatus. The measurement of the electrolyte volume change and contact angle was conducted under constant voltage polarization for 6 minutes. For comparison, a reference measurement of the sample without polarization was performed. This experiment was performed only for the electrode composed of SX2A carbon. The droplets were dispensed by an automatically controlled syringe of the volume of 3 μL. The results are presented in Fig. 3.

As expected, the carbon electrode shows hydrophobic properties. After placing the electrolyte droplet without polarization, the measured contact angle was approximately 134° for both 1 mol L⁻¹ pure Li₂SO₄ and Li₂SO₄ with 3% CMC. The electrolyte

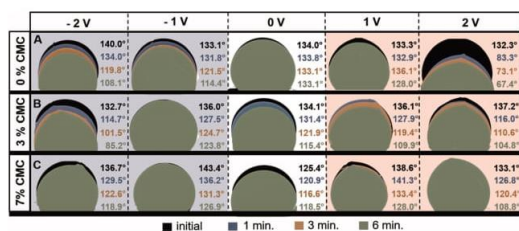


Fig. 3 Dynamic contact angle measurements of pristine and modified 1 mol L⁻¹ Li₂SO₄ electrolyte droplet adsorption on nonpolarized and polarized SX2A electrodes.

with 7% CMC had a contact angle of 125.5° (white background). For the non-modified electrolyte, the contact angle did not change during 6 minutes. However, the addition of CMC to the electrolyte significantly increased the electrolyte affinity to the carbon, as observed by a significant change in the contact angle over time; for the 3% additive, it decreased from 134.0° to 115.4°, and for the 7% CMC, it decreased from 125.4° to 118.5°. Additionally, the change in the droplet volume suggests spontaneous wetting of the carbon material. The application of potential has a significant influence on electrolyte behaviour. The cathodic polarization of non-modified 1 mol L⁻¹ Li₂SO₄ induces gradual wetting of the electrode, as observed both by a change in the contact angle and a decrease in the electrolyte volume. However, the effect of electrolyte modified by the addition of CMC on cathodic polarization is somewhat different, and repulsion of the electrolyte is observed. The behaviour of the electrolyte at a polarization of -1 V might be explained by an ion exchange equilibrium. One may agree that at the interface of the electrolyte and electrode, part of the electrode is spontaneously wetted by the adsorbed electrolyte with a mixture of ions. When cathodic polarization is applied, cations move deeper into the pores of the materials and exchange with previously adsorbed anions. Due to increased viscosity, ion exchange is hindered, and a higher force needs to be applied to exchange them. The change in contact angle suggests similar changes in the affinity of electrolytes towards the electrode. Moreover, one must consider the increased viscosity and surface tension (@ 100 mN m⁻¹) of electrolytes, making it more difficult to penetrate the electrode porous structure. The aforementioned consideration is more pronounced after increasing the cathodic polarization to -2 V. For electrolytes with 3% CMC, a stronger driving force results in faster wetting of the electrode. It is observed that both the contact angle and electrolyte droplet volume decrease. In the case of the electrolyte with 7% CMC, the repulsion effect is observed even when -2 V is applied.

The situation changes significantly for anodic polarization; for non-modified 1 mol L⁻¹ Li₂SO₄ polarized at 1 V, no remarkable electrode wetting is observed. The contact angle changes negligibly, and the adsorbed volume is marginal. Such a behaviour is explained by the low affinity of anions towards carbon electrodes and low pore penetration ability, as observed by dilatometry experiments.⁶⁰ However, the situation changes

when a voltage of 2 V is applied; a significant change in droplet volume accompanied by a decrease in the contact angle is observed. For 0% and 3% CMC additive, the contact angle changes similarly, and the adsorbed volume is comparable. The only difference is the intensity of the process. However, when 7% CMC is added to the electrolyte, no wetting is observed. For 1 V polarization, there is an insignificant change in the contact angle, and no visible decrease in droplet volume. Even the application of 2 V does not induce penetration of the electrolyte into the electrode pores, despite the decrease in the contact angle from 133.1° to 108.8°. The behaviour of the electrolyte with 3% and 7% CMC additive under anodic polarization confirms the aforementioned consideration regarding the hindered ion exchange in the pores of the material. This shows that in the case of viscous electrolytes, the wetting of the electrode is strictly connected to the applied polarization, viscosity, and surface tension.

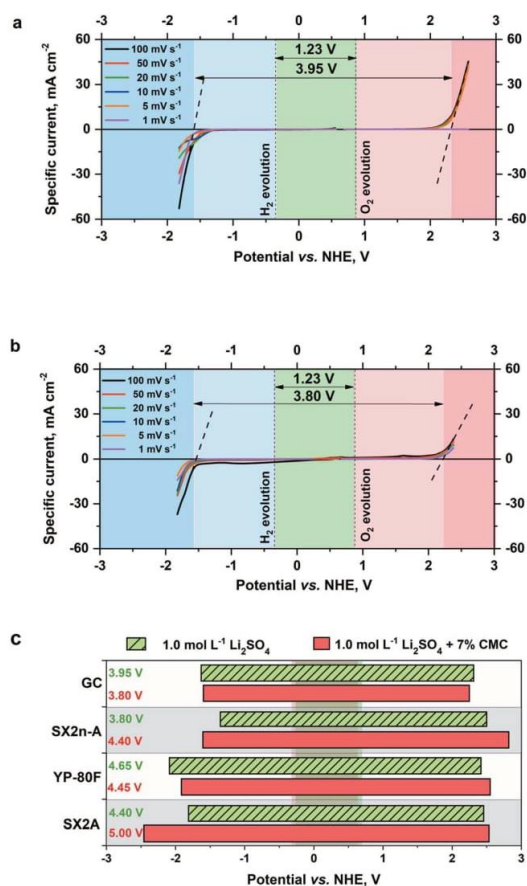


Fig. 4 Potential window determination by LSV in a 3-electrode cell configuration: (a) pristine 1 mol L⁻¹ Li₂SO₄ on glassy carbon, (b) 1 mol L⁻¹ Li₂SO₄ with 7% CMC additive on glassy carbon, (c) comparison of potential limitation on different electrode materials.

The electrochemical stability of modified and non-modified electrolytes was determined by linear sweep voltammetry (LSV) on a glassy carbon electrode. The voltammograms of pure $1 \text{ mol L}^{-1} \text{ Li}_2\text{SO}_4$ and a sample with the addition of 7% CMC are shown in Fig. 4a and b.

The maximum electrochemical window of the examined electrolytes was determined by significant current changes related to hydrogen and oxygen evolution. It can be observed that the addition of CMC does not introduce additional redox activity, and the LSV plot is typical for charge/discharge of the electrical double layer. The disturbance observed for a scan at 100 mV s^{-1} relates to the reduction and oxidation of hydrogen accumulated at the electrode/electrolyte interface. The limited diffusion of species in the modified electrolytes causes gas accumulation at the electrode surface. A comparison of the hydrogen/oxygen evolution potentials and theoretical maximum voltage shows no influence of CMC on these parameters. For the pristine electrolyte, the maximum voltage was 3.95 V, and for the modified electrolyte, it was 3.99 V. The abnormal values of the stability window exceed the thermodynamic correct value of 1.23 V because of the cell construction, where the overpotential, planar electrode, and excess electrolyte increase the overall result. Nevertheless, this method is ideal to observe the influence of electrolyte and electrode parameters on theoretical electrochemical stability. No significant differences are observed, regardless of whether CMC is present in the solution. However, in the case of the porous carbon electrodes, the influence of the CMC is more pronounced.

Fig. 4c presents a comparison of the maximum potential limitations of carbon electrodes estimated by the LSV method. In the case of typical mesoporous materials, SX2n-A and SX2A, during cathodic polarization, the hydrogen evolution potential is shifted towards more negative potentials when CMC is engaged. On the other hand, the oxygen evolution potential is not modified during anodic polarization. In the case of the microporous YP-80F material, hydrogen evolution is in the range of less negative values during cathodic polarization than in the case of the pristine electrolyte. Such behaviour might be explained by the aforementioned electro-wetting properties of modified electrolytes. In the case of mesopores, the electrolyte is electrochemically adsorbed and may reach the micropores. The shift of the potential towards more negative values is caused by hydrogen sorption overpotential.^{26,61,62} In the case of anodic polarization, the shift of the potential is marginal, and it is in the same range of values as in the case of the glassy carbon electrode. The situation is somewhat different in the case of microporous YP-80F carbon, where during cathodic polarization, the potential limitation is shifted towards less negative values. Such behaviour might relate to the inaccessibility of micropores by electrolytes and induces hydrogen evolution in wider pores. That is why for microporous carbon, the hydrogen evolution potential is the same as for glassy carbon electrodes. During anodic polarization, the oxygen evolution limit is shifted towards more positive values. This might be related to a lack of oxygen groups on the surface of the electrode and their formation. As shown by He *et al.*, the oxidation of carbon electrodes leads to the evolution of CO and CO₂.⁶³ This might mean

that in the case of YP-80F, the generated oxygen is used to recombine on the electrode surface and build up as surface groups. This leads further to a shift of the gas evolution potential during anodic polarization towards more positive values.

The real voltage limitation of the prepared electrolytes was estimated by GITT (galvanostatic intermittent titration technique), as shown in Fig. 5. During the GITT experiment, the current is applied to the system for a given time. After the specific charge is reached (titrated), the polarization is interrupted by open-circuit conditions until the potential stabilizes (or for a given time). The process is repeated until the desired electrode potential (or the total charge titrated) is reached. This experiment allows the equilibrium potentials to be determined.

The experiment was conducted in a three-electrode setup. The technique itself enables the determination of equilibrium potentials of the electrodes. Briefly, a constant current of low magnitude is applied to the capacitor to reach the potential plateau. After the plateau is maintained, the current is terminated, and the electrode tends to reach its equilibrium potential. The maximum theoretical capacitor voltage was estimated by the offset of the resting potential during hydrogen sorption at the negative electrode and carbon oxidation at the positive electrode. The obtained value of the voltage window is 1.9 V. Such a value would be acceptable for the capacitor if the potentials were equally distributed among the electrodes. In the real system, as shown by other authors, the safe voltage limitation for a $1 \text{ mol L}^{-1} \text{ Li}_2\text{SO}_4$ aqueous-based capacitor is 1.5–1.6 V. The presented result shows that the addition of CMC does not influence the performance^{26,64–66} of electrolytes on the carbon electrode. Although an earlier experiment showed shifting of the hydrogen evolution potential towards lower potential values for modified electrolytes, in this case, such behaviour is not observed. Consequently, for the full capacitor cell, the voltage limitation should be the same, regardless of the modification of the electrolyte. Additionally, the shape of the hydrogen desorption hysteresis is the same, meaning that an increase in viscosity did not influence the hydrogen sorption/desorption efficiency.

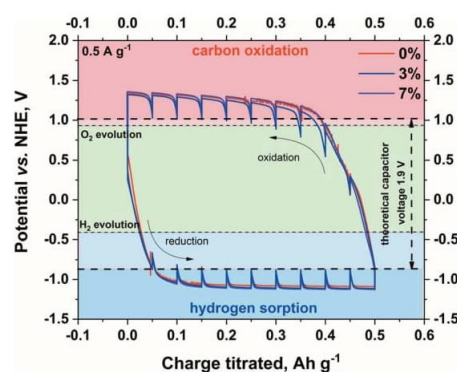


Fig. 5 Determination of the maximum stability window of pristine and modified electrolytes on SX2A electrode by GITT (current regime – 0.5 A g^{-1}).

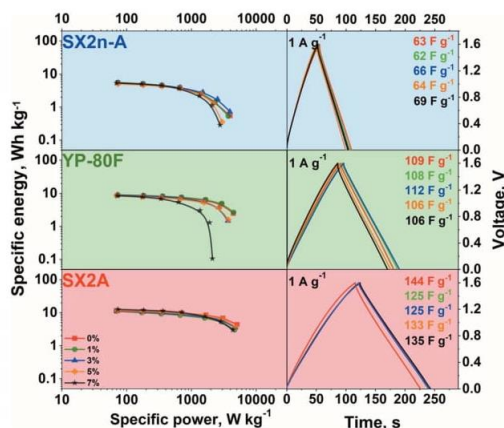


Fig. 6 The graphs on the left are Ragone plots for different carbons with non-modified and CMC-modified 1 mol L⁻¹ Li₂SO₄ electrolyte, and the graphs on the right are the corresponding galvanostatic charge/discharge profiles at the 1 A g⁻¹ current regime.

The capacitor performance with modified electrolytes was examined by galvanostatic charge/discharge at 0.5–10 A g⁻¹ current regimes. The galvanostatic charge/discharge profiles from 0 to 1.6 V are presented in Fig. 6.

Typical linear voltage increases on charging and decreases on discharging are observed, confirming additional redox reaction occurrence, irrespective of the carbon material used and CMC content. Nonetheless, the hydrogen sorption phenomena characteristic for aqueous neutral electrolytes cannot be neglected. As the discharge time increases, the capacitance of the carbon material increases in the order SX2n-A, YP-80F, and SX2A. This difference is strictly connected with carbon differences in the surface area and pore accessibility. What may be noticed is that the CMC addition does not impact the shape of galvanostatic curves or the polarizability, recorded at 1 A g⁻¹. The calculated power and energy values are presented on the Ragone plot.

For all carbons, the modification of the electrolyte did not influence the maximum energy recorded at a low power regime. This suggests that in all cases, the same active surface area is in contact with the electrolyte with the same capacitance. Such performance might be explained by the application of so-called conditioning cycles, just before the collection of data for the Ragone plot. The conditioning was performed to stabilize the system. For this reason, one cannot exclude the effect of gradual wetting of the electrode and pore penetration by the electrolyte during continuous charge/discharge cycles. However, this observation once more confirms that even highly viscous electrolytes might demonstrate satisfactory performance. Nevertheless, the structural properties of carbon have a significant influence on the maximum recorded power. On the one hand, in mesoporous carbon materials (SX2n-A and SX2A), the loss of power with an increase in electrolyte viscosity is marginal. However, the visible deterioration of the power in the case of

SX2n-A carbon can be explained by the inaccessibility of the strict microporosity. This carbon is characterized by the smallest average micropore size *ca.* 0.7 nm, while in the case of SX2A and YP-80F carbon, the average pore size is *ca.* 0.9 and 1 nm respectively. On the other hand, for microporous carbon (YP-80F), the loss of power with an increase in viscosity is significant. This loss of power may be related to the accessibility of the electrolyte to the slit porosity without ensuring enough mesoporosity to serve as transport channels. During polarization, the continuous dragging of the electrolyte towards the pore surface is ongoing. As ions together with their solvation shell enter the micropores, they may also be accompanied by their counterions *via* so-called co-insertion. As the mixture of ions is attracted to the micropores, those contributing to charge storage must exchange places with “inert” ions. In the case of viscous electrolytes applied to microporous electrodes, the mobility of ions is limited, which results in limited power performance. In the case of mesoporous carbons, this effect is less visible, the ions have more space, and the exchange is easier. Therefore, in this case, the power is less affected by the viscosity of the electrolyte. This finding stresses that micropore accessibility is a power limiting factor in the case of viscous electrolytes.

The effect of viscosity was also examined in terms of internal pressure build-up. The measurement was performed for the capacitor placed in the thermostatic chamber at 30 °C. The electrochemical experiment involved galvanostatic charging to the desired voltage, followed by 2 h of constant voltage hold. The gas generation rate was then calculated as the slope of the pressure build-up during the voltage hold period. The change in the gas generation rate and leakage current with voltage is shown in Fig. 7a.

A positive impact of increased viscosity on these two parameters is observed. With increasing viscosity, the internal pressure build-up and leakage current decrease. As the reduction of ionic mobility is not considered (no change of conductivity was recorded with increased viscosity), the leakage current reduction is most likely not connected with limited ion redistribution. Nonetheless, in the case of the aqueous electrolytes, the hydrogen sorption phenomenon needs to be here considered. Generally, at the negative electrode the water decomposes, and the generated hydrogen is *ad-hoc* adsorbed in the electrode microporosity. Additionally, as shown by He *et al.*,⁶⁷ even at low voltage the CO and CO₂ evolution might be observed. As the leakage current measurement is performed for 2 hours and the constant (equilibrated) current is reached, the electrode in such conditions might be considered as a reactor. In that case, the oxidation process will be performed until the equilibrium between substrate and product will be reached. In the case of the non-viscous electrolytes, the generated CO and CO₂ can easily diffuse and can shift the equilibrium towards substrate, resulting in increased leakage current. In the case of viscous electrolytes the mobility of gaseous product is limited and less current is necessary to stabilize equilibrium in the system. In case of the YP-80F carbon due to high microporosity the CO and CO₂ have limited mobility and the effect of electrolyte viscosity is less pronounced. However, in the case 1.6 V additional H₂

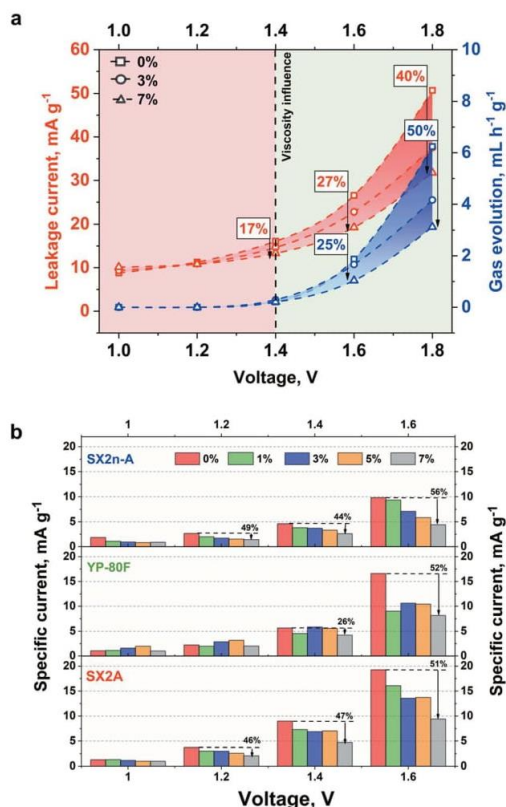


Fig. 7 (a) Leakage current and volume of generated gases in the system working based on electrolytes with different viscosities. (b) Comparison of leakage current for selected carbons with increasing voltage limitation.

recombination and evolution on negative electrode need to be considered. This case might be explained in similar manner as for CO and CO₂ evolution. There is an equilibrium between *ad-hoc* hydrogen adsorption and recombination. In case of the viscous electrolytes the evacuation of gaseous product is limited this current of lower density is necessary to keep the electrode charged. The leakage current itself depends on the susceptibility of the ions for their redistribution in the EDL. The diffusion parameter at a given potential does not change with time at a given potential step. Therefore, this parameter is closely related to the value of the leakage current. The increased electrolyte viscosity should limit the gas diffusion from the material pores and thus reduce the value of the leakage current. Our results also prove this concept. We assume that narrow micropores (like in YP-80F) up to 1.4 V strongly limit the gas diffusion. In this case, the narrow pores constitute a barrier. The second factor is higher electrolyte viscosity and the addition of 7% CMC at 1.4 V reduced the leakage current by 26%. Voltage of 1.6 V is already high (so the driving force of the decomposition process) that the narrow pores are not able to hold the generated gases.

In this case, viscosity begins to play a leading role (reduction of leakage current by 52%). In mesoporous materials and materials with a mixed pore content, viscosity begins to play a major role. Wider mesopores provide a more flexible path for gas diffusion. For SX2n-A and SX2A materials, the viscosity at relatively low voltage values (1, 1.2, 1.4 V) reduces gas diffusion. The pore width for mesoporous materials is not so small as to significantly limit the diffusion of gas.

The self-discharge measurement also showed interesting results. For YP-80F systems operating with 1 mol L⁻¹ Li₂SO₄ and with the addition of 7% CMC (Fig. 8a), the self-discharge course is nearly the same. For SX2A-based capacitor, the addition of CMC slightly reduces the self-discharge, especially in the first 2 hours. The biggest difference was observed for SX2n-A, for which the CMC addition significantly reduces the self-discharge process. For 1 mol L⁻¹ Li₂SO₄ the voltage dropped to 0.63, 0.7, 0.83 and 0.97 V for 1.0, 1.2, 1.4 and 1.6 V respectively. For electrolytes with 7% CMC, the voltage reached 0.79, 0.9, 1.02, and 1.1 V. Thus, one can conclude that to stabilize the voltage in the system based on mesoporous electrode material, the higher electrolyte viscosity should be applied. The stabilization most likely results from preventing the charge reorganization in the

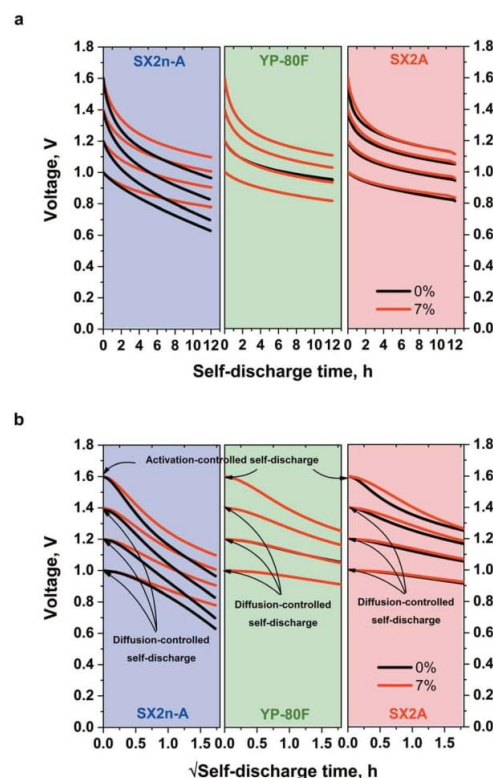


Fig. 8 Self-discharge profiles of capacitors operating with 1 mol L⁻¹ Li₂SO₄ and with 7% CMC addition dependence on (a) linear self-discharge time and (b) self-discharge time in a square-root time scale.

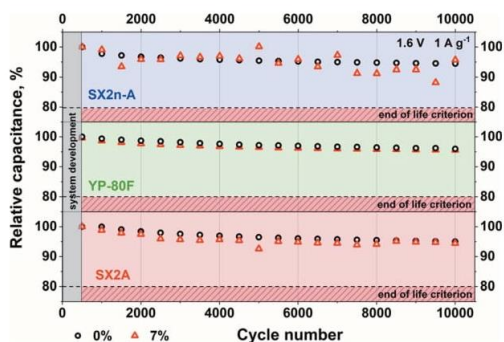


Fig. 9 Long-term cycling test for a capacitor with $1 \text{ mol L}^{-1} \text{ Li}_2\text{SO}_4$ and 7% CMC addition.

EDL once the polarization has subsided. As mentioned, the self-discharge process is caused by at least three types of processes: activation-controlled, diffusion-controlled, or so-called ohmic leakage. The diffusion-controlled process can be associated with the ions redistribution inside the micropores; activation-controlled processes are usually redox reactions resulting from the presence of pollutants, redox-active species in the electrolyte (or at electrode surface), and electrolyte decomposition. The ohmic leak usually occurs in the event of an internal short-circuit.

Based on the profile of the voltage vs. the self-discharge square root time (Fig. 8b), it can be concluded that, in fact, there are two self-discharge processes in the tested systems. At a 1, 1.2, and 1.4 V the linear course of the self-discharge indicates nearly typical diffusion-controlled process. The non-linear curve for 1.6 V for all materials, regardless of the electrolyte viscosity, indicates the appearance of additional, parasitic reactions, such as electrolyte decomposition that govern and accelerate the self-discharge process.

The influence of the increased electrolyte viscosity on the long-term performance was tested by the application of 10 000 charge/discharge cycles at 1 A g^{-1} current load (Fig. 9). One can easily notice that for all electrode materials, the capacitance reached 95% of its initial value after the same number of cycles. Therefore, we claim that no negative effect of increased electrolyte viscosity is observed.

4. Conclusions

This article describes the influence of increased electrolyte viscosity on electrochemical capacitor performance. The interaction between the viscous electrolyte and the porous carbon electrode is a complex relationship. It is postulated that unveiling its limiting factors can lead to further development of high-power-energy storage devices. The obtained results might be especially interesting in terms of the application of ionic liquids.

One of the major conclusions that we should underline is that increase in the electrolyte viscosity does not significantly reduce the mobility of the ions (conductivity). However, the

increased viscosity of the electrolyte reduces the electro-wetting phenomenon; nonetheless, it depends on the polarization magnitude. The ion exchange in viscous electrolytes inside porous structures is certainly hindered. This might lead to insufficient pore penetration (especially for micropores) and deterioration of the electrochemical capacitor performance. It is recommended, before the actual operation of the capacitor based on high-viscous electrolyte, to condition the system. This solution should increase electrode wettability and device performance. The stability of the electrolytes verified with LSV technique shows that there are no significant differences between the low- and high-viscous electrolytes upon application of a glassy carbon electrode. While using a porous electrode, the differences become observable. However, they strongly depend on the carbon porous structure; surprisingly, mesoporous materials are more affected than microporous ones. The GITT technique is better suited to estimate the electrolyte stability window than the LSV technique, which tends to overestimate the potential stability. The increased viscosity has a marginal effect on the final voltage window of the device. The increased electrolyte viscosity does not affect the hydrogen sorption/desorption process efficiency. Moreover, in this article, we present that the impact of the electrolyte viscosity on the electrochemical capacitor energy and power performance is determined by the pore structure of carbon and pore accessibility. Higher electrolyte viscosity does not necessarily result in an energy decrease. Proper selection of the electrode material porosity is required. A significant advantage of increased viscosity (the case in which 7% CMC was used) is reducing the parasitic reactions of water decomposition at high voltage, as observed in the gas generation experiment (twice as low at 1.8 V). In a microporous AC based system higher electrolyte viscosity slightly reduce the discharge degree. However, a significant reduction in self-discharge by limiting the charge delocalization in the EDL was noticed in mesoporous materials. Another positive aspect seems to be the lack of electrolyte viscosity influence on the long-term performance stability, regardless of the electrode material porosity.

The presented results highlight the topic of viscous electrolyte/porous carbon interactions. Finally, these results give rise to be more sceptical to the overall statement that the viscosity being itself the limiting factor of electrochemical capacitor performance.

Conflicts of interest

There are no conflicts to declare.

Acknowledgements

The authors would like to acknowledge the financial support from the European Research Council within the Starting Grant project (GA 759603) under the European Unions' Horizon 2020 research and innovation programme.

Notes and references

- 1 J. Khan and M. H. Arsalan, *Renewable Sustainable Energy Rev.*, 2016, **55**, 414–425.
- 2 P. Simon and Y. Gogotsi, *Nat. Mater.*, 2008, **7**, 845–854.
- 3 R. Kötz and M. Carlen, *Electrochim. Acta*, 2000, **45**, 2483–2498.
- 4 E. Frackowiak and F. Beguin, *Carbon*, 2001, **39**, 937–950.
- 5 B. E. Conway and W. G. Pell, *J. Solid State Electrochem.*, 2003, **7**, 637–644.
- 6 K. Fic, A. Platek, J. Piwek and E. Frackowiak, *Mater. Today*, 2018, **21**, 437–454.
- 7 M. Mirzaeian, Q. Abbas, A. Ogwu, P. Hall, M. Goldin, M. Mirzaeian and H. F. Jirandehi, *Int. J. Hydrogen Energy*, 2017, **42**, 25565–25587.
- 8 Y. Zhu, S. Murali, M. D. Stoller, K. J. Ganesh, W. Cai, P. J. Ferreira, A. Pirkle, R. M. Wallace, K. A. Cychoz, M. Thommes, D. Su, E. A. Stach and R. S. Ruoff, *Science*, 2011, **332**, 1537–1541.
- 9 C. Niu, E. K. Sichel, R. Hoch, D. Moy and H. Tennent, *Appl. Phys. Lett.*, 1997, **70**, 1480–1482.
- 10 C. S. Du and N. Pan, *Nanotechnology*, 2006, **17**, 5314–5318.
- 11 G. Moussa, C. M. Ghimbeu, P. L. Taberna, P. Simon and C. Vix-Guterl, *Carbon*, 2016, **105**, 628–637.
- 12 R. Borgohain, J. C. Li, J. P. Selegue and Y. T. Cheng, *J. Phys. Chem. C*, 2012, **116**, 15068–15075.
- 13 B. Anasori, M. R. Lukatskaya and Y. Gogotsi, *Nat. Rev. Mater.*, 2017, **2**, 16098.
- 14 Y. Gogotsi and B. Anasori, *ACS Nano*, 2019, **13**, 8491–8494.
- 15 H. Marsh and F. Rodríguez-Reinoso, in *Activated Carbon*, 2006, pp. 13–86.
- 16 E. Frackowiak and F. Beguin, *Carbon*, 2002, **40**, 1775–1787.
- 17 J. Lee, P. Srimuk, S. Fleischmann, X. Su, T. A. Hatton and V. Presser, *Prog. Mater. Sci.*, 2019, **101**, 46–89.
- 18 J. Krummacher, C. Schutter, L. H. Hess and A. Balducci, *Curr. Opin. Electrochem.*, 2018, **9**, 64–69.
- 19 F. Ghamouss, A. Brugere and J. Jacquemin, *J. Phys. Chem. C*, 2014, **118**, 14107–14123.
- 20 E. Frackowiak, Q. Abbas and F. Beguin, *J. Energy Chem.*, 2013, **22**, 226–240.
- 21 K. Fic, M. Meller and E. Frackowiak, *Electrochim. Acta*, 2014, **128**, 210–217.
- 22 V. Khomeiko, E. Raymundo-Pinero, E. Frackowiak and F. Beguin, *Appl. Phys. A: Mater. Sci. Process.*, 2006, **82**, 567–573.
- 23 J. Menzel, K. Fic and E. Frackowiak, *Prog. Nat. Sci.: Mater. Int.*, 2015, **25**, 642–649.
- 24 A. Slesinski, C. Matei-Ghimbeu, K. Fic, F. Beguin and E. Frackowiak, *Carbon*, 2018, **129**, 758–765.
- 25 L. Suo, O. Borodin, T. Gao, M. Olguin, J. Ho, X. Fan, C. Luo, C. Wang and K. Xu, *Science*, 2015, **350**, 938–943.
- 26 K. Fic, A. Platek, J. Piwek, J. Menzel, A. Ślesiński, P. Bujewska, P. Galek and E. Frackowiak, *Energy Storage Mater.*, 2019, **22**, 1–14.
- 27 M. P. Mousavi, B. E. Wilson, S. Kashefolgheta, E. L. Anderson, S. He, P. Buhlmann and A. Stein, *ACS Appl. Mater. Interfaces*, 2016, **8**, 3396–3406.
- 28 A. Balducci, *J. Power Sources*, 2016, **326**, 534–540.
- 29 A. Brandt, S. Pohlmann, A. Varzi, A. Balducci and S. Passerini, *MRS Bull.*, 2013, **38**, 554–559.
- 30 A. Balducci, U. Bardi, S. Caporali, M. Mastragostino and F. Soavi, *Electrochem. Commun.*, 2004, **6**, 566–570.
- 31 W. Y. Tsai, R. Y. Lin, S. Murali, L. L. Zhang, J. K. McDonough, R. S. Ruoff, P. L. Taberna, Y. Gogotsi and P. Simon, *Nano Energy*, 2013, **2**, 403–411.
- 32 A. Lewandowski, A. Olejniczak, M. Galinski and I. Stepniak, *J. Power Sources*, 2010, **195**, 5814–5819.
- 33 A. B. McEwen, S. F. McDevitt and V. R. Koch, *J. Electrochem. Soc.*, 1997, **144**, L84–L86.
- 34 Q. Zhang, J. P. Rong, D. S. Ma and B. Q. Wei, *Energy Environ. Sci.*, 2011, **4**, 2152–2159.
- 35 T. Abdallah, D. Lemordant and B. Claude-Montigny, *J. Power Sources*, 2012, **201**, 353–359.
- 36 A. Krause and A. Balducci, *Electrochem. Commun.*, 2011, **13**, 814–817.
- 37 H. N. Kwon, S. J. Jang, Y. C. Kang and K. C. Roh, *Sci. Rep.*, 2019, **9**, 1180.
- 38 J. Barthel, R. Neueder and H. Roch, *J. Chem. Eng. Data*, 2000, **45**, 1007–1011.
- 39 M. Anouti, E. Couadou, L. Timperman and H. Galiano, *Electrochim. Acta*, 2012, **64**, 110–117.
- 40 P. Leung, A. A. Shah, L. Sanz, C. Flox, J. R. Morante, Q. Xu, M. R. Mohamed, C. P. de Leon and F. C. Walsh, *J. Power Sources*, 2017, **360**, 243–283.
- 41 D. R. MacFarlane, N. Tachikawa, M. Forsyth, J. M. Pringle, P. C. Howlett, G. D. Elliott, J. H. Davis, M. Watanabe, P. Simon and C. A. Angell, *Energy Environ. Sci.*, 2014, **7**, 232–250.
- 42 Z. Y. Li, M. S. Akhtar and O. B. Yang, *J. Alloys Compd.*, 2015, **653**, 212–218.
- 43 M. Kunze, S. Jeong, E. Paillard, M. Winter and S. Passerini, *J. Phys. Chem. C*, 2010, **114**, 12364–12369.
- 44 L. Timperman, A. Vigeant and M. Anouti, *Electrochim. Acta*, 2015, **155**, 164–173.
- 45 C. Zhong, Y. Deng, W. Hu, J. Qiao, L. Zhang and J. Zhang, *Chem. Soc. Rev.*, 2015, **44**, 7484–7539.
- 46 W. T. Gu and G. Yushin, *WIREs Energy Environ.*, 2014, **3**, 424–473.
- 47 B. E. Conway, W. G. Pell and T. C. Liu, *J. Power Sources*, 1997, **65**, 53–59.
- 48 W. G. Pell, B. E. Conway, W. A. Adams and J. de Oliveira, *J. Power Sources*, 1999, **80**, 134–141.
- 49 A. M. Oickle and H. A. Andreas, *J. Phys. Chem. C*, 2011, **115**, 4283–4288.
- 50 H. A. Andreas, *J. Electrochem. Soc.*, 2015, **162**, A5047–A5053.
- 51 A. Lewandowski, P. Jakobczyk, M. Galinski and M. Biegun, *Phys. Chem. Chem. Phys.*, 2013, **15**, 8692–8699.
- 52 M. Y. Xia, J. H. Nie, Z. L. Zhang, X. M. Lu and Z. L. Wang, *Nano Energy*, 2018, **47**, 43–50.
- 53 T. Tevi, H. Yaghoubi, J. Wang and A. Takshi, *J. Power Sources*, 2013, **241**, 589–596.



- 54 L. B. Chen, H. Bai, Z. F. Huang and L. Li, *Energy Environ. Sci.*, 2014, 7, 1750–1759.
- 55 K. Fic, G. Lota and E. Frackowiak, *Electrochim. Acta*, 2010, 55, 7484–7488.
- 56 J. X. Li, Y. Gao, K. H. Han, J. H. Qi, M. Li and Z. C. Teng, *Sci. Rep.*, 2019, 9, 17270.
- 57 T. Sato, G. Masuda and K. Takagi, *Electrochim. Acta*, 2004, 49, 3603–3611.
- 58 C. Wolff, S. Jeong, E. Paillard, A. Balducci and S. Passerini, *J. Power Sources*, 2015, 293, 65–70.
- 59 N. Handa, T. Sugimoto, M. Yamagata, M. Kikuta, M. Kono and M. Ishikawa, *J. Power Sources*, 2008, 185, 1585–1588.
- 60 M. M. Hantel, V. Presser, R. Kotz and Y. Gogotsi, *Electrochem. Commun.*, 2011, 13, 1221–1224.
- 61 L. Demarconnay, E. Raymundo-Pinero and F. Beguin, *Electrochem. Commun.*, 2010, 12, 1275–1278.
- 62 Q. Gao, L. Demarconnay, E. Raymundo-Pinero and F. Beguin, *Energy Environ. Sci.*, 2012, 5, 9611–9617.
- 63 M. L. He, K. Fic, E. Frackowiak, P. Novak and E. J. Berg, *Energy Environ. Sci.*, 2016, 9, 623–633.
- 64 P. Ratajczak, K. Jurewicz, P. Skowron, Q. Abbas and F. Beguin, *Electrochim. Acta*, 2014, 130, 344–350.
- 65 Q. Abbas, P. Ratajczak, P. Babuchowska, A. Le Comte, D. Belanger, T. Brousse and F. Beguin, *J. Electrochem. Soc.*, 2015, 162, A5148–A5157.
- 66 A. Platek, C. Nita, C. M. Ghimbeu, E. Frackowiak and K. Fic, *Electrochim. Acta*, 2020, 338, 135788.
- 67 M. He, K. Fic, E. Frackowiak, P. Novak and E. J. Berg, *Energy Environ. Sci.*, 2016, 9, 623–633.

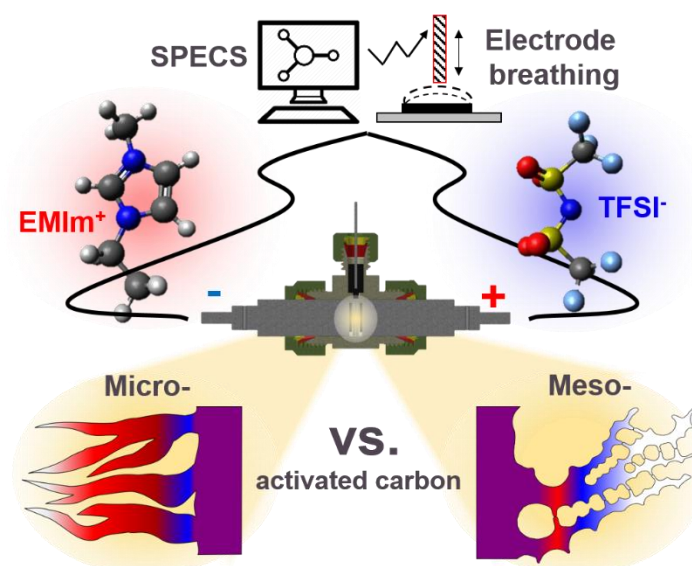
9. Article A4

Title: ***New insight into ion dynamics in nanoporous carbon materials: an application of the Step Potential Electrochemical Spectroscopy (SPECS) technique and Electrochemical Dilatometry***

Authors: Przemysław Galek, Paulina Bujewska, Scott Donne, Krzysztof Fic, Jakub Menzel

Journal: *Electrochimica Acta*, 2021, vol. 377, 138115-1 - 138115-7

DOI: 10.1016/j.electacta.2021.138115



Motivation

Advanced analytical techniques (in situ or operando) are used to describe the flow of ion fluxes in the ECs. We can find here measurement of the frequency changes of the piezoelectric resonator acting as a working electrode (electrochemical a quartz crystal microbalance, EQCM) [205, 206] or electrode volume changes under polarization (electrochemical dilatometry, ECD) [207, 208]. However, the correlation of the recorded changes with ion adsorption/desorption still does not provide full insight into the ion transport mechanism. However, comparisons of the results obtained with both methods do not always lead to unequivocal conclusions. This caught our attention

and prompted us to propose a new approach for determining the charge accumulation mechanism at the electrode/electrolyte interface.

Summary

In **Article A4** – ‘*New insight into ion dynamics in nanoporous carbon materials: An application of the step potential electrochemical spectroscopy (SPECS) technique and electrochemical dilatometry*’ proposed a new methodology to determine a type of ion exchange mechanism in AC electrodes in symmetric ECs. Research was carried out using an electrolyte with a similar anion and cation size – the IL bis(trifluoromethylsulfonyl) imide 1-ethyl-3-methylimidazolium (EMIM⁺TFSI⁻). Due to the combination of the step potential electrochemical spectroscopy (SPECS) technique and electrochemical dilatometry (ECD), the E ranges were distinguished, where the ion mixing region and the permselective adsorption regions occur. It was found that the mechanism of EDL formation strongly depends on the type of electrode material porous structure. The calculations allowed to extract and quantify the charge responsible for the movement of ions in the micropores. Experiments carried out have shown that the mass transport mechanisms are determined by the availability of the electrode pores. In microporous AC, cations are adsorbed by ion exchange and co-adsorption mechanisms, while the anions were initially adsorbed by ion exchange followed by a selective adsorption mechanism. In a micro/mesoporous AC, the anodic and cathodic polarization of carbon causes an analogous ion mixing mechanism, followed by selective adsorption of both ions. The data obtained are consistent with the data in the literature and provide new possibilities for measuring ion transport mechanisms in pores. A comparison of the collected and published data indicates that there is no universal description of the ion transport and the charge/discharge mechanism of the EDL in AC. Therefore, it can be concluded that it is a mixture of different mechanisms that depend on the size and availability of pores, the applied electrolyte type and electrolyte type.



Contents lists available at ScienceDirect

Electrochimica Acta

journal homepage: www.elsevier.com/locate/electacta



New insight into ion dynamics in nanoporous carbon materials: An application of the step potential electrochemical spectroscopy (SPECS) technique and electrochemical dilatometry



Przemysław Galek^a, Paulina Bujewska^a, Scott Donne^b, Krzysztof Fic^{a,*}, Jakub Menzel^{a,*}

^a Poznan University of Technology, Institute of Chemistry and Technical Electrochemistry, Berdychowo 4, Poznan 60965, Poland

^b University of Newcastle, Discipline of Chemistry, Callaghan NSW 2308, Australia

ARTICLE INFO

Article history:

Received 8 January 2021

Revised 1 March 2021

Accepted 7 March 2021

Available online 9 March 2021

Keywords:

Electrochemical capacitors

Electrochemical dilatometry

Carbon materials

Ionic liquids

ABSTRACT

This paper reports on the charging mechanism of an activated carbon electrode in a symmetric electrochemical capacitor operating in an ionic liquid electrolyte (EMIm⁺TFSI⁻). With the application of step potential electrochemical spectroscopy (SPECS) and electrochemical dilatometry, it is determined that the electrical double-layer formation mechanism strongly depends on the porous structure of the electrode material. Furthermore, SPECS calculations allow us to separate and quantify the charge component responsible for the ionic movement.

© 2021 The Authors. Published by Elsevier Ltd.

This is an open access article under the CC BY license (<http://creativecommons.org/licenses/by/4.0/>)

1. Introduction

In recent years, much attention has been paid to the development of electrochemical capacitors (ECs). ECs, characterized by high power, moderate energy, and an excellent life span, are considered either as an alternative or a good support system for electrochemical cells [1-3]. In contrast to other energy storage systems, the ECs charging/discharging process is achieved by the reversible attraction of ions at the electrode/electrode interface, as well as the formation of an electrical double-layer (EDL). As the capacitance of an EC is determined by the surface area accessible to ions, through the years many porous materials have been used to manufacture electrodes [4-8] including MXenes [9-15], transition metals [16-19] or carbon materials, such as graphene [20-25], nanotubes [26-30], nanoions [31,32], and carbide-derived carbon (CDC) [33-35]. However, due to its low production costs, the most applied electrode material is activated carbon [4,5,36-38].

To improve the performance of ECs, it is necessary to explore and describe the electrical double-layer formation mechanism in nanoconfined spaces. Research on this topic has been performed throughout the years, both with the application of theoretical modelling methods [39,40] and experimental in situ measurements, with such techniques as electrochemical quartz crystal

microbalance (EQCM) [41-44], electrochemical dilatometry [45,46], atomic force microscopy [47,48], and NMR studies [49-51]. It was determined that charge/discharge can be generally realized via two mechanisms: selective adsorption of the counterion or co-adsorption and desorption. This research was mostly realized with the application of ionic liquids (ILs) and organic solvent-based formulations as model electrolytes to observe both the dynamics of singular ions and the influence of the solvents. It was determined that cation and anion adsorption is different and highly related to the size and type of pores. Research performed with the application of CDCs with strict microporosity has shown that the charging mechanism differs with the pore size. In the case of research performed by Tsai et al. on materials with average pore sizes of 0.6 and 1 nm, the electrode charge was realized via a permselective mechanism for EMIm⁺ and an ion exchange for TFSI⁻ anions [41]. This conclusion was drawn from EQCM experiments, where the masses of the adsorbed anions and cations were compared to the theoretical prediction of the mass change required to charge the electrode. It was determined that charging of the negatively polarized electrode follows the theoretical trend; however, in the case of positive polarization, a lower mass of ions is involved. Moreover, in an experiment Jäckel N. applied a material with a strict 1.2 nm average pore diameter and found that while applying negative polarization, more cations entered than anions evacuated [46]. Finally, it was concluded that when close to the point of zero charge (PZC), small ions are more involved in the charging mechanism and are exchanged by larger ions, while for higher

* Corresponding authors.

E-mail addresses: krzysztof.fic@put.poznan.pl (K. Fic), jakub.menzel@put.poznan.pl (J. Menzel).

<https://doi.org/10.1016/j.electacta.2021.138115>

0013-4686/© 2021 The Authors. Published by Elsevier Ltd. This is an open access article under the CC BY license (<http://creativecommons.org/licenses/by/4.0/>)

potentials, counteranion adsorption is preferred. Recently, in research performed by Y. Wang et al., electrochemical dilatometry coupled with ^{19}F NMR was applied to describe the charge storage mechanism at the electrode/electrolyte interface. The EC with 1-ethyl-3-methyl-imidazolium ferrocenylsulfonyl-(trifluoromethylsulfonyl)-imide ($\text{EMIm}^+\text{FcTFSI}^-$) IL as the electrolyte and microporous activated carbon was investigated. The author showed that the pores were immediately filled with ions after soaking the electrode in the electrolyte. The system was polarized up to 1 V, and different ion movements were observed for the positive and negative electrodes: co-ion desorption with faradaic electron transfer was detected for the positive electrode, and counterion adsorption was detected for the negative electrode. Moreover, the charge storage mechanism for the positive electrode changed at an elevated voltage (2 V), where counterion adsorption was additionally assumed [49].

Step potential electrochemical spectroscopy (SPECS) is an electrochemical technique designed for the separation of Faradaic and non-Faradaic charge storage contributions in ECS, proposed in 2015 by S. Donne and M.F. Dupont [52,53]. The SPECS technique allows for deconvoluting the current response of the system into its components that correspond to the diffusion and activated controlled mechanisms of the charge storage. This technique has found the application in determining the mechanisms of charge storage [54], properties of activated carbons and the EC performance [55]. Application of SPECS demonstrates that the electrochemical properties of carbons might vary significantly with the temperature, current density, substrate and type of electrolyte. Additionally, SPECS technique found application in tracking of electrode structural changes related with formation of EDL and pseudocapacitance [56]. Furthermore, SPECS gives several advantages over conventional electrochemical techniques such as cyclic voltammetry or chronoamperometry [57].

Electrochemical dilatometry is an analytical technique [58], used for characterization of the electrode materials in energy storage devices. It allows the dimensional changes of the electrode during polarization to be monitored. This technique is suitable for an investigation of a different material types like graphite and graphitized materials [59–61], carbon nanotubes [62], activated carbons and activated carbon fibre cloth [60,61]. It was shown that the electrode height changes depend not only on the porosity of the materials but also on their density [60]. The results for different scan rates applied showed that the dilatation decreased with an increasing sweep rate [61].

Organic electrolytes are the most often used in recently reported dilatometric studies [60–65], most likely to avoid corrosion or other solvent-related issues. Generally, it is observed that cation insertion causes a higher electrode expansion than anion insertion. The impact of a solvent on dilatometric response was also described, based on acetonitrile and propylene carbonate (PC)-based electrolytes [60,65]. It appears that PC causes a higher electrode expansion than AN does. This fact can be easily explained by taking the AN and PC molecular size and volume of solvated cations and anions into account [66,67].

In this study, the ionic movement is measured via application of electrochemical dilatometry, and the quantification of the current responsible for ion transport is extracted by the SPECS technique. The utilization of the ionic liquid as an electrolyte allows us to observe the specific ionic interactions without a solvation shell. Additionally, considering the lack of redox activity in the applied electrolytes, the calculated SPECS parameters will only contribute to the charging of the electrical double-layer and ion diffusion in the porous structure. The correlation between the electrode volumetric changes and the calculated diffusion parameter allow us to quantify the charge responsible for ionic movement. A comparison of the electrochemical and volumetric responses in two car-

bons with comparable surface areas and different pore accessibilities provides new insight into the charge/discharge mechanisms at the electrode/electrolyte interface.

2. Experimental

2.1. Electrode preparation and characterization

The electrodes were prepared by mixing 95% activated carbon and 5% PTFE – 60% solution in water (Sigma Aldrich®, USA) as a binder. The electrodes were then prepared using a wet method followed by pressing to a 200 μm thickness and drying. Then, the self-standing, circular electrodes ($\varnothing = 10$ mm, 9.5 mg) were cut. Before the experiments, the electrodes were dried at 120 °C for 8 h in a vacuum to remove any moisture. Two types of active materials were applied: YP-50F (Kuraray®, Japan) and BP2000 (Cabot®, USA).

The nitrogen adsorption isotherm of the activated carbons was recorded by an ASAP 2460 analyser (Micromeritics®, USA) at 77 K. The specific surface area and the pore size distribution were calculated using the 2D nonlocal density functional theory (2D NLDFT) method. Both materials were characterized by a type I isotherm, which is characteristic of a microporous structure. Additionally, the 2D NLDFT surface area was ca. 1500 $\text{m}^2 \text{g}^{-1}$ for YP-50F and 1400 $\text{m}^2 \text{g}^{-1}$ for BP2000.

2.2. Electrochemical measurements

The electrochemical measurements were performed in a symmetric, two-electrode cell (Swagelok®, USA) with a reference electrode. Due to the application of aprotic electrolytes, an activated carbon-based quasi reference electrode (QRE) was applied. A piece of YP-50F carbon was placed at the perimeter of the separator between the working and counter electrodes and additionally separated by a Whatman GFA/D porous membrane. Contact with the potentiostat/galvanostat was provided via a platinum wire. The reference electrode was used to monitor the electrode potentials.

The $\text{EMIm}^+ \text{TFSI}^-$ ionic liquid (Solvionic®, France) with ~20 ppm water, measured by the Carl-Fisher method, was applied as the electrolyte. The electrodes were soaked in the electrolyte prior to measurement and separated by a GFA/D (Whatman®, UK) porous membrane. The electrochemical cells were set up in a moisture- and oxygen-free argon-filled glovebox (Jacomex®, France).

The electrochemical measurements were conducted with a computer-controlled multichannel potentiostat/galvanostat VMP3 (biologic®, France). The electrochemical systems were initially examined with the application of a galvanostatic charge/discharge within a 0.1–10 A g^{-1} current load, cyclic voltammetry at 1 and 10 mV s^{-1} scan rates, and electrochemical impedance spectroscopy (100 kHz–100 mHz for the ac frequency range and ± 5 mV for the voltage amplitude). All the current and capacitance values are expressed per mass of one electrode, if not stated otherwise.

The SPECS measurements were performed with the application of a series of 5-minute potentiostatic hold periods with 10 mV potential steps until the desired electrode potentials were achieved.

2.3. Electrochemical dilatometric measurements

Electrochemical dilatometric measurements were performed in an ECD-3-nano electrochemical dilatometer (EL-Cell®, Germany). The measurements were performed in a two-electrode configuration with a carbon QRE. The electrochemical measurements were performed after 6 h hold at constant potential in order to baseline stabilization. The cyclic voltammograms were recorded at 1 mV s^{-1} .

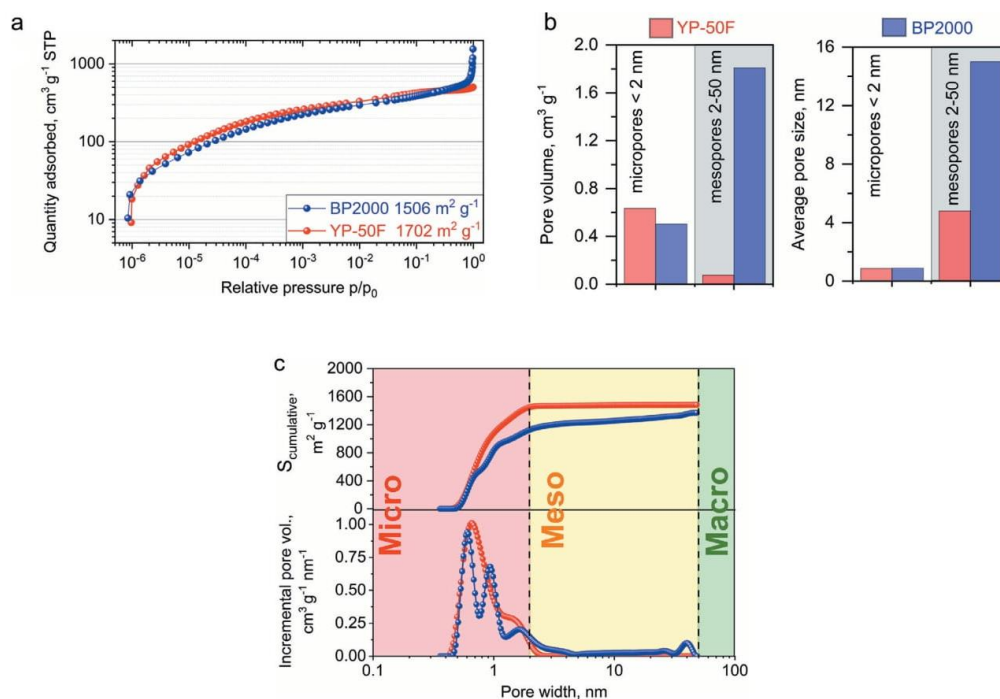


Fig. 1. (a) Nitrogen adsorption/desorption isotherm at 77 K; (b) pore volume and average pore size ratio of micro- to mesoporosity for the selected carbon materials; (c) cumulative surface area calculated with the NL-DFT method and corresponding pore size distributions.

3. Results and discussion

Two carbon materials were applied to prepare the electrodes for the EC: YP-50F (microporous) and BP2000 (micro/mesoporous). Fig. 1a shows the adsorption/desorption isotherms for both carbons, where one might observe that most of the gas adsorbs at a low relative pressure, indicating a significant share of micropores. In the case of YP-50F, the adsorption curve stabilizes, and a minimal amount of mesopores are involved in the N₂ adsorption process. However, for the BP2000 carbon, there is no stabilization of the adsorption curve, indicating adsorption in mesopores. Moreover, the significant increase in the gas quantity adsorbed above a relative pressure of 0.9 indicates the fraction of the macropores in the carbon structure. In Fig. 1b, the pore volume and the average pore size of both selected carbons are compared. Additionally, it can be seen that the micropore structures considering the volume and average pore size are similar. The main difference between the two carbons is the share of mesopores. The BP2000 is characterized by strongly developed mesoporous structures, while in the case of YP-50F, almost no mesopores are observed. Fig. 1c presents the cumulative surface area and the corresponding pore size distribution calculated by the 2D NLDFT model. In the case of the YP-50F, one can acknowledge a significant increase in the surface area of up to approximately 1500 m² g⁻¹ in the regime of micropores <2 nm, followed by a stabilization region for larger pores. For the BP2000, an initially similar build-up of the surface area is observed up to approximately 1200 m² g⁻¹. However, in this case, it is followed by a gradual increase due to the significant contribution of 2–50 nm mesopores up to approximately 1400 m² g⁻¹. Finally, both carbons are characterized by com-

parable NLDFT cumulative surface areas in the range of 1400 – 1500 m² g⁻¹.

The selection of the activated carbons was motivated to have two materials characterized by analogous surface areas but with different pore accessibility. It was desired that materials with different ion transport properties (provided by the different fractions of mesopores) be applied. YP-50F is a typical microporous flake-like material with “internal” microporosity. However, BP2000 is a carbon black with a high surface area and easily accessible “external” micropores.

The prepared electrochemical systems were examined with a SPECS technique in Swagelok® cells and by a CV technique with the application of an electrochemical dilatometer. The collective results of these investigations are presented in Fig. 2. The SPECS measurements were performed with using 10 mV steps and a 5-minute hold. The obtained current vs. time plots were used to calculate the capacitance, diffusion and residual parameters. The differential capacitance was divided into two modules, i.e., “geometric” and “porous” capacitance, which correspond to the easily and hardly accessible carbon surface areas, respectively. In the considered case, i.e., for the system without redox activity, the diffusion parameter corresponds to the charge required to promote ion movement. The time constant calculated as a product of cell resistance and capacitance refers to the minimum time necessary to fully charge the electrode and is divided into two modules: “geometric” and “porous”. The bottom graph represents the voltammetric response at a 1 mV s⁻¹ scan rate and the corresponding dilatometric changes of the working electrode.

Fig. 2a shows the collective data for the system operating with YP-50F activated carbon in the EMIm⁺TFSI⁻ ionic liquid electrolyte.

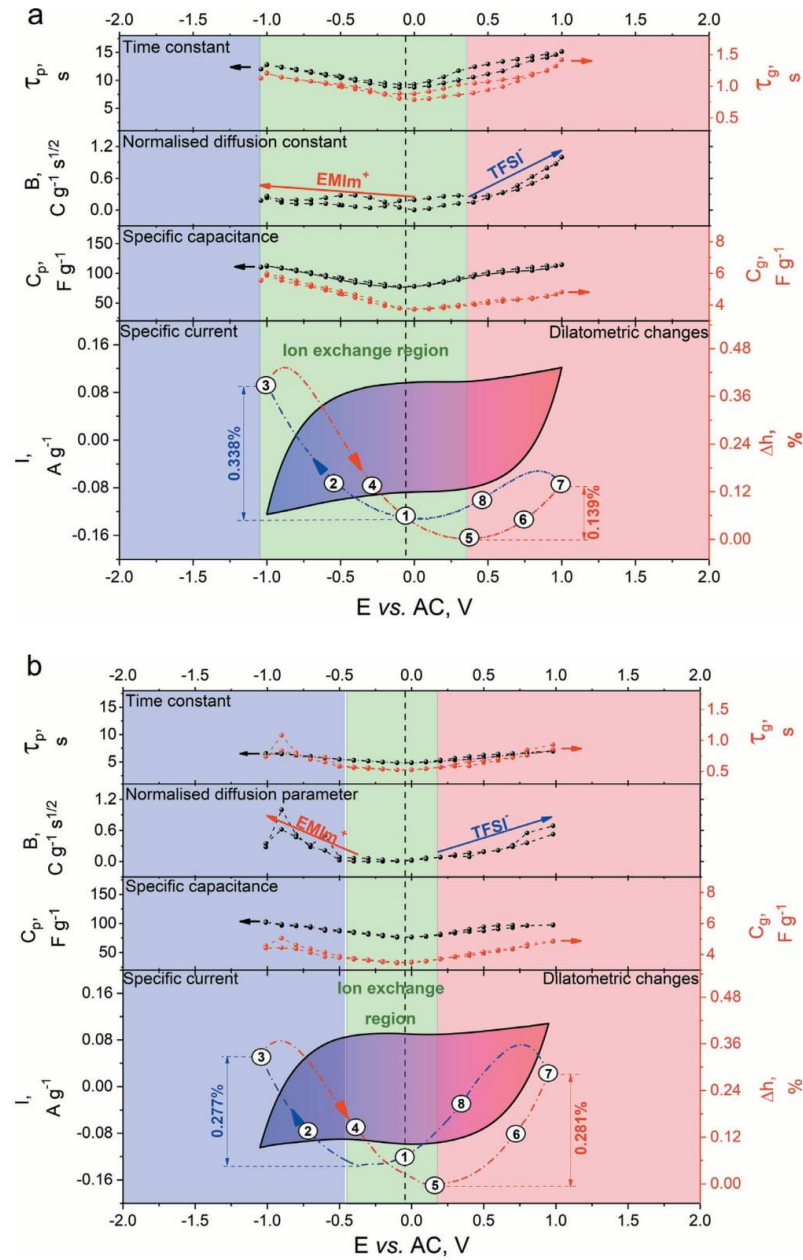


Fig. 2. Comparison of the calculated SPECS parameters (from the top: Time Constant, Normalised diffusion parameter, and Specific capacitance) and electrode dilatometry, and cyclic voltammetry characteristics for selected carbons: (a) YP-50F; (b) BP2000.

The selection of the electrolyte composition was determined by a similar anion and cation effective ion size, which was approximately 0.7 nm [70].

The system is characterized by the typical rectangular shape of cyclic voltammogram corresponding to the charge of the electrical double-layer. The potential limitation of the electrode was in the range of -1 to 1 V vs. AC QRE, which refers to the system being

charged up to 2 V. The 2 V limitation was applied to avoid any possible unwanted redox contribution, either from carbon functionalities or electrolyte decomposition.

The recorded dilatometric changes are comparable to the results obtained by other authors for this type of carbon material and ionic liquid [65]. In Fig. 2a, the results for the YP-50F carbon are presented. One may observe a larger displacement increase for

cathodic polarization than for anodic polarization, which are approximately 0.338% and 0.139%, respectively. First, the system was polarized from open circuit voltage (OCV) at 0 V towards negative potential values. One needs to acknowledge that the PZC, marked as "1" on the graph, determined by the lowest differential capacitance of the electrode, is not the same as the OCV, and it is shifted towards negative potentials. Further polarization leads to a gradual increase in both the "porous" and "geometric" differential capacitance, followed by a significant increase in the electrode displacement (points 2 and 3). Interestingly, the increasing trend of both the displacement and differential capacitance is not followed by a change in the diffusion parameter. This might suggest that the porous structure is occupied by both cations and anions. In this case, it might be concluded that electrode charging is realized via ion exchange and co-adsorption mechanisms. The change in polarization to the anode results in a typical dilatation hysteresis and a decrease in the displacement. After repolarization, the cations leave the active sites, and the system reaches PZC before reaching the minimum displacement. After changing the current flow, the TFSI⁻ anions are adsorbed at the carbon electrode/electrolyte interface and the differential capacitance increases. However, during the initial anion adsorption one can observe the displacement depression with the minimum of 0.4 V at point "5". This depression corresponds to the end of the ion exchange charge mechanism at the electrolyte/electrode interface. At this point, two phenomena need to be considered. First, the more mobile EMIm⁺ cations are easily adsorbed and desorbed from the microporous structure. Moreover, their movement is strongly determined by the electrode polarization direction. Second, heavy TFSI⁻ anions occupy the active sites in close proximity, and at the initial state of electrode charging, they exchange with cations that leave micropores. Anodic charging via an ion-exchange mechanism is realized until the micropores are deprived of available ions to adsorb. Further polarization promotes the charge realized via the permselective mechanism, and an insignificant increase in the displacement is observed. Moreover, it seems that selective adsorption is realized by sacrificing an additional charge to move the ions. Moreover, one may observe that both the cation to anion and anion to cation exchange regions are shifted towards more positive values. This additionally confirms that the more mobile EMIm⁺ cations enter the pores before heavy TFSI⁻ anions leave the carbon structure. The calculated time constant suggests that during the charge/discharge process only electrostatic interactions were involved. This thesis is supported by the noticeable regular increasing trend reflecting gradual penetration of porous structure. In case of the redox process the rapid fluctuations to higher time constant values would be observed, as a result of ongoing slow charge transfer process. Additionally, one might notice that the accessibility to the surface reflected by the "geometric" capacitance parameter is easier for EMIm⁺. Applying cathodic polarization results in a higher recorded "geometric" capacitance.

Interestingly, one can observe a significant increase in the diffusion parameter for cathodic polarization when heavy TFSI⁻ anions are adsorbed. However, the displacement change for the cathodic process is approximately 1/3 that of the anodic process. Keeping in mind that both anions and cations are characterized by similar effective volumes, it can be concluded that in the case of YP-50F activated carbon, the charging of the positive electrode is first realized via ion exchange mechanism and desorption of cation followed by permselective adsorption of anion. However, in the case of the negative electrode up to 1 V vs. QRE, the ion exchange and co-adsorption mechanisms are dominant. Additionally, an increase in the diffusion current for the permselective ion adsorption mechanism can be observed. This suggests that a greater charge is necessary to attract the selected ions into the porous structure. For the ion exchange adsorption mechanism, a stable charge is recorded

due to the unlimited ion accessibility at the electrode/electrolyte interface.

Fig. 2b presents the collective data for the system operating with BP2000 activated carbon in the EMIm⁺TFSI⁻ ionic liquid electrolyte. Similar to the aforementioned system, for this carbon, the characteristic rectangular shape of the cyclic voltammetry response was recorded, suggesting pure electrostatic charge accumulation mechanisms. However, one might observe a significant difference in the dilatometric response of the micro/mesoporous carbon material in comparison to YP-50F. In the case of the BP2000 carbon, the displacements for both the positive and negative electrodes are similar. As follows, it can be concluded that a similar number of cations and anions are involved in the charge accumulation process. Similar to the YP-50F case, for the BP2000 carbon, the PZC is shifted towards negative potential values. As in the previous system, first, cathodic polarization was applied to the electrode, promoting EMIm⁺ adsorption. One can observe a significant displacement increase as the charge storage process is involved (points 2 and 3). After reaching a potential of -1 V vs. QRE, the polarization is changed to anodic. The change in the polarization results in a typical delayed mass transport response observed at the maximum displacement recorded during the electrode discharge. Similar to the microporous carbon in the case of BP2000 carbon, there is a depression of the displacement beyond the PZC. However, in this case the minimum displacement (point "5") is close to the PZC and OCV. One can observe that the adsorption of TFSI⁻ anions results in a rapid increase in displacement up to 1 V vs. QRE. Again, as mentioned above, the change in polarization results in a delayed displacement response; however, it is more pronounced due to the large ionic mass of TFSI⁻. Interestingly, in contrast to the previous results, during cathodic polarization the anion-to-cation exchange point is in a small depression. Moreover, for *meso*/microporous carbon it is shifted towards more negative values. Such behaviour suggests undisturbed ion exchange mechanisms for both positive and negative polarization close to the PZC. One can additionally notice that a significant change in the diffusion parameter is recorded after both anions to cations and cations to anions exchange. The observed minimum diffusion parameter corresponds to the undisturbed ion exchange process. The calculated time constants in the range of 5 to 8 s for porous parameters exclude the possible impact of the red-ox activity on the recorded displacement and calculated diffusion parameter.

In the case of *meso*/microporous carbon for both the positive and negative electrodes, combined ion-exchange and permselective adsorption mechanisms can be observed. As mentioned above, the displacement changes for cathodic and anodic polarization are nearly identical, and the same can be noticed in the case of the diffusion parameter. This shows that in both cases, after initial ion exchange analogous volumes of the ions are selectively adsorbed with the same ease.

The present study has shown that the type of carbon material has a significant difference in terms of the ion adsorption mechanism determined by the porous structure of the activated carbon. In the case of a microporous material, anodic polarization promotes ion exchange with a co-adsorption mechanism, while for cathodic polarization, ion selective adsorption is the dominating mechanism. For the micro/mesopores, both electrodes are characterized by an analogous ion adsorption mechanism; ion exchange followed by permselective adsorption. Moreover, the ion transport properties are determined by the microscopic characteristics of the activated carbon material, rather than the electrolyte properties.

On one hand, the obtained results are in contrast to the data observed by W. Tsai et al. by application of EQCM where permselective adsorption was observed for EMIm⁺ ions, while TFSI⁻ adsorption was achieved via ion exchange with co-adsorption How-

ever, their experiment was performed on carbide-derived carbon electrodes with a strict 1 nm pore size [41].

On the other hand, our results are comparable to the data recorded by N. Jäckel et al. via application of EQCM, where the authors determined that when a negative potential is applied, more anions enter the pores than there are ejected cations. Thus, EMIm⁺ cations dominate during the charge/discharge process. Additionally, it was reflected in small dilatometric changes of the positive electrode. Notably, in this research novolac-derived carbon beads with narrow pore size distributions and 1.2 nm average pore sizes were applied. It seems that the increased pore size dimensions have a significant effect on the ion dynamics in the carbon material [46]. Moreover, A. C. Forse et al. applied NMR to study the spontaneous wetting of micropores in the case of YP-50F activated carbon. Additionally, as in our case for this carbon, the authors also observed the counterion adsorption and co-ion desorption mechanism [50].

In our case, we apply activated carbon with micropores in the range of 0.9 – 2 nm with a slight contribution of mesopores. Additionally, one needs to consider that the type of surface oxygen functionality determines the carbon adsorption properties and can influence the electrolyte pore penetration abilities.

Conclusions

Electrochemical dilatometry with the SPECS technique was applied to examine the EMIm⁺TFSI⁻ pristine electrolyte in two different activated carbon materials. The step voltage hold curves were deconvoluted and the differential components of the capacitance and diffusion parameters were calculated. The measured volumetric changes of the electrodes were in good arrangement with the published data by other authors. However, the analysis of the ion mobility driving forces led to a different conclusion compared to the data obtained for EQCM on model materials. Moreover, in the case of the examined materials different electrolyte behaviours were observed. However, in this study, by the deconvolution of the current with the application of the SPECS technique, the share of charge responsible for ion movement was extracted and compared with the corresponding dilatometric data. The performed experiments showed that the mass transport mechanisms are determined by the pore accessibility from the bulk of the electrode. In the case of microporous activated carbon, the EMIm⁺ cations were adsorbed via ion-exchange and co-adsorption mechanisms, while the TFSI⁻ anion was initially adsorbed via ion exchange followed by a permselective mechanism. The micro/mesoporous carbon anodic and cathodic polarization results in analogous ion adsorption mechanisms an ion-exchange followed by selective ion adsorption.

With the application of the SPECS technique, it was possible to extract and quantify the current responsible for charge transfer in the micropores of the carbon material. The obtained data are consistent with the literature data and provide new possibilities for measuring the ion transport mechanisms in nanoconfined spaces.

A comparison of the gathered and literature data shows that there is no universal description of the ion mobility and charge/discharge mechanism of the electrical double-layer in activated carbon. It can thus be concluded that it is a mixture of various mechanisms that depends on the pore size and accessibility, applied potential, and type of electrolyte.

CRedit author statement

Przemysław Galek: Visualization, Investigation, Writing - Review & Editing **Paulina Bujewska:** Investigation, Writing - Review & Editing **Scott Donne:** Validation, Methodology **Krzysztof Fic:** Funding acquisition, Project administration, Resources, Supervision **Jakub Menzel:** Conceptualization, Methodology, Software, Writing - Original Draft, Writing - Review & Editing, Supervision.

Declaration of Competing Interest

The authors declare that they have no known competing financial interests or personal relationships that could have appeared to influence the work reported in this paper.

Acknowledgements

The authors acknowledge the financial support from the European Commission and European Research Council received in the form of the Starting Grant (StG-2017, GA 759603).

References

- [1] P. Simon, Y. Gogotsi, Perspectives for electrochemical capacitors and related devices, *Nat. Mater.* 19 (11) (2020) 1151–1163.
- [2] P. Kurzweil, J. Schottenbauer, C. Schell, Past, present and future of electrochemical capacitors: pseudocapacitance, aging mechanisms and service life estimation, *J. Energy Storage* (2021) 102311.
- [3] J. Zhao, A.F. Burke, Electrochemical capacitors: materials, technologies and performance, *Energy Storage Mater.* 36 (2021) 31–55.
- [4] K. Fic, A. Platek, J. Piwek, E. Frackowiak, Sustainable materials for electrochemical capacitors, *Mater. Today* 21 (4) (2018) 437–454.
- [5] E. Frackowiak, F. Beguin, Carbon materials for the electrochemical storage of energy in capacitors, *Carbon N Y* 39 (6) (2001) 937–950.
- [6] Y.-Q. Dai, G.-C. Li, X.-H. Li, H.-J. Guo, Z.-X. Wang, G.-C. Yan, J.-X. Wang, Ultrathin porous graphitic carbon nanosheets activated by alkali metal salts for high power density lithium-ion capacitors, *Rare Met.* (2020).
- [7] Y.G. Wang, Y.F. Song, Y.Y. Xia, Electrochemical capacitors: mechanism, materials, systems, characterization and applications, *Chem. Soc. Rev.* 45 (21) (2016) 5925–5950.
- [8] C.C. Ji, H.Y. Mi, S.C. Yang, Latest advances in supercapacitors: from new electrode materials to novel device designs, *Chin. Sci. Bull. -Chin.* 64 (1) (2019) 9–34.
- [9] B. Anasori, M.R. Lukatskaya, Y. Gogotsi, 2D metal carbides and nitrides (MXenes) for energy storage, *Nat. Rev. Mater.* 2 (2) (2017).
- [10] Y. Dall'Agnese, P. Rozier, P.L. Taberna, Y. Gogotsi, P. Simon, Capacitance of two-dimensional titanium carbide (MXene) and MXene/carbon nanotube composites in organic electrolytes, *J. Power Sources* 306 (2016) 510–515.
- [11] C.F. Zhang, M.P. Kremer, A. Seral-Ascaso, S.H. Park, N. McEvoy, B. Anasori, Y. Gogotsi, V. Nicolosi, Stamping of flexible, coplanar micro-supercapacitors using MXene inks, *Adv. Funct. Mater.* 28 (9) (2018).
- [12] L.-Y. Xiu, Z.-Y. Wang, J.-S. Qiu, General synthesis of MXene by green etching chemistry of fluoride-free Lewis acidic melts, *Rare Met.* 39 (11) (2020) 1237–1238.
- [13] Z.F. Lin, P. Rozier, B. Duployer, P.L. Taberna, B. Anasori, Y. Gogotsi, P. Simon, Electrochemical and in-situ X-ray diffraction studies of Ti3C2Tx MXene in ionic liquid electrolyte, *Electrochim. Commun.* 72 (2016) 50–53.
- [14] Z. Ling, C.E. Ren, M.Q. Zhao, J. Yang, J.M. Giammarco, J. Qiu, M.W. Barsoum, Y. Gogotsi, Flexible and conductive MXene films and nanocomposites with high capacitance, *Proc. Natl. Acad. Sci. U S A* 111 (47) (2014) 16676–16681.
- [15] G.S. Gund, J.H. Park, R. Harpalsinh, M. Kota, J.H. Shin, T.I. Kim, Y. Gogotsi, H.S. Park, MXene/polymer hybrid materials for flexible AC-filtering electrochemical capacitors, *Joule* 3 (1) (2019) 164–176.
- [16] G.F. Ma, H. Peng, J.J. Mu, H.H. Huang, X.Z. Zhou, Z.Q. Lei, In situ intercalative polymerization of pyrrole in graphene analogue of MoS2 as advanced electrode material in supercapacitor, *J. Power Sources* 229 (2013) 72–78.
- [17] M.A. Bissett, I.A. Kinloch, R.A.W. Dryfe, Characterization of MoS2-graphene composites for high-performance coin cell supercapacitors, *ACS Appl. Mater. Interfaces* 7 (31) (2015) 17388–17398.
- [18] E.E. Miller, Y. Hua, F.H. Tezel, Materials for energy storage: review of electrode materials and methods of increasing capacitance for supercapacitors, *J. Energy Storage* 20 (2018) 30–40.
- [19] H. Liu, X. Liu, S. Wang, H.-K. Liu, L. Li, Transition metal based battery-type electrodes in hybrid supercapacitors: a review, *Energy Storage Mater.* 28 (2020) 122–145.
- [20] G.K. Maron, J.H. Alano, B. da Silveira Noremberg, L. da Silva Rodrigues, V. Stolojan, S.R.P. Silva, N.L. Villarreal Carreño, Electrochemical supercapacitors based on 3D nanocomposites of reduced graphene oxide/carbon nanotube and ZnS, *J. Alloys Compd.* 836 (2020) 155408.
- [21] M. Parmeggiani, P. Zaccagnini, S. Stassi, M. Fontana, S. Bianco, C. Nicosia, C.F. Pirri, A. Lamberti, PDMS/polyimide composite as an elastomeric substrate for multifunctional laser-induced graphene electrodes, *ACS Appl. Mater. Interfaces* 11 (36) (2019) 33221–33230.
- [22] A. Viswanathan, B.G. Prakasahiah, V. Subburaj, A.N. Shetty, High energy reduced graphene oxide/vanadium Pentoxide/polyaniline hybrid supercapacitor for power backup and switched capacitor converters, *J. Colloid Interface Sci.* 545 (2019) 82–93.
- [23] T. Beyazay, F.E.S. Oztuna, U. Unal, Self-standing reduced graphene oxide papers electrodeposited with manganese oxide nanostructures as electrodes for electrochemical capacitors, *Electrochim. Acta* 296 (2019) 916–924.

- [24] F.Y. Chi, C. Li, Q.Q. Zhou, M. Zhang, J. Chen, X.W. Yu, G.Q. Shi, Graphene-based organic electrochemical capacitors for AC line filtering, *Adv. Energy Mater.* 7 (19) (2017) 7.
- [25] Q.Q. Zhou, M.M. Wu, M. Zhang, G.C. Xu, B.W. Yao, C. Li, G.Q. Shi, Graphene-based electrochemical capacitors with integrated high-performance, *Mater. Today Energy* 6 (2017) 181–188.
- [26] E. Iwama, N. Kawabata, N. Nishio, K. Kisu, J. Miyamoto, W. Naoi, P. Rozier, P. Simon, K. Naoi, Enhanced electrochemical performance of ultracentrifugation-derived nc-Li 3 VO 4 /MWCNT composites for hybrid supercapacitors, *ACS Nano* 10 (5) (2016) 5398–5404.
- [27] C.M. Ghimbeu, E. Raymundo-Pinero, P. Fioux, F. Beguin, C. Vix-Guterl, Vanadium nitride/carbon nanotube nanocomposites as electrodes for supercapacitors, *J. Mater. Chem.* 21 (35) (2011) 13268–13275.
- [28] C. Emmenegger, P. Mauron, P. Sudan, P. Wenger, V. Hermann, R. Gallay, A. Zuttel, Carbon nanotubes as active electrode material, *Processing and Fabrication of Adv. Mater.* Xi (2003) 480–491.
- [29] R. Vicentini, W.G. Nunes, L.H. da Costa, L.M. Da Silva, B. Freitas, A.M. Pascon, O. Vilas-Boas, H. Zanin, Multi-walled carbon nanotubes and activated carbon composite material as electrodes for electrochemical capacitors, *J. Energy Storage* 33 (2021) 100738.
- [30] D.D. Potphode, L. Sinha, P.M. Shirage, Redox additive enhanced capacitance: multi-walled carbon nanotubes/polyaniline nanocomposite based symmetric supercapacitors for rapid charge storage, *Appl. Surf. Sci.* 469 (2019) 162–172.
- [31] Y. Gao, Y.S. Zhou, M. Qian, X.N. He, J. Redepenning, P. Goodman, H.M. Li, L. Jiang, Y.F. Lu, Chemical activation of carbon nano-onions for high-rate supercapacitor electrodes, *Carbon N Y* 51 (2013) 52–58.
- [32] G. Moussa, C.M. Ghimbeu, P.L. Taberna, P. Simon, C. Vix-Guterl, Relationship between the carbon nano-onions (CNOs) surface chemistry/defects and their capacitance in aqueous and organic electrolytes, *Carbon N Y* 105 (2016) 628–637.
- [33] P.C. Gao, W.Y. Tsai, B. Daffos, P.L. Taberna, C.R. Perez, Y. Gogotsi, P. Simon, F. Favier, Graphene-like carbide derived carbon for high-power supercapacitors, *Nano Energy* 12 (2015) 197–206.
- [34] C.R. Perez, S.H. Yeon, J. Segalini, V. Presser, P.L. Taberna, P. Simon, Y. Gogotsi, Structure and electrochemical performance of carbide-derived carbon nanopowders, *Adv. Funct. Mater.* 23 (8) (2013) 1081–1089.
- [35] C. Portet, M.A. Lillo-Rodenas, A. Linares-Solano, Y. Gogotsi, Capacitance of KOH activated carbide-derived carbons, *Phys. Chem. Chem. Phys.* 11 (25) (2009) 4943–4945.
- [36] P. Ratajczak, M.E. Suss, F. Kaasik, F. Beguin, Carbon electrodes for capacitive technologies, *Energy Storage Mater.* 16 (2019) 126–145.
- [37] F. Béguin, V. Presser, A. Balducci, E. Frackowiak, Carbons and electrolytes for advanced supercapacitors, *Adv. Mater.* 26 (14) (2014) 2219–2251.
- [38] C.F. Liu, Y.C. Liu, T.Y. Yi, C.C. Hu, Carbon materials for high-voltage supercapacitors, *Carbon N Y* 145 (2019) 529–548.
- [39] E. Lahrar, A. Belhboub, P. Simon, C. Merlet, Ionic liquids under confinement: from systematic variations of the ion and pore sizes toward an understanding of the structure and dynamics in complex porous carbons, *ACS Appl. Mater. Interfaces* 12 (1) (2020) 1789–1798.
- [40] A.C. Forse, C. Merlet, J.M. Griffin, C.P. Grey, New perspectives on the charging mechanisms of supercapacitors, *J. Am. Chem. Soc.* 138 (18) (2016) 5731–5744.
- [41] W.Y. Tsai, P.L. Taberna, P. Simon, Electrochemical quartz crystal microbalance (EQCM) study of ion dynamics in nanoporous carbons, *J. Am. Chem. Soc.* 136 (24) (2014) 8722–8728.
- [42] N. Shpigel, M.D. Levi, S. Sigalov, L. Daikhin, D. Aurbach, In situ real-time mechanical and morphological characterization of electrodes for electrochemical energy storage and conversion by electrochemical quartz crystal microbalance with dissipation monitoring, *Acc. Chem. Res.* 51 (1) (2018) 69–79.
- [43] T. Le, D. Aradilla, G. Bidan, F. Billon, M. Delaunay, J.M. Gerard, H. Perrot, O. Sel, Unveiling the ionic exchange mechanisms in vertically-oriented graphene nanosheet supercapacitor electrodes with electrochemical quartz crystal microbalance and ac-electrogravimetry, *Electrochem. Commun.* 93 (2018) 5–9.
- [44] J.L. Ye, Y.C. Wu, K. Xu, K. Ni, N. Shu, P.L. Taberna, Y.W. Zhu, P. Simon, Charge storage mechanisms of single-layer graphene in ionic liquid, *J. Am. Chem. Soc.* 141 (42) (2019) 16559–16563.
- [45] M.M. Hantel, V. Presser, R. Kotz, Y. Gogotsi, In situ electrochemical dilatometry of carbide-derived carbons, *Electrochem. Commun.* 13 (11) (2011) 1221–1224.
- [46] N. Jackel, S.P. Emge, B. Krüner, B. Roling, V. Presser, Quantitative information about electroadsorption of ionic liquids in carbon nanopores from electrochemical dilatometry and Quartz crystal microbalance measurements, *J. Phys. Chem. C* 121 (35) (2017) 19120–19128.
- [47] T.M. Arruda, M. Heon, V. Presser, P.C. Hillesheim, S. Dai, Y. Gogotsi, S.V. Kalinin, N. Balke, In situ tracking of the nanoscale expansion of porous carbon electrodes, *Energy Environ. Sci.* 6 (1) (2013) 225–231.
- [48] J.M. Black, G. Feng, P.F. Fulvio, P.C. Hillesheim, S. Dai, Y. Gogotsi, P.T. Cummings, S.V. Kalinin, N. Balke, Strain-based in situ study of anion and cation insertion into porous carbon electrodes with different pore sizes, *Adv. Energy Mater.* 4 (3) (2014).
- [49] Y. Wang, D. Rochefort, Solid-state NMR and electrochemical dilatometry study of charge storage in supercapacitor with redox ionic liquid electrolyte, *Energy Storage Mater.* 20 (2019) 80–88.
- [50] A.C. Forse, J.M. Griffin, C. Merlet, P.M. Bayley, H. Wang, P. Simon, C.P. Grey, NMR study of ion dynamics and charge storage in ionic liquid supercapacitors, *J. Am. Chem. Soc.* 137 (22) (2015) 7231–7242.
- [51] J.M. Griffin, A.C. Forse, W.Y. Tsai, P.L. Taberna, P. Simon, C.P. Grey, In situ NMR and electrochemical quartz crystal microbalance techniques reveal the structure of the electrical double layer in supercapacitors, *Nat. Mater.* 14 (8) (2015) 812–+.
- [52] M.F. Dupont, S.W. Donne, Separating faradaic and non-faradaic charge storage contributions in activated carbon electrochemical capacitors using electrochemical methods I. Step potential electrochemical spectroscopy, *J. Electrochem. Soc.* 162 (7) (2015) A1246–A1254.
- [53] M. Forghani, S.W. Donne, Modification of the step potential electrochemical spectroscopy analysis protocol to improve outcomes, *J. Electrochem. Soc.* 166 (13) (2019) A2727–A2735.
- [54] A.J. Gibson, S.W. Donne, A step potential electrochemical spectroscopy (SPECS) investigation of anodically electrodeposited thin films of manganese dioxide, *J. Power Sources* 359 (2017) 520–528.
- [55] M.A. Hughes, J.A. Allen, S.W. Donne, The properties of carbons derived through the electrolytic reduction of molten carbonates under varied conditions: part I. A study based on step potential electrochemical spectroscopy, *J. Electrochem. Soc.* 165 (11) (2018) A2608–A2624.
- [56] A.J. Gibson, M.F. Dupont, R.J. Wood, Q. Gu, A.P. Cameron, S.W. Donne, A synchrotron X-ray powder diffraction and step potential electrochemical spectroscopy study on the change in manganese dioxide capacitive behaviour during cycling, *Electrochim. Acta* 260 (2018) 630–639.
- [57] M.A. Hughes, J.A. Allen, S.W. Donne, The properties and performance of carbon produced through the electrochemical reduction of molten carbonate: a study based on step potential electrochemical spectroscopy, *Electrochim. Acta* 278 (2018) 340–351.
- [58] A. Métrot, P. Willmann, A. Hérodin, Insertion électrochimique du complexe BF₃(C₂H₅)₂O dans un pyrographite, *Mater. Sci. Eng.* 31 (1977) 83–86.
- [59] W. Biberacher, A. Lerf, J.O.M. Besenhard, H. Möhwald, T. Butz, A high resolution dilatometer for in situ studies of the electrointercalation of layered materials, *Mater. Res. Bull.* 17 (11) (1982) 1385–1392.
- [60] M. Hahn, O. Barbieri, R. Gallay, R. Kötz, A dilatometric study of the voltage limitation of carbonaceous electrodes in aprotic EDLC type electrolytes by charge-induced strain, *Carbon N Y* 44 (2006) 2523–2533.
- [61] M. Hahn, O. Barbieri, F.P. Campana, R. Kötz, R. Gallay, Carbon based double layer capacitors with aprotic electrolyte solutions: the possible role of intercalation/insertion processes, *Appl. Phys. A* 82 (4) (2006) 633–638.
- [62] P.W. Ruch, R. Kötz, A. Wokaun, Electrochemical characterization of single-walled carbon nanotubes for electrochemical double layer capacitors using non-aqueous electrolyte, *Electrochim. Acta* 54 (19) (2009) 4451–4458.
- [63] P.W. Ruch, D. Cericola, A. Foelske, R. Kötz, A. Wokaun, A comparison of the aging of electrochemical double layer capacitors with acetonitrile and propylene carbonate-based electrolytes at elevated voltages, *Electrochim. Acta* 55 (2010) 2352–2357.
- [64] M.M. Hantel, R. Nesper, A. Wokaun, R. Kötz, In-situ XRD and dilatometry investigation of the formation of pillared graphene via electrochemical activation of partially reduced graphite oxide, *Electrochim. Acta* 134 (2014) 459–470.
- [65] M.M. Hantel, D. Weingarth, R. Kötz, Parameters determining dimensional changes of porous carbons during capacitive charging, *Carbon N Y* 69 (2014) 275–286.
- [66] Y.-J. Kim, Y. Masuzawa, S. Ozaki, M. Endo, M.S. Dresselhaus, PVDC-based carbon material by chemical activation and its application to non-aqueous EDLC, *J. Electrochem. Soc.* 151 (6) (2004) E199.
- [67] J.A. Gardecki, M. Maroncelli, Solvation and rotational dynamics in acetonitrile/propylene carbonate mixtures: a binary system for use in dynamical solvent effect studies, *Chem. Phys. Lett.* 301 (5) (1999) 571–578.

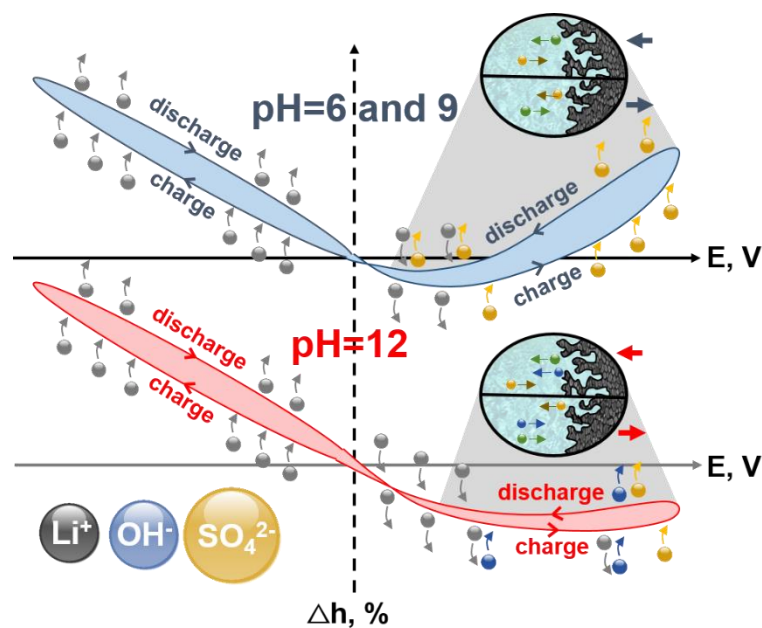
10. Article A5

Title: ***Impact of electrolyte pH on the ion population at the electrode/electrolyte interface monitored by electrochemical dilatometry***

Authors: Paulina Bujewska, Przemysław Galek, Krzysztof Fic

Journal: unpublished, restricted access until 29.09.2022

DOI: -



Motivation

Aqueous solutions are often used as electrolytes in ECs because of safety and ecological issues [209]. The best energy/power/cycle life performance is reported when neutral pH electrolytes are used [210, 211]. Papers published to date indicate that the electrode porosity should match the a respective ion size. However, the question of which ions should be taken into account in such considerations is still open. In IL-based systems, the situation seems to be relatively straightforward, since only cations and anions, making an IL structure, are present in the electrolyte. In the case of electrolytes based on aqueous solutions, more factors must be considered: ions from a dissolved salt, their solvation shell, which certainly vary depending on several conditions, and hydrogen-based cations (H^+ , H_3O^+) as well as hydroxyl groups (OH^-) coming

from water itself. To determine ionic fluxes within electrodes, different techniques can be adopted, e.g., electrochemical quartz crystal microbalance (EQCM), electrochemical dilatometry (ECD), scanning electrochemical microscopy (SECM), coupled with solid-state NMR or Raman spectroscopy.

Summary

Article A5 – *‘Impact of electrolyte pH on the ion population at the electrode/electrolyte interface monitored by electrochemical dilatometry’* in a comprehensive way presents the impact of OH^- and H^+ ions concentration in aqueous electrolyte on charge storage possibilities and ion flow in bulk of porous carbon electrodes. The EC performance is strongly dependent on the electrolyte pH. There is a significant alkalization of the electrolyte pH near the electrode during EC operation. It was concluded that the higher the pH of the electrolyte, the higher the OH^- contribution to EDL formation. Furthermore, the transport of SO_4^{2-} anions requires a very high driving force and causes irreversible changes within the texture of the material. The EC operating in an electrolyte of pH 6 is more stable and the electrode’s textural changes are reversible, even at very harsh conditions. The trend was shown to be comparable for electrolytes of pH 6 and 9. However, ECs with the pH 12 solution exhibit similar behaviour to the LiOH solution, suggesting that during positive polarization, the primary role is played by OH^- – despite the same salt concentration. Therefore, we conclude that different ions (or ions with various solvation shells) participate in the formation of EDL. This result raises an essential concern for the actual ion population at the electrode/electrolyte interface, which affects the water decomposition potential and triggers various parasitic reactions that impact the long-term performance.

Impact of electrolyte pH on the ion population at the electrode/electrolyte interface monitored by electrochemical dilatometry

Paulina Bujewska, Przemyslaw Galek, Krzysztof Fic*

Poznan University of Technology, Institute of Chemistry and Technical Electrochemistry, Berdychowo 4, 60965, Poland

*Corresponding author: krzysztof.fic@put.poznan.pl

Keywords

Electrochemical capacitors; Electrochemical dilatometry; Step potential electrochemical spectroscopy; Ionic fluxes; pH influence

Abstract

Electrode height changes in electrochemical capacitors (ECs) strongly depend on the electrolyte pH. Hence, different ions (or ions with various solvation shells) participate in EDL formation. In this work, operando electrochemical dilatometry (ECD) experiments, incorporating various electrochemical techniques like cyclic voltammetry, large amplitude sinusoidal voltammetry (LASV) and step potential electrochemical spectroscopy (SPECS) were performed for the ECs operating in $1 \text{ mol L}^{-1} \text{ Li}_2\text{SO}_4$ of different pH (6, 9 and 12) and $1 \text{ mol L}^{-1} \text{ LiOH}$ (for comparative purposes); a microporous carbon (Kuraray® YP-80F) was used as an electrode material. It was shown that the trend is comparable for electrolytes of pH 6 and 9; however, the cell with the solution of pH 12 exhibits similar behavior to LiOH solution, suggesting that during positive polarization, the primary role is played by OH^- – despite the same salt concentration. This result raises an essential concern of the actual ion population at the electrode/electrolyte interface, affecting the water decomposition potentials and triggers various parasitic reactions impacting the long-term electrochemical capacitors performance.

1. Introduction

The increase in energy consumption in recent years has caused a great deal of interest in energy harvesting, conversion, and storage devices. As part of sustainable development, the trend is towards the search for environmentally friendly solutions due to the depletion of natural resources and environmental issues [1-4]. For example, lithium is often replaced by sodium or potassium in batteries [5-8] and aqueous solutions are used as electrolytes instead of organic ones in electrochemical capacitors (ECs) [9-14]. Undoubtedly, progress in materials research for ECs requires extensive fundamental knowledge and insightful study, but it is not only about the development of materials with promising metrics. The key is to match the properties of the electrode material with the electrolytic solution. Considerations on the pore diameter versus the size and number of ions at the interface are crucial for the device performance improvement. Hence, a comprehensive description of ionic fluxes at the electrode/electrolyte interface during polarization is of great importance. There are numerous reports in the literature regarding the reasons for fading of EC performance, shortening of cycle life, or increased self-discharge under different medium and operating conditions [15-18]. Various research pathways, including different techniques, can be taken for the fundamental studies on the interface between the carbon electrode and the electrolytic

solution, as well as for an explanation of the ageing mechanisms in ECs. Such considerations quite often use a sophisticated approach; lately, *postmortem* analyzes are coupled with *in situ* experiments [19-26]. Nuclear magnetic resonance spectroscopy (NMR) [27-29], X-ray neutron scattering [30-32], Raman spectroscopy [12, 33], atomic force microscopy [34, 35], electrochemical quartz crystal microbalance (EQCM) [22, 36-41] or electrochemical dilatometry (ECD) [20, 27, 42-46] are powerful techniques that provide insightful information on charge storage in ECs. However, published papers mainly concern ionic liquid-based systems (ILs) or organic electrolyte-based systems. It has been found that during the EC charging, the cations are indeed adsorbed at the negative electrode, while at the positive electrode this mechanism is more complicated. At low potential values (near so-called point of zero charge), the ion-mixing effect, i.e., cation desorption coupled with anion adsorption, is observed. The potential range of ion mixing depends on the electrolyte composition, in the case of water-based electrolytes, but also on an electrode material used: its accessible surface area and pore size distribution. With further potential increase, anion adsorption is assumed, playing an important role in electrode charge balancing; however, cations are still expelled from the material porosity or the electrode surface [20, 22, 27, 47-49]. The differences in charge storage mechanism during the electrode polarization are clearly reflected in the volumetric changes

1

of the electrode. The effect of solvent on the volumetric changes of the electrode studied in an organic medium is well pronounced; the larger the solvent molecules, the greater the electrode expansion [42, 43]. It is worth mentioning that the solvent effect was much more pronounced for the negatively polarized electrode than for the positively polarized one. However, solvent molecules were detected within the porosity of the material regardless the direction of polarization [43]. These results allow for the assumption of the significant impact of electrolyte pH on ionic fluxes and the charge storage mechanism in aqueous-based EC.

The charge storage and ionic fluxes at the porous electrode/aqueous electrolyte interface are affected by many factors and the electrolyte pH is one of the most important ones. It has been claimed that in a pH-neutral electrolytic solution, it is possible to increase the maximum operating voltage of the cell above the theoretical voltage of water decomposition (1.23 V). This is attributed to the balance between H_3O^+ and OH^- species, strong ion-solvent interactions and other factors such as reversible hydrogen electroadsorption on the negative electrode. For electrolytes of acidic or alkaline pH, the oxygen and hydrogen evolution overpotentials are low and several unwanted reactions (hydrogen/oxygen evolution, carbon oxidation, and electrolyte decomposition) even at low capacitor voltage may occur. Moreover, extreme pH values negatively impact current collectors; typical corrosion is expected at low pH, whereas a passive layer can introduce another resistive component at high pH. Both impede the current flow between the current collector and the electrode, resulting in high cell resistance. The possible issues listed above have a negative impact on the cycle life of ECs. However, it should be noted that even under relatively mild conditions (pH between 6-9), the local pH changes nearly polarized electrode affect EC performance and shorten its life [50].

Since several decades pH has been considered as a 'measure' of hydrogen ion concentration/activity ($pH = -\log[C_{H^+}]$); it is clear that each increase in pH unit means an increase of an order of magnitude in H^+ concentration. Of course, the concentration of hydroxyl groups also varies with the change in pH ($pH + pOH = 14$). Variable concentrations of H^+ and OH^- can significantly impact the charge storage mechanism because not only ions that come from the salt dissolved in water can play the role of charge carriers. Interestingly, in EC operating in acidic electrolyte, the EQCM detected an increased contribution of protons (H^+), or to be more specific – hydrated protons (H_3O^+) [51, 52], in electrode charge balancing [22, 47]. A similar effect was observed for alkaline-based electrolytes; the charge at the positively polarized electrode is (partially) balanced by OH^- anions [22].

Taking into account that the concentrations of H^+ and OH^- are definitely lower than the concentrations of dissolved salt, one should consider further electrode

charge balancing by cation and anions coming from the salt used. A significant contribution of protons and hydroxide anions in charge storage is attributed to their outstanding ionic mobility. Theoretically, the smaller the ion, the stronger its interactions with water molecules; hence, the hydrated diameters of (smaller) bare ions are *de facto* notably larger [53]. The comparison of ionic diameter and ion mobility for the proton with Li^+ cation and hydroxide with SO_4^{2-} anions is presented in Fig. 1.

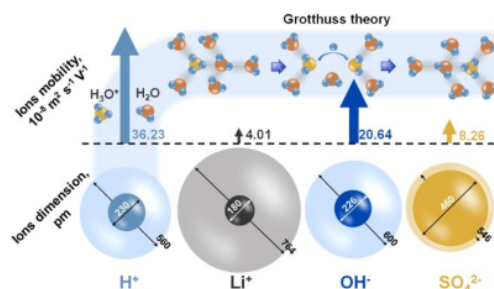


Fig. 1. Diameter of the selected bare and solvated ions and their mobility [51-53]; mechanism of proton transfer based on the Grotthuss theory.

The proton (hydrated or not), as an ion always smaller than Li^+ , is supposed to be more mobile. However, there is a huge difference in their mobility: the value is almost one order of magnitude higher for H^+ : $36.23 \text{ vs. } 4.01 \cdot 10^{-8} \text{ m}^2 \text{ s}^{-1} \text{ V}^{-1}$. Similar observation can be made for OH^- and SO_4^{2-} mobility. The diameter of these anions in hydrated form is comparable, whereas the mobility of OH^- is definitely higher ($20.64 \text{ vs. } 8.29 \cdot 10^{-8} \text{ m}^2 \text{ s}^{-1} \text{ V}^{-1}$, respectively). Note that the values presented refer to the nondiffusive transport of these ions. The behavior of protons in water is described by the Grotthuss mechanism, in which a proton from a hydronium ion 'diffuses' through a hydrogen bond (network) to another water molecule (schematically presented in Fig. 1). An analogous mechanism for the hydroxide anion was described [51, 52] and explains its high mobility.

It should be taken into account that, depending on the pH of the solution, the number of cations and anions solvated so that their mobility, as well as their affinity to solvent molecules, can change. Therefore, it seems reasonable to consider ionic fluxes under various pH conditions.

Measuring the height change of the electrode during EC operation is expected to be extremely helpful in describing the processes ongoing at the electrode/electrolyte interface. Nevertheless, a solely volumetric probing of the electrode is not sufficient for a detailed description of the EC charging mechanism because no information on surface interactions is provided by such a study. As already presented, step potential electrochemical spectroscopy (SPECS), developed by Donne and Dupont, allows the current and capacitance to be resolved into several

components – related to electric double-layer (EDL) formation, ion diffusion, and other residual processes [56, 57]. Hence, the SPECS data considered with the dilatometry results enable identifying and quantifying the ions responsible for the formation of EDL at the surface of the porous material and within pores. Thus, merging both techniques allows correlation of the calculated diffusion parameter with the observed ionic fluxes [20].

In this paper, the results from *operando* electrochemical dilatometry coupled with SPECS are presented. These two techniques were applied to better understand and describe the fundamental aspects concerning the behavior and solvation effect of cations and anions at various electrolyte pH. The results of this work provide useful information in the development of energy storage and conversion devices.

2. Experimental

2.1. Electrode material and electrolyte

An activated carbon (AC) YP-80 F (Kuraray[®], Japan) was used as the electrode material for the electrochemical tests. The AC (97%) was mixed with a binder (3%) – 60% polytetrafluoroethylene (PTFE) solution in water (Sigma Aldrich[®], USA) in ethanol (96%, POCH[®], USA) as a solvent. The slurry was mixed at an elevated temperature (70°C) until the solvent evaporated. The powder was then wet with ethanol and the material was rolled to a film of 250 μm thickness. The electrodes of 10 mm diameter (~9 mg) were cut and dried at 120°C for 8 h.

Electrodes were characterized with N_2 adsorption-desorption at 77 K (ASAP 2460, Micromeritics[®], USA). The specific surface area was calculated using the Brunauer-Emmett-Teller (BET) equation; two-dimensional non-local density functional theory (2DNLDFT) was used to determine the distribution of pore size within the material [58, 59].

Electrodes were investigated in several aqueous solutions: 1 mol L⁻¹ Li_2SO_4 ($\geq 98\%$, Sigma Aldrich[®], USA) of different pH – 6, 9 and 12, and in 1 mol L⁻¹ LiOH ($\geq 98\%$, Sigma Aldrich[®], USA) of pH 12. Electrolytes were prepared by dissolution of salt or LiOH in water. The initial pH (9) of Li_2SO_4 was adjusted to pH 6 with H_2SO_4 (95%, POCH[®], USA) and to pH 12 with LiOH.

The pH of the electrolytes was measured with the S220 SevenCompact pH meter (a relative accuracy ± 0.002 , Mettler Toledo[™]; USA) at ambient temperature.

2.2. Electrochemical dilatometry

Operando electrochemical experiments were performed on the high-resolution (5 nm) electrochemical dilatometer ECD-3-nano (EI-Cell[®], Germany) to measure the height change of the electrodes during polarization. The electrodes were separated by a stiff glass frit and a 0.26mm thick

GF/A glass microfiber membrane with a pore size 1.6 μm (Whatman[®], UK). Charge-induced height changes of the working electrode were monitored. It is noteworthy that the glass frit is fixed in position, hence the dimensional change of the counter electrode did not affect the measurement. The experiments were performed in a two-electrode configuration with the AC YP-80F-based *quasi* reference electrode (hereinafter denoted as AC). Before the electrochemical tests, the cell was kept at constant voltage for 6 hours to allow baseline stabilization. The electrode height change is expressed as a percentage, on the basis of its thickness, or as a direct micrometric change.

2.3. Electrochemical protocols

Computer-controlled multichannel potentiostat/galvanostat VMP3 (BioLogic[®], France) was used for electrochemical investigations. The experiments were controlled by EC-Lab[®] software (BioLogic[®], France).

Electrochemical techniques

The electrochemical studies involved cyclic voltammetry (CV) at 1 mV s⁻¹ in two-electrode configuration and 0.5 mV s⁻¹ in three-electrode configuration. To gain more detailed information, large amplitude sinusoidal voltammetry (LASV) was used. In this technique, the scan rate is determined by applied frequency. The frequency (0.15 mHz) was adjusted to reproduce the scan rate applied in CV, since dilatometric changes strongly depend on this parameter.

Raman spectroscopy

Operando Raman spectroscopy was incorporated as a technique supporting the ECD. The spectra were recorded on a DXR-2 computer-controlled Raman microscope (ThermoFisher Scientific[®], USA) with a 532 nm wavelength laser (power adjusted 8 mW) within the wave numbers of 100 – 3565 cm⁻¹.

The experiment was carried out in a typical three-electrode cell with the electrolyte excess; the quartz crystal electrochemical cell was assembled with a 5 mm diameter AC electrode (working) and a platinum wire as the counter electrode; Ag/AgCl electrode served as the reference electrode. The examined AC electrode, placed behind a quartz glass window on the gold current collector, was exposed to the laser beam. Raman spectra were recorded every 2.5 min during the LASV experiment, with a frequency of 0.21 mHz.

Step potential electrochemical spectroscopy

SPECS experiment was carried out in the ECD assembled with 1 mol L⁻¹ Li_2SO_4 solution of pH 6 and 12 as the electrolyte. The electrode pretreatment and the potential of the individual electrode determination (E_{min} , E_{max}) involved three cycles of CV between the cell voltage 0 – 1.6 V and 0 – -1.6 V (1 mV s⁻¹). E_{max} and E_{min} were measured as +0.53 and -

1.08 V vs. AC for the electrolyte of pH 6 and +0.43 and -1.17 V vs. AC for the solution of pH 12. Before the SPECS measurement, the system was held at E_{min} for 30 min, to stabilize the current response. Afterward, SPECS was performed on one electrode in the full, previously determined, potential range. Starting from the E_{min} , the potential was gradually increased by 10 mV and held for 300 s at each potential step. After that, the system was polarized in the opposite direction. Five full charge/discharge cycles were performed.

3. Results and discussion

To understand how pH variations influence the characteristic of EC (the operating potential of the electrodes, the current response, and capacitance), the cells operating in 1 mol L⁻¹ Li₂SO₄ solutions of different pH were charged up to 1.6 V. The operating potential of the negative and positive electrodes was determined in the two-electrode configuration. After that, the working electrode was polarized in a given potential range in the three-electrode configuration with the CV technique (Fig. 2).

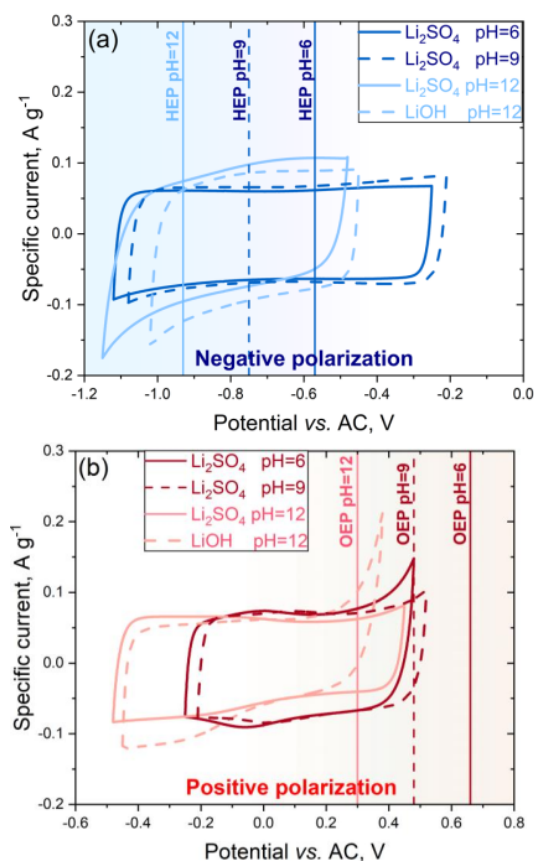


Fig. 2. Cyclic voltammograms (0.5 mV s^{-1}) recorded for the electrode negatively (a) and positively (b) polarized in sulfate-based electrolytes of different pH and LiOH solution.

Moreover, the hydrogen and oxygen evolution potentials (HEP and OEP, respectively) were calculated from the Nernst equation and presented in Fig. 2. However, one should consider that the calculated values are valid only in the electrochemical equilibrium state; hence, with applied polarization, they can be slightly shifted. Another issue concerns local pH changes during electrode polarization that could seriously affect the calculated HEP and OEP values [60].

The rest potential (OCP) strongly depends on the solution's pH – it is considerably shifted towards lower potentials at the electrolyte of pH 12 in comparison to the electrolyte of pH 6 and 9. This shift does not straightforwardly follow the trend of 59 mV/pH decade but is in agreement with the Pourbaix diagram and water stability potentials – the higher electrolyte pH, the lower OCP is expected [61].

When the electrode is negatively polarized (Fig. 2a), the current response is comparable for the electrolytes of pH 6 and 9, and no rapid current increase was recorded despite the HEP exceeding; the voltammogram only slightly deviates from the ideal rectangular shape in both cases, denoting mostly electrostatic charge accumulation. No redox reactions related to the hydrogen storage process are assumed due to the high overpotential of H₂ evolution under these conditions. It may again suggest that the pH increases near the (polarized) electrode. The voltammogram of the electrode operating in the pH 12 solution exhibits a different character. The increase in current is seen from the very beginning of charging, with the slope change below -1.0 V vs. AC, which is in agreement with the calculated HEP for this electrolyte (-0.93 V vs. AC); the hydrogen reduction can be considered here. The behavior of the electrode in 1 mol L⁻¹ LiOH solution was investigated for comparison purposes. As it was impossible to polarize the hydroxide-based EC up to 1.6 V (electrolyte decomposition), the studies were performed until the cell voltage was 1.4 V. The recorded voltammogram is analogous to the one recorded for the electrode operating in sulfate-based electrolyte (of pH 12), showing a similar charge storage mechanism. The difference is in slope change during charging – the current increase seems to appear at higher potential value, despite the narrower potential range.

In the case of positive polarization (Fig. 2b), the current increase at potentials higher than +0.3 V vs. AC is seen for the electrolyte of pH 6. This result is specific because the operating potential of the electrode (+0.48 V vs. AC) is below the OEP (+0.66 V vs. AC). It indirectly indicates a remarkable local pH increase during polarization that results in a shift of the equilibrium potential. The OEP was exceeded for the solutions of pH 9 and 12; however, no peaks are visible at the CV profiles recorded for these electrodes. Apart from the current increase at the electrolyte of pH 6, the data obtained is comparable for pH 6 and 9. In the case of the electrode working in the alkaline sulfate solution and the hydroxide-

based electrolyte, the voltammograms' shape differs from that previously discussed. The OCP values are obviously shifted, but also the recorded current is lower, suggesting lower capacitance. Moreover, for the cell with LiOH solution, a rapid current increase is seen above +0.25 V vs. AC (just after OEP exceeding) and its response is visible during discharging, an increase in current measured below -0.1 V versus AC. The presented data lead to the conclusion that the charge storage mechanism is similar for electrodes operating with sulfate-based electrolytes of pH 6 and 9. In the alkaline electrolyte similar ion movement and the electrode behavior to those observed in LiOH as the electrolyte can be assumed. The dilatometry data are expected to help to substantiate this assumption.

The dilatation changes vs. potential are presented in **Fig. 3**. It is worth mentioning that the presented dilatation is a relative value. The electrode height change equal to zero is set to be at the same potential (0 V vs. AC) for the data presented below.

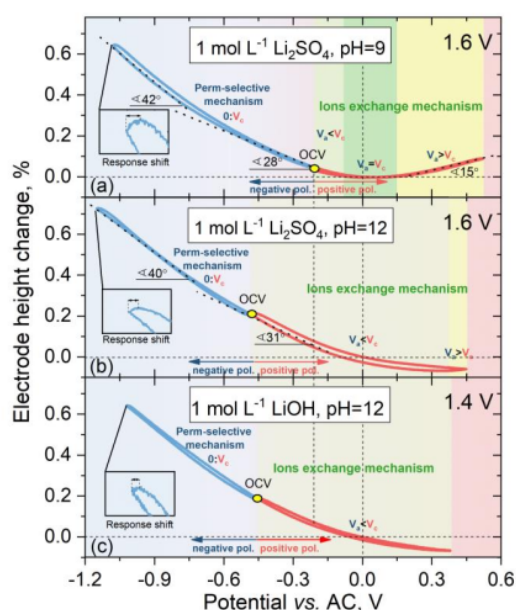


Fig. 3. Changes in electrode height in the function of potential applied for the electrodes polarized negatively (blue curves) and positively (red curves) in 1 mol L⁻¹ Li₂SO₄ of pH (a) 9 and (b) 12, as well as in (c) 1 mol L⁻¹ LiOH.

As the greatest differences in electrode height changes were observed for those operating in electrolytes of pH 9 (**Fig. 3a**) and 12 (**Fig. 3b**), these two results are compared (a detailed description of the electrode behavior operating in electrolytes of pH 6 and 9 will be provided below with the LASV results). If consider the polarization from the OCP down to lower potentials, where the perm-selective mechanism with the cations insertion is assumed (anions volume : cations volume denoted as $0:V_c$), the electrode

expansion was recorded. However, the character of the electrode height change differs in both electrolytes. In the case of the solution of pH 9 a linear increase of the electrode height change is seen down to -0.6 V vs. AC with a slope of 28°; below this potential the electrode expands even faster as the slope is 42°. It suggests that small cations (H₃O⁺) penetrate the porosity of the material first and after more bulky cations (solvated Li⁺) contribute to the charge balance of the electrode. The second possibility is related to the texture of the material. The pore channels may be the widest at the entrance, hence cations, both Li⁺ and H₃O⁺ can easily move in, without any remarkable electrode height change. However, with a potential decrease, the ions are pushed deeper into the narrow channels, and the electrode expansion rate is higher. Moreover, a hysteresis loop is visible – despite the polarization change, an increase in the electrode height is seen, suggesting the delayed ion response to the polarization change. The mechanism of positively charged ions expelling from the material porosity with the potential increase appears to be similar to that observed during electrode charging: more pronounced electrode shrinkage at the beginning, when larger cations move out of narrow pore channels, and mild electrode height changes closer to the OCP. All changes are reversible in the applied potential range.

When the electrode is polarized from the OCP to higher values, shrinkage of the electrode is still observed, meaning that ions leave the porosity. In the potential range from -0.1 to +0.15 V vs. AC, no change in electrode volume was recorded. It may suggest that the cations are continuously evacuated from the material, and simultaneously the anions enter the pores, and their volume is balanced ($V_a = V_c$). This effect is called ion exchange. With further potential increase, the electrode expansion is seen. However, taking into account the size of anions and cations present in the electrolytic solution, which are at least comparable $SO_4^{2-} \approx OH^- \approx H^+$, only Li⁺ is slightly larger than the others, the dilatation for both polarizations was expected to be similar. However, the difference in the electrode height change recorded for the negative and positive polarization is notable – 0.64% vs. 0.09%; the slope of the change is also smaller (15°). Here, we postulate that above +0.15 V vs. AC anions are adsorbed and cause an increase in electrode height but cations are still expelled from the material ($V_a > V_c$). The proposed mechanism is in agreement with the one described by Wang *et al.* in IL as the electrolyte [27].

The dilatometry data recorded for the electrode operating in the alkaline electrolyte (**Fig. 3**) is evidence of charge storage mechanisms different from those postulated on the basis of the voltammograms. Going into details, during polarization toward negative potentials from the OCP the electrode expansion is observed ($0:V_c$). However, it should be taken into account that the increase of the electrode height started much above the OCP. For easier comparison with the results discussed above, the negative

polarization will now be considered from the same potential as it was for the electrolyte of pH 9, i.e. -0.22 V vs. AC. Continuous electrode expansion was measured in the analyzed potential range. A linear increase in this parameter was determined to be -0.65 V vs. AC, with a slope of 31° . Below this potential, the electrode expansion rate is even higher – the slope of the curve increased by 9° . These values are comparable to those calculated for pH 9. However, there is no such well-pronounced hysteresis loop. The electrode height increase after the change of polarization direction is smaller. It suggests that the cations move out of the carbon porosity easier at higher pH.

When the electrode is polarized toward higher potentials, the electrode shrinkage is observed and the rate is constant between -0.65 V and -0.15 V vs. AC. Unlike the data obtained at pH 9, there is no plateau at pH 12 – with increasing potential, the electrode volume decreases. Therefore, no ion exchange region can be distinguished, where the volume of adsorbed anions is equal to cations desorbed ($V_a = V_c$). The electrode height change above -0.15 V up to $+0.44$ V vs. AC can be described as a polynomial function of degree two with the minimum reached at $+0.37$ V vs. AC. Up to this potential, evacuated cations are believed to be responsible for positive polarized electrode charge balancing ($V_a < V_c$). At potentials higher than $+0.37$ V vs. AC, an increase in the electrode volume was measured; therefore, anions are mainly considered to contribute to the formation of EDL ($V_a > V_c$).

As the differences of the electrode behavior at pH 9 and 12 are the most pronounced for the positive polarization, it can be assumed that various anions are responsible for charge balancing within the electrode. In order to identify the ionic fluxes at various pH levels, the dilatometric changes recorded in sulfate-based electrolytes are compared with those recorded in 1 mol L^{-1} LiOH (Fig. 3c). As already mentioned, the voltage applied for the cell operating in LiOH solution was limited to 1.4 V. However, in the potential range presented, the electrode behavior is analogous to that exhibited by the electrode operating with alkaline Li_2SO_4 solution. During the polarization toward potentials lower than the OCP, the electrode expansion is observed. It is worth mentioning that when the polarization changes, the cations move very quickly from the porosity. The shift in time of this response is smaller than in the previous cases. When the electrode was polarized to higher potential values, continuous electrode shrinkage is observed up to maximum applied potential, suggesting that the volume of adsorbed anions is lower than the volume of cations ($V_a < V_c$). Approximately at the same potential at the electrolyte of pH 12 the minimum dilatation was recorded. The compared results clearly demonstrate that in the case of both LiOH and alkaline Li_2SO_4 solutions, the same ions are involved in the electrode charge balancing. Hence, due to high concentration and mobility of the hydroxide anion, this ion is initially attracted to the electrode surface from the electrolyte

of pH 12 and the electrode expansion caused by SO_4^{2-} is seen at relatively high potentials. At the electrolyte of pH 9 penetration of pores by sulfate anion, visible as the electrode height increase, is seen at lower potentials because of the higher $\text{SO}_4^{2-}:\text{OH}^-$ ratio.

The results of cyclic voltammetry provided general information on the electrochemical behavior and volume changes of the polarized electrode at various pHs, showing the similarities and dissimilarities between the electrolytes used. In order to explain the ambiguous mechanism of charge storage during positive polarization, the LASV technique was applied.

Fig. 4 presents the voltage (grey dashed line) and the current (red dashed line) in time recorded for the polarized electrode in sulfate-based electrolytes of different pH.

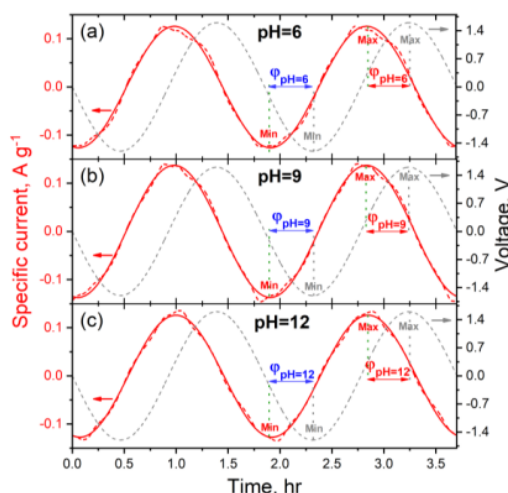


Fig. 4. LASV profiles, presenting the phase shift between the applied voltage, the recorded current (dashed line) and the sinusoidal fitting (solid line) of the current in time for cells assembled with 1 mol L^{-1} Li_2SO_4 of pH 6 (a), 9 (b) and 12 (c).

In the LASV technique, the voltage applied periodically varies as a sine wave. At the same time, the current is registered. In the case of ideal capacitive character, the current leads the voltage by $\phi = +90^\circ$. It is said that these parameters are shifted in phase. Any deviation from this ideal phase shift denotes changes in the charge storage mechanism. A phase shift approaching 0° indicates increasing contribution of resistive character (for the resistors the voltage and the current are in one phase), here denoting certain redox processes.

To investigate the impact of pH on the charging mechanism, the electrochemical cell was polarized in a two-electrode configuration from -1.6 V to 1.6 V. The investigated electrode was repolarized to describe its behavior during both polarities. The LASV profiles are presented in Fig. 4. For current recorded the sine function was fitted to the experimental data (solid red line) and the phase shift was determined based

on the equation: $y=y_0+A\sin\left(\pi\frac{x-x_c}{w}\right)$, where y_0 – offset, A – amplitude, x_c – phase shift and w – period.

A scan rate is variable in the LASV – the higher the cell potential difference, the slower the scan rate. Therefore, the redox activity and electrolyte decomposition are revealed at a low scan rate at the maximum and minimum applied voltages. As expected, similarities are observed between the electrolyte of pH 6 (Fig. 4a) and 9 (Fig. 4b). The deviations of the current curve have the same character, and they occur at the same time. Phase shifts determined in both electrolytes are equal to 23.5°. In the case of the electrolyte of pH 12 (Fig. 4c) the peaks are also seen at the highest cell potential difference. However, they are shifted in time if compared to those registered for pH 6 and 9. The phase shift is 22.4°. For comparison purposes, a commercial EC based on organic electrolyte was tested under the same conditions, and its phase shift was found to be 20.3°.

As the analysis of the electrode height change as a function of voltage/potential applied provided only a general picture of the processes ongoing during the AC electrode polarization, it is worth considering the recorded dilatation vs. charge stored presented for sulfate-based electrolytes of pH 6 (Fig. 5b), 9 (Fig. 5c) and 12 (Fig. 5d). The charge was calculated from the current in time integration and presented as the absolute value.

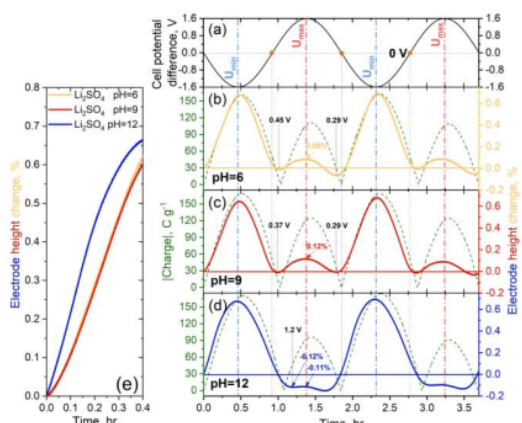


Fig. 5. LASV profiles, presenting the changes in cell voltage in time (a) and the changes in accumulated charge and electrode height simultaneously for cells assembled with 1 mol L⁻¹ Li₂SO₄ of pH 6 (b), 9 (c) and 12 (d); dilatometry recorded during insertion of the cations at the beginning of negative polarization (e).

Fig. 5a presents the cell potential difference in time – the cell was polarized from 0 V down to -1.6 V and up to 1.6 V; the charge stored and the electrode height changes are presented for the negatively and positively polarized electrode, respectively. The minimum/ maximum cell potential differences, as well as 0 V, are marked as the dash-dotted blue/red and grey lines to facilitate careful data interpretation.

The charge exhibits the same trend, regardless of the electrolyte used – it obviously increases with increasing voltage, reaching 160 A s g⁻¹ at pH 6, and 170 A s g⁻¹ at pH 9 and 12 (Fig. S1). The characteristic of charge accumulation during charging is comparable for all the systems. Nevertheless, when the polarization direction is changed, this process is slower in the case of the alkaline electrolyte. It can be suggested that the charge carriers are not easily expelled from the material. Moreover, during discharge, the charge accumulated on the negatively polarized electrode is not fully recovered. There is still 50, 50 and 70 A s g⁻¹ stored at 0 V in the case of the electrolyte of pH 6, 9 and 12, respectively. When the cell is polarized up to 1.6 V, the amount of charge accumulated on the electrode is the same as in the case of a 'negative' voltage and certain charge remains in the system at 0 V. The charge loss is related to the redox reactions/electrolyte decomposition, which were seen on the specific current curve at LASV profiles (Fig. 4).

With a comparable amount of charge stored at the negatively polarized electrode and the same cations in the electrolytic solution taken into account, the dilatometric changes are expected to be similar as well. The maximum electrode expansion reaches 0.65 – 0.68% (Fig. 5b, c, d). However, it is clearly seen that electrode swelling has a different character in 'neutral' electrolytes compared to alkaline one. When the cell is being charged from 0 V down to -1.6 V (the beginning of this process is presented in Fig. 5e), the electrode height change is slower for the electrolytes of pH 6 and 9 (the slope is 56° vs. 65° for pH 12). We assume that the reason for those differences comes from Li⁺/H⁺ concentration ratio and solvation shell of the cation. The mild change in electrode height can be attributed to protons adsorption. Because of their higher concentration at lower pH values and high mobility, they can reach the electrode surface faster than larger and slower Li⁺ cations, but not cause such a fast electrode expansion. With further negative electrode polarization (when -0.9 V is exceeded), the slope of the height change is comparable to the one measured for pH 12. It means that by this cell potential difference, the cations of similar diameter are responsible for the charge accumulated into the electrode. Just before reaching the minimum voltage, the electrode dilatation is even slightly faster for electrolytes of lower pH (6 and 9), suggesting that larger cations are attracted to the electrode. It is in agreement with the theory of the solvation shell of the cations at various pH – the highest solvation occurs at neutral pH. Hence, the solvated Li⁺ cation is bigger and not as mobile in the case of electrolytes of pH 6 and 9, in comparison to the solution of pH 12, therefore, it moves into the porosity as the last one. The recorded electrode height change in the alkaline electrolyte is linear as long as the charge increases linearly. It suggests that only solvated Li⁺ cations penetrate the electrode porosity or that protons are attracted to the electrode surface simultaneously

with Li^+ and that the recorded dilatation is rather related to the accumulation of the bigger metal cations. When the cells are discharged, the dilatometric response is analogous to the charging process; in the case of electrolytes of pH 6 and 9, first cations with high solvation degree are expelled from the material, causing delay (because of low mobility) but noticeable (because of size) electrode shrinkage. Then, approaching -0.2 V, the electrode height change slope decreases, indicating that the protons are moving out. In the electrolyte of pH 12, this change is linear. When the voltage reaches 0 V, the electrode height change is not equal to 0, which is related to the previously mentioned charge stored despite the theoretically discharged cell.

During the cell polarization towards 1.6 V, the charge accumulated at the positive electrode is the same as it was in the case of the negative one. Moreover, the charge loss is the same; it shows that the charge is well balanced at both electrodes. It is known that anions (here SO_4^{2-} and OH^-) are attracted to the positively polarized electrode in order to balance its charge. When the ions diameter was taken into account, the electrode height changes were expected to be similar or slightly lower if compared to the negative polarization. However, it is seen in **Fig. 5**, that the difference between both polarities is significant. The height increase of the electrode operating at the electrolyte of pH 6 and 9 reaches 0.09% and 0.12%, respectively, while at pH 12 this value is even noticeably lower than the initial: -0.11% (for the electrode negatively polarized, this change reached almost 0.7%). It can be caused by the already reported charging mechanism for the positively polarized electrode, where the charge is first balanced by cations expulsion and then, at higher potentials, counterions are attracted to the electrode [27].

Herein, initially, with increasing the voltage, the electrode height decreases (according to decreasing charge) in all tested electrolytes. The minimum value in mild electrolytes is reached at 0.45 V (pH 6) and 0.37 V (pH 9). Subsequently, electrode expansion is observed to reach 1.6 V, reaching a similar electrode height change at both electrolytes. In the reversed process, when the voltage decreases, the electrode shrinkage is seen. The rate of these changes is comparable in both cases (small differences can be related to the natural drift of the ECD or slight temperature variations) and the minimum dilatation was recorded at the same voltage (0.29 V). Taking all the above-mentioned results, the same anion (or anions) is supposed to be responsible for charge balancing during positive polarization at pH 6 and 9, confirming the preliminary assumptions made based on the cyclic voltammetry results.

As already noticed, both electrochemical behavior and electrode height change for the electrolyte of pH 12 are significantly different from those obtained under milder conditions. The LASV results, presented in **Fig. 5d**, are consistent with the previously gained data. Despite the increase in voltage, the electrode shrinkage was recorded to 1.2 V, reaching -0.12%.

With further positive polarization, a very small electrode expansion is seen. Bearing in mind that the charge is balanced by the anions, such a slight dilatation may be counter-intuitive. However, data recorded at lower pH values and literature reports clearly demonstrate that anions accumulate within the porosity of the material [22, 37, 44, 48]. One needs to remember about the definitely higher concentration of very mobile OH^- in alkaline medium (six orders of magnitude higher if compared with pH 6). Hence, this anion is mostly considered to be responsible for the charge balancing of the positively polarized electrode. Its solvated size is comparable to the size of SO_4^{2-} thus a high degree of OH^- desolvation is assumed. As a consequence, with increasing voltage, the bulky lithium ions are expelled from the material and smaller desolvated OH^- ions take their place, which is seen as the prolonged electrode shrinkage. At adequately high voltages, when the SO_4^{2-} ions are attracted to the electrode and the Li^+ ions are not evacuated from the porosity (or their evacuation is not as fast as at lower voltages), the electrode expansion is visible. It should also be taken into account that sulfate anions might be attracted only at the electrode surface without causing any electrode swelling. When the cell is discharged, the processes are reversed – the anions (first SO_4^{2-} and then OH^-) are moving out from the electrode and the cations penetrate the porosity.

The results obtained with the LASV technique are in accordance with the CV data. The current response, as well as the dilatometry results, are comparable with cycles. To look at the ongoing processes from another perspective, Raman spectroscopy in *operando* mode was chosen as a supporting technique. As activated carbons are made up of C-C bonds, Raman spectroscopy is sensitive to changes in their orientation. Therefore, to study the changes of carbon electrodes, the most important are the bands corresponding to the ordered and defected structure of the material. The former is named the G-band ($\sim 1580\text{ cm}^{-1}$) and originates from the C-C stretching vibration, while the later one – D-band ($\sim 1355\text{ cm}^{-1}$) comes from a decrease in the graphite lattice and carbon disordered structures [62, 63].

The LASV experiment with a relatively low frequency applied (because of high resistance within the typical three-electrode cell) was performed. Simultaneously, the electrode dilatation with ECD was measured with the same experimental setup. The experiments were performed in $1\text{ mol L}^{-1}\text{ Li}_2\text{SO}_4$ of pH 6 at the potential range determined in the ECD (from +0.47 V down to -1.13 V vs. AC). The potential and the electrode height change in time (for one cycle) are presented in **Fig. 6a**.

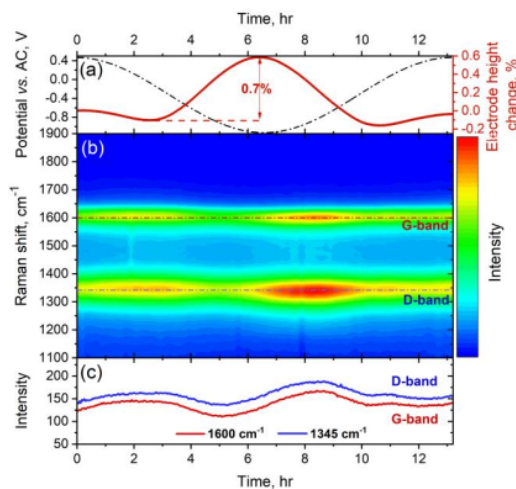


Fig. 6. LASV profile of one cycle in three-electrode configuration, presented as the potential change in time with the electrode height change recorded (a) and Raman spectrum (heat map), at specified Raman shift range: 1100 – 1900 cm^{-1} , obtained during operando measurements (b); intensity changes of the D and G bands (c).

The electrode was polarized from the maximum potential to the minimum potential. The trend in dilatometry results is comparable to the previously recorded data (Fig. 4), showing that despite the slower sweep rate, the electrode height change range is equal to 0.7%. Fig. 6b presents the Raman spectra in the form of a so-called heat map of the polarized electrode (Raman shift range limited to 1100 – 1900 cm^{-1} to easily follow the intensity changes of the D and G bands). On the basis of such an experiment, it is possible to monitor the whole spectrum changes in time, as well as to study the intensity of the selected band. It is seen that both D and G band change their intensity during electrode polarization (Fig. 6c). The intensity ratio of the bands clearly changes. However, if these changes are compared with the fluctuation of the potential, it is seen that the Raman response is, somewhat, delayed. This shift was described to be related to a better pronounced Raman signal during the desorption of gaseous products rather than during their adsorption [64]. Therefore, in this experiment, all changes in the material are seen for the ions moving out of the porosity of the electrode.

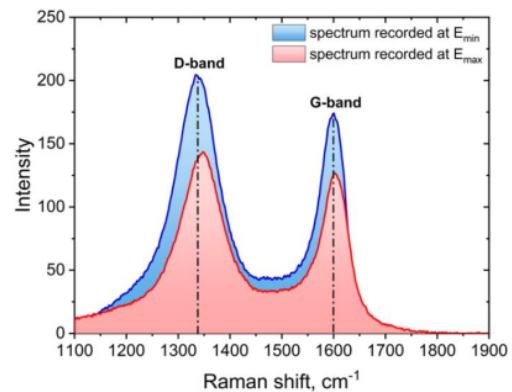


Fig. 7. Raman spectra recorded at maximum and minimum potential during the LASV experiment.

As the G-band intensity increases and its position slightly changes after reaching maximum/minimum potential (Fig. 7), it can be concluded that the distance between the graphene layers increases. Moreover, the variations of intensity are more noticeable when the electrode is negatively polarized. The change in the D-band position is also significant, showing that the ions are inserted between the graphene layers and the number of defects in the carbon matrix increases. Hence, Raman spectroscopy results confirm different mechanism of charge storage if the results are compared with negative polarization.

The last analysis was performed with the SPECS technique. The results provide information about charge accumulation and ion fluxes in the vicinity of the polarized electrode. The parameters obtained with this technique can thus be correlated with the changes in electrode height. The fit curves (I_{fit}) were matched to the experimental current curves (I_{exp} , registered at each potential step). Each total I_{fit} current consists of four components ($I_{fit} = I_p + I_G + I_D + I_R$): current related with EDL formation in the bulk electrode (porous surface; I_p) and on the outer surface (geometric surface; I_G), the current connected with ion diffusion (I_D), and the equilibrium current (I_E) attributed to side reactions. Each current component is characterized by individual parameters. For the purpose of this study, we consider resistance of EDL formation (R ; ohm) and differential capacitances (C ; F). The product of R and C gives the time constant (τ , s) of EDL formation. The charge delivered to the system necessary for EDL formation is specified by the normalized diffusion parameter (B ; $\text{A s}^{0.5}$). The profiles of individual parameters are summarized in Fig. S2 for five cycles of the electrode repolarization at the full potential range (determined during two-electrode with the reference experiment at 1.6 V) for the systems operating in 1 mol L^{-1} Li_2SO_4 of pH 6 and 12. Here, only extreme pH values were taken into consideration, because of high similarity in the electrochemical and dilatometric response registered in electrolytes of pH 6 and 9 (confirmed by the previously presented results in Fig. 2).

For both systems, the reproducibility of the results in each cycle is very high. The identical systems' response is observed for the given potential. Such reproducibility proves the system stability during the operation despite the harsh conditions of SPECS experiments.

Data from the first repolarization cycle for both electrolytes are presented as voltammograms (Fig. 8).

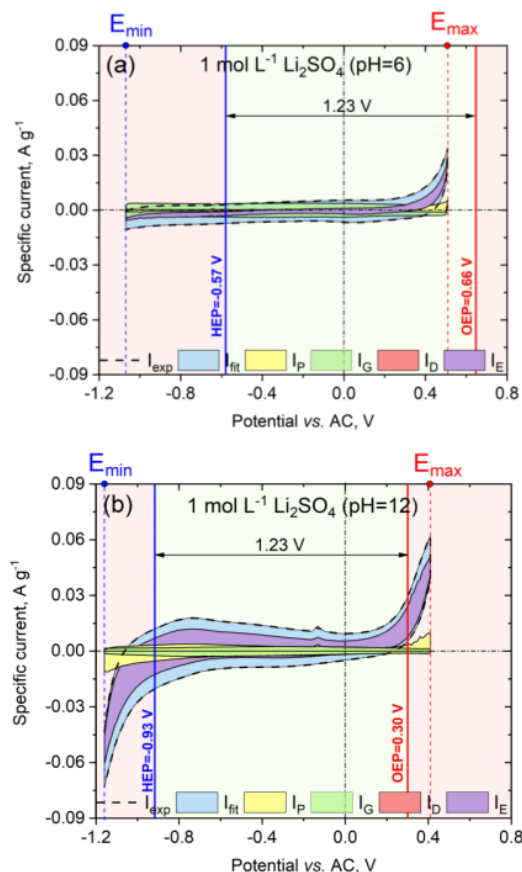


Fig. 8. SPECS results presented as voltammetry profiles for ECs operating in 1 mol L⁻¹ Li₂SO₄ of (a) pH 6 and (b) pH 12.

The I_{fit} curves perfectly reflect the profiles of the voltammograms represented by I_{exp} . It proves high coefficient of determination. The results for both electrolytes differ significantly from each other. For an electrolyte of pH 6 (Fig. 8a; zoom in on data presented in Fig. S3) the I_G current is a significant share of I_{fit} . There is a noticeable additional contribution of the I_P current (however, much lower than the I_G). The surface in the electrode bulk is much more developed than the surface remaining in direct contact with the electrolyte. Theoretically, the porous structure should accumulate more charge. This phenomenon can be explained by the limited insertion of ions into

the electrode bulk caused by the retention of large SO_4^{2-} ions at the entrance to the micropores (on the surface of the external electrode surface). It leads to the accumulation of ions in the EDL diffusion layer in the mesopores and increase in I_G response. With increasing potential, the current increase at E_{max} is observed, indicating electrolyte decomposition and possible oxygen evolution. The evolution of oxygen in the form of a gas leads to the reorganization of ions in the mesoporous EDL layer and leads to a partial ion takeover from the outer electrode layers into the pores (increase in I_P and decrease in I_G near E_{max}). The I_E current, strongly affects the total I_{fit} . The greater the redox activity, including the electrolyte decomposition, the greater the I_E . This is confirmed by the rapid increase in this current response at E_{max} . Based on our knowledge, previously performed experiments and mathematical considerations, it is known that the share of the I_E decreases with the data recording time shortening at a specific potential step. However, in order to fit the I_{fit} curves to I_{exp} and obtain satisfactory insight into the behavior of both systems at the given potential on the electrochemical dilatometer, it was necessary to apply five-minute steps. However, both systems are characterized by relatively high stability under these conditions. As mentioned earlier, the electrolyte decomposition is noticeable only near E_{max} . However, this potential is still far from the theoretical OEP (+0.66 V vs. AC). On the other hand, at E_{min} , there are no signs of electrolyte decomposition and hydrogen evolution despite the definitely exceeded HEP (-0.57 V vs. AC). It indicates a high overpotential for H₂ evolution, suggesting local pH change (alkalization) during electrode polarization, causing the HEP and the OEP to shift towards lower values. The results are consistent with the voltammograms presented in Fig. 2. Completely different behavior is observed for the EC operating in the electrolyte of pH 12 (Fig. 8b). Here, the total I_{fit} varies significantly over the entire potential range. In E_{min} and E_{max} , much more pronounced electrolyte decomposition is evident, if compared with the results presented for the electrolyte of pH 6. Electrolyte decomposition occurs near the OEP (+0.30 V vs. AC) and the HEP (-0.93 V vs. AC). It can be assumed that the safe operating potential range of such a system is narrower than for Li₂SO₄ solution of pH 6. Moreover, a much smaller difference between I_G and I_P is seen than in the previously discussed electrolyte. In this case, the amount of charge accumulated in the bulk and on the outer surface is comparable (excluding the extreme potentials). The decrease in I_G and the increase in I_P response lead to the conclusion that much of the available charge penetrates the micropores. This is consistent with the presence of a large number of small OH⁻ ions which easily penetrate micropores. Similarly, as for pH 6, the dominance of I_P share over I_G takes place at E_{max} and E_{min} , where the electrolyte decomposition is observed more. It should also be mentioned that the total I_{fit} response is dominated by the I_E . Additional

side reactions are registered throughout the potential range.

Fig. 9 presents the calculated SPECS parameters and the changes in electrode height. To present the result clearly and ease the interpretation of the data, it was necessary to choose a common starting point, which is E_{min} (because of the different potential ranges at various electrolytes' pH).

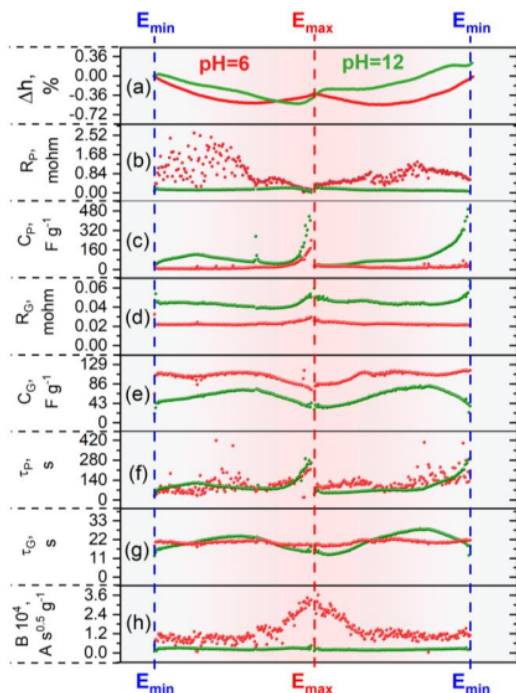


Fig. 9. Parameters calculated based on the SPECS technique for the first cycle of electrode repolarization in the full potential range (for the maximum voltage 1.6 V) for the cell with 1 mol L⁻¹ Li₂SO₄ at pH 6 and 12: (a) change in electrode height Δh ; (b, d) porous and geometric resistance R ; (c, e) differential specific porous and geometric capacitance C ; (f, g) time constant T of EDL formation within porosity and electrode surface, and (h) specific normalized diffusion parameter B .

The dilatometric response for pH=6 is reproducible over five cycles of electrode repolarization (**Fig. S2a**). The dilatometric change (for the first cycle, presented in **Fig. 9a** as a red curve) is symmetrical – the change recorded from E_{min} to E_{max} looks like a 'mirror reflection'. It indicates fully reversible and repeatable ions movement as well as insertion/deinsertion into/from the material porosity. Furthermore, the difference in electrode height between E_{min} and E_{max} is less pronounced than the change recorded during the LASV experiment. It is probably caused by deeper penetration of SO_4^{2-} ions into the electrode or a higher number of adsorbed anions, because of a much slower scan rate and a longer hold time at maximum potential.

The dilatometry profile of the electrode polarized in the alkaline electrolyte is also presented in **Fig. 9a**

(green curve). The significant and relatively sharp (if compared with the dilatometric response observed previously in **Fig. 3b** and **Fig. 5d**) of the electrode height close to E_{max} is seen. This increase is caused by the adsorption of SO_4^{2-} ions at an extremely low scan rate (here ~ 0.033 mV s⁻¹); therefore, such an increase was not observed when CV or LASV techniques were used with a scan rate ~ 1 mV s⁻¹, where the electrode's charge balancing was connected to OH⁻ adsorption rather than bulky SO_4^{2-} . Under these conditions (very low scan rate, relatively high potential value, and, consequently, high driving force), low-mobility SO_4^{2-} can be adsorbed into the pores of the positively polarized electrode. When the polarization is changed and directed toward negative values, the dilatometry response is not symmetric (like it was observed in the case of pH 6). After reaching E_{max} , the electrode continuously increases its volume, indicating further adsorption of SO_4^{2-} anions (down to -0.1 V after E_{max} exceeding). The dilatometric response is constant at relatively high potentials, suggesting that sulfate anions can be partially trapped in the pores or their desorption from the material is a very slow process, and hence there is no significant electrode height change. The other possibility is an exchange of equilibrated ions – SO_4^{2-} anions leave the porosity and their place is immediately taken by partially/completely desolvated Li⁺ cations.

The balance of one divalent anion can be done by two monovalent cations and the size of the sulfate anion is comparable to that of two lithium cations. In the next stage, as the potential approaches E_{min} , a significant change in the height of the electrode is observed indicating that Li⁺ is adsorbed (as discussed). Attention should also be paid to the dilatometric response which changes over cycles; hence it is not fully reproducible (**Fig. S2b**). If SO_4^{2-} ions are trapped inside the material, a significant loss of charge would be expected during discharge of the system. The charge loss was shown to be comparable for both polarities in the case of electrolytes of pH 6 and 12 (**Fig. S1**). In this connection, the theory of quite fast anions/cations exchange seems to be more appropriate. This non-reproducible change in electrode height can be related to irreversible changes in the porous texture of the material. Micropores may increase their size, and hence, the insertion of ions will not be well-pronounced anymore during ECD experiment. Furthermore, at the positive potentials, participation of OH⁻ in EDL formation is expected (due to the very high concentration of OH⁻, compared to its number in the electrolyte of pH 6). However, because of the small diameter of this anion, its impact on the dilatometry response can be difficult to notice.

As the resistance R_p (**Fig. 9b**) and capacitance C_p (**Fig. 9c**) are directly related to each other, these parameters will be discussed simultaneously. The R_p for pH 6 is strongly disturbed and takes higher values compared to pH 12. However, C_p values are much lower in the electrolyte of higher pH. This result confirms

the difficulty in penetrating large SO_4^{2-} in the bulk and the ease of effective EDL formation by OH^- . At the same time, attention should be paid to parameters related to the EDL formation on the electrode surface that is easily accessible for the ions (Fig. 9d and e). The R_G for pH 12 is two times higher and the C_G is two times lower than those components calculated for pH 6. This leads to the conclusion that SO_4^{2-} ions in pH 6 are willingly attracted to the electrode, but they remain on its surface (with limited penetration into the porosity). The basic criterion for assigning the index 'P – porous' and 'G – geometrical' to the R and C parameters was the value of the time constant. The EDL formation is faster as the electrode surface is easily accessible to ions (geometric surface). For the electrolyte of pH 6 (Fig. 9g), the T_G has an almost constant value throughout the polarization range, demonstrating that there is no disturbance in EDL formation. In the alkaline solution, the T_P has variable values (Fig. 9f), depending on the driving force of EDL formation, that is, the applied potential. Interpretation of T_P may be a bit more difficult due to large fluctuations for the electrolyte of pH 12 (caused by high R_P noise for this electrolyte). However, based on the trend observed in RP , the system with pH 12 is characterized by a lower value of T_P . Significant differences in the values and curve profiles can be observed for parameter B (Fig. 9h). For the electrode polarized in the electrolyte of pH 6, the charge needed for the ions movement/transport is much higher compared to the charge necessary in pH 12. This result is logical and coherent if takes into account lower Li^+ and SO_4^{2-} mobility (4.01 and $8.28 \cdot 10^{-8} \text{ m}^2 \text{ s}^{-1} \text{ V}^{-1}$, respectively) in comparison to OH^- mobility ($20.64 \cdot 10^{-8} \text{ m}^2 \text{ s}^{-1} \text{ V}^{-1}$). This relates particularly to SO_4^{2-} transport (in the electrolyte of pH 6) for which a large increase in the B value at E_{max} is observed. The changes in parameter B are incomparably smaller in the case of the pH 12 solution, which results from the ease in the diffusion of highly mobile OH^- .

Conclusions

1. The electrochemical behavior of $1 \text{ mol L}^{-1} \text{ Li}_2\text{SO}_4$ strongly depends on the pH of the electrolyte.
2. There is a significant alkalization of the electrolyte pH near the electrode during EC operation.
3. The $1 \text{ mol L}^{-1} \text{ Li}_2\text{SO}_4$ electrolyte of pH 12 exhibits a behavior similar to the LiOH -based system.
4. Repolarization of the electrode and its polarization separately at positive and then negative polarization gives a similar dilatometry response.
5. Electrode height changes measured with different technique (CV, LASV) give the same reproducible results if the experiment conditions are comparable.
6. The mechanism of charge storage strongly depends on the electrolyte pH; at pH 6 and 9 ongoing processes are comparable, whereas at pH 12 the differences are visible, especially during positive polarization.

7. The higher the electrolyte pH, the higher the OH^- contribution to EDL formation.
8. The transport of SO_4^{2-} anions requires a very high driving force.
9. EC operating at pH 6 electrolyte is more stable and the textural changes of the electrode are reversible, even under very harsh conditions.
10. SO_4^{2-} anions cause irreversible changes within the material texture.

Declaration of Competing Interest

The authors declare that they have no known competing financial interests or personal relationships that could have appeared to influence the work reported in this paper.

Acknowledgements

The authors acknowledge the financial support from the European Research Council within the Starting Grant project (GA 759603) under the European Unions' Horizon 2020 research and innovation programme.

References

- [1] D. Larcher, J.M. Tarascon, Towards greener and more sustainable batteries for electrical energy storage, *Nature Chemistry*, 2015, pp. 19-29.
- [2] B. Dunn, H. Kamath, J.M. Tarascon, Electrical energy storage for the grid: a battery of choices, *Science* 334(6058) (2011) 928-35.
- [3] J.Y. Zhao, A.F. Burke, Review on supercapacitors: Technologies and performance evaluation, *Journal of Energy Chemistry* 59 (2021) 276-291.
- [4] P. Simon, Y. Gogotsi, Perspectives for electrochemical capacitors and related devices, *Nat Mater* 19(11) (2020) 1151-1163.
- [5] N. Yabuuchi, K. Kubota, M. Dahbi, S. Komaba, Research development on sodium-ion batteries, *Chem Rev* 114(23) (2014) 11636-82.
- [6] M.D. Slater, D. Kim, E. Lee, C.S. Johnson, Sodium-Ion Batteries, *Advanced Functional Materials* 23(8) (2013) 947-958.
- [7] L.M. Wu, D. Buchholz, C. Vaalma, G.A. Giffin, S. Passerini, Apple-Blowaste-Derived Hard Carbon as a Powerful Anode Material for Na-Ion Batteries, *Chemelectrochem* 3(2) (2016) 292-298.
- [8] J.Y. Hwang, S.T. Myung, Y.K. Sun, Sodium-ion batteries: present and future, *Chem Soc Rev* 46(12) (2017) 3529-3614.
- [9] D. Yu, Q. Qian, L. Wei, W. Jiang, K. Goh, J. Wei, J. Zhang, Y. Chen, Emergence of fiber supercapacitors, *Chem Soc Rev* 44(3) (2015) 647-62.
- [10] J. Halim, S. Kota, M.R. Lukatskaya, M. Naguib, M.-Q. Zhao, E.J. Moon, J. Pitcock, J. Nanda, S.J. May, Y. Gogotsi, M.W. Barsoum, Synthesis and Characterization of 2D Molybdenum Carbide (MXene), *Advanced Functional Materials* 26(18) (2016) 3118-3127.
- [11] M. Mirzaeiian, Q. Abbas, A. Ogwu, P. Hall, M. Goldin, M. Mirzaeiian, H.F. Jirandehi, Electrode and electrolyte materials for electrochemical capacitors, *International Journal of Hydrogen Energy* 42(40) (2017) 25565-25587.
- [12] J. Menzel, E. Frackowiak, K. Fic, Agar-based aqueous electrolytes for electrochemical capacitors with reduced self-discharge, *Electrochimica Acta* 332 (2020).
- [13] K. Fic, G. Lota, M. Meller, E. Frackowiak, Novel insight into neutral medium as electrolyte for high-voltage supercapacitors, *Energy & Environmental Science* 5(2) (2012) 5842-5850.
- [14] S. Yamazaki, T. Ito, Y. Murakumo, M. Naitou, T. Shimooka, M. Yamagata, M. Ishikawa, Hybrid capacitors utilizing halogen-based redox reactions at interface between carbon positive

- electrode and aqueous electrolytes, *Journal of Power Sources* 326 (2016) 580-586.
- [15] J. Piwek, A. Platek, E. Frackowiak, K. Fic, Mechanisms of the performance fading of carbon-based electrochemical capacitors operating in a LiNO₃ electrolyte, *Journal of Power Sources* 438 (2019) 227029.
- [16] P.W. Ruch, D. Cericola, A. Foelske, R. Kotz, A. Wokaun, A comparison of the aging of electrochemical double layer capacitors with acetonitrile and propylene carbonate-based electrolytes at elevated voltages, *Electrochimica Acta* 55(7) (2010) 2352-2357.
- [17] S.E.M. Pourhosseini, A. Bothe, A. Balducci, F. Beguin, P. Ratajczak, Strategy to assess the carbon electrode modifications associated with the high voltage ageing of electrochemical capacitors in organic electrolyte, *Energy Storage Materials* 38 (2021) 17-29.
- [18] J.W. Graydon, M. Panjehshahi, D.W. Kirk, Charge redistribution and ionic mobility in the micropores of supercapacitors, *Journal of Power Sources* 245 (2014) 822-829.
- [19] A. Bothe, S.E.M. Pourhosseini, P. Ratajczak, F. Beguin, A. Balducci, Towards understanding the impact of operating voltage on the stability of adiponitrile-based electrical double-layer capacitors, *Journal of Power Sources* 496 (2021).
- [20] P. Galek, P. Bujewska, S. Donne, K. Fic, J. Menzel, New insight into ion dynamics in nanoporous carbon materials: An application of the step potential electrochemical spectroscopy (SPECS) technique and electrochemical dilatometry, *Electrochimica Acta* 377 (2021) 138115.
- [21] H. Li, Z. Li, F.C. Lin, Q.R. Chen, T. Qiu, Y. Liu, Q. Zhang, Capacitance Loss Mechanism and Prediction Based on Electrochemical Corrosion in Metallized Film Capacitors, *Ieee Transactions on Dielectrics and Electrical Insulation* 28(2) (2021) 661-669.
- [22] A. Platek-Mielczarek, E. Frackowiak, K. Fic, Specific carbon/iodide interactions in electrochemical capacitors monitored by EQCM technique, *Energy & Environmental Science* 14(4) (2021) 2381-2393.
- [23] P. Kurzweil, J. Schottenbauer, C. Schell, Past, Present and Future of Electrochemical Capacitors: Pseudocapacitance, Aging Mechanisms and Service Life Estimation, *Journal of Energy Storage* 35 (2021) 102311.
- [24] U. Samukaite-Bubniene, A. Valiuniene, V. Buciskas, P. Genys, V. Ratautaite, A. Ramanaviciene, E. Aksun, A. Tereshchenko, B. Zeybek, A. Ramanavicius, Towards supercapacitors: Cyclic voltammetry and fast Fourier transform electrochemical impedance spectroscopy based evaluation of polypyrrole electrochemically deposited on the pencil graphite electrode, *Colloids and Surfaces A-Physicochemical and Engineering Aspects* 610 (2021).
- [25] M. Zhu, C.J. Weber, Y. Yang, M. Konuma, U. Starke, K. Kern, A.M. Bittner, Chemical and electrochemical ageing of carbon materials used in supercapacitor electrodes, *Carbon* 46(14) (2008) 1829-1840.
- [26] P.W. Ruch, D. Cericola, A. Foelske-Schmitz, R. Kotz, A. Wokaun, Aging of electrochemical double layer capacitors with acetonitrile-based electrolyte at elevated voltages, *Electrochimica Acta* 55(15) (2010) 4412-4420.
- [27] Y.Y. Wang, C. Malveau, D. Rochefort, Solid-state NMR and electrochemical dilatometry study of charge storage in supercapacitor with redox ionic liquid electrolyte, *Energy Storage Materials* 20 (2019) 80-88.
- [28] A.C. Forse, J.M. Griffin, C. Merlet, J. Carretero-Gonzalez, A.R.O. Raji, N.M. Trease, C.P. Grey, Direct observation of ion dynamics in supercapacitor electrodes using in situ diffusion NMR spectroscopy, *Nature Energy* 2(3) (2017).
- [29] H. Wang, T.K. Koster, N.M. Trease, J. Segalini, P.L. Taberna, P. Simon, Y. Gogotsi, C.P. Grey, Real-time NMR studies of electrochemical double-layer capacitors, *J Am Chem Soc* 133(48) (2011) 19270-3.
- [30] C. Prehal, D. Weingarh, E. Perre, R.T. Lechner, H. Amenitsch, O. Paris, V. Presser, Tracking the structural arrangement of ions in carbon supercapacitor nanopores using in situ small-angle X-ray scattering, *Energy & Environmental Science* 8(6) (2015) 1725-1735.
- [31] C. Prehal, C. Koczwara, N. Jackel, A. Schreiber, M. Burian, H. Amenitsch, M.A. Hartmann, V. Presser, O. Paris, Quantification of ion confinement and desolvation in nanoporous carbon supercapacitors with modelling and in situ X-ray scattering, *Nature Energy* 2(3) (2017).
- [32] C. Koczwara, C. Prehal, S. Haas, P. Boesecke, N. Huesing, O. Paris, Towards Real-Time Ion-Specific Structural Sensitivity in Nanoporous Carbon Electrodes Using In Situ Anomalous Small-Angle X-ray Scattering, *ACS Appl Mater Interfaces* 11(45) (2019) 42214-42220.
- [33] R. Vicentini, L.M. Da Silva, D.V. Franco, W.G. Nunes, J. Fiates, G. Doubek, L.F.M. Franco, R.G. Freitas, C. Fantini, H. Zanin, Raman probing carbon & aqueous electrolytes interfaces and molecular dynamics simulations towards understanding electrochemical properties under polarization conditions in supercapacitors, *Journal of Energy Chemistry* 60 (2021) 279-292.
- [34] J.M. Black, G. Feng, P.F. Fulvio, P.C. Hillesheim, S. Dai, Y. Gogotsi, P.T. Cummings, S.V. Kalinin, N. Balke, Strain-Based In Situ Study of Anion and Cation Insertion into Porous Carbon Electrodes with Different Pore Sizes, *Advanced Energy Materials* 4(3) (2014) 1300683.
- [35] F. Endres, N. Borisenko, S.Z. El Abedin, R. Hayes, R. Atkin, The interface ionic liquid(s)/electrode(s): in situ STM and AFM measurements, *Faraday Discuss* 154 (2012) 221-33; discussion 313-33, 465-71.
- [36] M. Salanne, B. Rotenberg, K. Naoi, K. Kaneko, P.L. Taberna, C.P. Grey, B. Dunn, P. Simon, Efficient storage mechanisms for building better supercapacitors, *Nature Energy* 1(6) (2016).
- [37] N. Jäckel, S. Patrick Emge, B. Krüner, B. Röhling, V. Presser, Quantitative Information about Electrosorption of Ionic Liquids in Carbon Nanopores from Electrochemical Dilatometry and Quartz Crystal Microbalance Measurements, *The Journal of Physical Chemistry C* 121(35) (2017) 19120-19128.
- [38] S. Sigalov, M.D. Levi, L. Daiqin, G. Salitra, D. Aurbach, Electrochemical quartz crystal admittance studies of ion adsorption on nanoporous composite carbon electrodes in aprotic solutions, *Journal of Solid State Electrochemistry* 18(5) (2014) 1335-1344.
- [39] F. Escobar-Teran, A. Arnau, J.V. Garcia, Y. Jimenez, H. Perrot, O. Sel, Gravimetric and dynamic deconvolution of global EQCM response of carbon nanotube based electrodes by Ac-electrogravimetry, *Electrochemistry Communications* 70 (2016) 73-77.
- [40] M.D. Levi, G. Salitra, N. Levy, D. Aurbach, J. Maier, Application of a quartz-crystal microbalance to measure ionic fluxes in microporous carbons for energy storage, *Nat Mater* 8(11) (2009) 872-5.
- [41] S. Sigalov, M.D. Levi, G. Salitra, D. Aurbach, J. Maier, EQCM as a unique tool for determination of ionic fluxes in microporous carbons as a function of surface charge distribution, *Electrochemistry Communications* 12(12) (2010) 1718-1721.
- [42] M. Hahn, O. Barbieri, R. Gally, R. Kotz, A dilatometric study of the voltage limitation of carbonaceous electrodes in aprotic EDLC type electrolytes by charge-induced strain, *Carbon* 44(12) (2006) 2523-2533.
- [43] M.M. Hantel, D. Weingarh, R. Kotz, Parameters determining dimensional changes of porous carbons during capacitive charging, *Carbon* 69 (2014) 275-286.
- [44] D. Moreno, Y. Bootwala, W.Y. Tsai, Q. Gao, F.Y. Shen, N. Balke, K.B. Hatzell, M.C. Hatzell, In Situ Electrochemical Dilatometry of Phosphate Anion Electrosorption, *Environmental Science & Technology Letters* 5(12) (2018) 745-749.
- [45] M.M. Hantel, V. Presser, R. Kotz, Y. Gogotsi, In situ electrochemical dilatometry of carbide-derived carbons, *Electrochemistry Communications* 13(11) (2011) 1221-1224.
- [46] N. Jackel, B. Krüner, K.L. Van Aken, M. Alhabeb, B. Anasori, F. Kaasik, Y. Gogotsi, V. Presser, Electrochemical in Situ Tracking of Volumetric Changes in Two-Dimensional Metal Carbides (MXenes) in Ionic Liquids, *ACS Appl Mater Interfaces* 8(47) (2016) 32089-32093.
- [47] Y.C. Wu, P.L. Taberna, P. Simon, Tracking ionic fluxes in porous carbon electrodes from aqueous electrolyte mixture at various pH, *Electrochemistry Communications* 93 (2018) 119-122.

- [48] W.Y. Tsai, P.L. Taberna, P. Simon, Electrochemical quartz crystal microbalance (EQCM) study of ion dynamics in nanoporous carbons, *J Am Chem Soc* 136(24) (2014) 8722-8.
- [49] M.D. Levi, N. Levy, S. Sigalov, G. Salitra, D. Aurbach, J. Maier, Electrochemical quartz crystal microbalance (EQCM) studies of ions and solvents insertion into highly porous activated carbons, *J Am Chem Soc* 132(38) (2010) 13220-2.
- [50] A. Slesinski, C. Matei-Ghimbeu, K. Fic, F. Béguin, E. Frackowiak, Self-buffered pH at carbon surfaces in aqueous supercapacitors, *Carbon* 129 (2018) 758-765.
- [51] N. Agmon, Mechanism of hydroxide mobility, *Chemical Physics Letters* 319(3-4) (2000) 247-252.
- [52] R. Ludwig, New insight into the transport mechanism of hydrated hydroxide ions in water, *Angew Chem Int Ed Engl* 42(3) (2003) 258-60.
- [53] A.G. Volkov, S. Paula, D.W. Deamer, Two mechanisms of permeation of small neutral molecules and hydrated ions across phospholipid bilayers, *Bioelectrochemistry and Bioenergetics* 42(2) (1997) 153-160.
- [54] P.W. Atkins, *Atkins' physical chemistry*, Eleventh edition / Peter Atkins, Julio de Paula, James Keeler... ed., Oxford, United Kingdom : Oxford University Press, Oxford, United Kingdom Oxford, 2018.
- [55] Z. Bo, J.Y. Yang, H.L. Qi, J.H. Yan, K.F. Cen, Z.J. Han, Revealing ion transport in supercapacitors with Sub-2 nm two-dimensional graphene channels, *Energy Storage Materials* 31 (2020) 64-71.
- [56] M.F. Dupont, S.W. Donne, A Step Potential Electrochemical Spectroscopy Analysis of Electrochemical Capacitor Electrode Performance, *Electrochimica Acta* 167 (2015) 268-277.
- [57] M. Forghani, S.W. Donne, Modification of the Step Potential Electrochemical Spectroscopy Analysis Protocol to Improve Outcomes, *Journal of the Electrochemical Society* 166(13) (2019) A2727-A2735.
- [58] J. Jagiello, J.P. Olivier, 2D-NLDFIT adsorption models for carbon slit-shaped pores with surface energetical heterogeneity and geometrical corrugation, *Carbon* 55 (2013) 70-80.
- [59] J. Jagiello, J.P. Olivier, Carbon slit pore model incorporating surface energetical heterogeneity and geometrical corrugation, *Adsorption*, 2013, pp. 777-783.
- [60] A. Slesinski, S. Sroka, K. Fic, E. Frackowiak, J. Menzel, Operando Monitoring of Local pH Value Changes at the Carbon Electrode Surface in Neutral Sulfate-Based Aqueous Electrochemical Capacitors, *Acs Applied Materials & Interfaces* (2022).
- [61] M. Pourbaix, *Atlas of electrochemical equilibria in aqueous solutions*, Oxford : Pergamon, Oxford, 1966.
- [62] N. Shimodaira, A. Masui, Raman spectroscopic investigations of activated carbon materials, *Journal of Applied Physics* 92(2) (2002) 902-909.
- [63] F. Tuinstra, J.L. Koenig, Raman Spectrum of Graphite, *The Journal of Chemical Physics* 53(3) (1970) 1126-1130.
- [64] S. Leyva-García, E. Morallón, D. Cazorla-Amorós, F. Béguin, D. Lozano-Castelló, New insights on electrochemical hydrogen storage in nanoporous carbons by in situ Raman spectroscopy, *Carbon* 69 (2014) 401-408.

Supplementary information

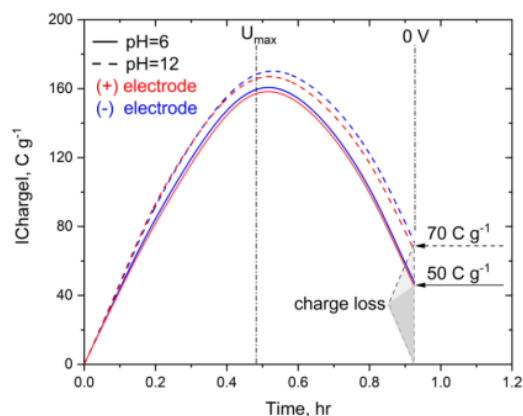
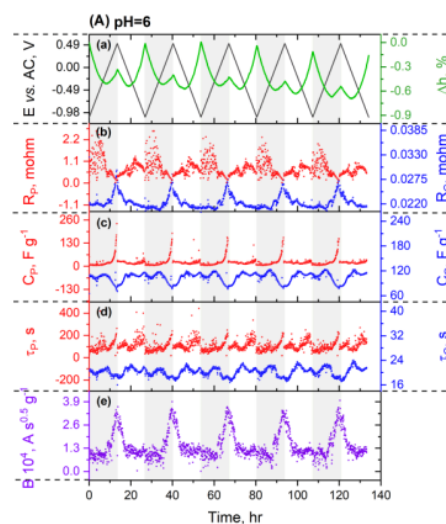


Fig. S1. Charge accumulated at the electrode polarized positively and negatively for the cell operating at 1.6 V at the electrolyte of pH 6 and 12.



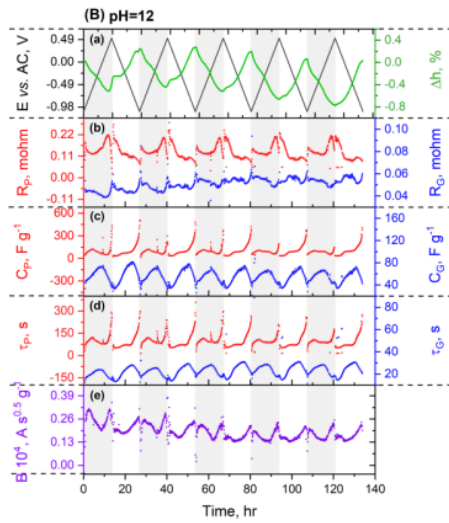


Fig. S2. Parameters obtained from the SPECS technique for the five cycles of electrode repolarization in full potential range for 1.6 V for cell with 1 mol L⁻¹ Li₂SO₄ at pH (A) 6 and (B) 12: (a) dilatometry displacement Δh , porous and geometric (b, d) resistance R , (c, e) differential specific capacitance C and (f, g) time constant τ , (h) specific normalized diffusion parameter B .

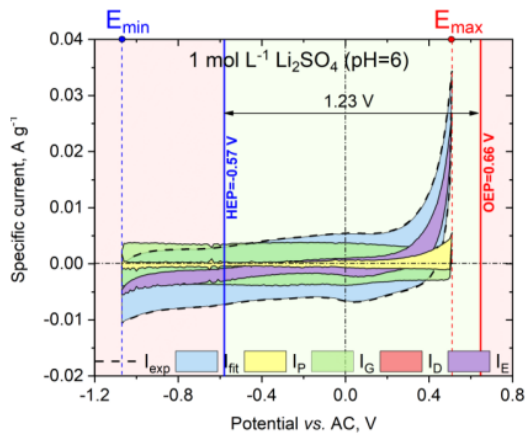


Fig. S3. SPECS results presented as voltammetry profiles for the ECs operating in 1 mol L⁻¹ Li₂SO₄ of pH 6 - zoom for Fig. 8a.

11. Computer software

Title: ***SPECSfit - application for data conversion from Step Potential Electrochemical Spectroscopy technique***

Authors: Przemysław Galek, Maciej Staszak, Krzysztof Fic



Motivation

The motivation for creating the '*SPECSfit*' software was the need to reduce the time spent on calculations and to increase the possibility of controlling the obtained results recorded with the Step Potential Electrochemical Spectroscopy (SPECS) technique. In the initial stage of using this technique, the recorded data was processed by the Origin® program, which did not allow automatic counting of the entire spectrum of the collected data. So far, only selected current curves recorded at a given potential step have been manually adjusted. It was related to the limitation of the time devoted to manual counting. The result of this procedure was to obtain results from only a part of a large data set. The generated charts were not liquid and often did not allow for a reliable interpretation of the results obtained. It was necessary to develop a tool allowing for quick data processing, calculations of the entire range in which they were collected, and real-time visualization of the obtained electrochemical parameters.

Summary

As a result of cooperation with Dr. Maciej Staszak, a '*SPECSfit*' computer program was created to automatically process the results obtained with the SPECS technique. The program is based on the Visual Basic.NET programming language, and it can run on any computer operating system. '*SPECSfit*' is compatible with BioLogic Science Instruments EC-Lab® software. The data are loaded into the program with the Microsoft Project Template (MPT) file extension. The finally converted data are obtained in the Microsoft Excel Open XML Spreadsheet (XLSX) file. This file is automatically created when

the calculation procedure is started in the 'SPECStfit' program. Data are collected systematically as the implementation of the calculation procedure progresses. The application also enables visualization of the electrochemical parameters calculated on graphs in real time.

Program description

The SPECStfit program dialog box is shown in **Fig. 7**.

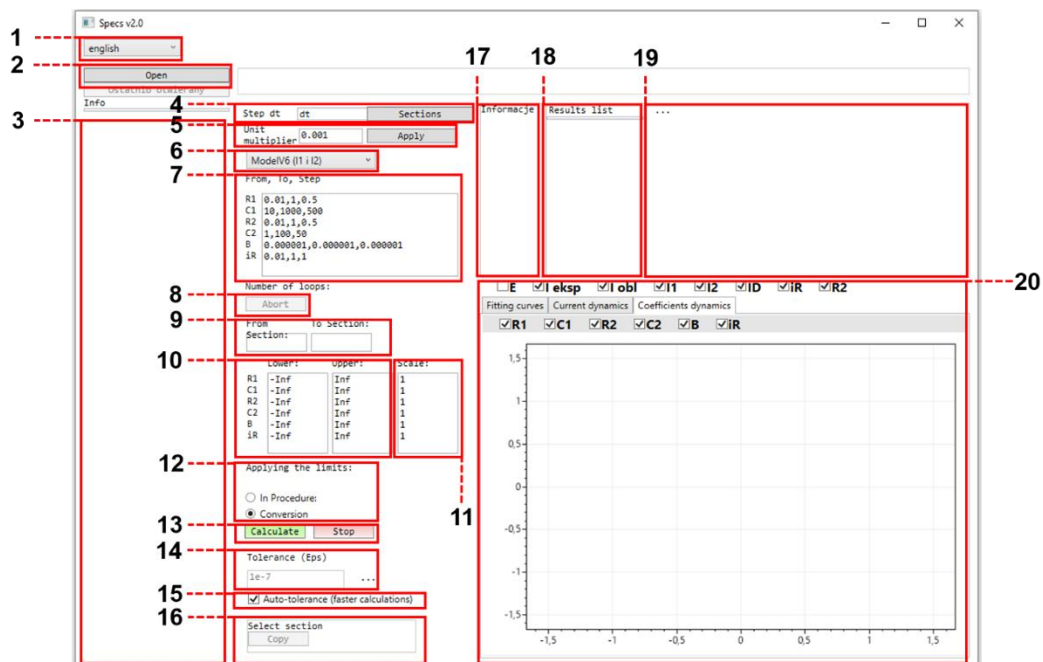


Fig. 7. Dialogue box of the 'SPECStfit' program.

- 1 – In this area, it is possible to select the language (English/Polish) in which the program dialog window will be displayed.
- 2 – '**Open**' button opens the source where the data are to be loaded from to the application. This source is previously exported as an MPT file from the EC-Lab program. The MPT file must be in the same folder as all 'SPECStfit' related files.
- 3 – The uploaded data are displayed in this area as sections. Each section represents a step potential for which data was recorded. In addition, next to the section, the range of time (in seconds) in which the data was collected during the experiment appears.
- 4 – The value of '**Step dt**' is usually read by the program automatically and means the time interval (in seconds) at which the points

of the recorded current curve were collected. This value is read from the specific line of the MPT file. However, the latest versions of the EC-Lab program do not always provide this value in the MPT source file.

- 5 – The '**Unit multiplier**' settings allow a quick change in the decimal place of the results obtained.
- 6 – In this area, the user can choose one of the four options. 1) '**ModellV6 (I1 and I2)**' where the component corresponding to the formation of EDL is divided into two components (porous *I1* and geometric *I2*). 2) '**ModellV4 (I)**' where the porous and geometric components are summed to one common component *I1*. 3) and 4) '**Diffusion model**' where basic equation for diffusion current *ID* appears in tabs 1) and 2):

$$i_D = \frac{B}{t^{0.5}}$$

is divided to an equation with more detailed parameters:

$$i_D = \frac{FD\Delta C}{h} \left(1 + 2 \sum_{k=1}^{\infty} \exp\left(-\frac{k^2\pi^2Dt}{h^2}\right) \right)$$

- 7 – In the given area, it is possible to make changes in the value range of individual components when calculations are realised. The first value is the initial value (always lower), the second one is the final value of the range (always higher). Selecting the range as close as possible to the final values increases the speed of the calculations performed. The third value in the line is the step at which the calculations are performed. The number of loops performed on the basis of the entered limit values and the number of steps performed is automatically displayed in the window. It is recommended to adjust the start values so that the number of loops ranges from 17 to 84. Too small loops number increases the calculation error, while too many loops unnecessarily extend the time of data processing without a further

error value reduction. A description of individuals' parameters is given below (more details are given in **Chapter 4**).

$R1, R2$ – porous and geometric resistance (ohm)

$C1, C2$ – porous and geometric differential capacitance (mF)

B – diffusion component ($C s^{0.5}$)

IR – residual current (mA)

ΔC – concentration difference of the diffusing species between the interface and bulk ($mol m^{-3}$)

H – diffusion layer thickness (m)

D – concentration independent diffusion coefficient ($m^2 s^{-1}$)

- 8 – By '**Abort**' button the user can stop the calculation procedure at any time.
- 9 – In the '*From section*' and '*To section*' windows, the user can define the range of calculated sections.
- 10 – This area was added mainly due to program errors occurring from time to time. Single points that should be in the trend of the calculated parameters $R1$ or $C1$ are sometimes assigned $R2$ or $C2$ and vice versa. It is possible to force the program to count the searched values by entering the predicted ranges in which the calculated parameters should fall. Such an action prevents them from being flipped to the twin terms of the equation.
- 11 - In '*SPECSfit*' there is also a possibility to modify the importance of the searched variables and this option can be found in the area '**Scale**'. It is a factor that determines the importance level of a given component in the calculation procedure performed. By default, for all components, the importance is set to '1', which means that there is no scaling. The larger the scale, the greater the weight of a given factor. This area allows us to control the obtained results. If the calculations are correct, assigning a different weight should not affect the final result.
- 12 – It is necessary to mark the '**Conversion**' item to correct the conversion of conversion of points using the method presented in the area (10).

- There is also the possibility of automatic point point exchange by selecting the item 'In procedure'. However, this option has some disadvantages and does not always result in component swapping.
- 13 – The '**Calculate**' button starts and the 'Stop' button interrupts the calculation procedure.
 - 14 – '**Tolerance (Eps)**' is an acceptable numerical relative error. The lower the value of this parameter, the longer the computational procedure takes, but more precisely.
 - 15 - After starting the application, the '**Auto tolerance (faster calculation)**' option is automatically selected.
 - 16 – It is possible to copy the experimental data of a given section from the area (2) by clicking the '**Copy**' button.
 - 17 – On the '**Information**' tab, in the right-hand side of the dialog box, information about the calculation progress is displayed.
 - 18 – In the '**Result List**' section numbers are displayed for which results have already been obtained. This list is completed as the procedure progresses.
 - 19 – The '**Description**' area is a preview of the preview of the results obtained for the selected section.
 - 20 – Graphs are represented in the area in the lower part of the dialog box on the right side. After selecting the '**Fit curves**' tab and the appropriate markers in the upper part of the area, the graph shows the dependence of the selected value (on the Y-axis) on the measurement time (in seconds) of a given section at a given E/U (X-axis). Symbol ' E ' means the E/U at which the given section was recorded. ' I_{exp}/I_{cal} ' is the experimental and the calculated (fit) current, respectively. The last box ' $R2$ ' defines the matching error value. In the '**Current dynamics**' tab, the results (I_{cal} , I_1 , I_2 , ID , IR , $R2$, without E and I_{exp}) are displayed for all completed sections depending on the duration of the experiment. The last tab '**Coefficients dynamics**' allows one to display the calculated parameters $R1$, $C1$, $R2$, $C2$, B , ΔC , h , D , and IR .

12. Summary

The dissertation consideration emphasizes both the current state of knowledge and experimental research (applied and fundamental) within electrochemical capacitors. The first and fundamental element of high-performance devices production is understanding the phenomena and processes related to the charge storage at the electrode/electrolyte interface at the molecular level. The research presented in this dissertation deals with this topic. The differences resulting from the wide application wide salt concentration in the aqueous electrolyte are discussed here, including the new concept of a saturated solution of ‘*water in salt*’ (**Article 2**). High salt concentration is associated with increased electrolyte viscosity, which has a significant impact on ECs performance (**Article 3**). Increased viscosity with system preconditioning and appropriate electrode material may lead to the improvement of such EC parameters as self-discharge or gas evolution. For effective charge storage in a given electrode material, it is necessary to match the ions' size with the pores diameter. The merging of electrochemical dilatometry with step potential electrochemical spectroscopy led to the definition of the type of charge storage mechanism depending on the electrolyte and electrode material (**Article A4**). However, manual data processing from SPECS is not the fastest way. The computer program developed ‘*SPECSfit*’, comes with help for fast and reliable data processing (**Chapter 12**). The influence of pH at the electrode surface has already been described, but only now has the influence of H^+ and OH^- ions concentration on ion movement in porous materials been thoroughly explained (**Article 5**). The electrodes production and device assembly are the last stage in which there is an opportunity to improve the ECs performance. This applies to improving the rheological properties of the electrode slurry, appropriate selection mixing technique, and current collector coverage (**Article 1**). The literature analysis and the presented experimental results cover a wide range of ECs elements and are to be the basis for undertaking new research paths in this subject.

13. Articles not included in the dissertation topic

Title: ***Revisited insights into charge storage mechanisms in electrochemical capacitors with Li₂SO₄-based electrolyte***

Authors: Krzysztof Fic, Anetta Płatek, Justyna Piwek, Jakub Menzel, Adam Ślesiński, Paulina Bujewska, Przemysław Galek, Elżbieta Frąckowiak

Journal: Energy Storage Materials, 2019, vol. 22, 1-14

DOI: 10.1016/j.ensm.2019.08.005

Abstract

The article comprehensively describes the latest achievements related to the use of neutral water-based electrolyte (1 mol L⁻¹ Li₂SO₄ solution) in ECs. The basic physicochemical properties of aqueous electrolytes (conductivity, viscosity, etc.), EC operating parameters and a proposal for a new approach in the study of systems – operando tests were discussed. The operando studies performed included the use of electrochemical quartz crystal microbalance (EQCM), Raman spectroscopy, and scanning electrochemical microscopy (SECM). Interesting results were obtained concerning the specific and selective adsorption of ions with the use of the given methods. In addition is presented a post-mortem analysis of carbon electrodes subjected to the aging protocol. The effect of an anti-aging additive (tocopherol - vitamin E) on the electrode material and the electrolyte was investigated. Finally, mechanisms governing the capacitive and redox interfacial interactions are proposed.



Title: ***Three-dimensional architectures in electrochemical capacitor applications – insights, opinions and perspectives***

Authors: Przemysław Galek, Adam Maćkowiak, Paulina Bujewska, Krzysztof Fic

Journal: Frontiers in Energy Research, 2020, vol. 8, 139-1 - 139-21

DOI: 10.3389/fenrg.2020.00139

Abstract

This article is a summary of the latest news on electrode materials with a 3D structure in ECs applications. The division of this group of structures was systematized, taking into account the method of their production: into template and non-template strategies. The advantages and disadvantages for the selected groups have been summarized. Special attention has been paid to the carbon materials for their structural connection as they not only create the desired hierarchical porous channels, but also provide high conductivity and mechanical stability. For individual solutions, numerous examples from the literature are presented. Finally, the future challenges for this type of material are summarized.



Title: ***Deep eutectic solvents for high-temperature electrochemical capacitors***

Authors: Adam Maćkowiak, Przemysław Galek, Krzysztof Fic

Journal: ChemElectroChem, 2021, vol. 8, 4028-4037

DOI: 10.1002/celec.202100711

Abstract

In this article authors propose the concept of EC operating in high-temperature conditions (100°C). This solution is an electrolyte in the form of a deep eutectic mixture based on lithium nitrate and acetamide. To describe the chemistry of the mixture, infrared and Raman spectroscopy, differential scanning calorimetry, and gas chromatography with mass spectrometry were used. Electrochemical analysis includes verification of system aging, self-discharge monitoring, leakage current measurement, and basic research related to determination of specific capacitance or maximum voltage. Additionally, a comprehensive analysis of the addition of lithium nitrate salt and an organic solvent to the operating system was performed, including the replacement of lithium ions with sodium or potassium.



Title: ***Contact angle analysis of surface topographies created by electric discharge machining***

Authors: Katarzyna Peta, Tomasz Bartkowiak, Przemysław Galek, Michał Mendak

Journal: Tribology International, 2021, vol. 163, 107139-1 - 107139-14

DOI: 10.1016/j.triboint.2021.107139

Abstract

The article specifies the relationship between the wettability and the surface microgeometry of the 6060 aluminum alloy resulting from electro-discharge machining (EDM). The analyzes were extended by calculating the strength of the correlation between the contact angles and the geometrical surface topography characteristics that change with the observation scale. Surface topographies are measured with a focal variation microscope and characterized by ISO parameters, geometric motifs, and multiscale curvature tensor analysis. The wettability of the finished structures was tested indirectly by measuring the contact angle. The analysis was performed by using aqueous solutions of a semi-synthetic polymer of various concentrations and viscosities. The study showed that aluminum alloy wetting can be easily controlled with a suitable EDM finish.

Title: ***Operando monitoring of activated carbon electrodes operating with aqueous electrolytes***

Authors: Jakub Menzel, Adam Slesinski, Przemyslaw Galek, Paulina Bujewska, Andrii Kachmar, Elżbieta Frąckowiak, Ayumi Washio, Hirofumi Yamamoto, Masashi Ishikawa, Krzysztof Fic

Journal: Energy Storage Materials, 2022, 518-528

DOI: 10.1016/j.ensm.2022.04.030

Abstract

Remarkable changes in the volume of activated carbon electrodes operating with aqueous electrolytes were measured with scanning electrochemical microscopy (SECM) and electrochemical dilatometry (ECD) techniques. It appears that the electrolyte volume absorbed by the carbon electrode strongly depends on the polarization direction and the electrode potential. It is assumed that these changes result from different ion adsorption properties and the volume of the electrolyte. Furthermore, the electrode surface functionalities appear to change. This has been confirmed by operando contact angle measurements. In addition to the observations of volume changes, a method of preconditioning electrochemical capacitors is proposed, which is an outcome of the observed electrode dilatations and modulated wettability. The conditioning method promotes deep electrochemical impregnation of the electrodes by an electrolyte. In fact, remarkably better wetting of the electrodes is reflected in significant changes in the potential distribution between electrodes. Moreover, the internal pressure build-up during the potentiostatic hold test is reduced. Finally, in situ observations of the electrodes with X-ray tomography suggest the precipitation of insoluble deposits at the surface of the positive electrode near the separator.

List of figures and tables

Figures

Fig. 1. Energy sources and methods of its conversion [2].	23
Fig. 2. Ragone plot for electrochemical energy storage systems [12, 13].	25
Fig. 3. Electrochemical capacitor: (a) construction, (b) types, and (c) principle of operation.	31
Fig. 4. Electrode materials for electrochemical capacitors.	33
Fig. 5. The advantages of carbon materials [32-34].	34
Fig. 6. Composition of electrode in electrochemical capacitor.	45
Fig. 7. Dialogue box of the 'SPECStit' program.	121

Tables

Tab. 1. Application of electrochemical energy storage systems (fuel cells, batteries, capacitors) [8-10].	27
Tab. 2. Advantages and disadvantages of electrochemical energy storage systems (fuel cells, batteries, capacitors) [8-10].	27

Scientific accomplishments

14. Publications

- 1) *'Revisited insights into charge storage mechanisms in electrochemical capacitors with Li₂SO₄-based electrolyte'*
Fic K., Płatek A., Piwek P., Menzel J., Ślesiński A., Bujewska P., **Galek P.**,
Frąckowiak E.
Energy Storage Materials, 22 (2019), 1-14 **IF=16.280**
- 2) *'Interfacial aspects induced by saturated aqueous electrolytes in electrochemical capacitor applications'*
Galek P., Frąckowiak E. Fic K.
Electrochimica Acta , 334 (2020), 135572-1-135572-12 **IF=6.901**
- 3) *'Three-dimensional architectures in electrochemical capacitor applications – insights, opinions and perspectives'*
Galek P., Maćkowiak A. Bujewska P., Fic K.
Frontiers in Energy Research, 8 (2020), 139-1-139-21 **IF=4.008**
- 4) *'Peculiar role of the electrolyte viscosity in the electrochemical capacitor performance'*
Galek P., Ślesiński A., Fic K., Menzel J.
Journal of Materials Chemistry A, 13 (2021), 8644-8654 **IF=12.732**
- 5) *'New Insight into Ion Dynamics in Nanoporous Carbon Materials: an Application of the Step Potential Electrochemical Spectroscopy (SPECS) Technique and Electrochemical Dilatometry'*
Galek P., Bujewska P., Donne S., Fic K., Menzel J.
Electrochimica Acta, 337 (2021), 138115-1-138115-7 **IF=6.901**
- 6) *'Contact angle analysis of surface topographies created by electric discharge machining'*
Peta K., Bartkowiak T., **Galek P.**, Mendak M.
Tribology International, 163 (2021), 107139-1-107139-14 **IF=4.872**
- 7) *'Deep Eutectic Solvents for High-Temperature Electrochemical Capacitors'*
Maćkowiak A., **Galek P.**, Fic K.,
ChemElectroChem, 8 (2021), 1-11 **IF=4.590**

- 8) 'Operando monitoring of activated carbon electrodes operating with aqueous electrolytes'

Menzel J., J, Ślesiński A., **Galek P.**, Bujewska P., Kachmar A., Frąckowiak E., Washio A., Yamamoto H., Ishikawa M., Fic K.

Energy Storage Materials, 49 (2022), 518-528

IF=17.789

Total Impact Factor: 74.073

Impact Factor Including Co-authors: 14.266

15. Chapter

- 1) 'Redox-active electrolytes in electrochemical capacitors'

Bujewska P., **Galek P.**, Frąckowiak E., Fic K

Book: 'Redox Chemistry - From Molecules to Energy Storage', edited by Prof. Olivier Fontaine, ISBN 978-1-80355-538-6, 15.04.2022

16. Patents and patents applications

Patents:

- 1) 'Kondensator elektrochemiczny'

Galek P., Frąckowiak E., Fic K.

Pat.238545

- 2) 'Wysokotemperaturowy kondensator elektrochemiczny'

Maćkowiak A., **Galek P.**, Frąckowiak E., Fic K.

P.434065

Patent application:

- 1) 'Kondensator elektrochemiczny bazujący na proekologicznym spoiwie'

Galek P., Tobis M., Maćkowiak A., Foroutan Koudahi M., Bujewska P., Piwek J., Ślesiński A., Menzel J., Jeżowski P., Fic K.

P.437690

17. Reports

- 1) *'Hydrogen as a future fuel source: electrochemical storage in carbon materials'*

Galek P., Menzel J., Fic K.

Joint Research Centre European Commission Rue du Champ de Mars 21
1050 Brussels, Belgium

- 2) *'Gluten jako proekologiczne spoiwo w kondensatorze elektrochemicznym'*

Galek P., Tobis M., Maćkowiak A., Foroutan Koudahi M., Bujewska P.,
Piwek J., Ślesiński A., Menzel J., Jeżowski P., Fic K.

Subsidy for conducting research and related tasks aimed
at the development of young scientists and participants of doctoral studies
and doctoral schools financed under the internal competition procedure
in 2020.

18. Scientific conferences

18.1. Oral presentations

International range

- 1) *'Impact of the Electrolyte Concentration on the Capacitor Performance'*
Fic K., **Galek P.**, Frąckowiak E.
The 69th Annual Meeting of the International Society of Electrochemistry
Bologna, Italy, 02-07.09.2018
- 3) *'Phenomena at Porous Carbon Electrode/Saturated Electrolyte Interface
in Electrochemical Capacitors'*
Fic K., **Galek P.**, Menzel J., Frąckowiak E.
Americas International Meeting on Electrochemistry and Solid State
Science
Cancun, Mexico, 30.09-04.10.2018

- 4) '*Saturated water-based electrolytes in electrochemical capacitor application*'
Fic K., **Galek P.**, Frąckowiak E.
International Symposium on Enhanced Electrochemical Capacitors
Nantes, France, 06-10.05.2019
- 5) '*Operando exploration of the ionic fluxes at the electrode/electrolyte interface for better electrochemical capacitors*'
Fic K., Płatek A., Menzel J., Ślesiński A., Bujewska P., Piwek J., **Galek P.**, Frąckowiak E
6th International Conference on Advanced Capacitors
Ueda, Japan, 08-12.09.2019
- 6) '*Electrolyte – Important Component of Electrochemical Capacitor*'
Frąckowiak E., Piwek J., Płatek A., Menzel J., **Galek P.**, Fic K
The Third International Conference on Energy Storage Materials
Shenzhen, China, 28.11-01.12.2019
- 7) '*Insights into Ionic Fluxes at Electrode/Electrolyte Interface in Carbon-Based Electrochemical Capacitors with SPECS Technique and Electrochemical Dilatometry*'
Galek P., Menzel J., Bujewska P., Donne S., Fic K.
2020 Virtual MRS Spring/Fall Meeting & Exhibit (online)
Boston, USA, 27.11-04.12.2020
- 8) '*New Insight into Ion Dynamics in Nanoporous Carbon Materials: an Application of the Step Potential Electrochemical Spectroscopy (SPECS) Technique and Electrochemical Dilatometry*'
Menzel J., **Galek P.**, Bujewska P., Donne S., Fic K.
72nd Annual Meeting of the International Society of Electrochemistry (online)
Jeju , Korea, 29.08-03.09.2021

- 9) *'Impact of OH^- and H^+ ions concentration on electrical double-layer formation and electrode expansion in porous carbon materials'*
Galek P., Bujewska P., Fic K.
International Symposium on Enhanced Electrochemical Capacitors
Bologne, Italy, 11-15.07.2022
- 10) *'Analysis of carbon electrode dilatometric strain determined by Scanning Electrochemical Microscopy and internal pressure measurements'*
Menzel J., Ślesiński A., **Galek P.**, Bujewska P., Frąckowiak E., Fic K.
International Symposium on Enhanced Electrochemical Capacitors
Bologne, Italy, 11-15.07.2022
- 11) *'A step potential electrochemical spectroscopy (SPECS) investigation of the lithium intercalation process'*
Maćkowiak A., **Galek P.**, Jeżowski P., Fic K.
Regional Meeting of the International Society of Electrochemistry
Prague, Czech Republic, 15-19.08.2022
- 12) *'Influence of the Cation Size and the Electrolyte pH on the Electrical Double-Layer Formation Determined by Electrochemical Dilatometry'*
Bujewska P., **Galek P.**, Fic K.
Regional Meeting of the International Society of Electrochemistry
Prague, Czech Republic, 15-19.08.2022
- 13) *'In-depth investigation of lithium intercalation into graphite layers using step potential electrochemical spectroscopy (SPECS)'*
Maćkowiak A., **Galek P.**, Jeżowski P., Fic K.
72rd Annual Meeting of the International Society of Electrochemistry
(online)
12-16.09.2022

National range

- 1) *'Impact of the Electrolyte Viscosity on the Electrochemical Capacitor Performance'*

Galek P., Menzel J., Fic K.

XI Konferencja Naukowo-Techniczna *'Materiały Węglowe i Kompozyty Polimerowe'*

Jaszowiec, Poland, 02-05.04.2019

- 2) *'Electrochemical capacitors – mutual interactions of rheology and electrochemistry'*

Galek P., Frąckowiak E., Fic K

II Polish Carbon Society Scientific Workshop "New trends in carbon research"

Poznan, Poland, 27.10.2019

18.2. Poster presentations

International range

- 1) *'Correlation of Rheological Parameters of Supercapacitor Components with Electrochemical Performance'*

Galek P., Frąckowiak E., Fic K.

The First International Conference on Energy Storage Materials

Shenzhen, China, 18-21.11.2017

- 2) *'Correlation of Rheological Parameters of Activated Carbon Coatings with their Electrochemical Response in Aqueous Electrolytes'*

Galek P., Frąckowiak E., Fic K.

Supercapacitors: Store for the Future

Goteborg, Sweden, 11-13.06.2018

- 3) *'Correlation of Rheological Parameters of Activated Carbon Coatings with their Electrochemical Response in Aqueous Electrolytes'*

Galek P., Frąckowiak E., Fic K.

Carbon 2018 – The World Conference on Carbon

Madrid, Spain, 01-06.07.2018

- 4) *'Electrolyte viscosity: limiting parameter of electrochemical capacitor efficiency?'*
Galek P., Menzel J., Fic K.
International Symposium on Enhanced Electrochemical Capacitors
Nantes, France, 06-10.05.2019
- 5) *'Deep Eutectic Solvents Based on Lithium Nitrate and Acetamide as Electrolyte in High-Temperature Electric Double-Layer Capacitors'*
Maćkowiak A., Galek P., Fic K.
71st Annual ISE Meeting (online)
Belgrad, Serbia, 30.08-04.09.2020
- 6) *'Unveiling the origin of carbon dilatometric changes with the application of novel SPECS technique'*
Menzel J., Galek P., Bujewska P., Donne S., Fic K.
71st Annual ISE Meeting (online)
Belgrad, Serbia, 30.08-04.09.2020
- 7) *'Deep Eutectic Solvents Based on Lithium Nitrate and Acetamide as Electrolytes in High-Temperature Electric Double-Layer Capacitors'*
Maćkowiak M., Galek P., Fic K.
12th European Symposium on Electrochemical Engineering (online)
Leeuwarden, Holland, 14-17.06.2021
- 8) *'Point of Zero Charge - Meaning and Determination with the Electrochemical Quartz Crystal Microbalance'*
Sroka S., Galek P., Płatek-Mielczarek A., Menzel J., Fic K.
72nd Annual Meeting of the International Society of Electrochemistry (online)
Jeju, Korea, 29.08-03.09.2021
- 9) *'New insights into Point of Zero Charge determination with Electrochemical Quartz Crystal Microbalance'*
Sroka S., Galek P., Płatek-Mielczarek A., Menzel J., Fic K.
International Symposium on Enhanced Electrochemical Capacitors
Bologne, Italy, 11-15.07.2022

National range

- 1) *'Correlation of Rheological Parameters of Activated Carbon Coatings with their Electrochemical Response in Aqueous Electrolytes'*
Galek P., Frąckowiak E., Fic K.
XI Konferencja Naukowo-Techniczna „Materiały Węglowe i Kompozyty Polimerowe”
Jaszowiec, Poland, 17-20.04.2018
- 2) *'Electrical energy storage systems - perspectives for the future'*
Galek P., Ślesiński A., Fic K.
Polish Scientific Networks 2019 Conference
Poznan, Poland, 19-21.10.2019

19. Awards

- 1) **Award for Master thesis:**
'Determination of rheological parameters of the electrode slurry and electrolyte solutions and their correlation with electrochemical properties'
Galek P., Fic K.
Polski Komitet Materiałów Elektrotechnicznych Stowarzyszenia Elektryków Polskich
Wrocław, Poland, 08.12.2017
- 2) **Poster prize:**
'Electrolyte viscosity: limiting parameter of electrochemical capacitor efficiency?'
Galek P., Menzel J., Fic K.
International Symposium on Enhanced Electrochemical Capacitors
Nantes, France, 09.05.2019
- 3) **Cover page:**
'Deep Eutectic Solvents for High-Temperature Electrochemical Capacitors'
(*ChemElectroChem* 21/2021)
Maćkowiak A., **Galek P.**, Fic K.

4) **Distinction:**

Award of the Poznan Department of the Polish Academy of Sciences for the best original creative work, the lead author of which is a PhD student from the Department area

Poznan, Poland, 07.06.2022

5) **Scholarship:**

Poznan City Scholarship for young researchers from the Poznan scientific community

Poznan, Poland, 27.06.2022

20. Research project

1) **Researcher in European Research Council (ERC) GA 759603 project**

'If immortality unveil...' – development of the novel types of energy storage systems with excellent long-term performance'

21. Memberships in scientific organizations and other functions/trainings

Memberships:

- 1) International Society of Electrochemistry
- 2) Polish Carbon Society

Conferences organizer:

- 1) *'Komerccjalizacja badań – wyzwanie dla młodych naukowców'*
(Warsaw, Poland, 15.11.2018)
- 2) *'Polish Scientific Networks: Science and Technology Conference'*
(Poznan, Poland, 19-21.09.2019)

Trainings:

- 1) *'International Summer School (ISS) on Energy Storage Systems: New Developments and Directions'* (Zaragoza, Spain, 18-21.07.2022)
- 2) *'Battery energy storages in smart grids'* – Eunice European University



- 3) Statistica software: '*DOE – computer aided planning and statistical analysis of innovative research*'
- 4) Autodesk AutoCAD software (basic level)
- 5) Origin software '*Basics of data analysis in the program environment*'
- 6) Autodesk Inventor (advanced level)
- 7) Summer school: '*Supercapacitors: Store for the Future*' (Goteborg, Sweden, 11-13.06.2018)

Literature

- [1] D. Larcher, J.M. Tarascon, Towards greener and more sustainable batteries for electrical energy storage, 2015, pp. 19-29.
- [2] A. Czerwiński, Akumulatory, baterie, ogniwa, Wydawnictwa Komunikacji i Łączności, Warszawa, 2018.
- [3] S. Shafiee, E. Topal, When will fossil fuel reserves be diminished?, *Energy Policy* 37(1) (2009) 181-189.
- [4] N. Abas, A. Kalair, N. Khan, Review of fossil fuels and future energy technologies, *Futures* 69 (2015) 31-49.
- [5] A. Poullikkas, A comparative overview of large-scale battery systems for electricity storage, *Renewable & Sustainable Energy Reviews* 27 (2013) 778-788.
- [6] K. Bradbury, L. Pratson, D. Patiño-Echeverri, Economic viability of energy storage systems based on price arbitrage potential in real-time U.S. electricity markets, *Applied Energy* 114 (2014) 512-519.
- [7] G.L. Kyriakopoulos, G. Arabatzis, Electrical energy storage systems in electricity generation: Energy policies, innovative technologies, and regulatory regimes, *Renewable & Sustainable Energy Reviews* 56 (2016) 1044-1067.
- [8] Z. Yang, J. Zhang, M.C. Kintner-Meyer, X. Lu, D. Choi, J.P. Lemmon, J. Liu, Electrochemical energy storage for green grid, *Chem Rev* 111(5) (2011) 3577-613.
- [9] M. Winter, R.J. Brodd, What are batteries, fuel cells, and supercapacitors?, *Chem Rev* 104(10) (2004) 4245-69.
- [10] A. Khaligh, Z.H. Li, Battery, Ultracapacitor, Fuel Cell, and Hybrid Energy Storage Systems for Electric, Hybrid Electric, Fuel Cell, and Plug-In Hybrid Electric Vehicles: State of the Art, *Ieee Transactions on Vehicular Technology* 59(6) (2010) 2806-2814.
- [11] J.r. Garche, C.K. Dyer, *Encyclopedia of electrochemical power sources* / editor-in-chief, Jürgen Garche ; section editors, Chris K. Dyer [and others], Academic Press, Amsterdam ;, 2009.
- [12] P. Simon, Y. Gogotsi, Materials for electrochemical capacitors, *Nat Mater* 7(11) (2008) 845-54.
- [13] Q. Cai, D.J.L. Brett, D. Browning, N.P. Brandon, A sizing-design methodology for hybrid fuel cell power systems and its application to an unmanned underwater vehicle, *Journal of Power Sources* 195(19) (2010) 6559-6569.
- [14] F. Béguin, E. Frąckowiak, *Supercapacitors*, 2013.
- [15] B.E. Conway, *Electrochemical Supercapacitors*, 1st 1999. ed., Springer US, New York, NY, 1999.
- [16] S.M.M. Ehteshami, S.H. Chan, The role of hydrogen and fuel cells to store renewable energy in the future energy network - potentials and challenges, *Energy Policy* 73 (2014) 103-109.
- [17] L.X. Fan, Z.K. Tu, S.H. Chan, Recent development of hydrogen and fuel cell technologies: A review, *Energy Reports* 7 (2021) 8421-8446.
- [18] J.O. Abe, A.P.I. Popoola, E. Ajenifuja, O.M. Popoola, Hydrogen energy, economy and storage: Review and recommendation, *International Journal of Hydrogen Energy* 44(29) (2019) 15072-15086.
- [19] B. Dunn, H. Kamath, J.M. Tarascon, Electrical energy storage for the grid: a battery of choices, *Science* 334(6058) (2011) 928-35.
- [20] N. Yabuuchi, K. Kubota, M. Dahbi, S. Komaba, Research development on sodium-ion batteries, *Chem Rev* 114(23) (2014) 11636-82.
- [21] W. Luo, J. Wan, B. Ozdemir, W. Bao, Y. Chen, J. Dai, H. Lin, Y. Xu, F. Gu, V. Barone, L. Hu, Potassium Ion Batteries with Graphitic Materials, *Nano Lett* 15(11) (2015) 7671-7.
- [22] P. Barber, S. Balasubramanian, Y. Anguchamy, S. Gong, A. Wibowo, H. Gao, H.J. Ploehn, H.C. zur Loye, Polymer Composite and Nanocomposite Dielectric Materials for Pulse Power Energy Storage, *Materials* 2(4) (2009) 1697-1733.
- [23] J. Ho, T.R. Jow, S. Boggs, Historical Introduction to Capacitor Technology, *Ieee Electrical Insulation Magazine* 26(1) (2010) 20-25.
- [24] F. Béguin, E. Frąckowiak, *Carbons for Electrochemical Energy Storage and Conversion Systems*, 2009.

- [25] G.C. Gschwend, A. Olaya, H.H. Girault, How to polarise an interface with ions: the discrete Helmholtz model, *Chem Sci* 11(39) (2020) 10807-10813.
- [26] K.B. Oldham, A Gouy-Chapman-Stern model of the double layer at a (metal)/(ionic liquid) interface, *Journal of Electroanalytical Chemistry* 613(2) (2008) 131-138.
- [27] D.C. Grahame, The electrical double layer and the theory of electrocapillarity, *Chem Rev* 41(3) (1947) 441-501.
- [28] B.E. Conway, V. Birss, J. Wojtowicz, The role and utilization of pseudocapacitance for energy storage by supercapacitors, *Journal of Power Sources* 66(1-2) (1997) 1-14.
- [29] S. Roldán, M. Granda, R. Menéndez, R. Santamaría, C. Blanco, Mechanisms of Energy Storage in Carbon-Based Supercapacitors Modified with a Quinoid Redox-Active Electrolyte, *The Journal of Physical Chemistry C* 115(35) (2011) 17606-17611.
- [30] G.H. Yu, X. Xie, L.J. Pan, Z.N. Bao, Y. Cui, Hybrid nanostructured materials for high-performance electrochemical capacitors, *Nano Energy* 2(2) (2013) 213-234.
- [31] E. Frackowiak, F. Beguin, Carbon materials for the electrochemical storage of energy in capacitors, *Carbon* 39(6) (2001) 937-950.
- [32] B. Xu, F. Wu, R.J. Chen, G.P. Cao, S. Chen, Z.M. Zhou, Y.S. Yang, Highly mesoporous and high surface area carbon: A high capacitance electrode material for EDLCs with various electrolytes, *Electrochemistry Communications* 10(5) (2008) 795-797.
- [33] C. Merlet, B. Rotenberg, P.A. Madden, P.L. Taberna, P. Simon, Y. Gogotsi, M. Salanne, On the molecular origin of supercapacitance in nanoporous carbon electrodes, *Nat Mater* 11(4) (2012) 306-10.
- [34] F. Xu, Z. Tang, S. Huang, L. Chen, Y. Liang, W. Mai, H. Zhong, R. Fu, D. Wu, Facile synthesis of ultrahigh-surface-area hollow carbon nanospheres for enhanced adsorption and energy storage, *Nat Commun* 6(1) (2015) 7221.
- [35] Y. Zhang, H. Feng, X.B. Wu, L.Z. Wang, A.Q. Zhang, T.C. Xia, H.C. Dong, X.F. Li, L.S. Zhang, Progress of electrochemical capacitor electrode materials: A review, *International Journal of Hydrogen Energy* 34(11) (2009) 4889-4899.
- [36] D.Y. Qu, H. Shi, Studies of activated carbons used in double-layer capacitors, *Journal of Power Sources* 74(1) (1998) 99-107.
- [37] L.H. Wang, M. Toyoda, M. Inagaki, Dependence of electric double layer capacitance of activated carbons on the types of pores and their surface areas, *New Carbon Materials* 23(2) (2008) 111-115.
- [38] Q.Y. Li, H.Q. Wang, Q.F. Dai, J.H. Yang, Y.L. Zhong, Novel activated carbons as electrode materials for electrochemical capacitors from a series of starch, *Solid State Ionics* 179(7-8) (2008) 269-273.
- [39] G. Lota, T.A. Centeno, E. Frackowiak, F. Stoeckli, Improvement of the structural and chemical properties of a commercial activated carbon for its application in electrochemical capacitors, *Electrochimica Acta* 53(5) (2008) 2210-2216.
- [40] C. Bouchelta, M.S. Medjram, O. Bertrand, J.P. Bellat, Preparation and characterization of activated carbon from date stones by physical activation with steam, *Journal of Analytical and Applied Pyrolysis* 82(1) (2008) 70-77.
- [41] J.A. Maciá-Agulló, B.C. Moore, D. Cazorla-Amorós, A. Linares-Solano, Activation of coal tar pitch carbon fibres: Physical activation vs. chemical activation, *Carbon* 42(7) (2004) 1367-1370.
- [42] Q. Lu, Z.X. Zhang, X. Wang, H.Q. Guo, M.S. Cui, Y.P. Yang, Catalytic Fast Pyrolysis of Biomass Impregnated with Potassium Phosphate in a Hydrogen Atmosphere for the Production of Phenol and Activated Carbon, *Front Chem* 6 (2018) 32.
- [43] S.H. Pak, M.J. Jeon, Y.W. Jeon, Study of sulfuric acid treatment of activated carbon used to enhance mixed VOC removal, *International Biodeterioration & Biodegradation* 113 (2016) 195-200.
- [44] Ö. Şahin, C. Saka, A.A. Ceyhan, O. Baytar, Preparation of High Surface Area Activated Carbon from *Elaeagnus angustifolia* Seeds by Chemical Activation with ZnCl₂ in One-Step Treatment and its Iodine Adsorption, *Separation Science and Technology* 50(6) (2014) 886-891.
- [45] J.C. Wang, S. Kaskel, KOH activation of carbon-based materials for energy storage, *Journal of Materials Chemistry* 22(45) (2012) 23710-23725.
- [46] K. Fic, A. Platek, J. Piwek, E. Frackowiak, Sustainable materials for electrochemical capacitors, *Materials Today* 21(4) (2018) 437-454.

- [47] K.L. Chiu, D.H.L. Ng, Synthesis and characterization of cotton-made activated carbon fiber and its adsorption of methylene blue in water treatment, *Biomass & Bioenergy* 46 (2012) 102-110.
- [48] N.A. Fathy, O.I. El-Shafey, L.B. Khalil, Effectiveness of Alkali-Acid Treatment in Enhancement the Adsorption Capacity for Rice Straw: The Removal of Methylene Blue Dye, *ISRN Physical Chemistry* 2013 (2013) 1-15.
- [49] X.J. He, P.H. Ling, J.S. Qiu, M.X. Yu, X.Y. Zhang, C. Yu, M.D. Zheng, Efficient preparation of biomass-based mesoporous carbons for supercapacitors with both high energy density and high power density, *Journal of Power Sources* 240 (2013) 109-113.
- [50] K. Yang, J. Peng, C. Srinivasakannan, L. Zhang, H. Xia, X. Duan, Preparation of high surface area activated carbon from coconut shells using microwave heating, *Bioresour Technol* 101(15) (2010) 6163-9.
- [51] C.S. Yang, Y.S. Jang, H.K. Jeong, Bamboo-based activated carbon for supercapacitor applications, *Current Applied Physics* 14(12) (2014) 1616-1620.
- [52] B. Goodell, X. Xie, Y. Qian, G. Daniel, M. Peterson, J. Jellison, Carbon nanotubes produced from natural cellulosic materials, *J Nanosci Nanotechnol* 8(5) (2008) 2472-4.
- [53] E. Raymundo-Piñero, F. Leroux, F. Béguin, A High-Performance Carbon for Supercapacitors Obtained by Carbonization of a Seaweed Biopolymer, *Advanced Materials* 18(14) (2006) 1877-1882.
- [54] N.S. Sulaiman, R. Hashim, M.H.M. Amini, M. Danish, O. Sulaiman, Optimization of activated carbon preparation from cassava stem using response surface methodology on surface area and yield, *Journal of Cleaner Production* 198 (2018) 1422-1430.
- [55] A. Álvarez-Murillo, S. Román, B. Ledesma, E. Sabio, Study of variables in energy densification of olive stone by hydrothermal carbonization, *Journal of Analytical and Applied Pyrolysis* 113 (2015) 307-314.
- [56] M. Mirzaeian, Q. Abbas, A. Ogwu, P. Hall, M. Goldin, M. Mirzaeian, H.F. Jirandehi, Electrode and electrolyte materials for electrochemical capacitors, *International Journal of Hydrogen Energy* 42(40) (2017) 25565-25587.
- [57] F.B. Sillars, S.I. Fletcher, M. Mirzaeian, P.J. Hall, Effect of activated carbon xerogel pore size on the capacitance performance of ionic liquid electrolytes, *Energy & Environmental Science* 4(3) (2011) 695-706.
- [58] A.G. Pandolfo, A.F. Hollenkamp, Carbon properties and their role in supercapacitors, *Journal of Power Sources* 157(1) (2006) 11-27.
- [59] E. Tee, I. Tallo, H. Kurig, T. Thomberg, A. Janes, E. Lust, Huge enhancement of energy storage capacity and power density of supercapacitors based on the carbon dioxide activated microporous SiC-CDC, *Electrochimica Acta* 161 (2015) 364-370.
- [60] J. Eskusson, A. Janes, A. Kikas, L. Matisen, E. Lust, Physical and electrochemical characteristics of supercapacitors based on carbide derived carbon electrodes in aqueous electrolytes, *Journal of Power Sources* 196(8) (2011) 4109-4116.
- [61] A. Jänes, T. Thomberg, E. Lust, Synthesis and characterisation of nanoporous carbide-derived carbon by chlorination of vanadium carbide, *Carbon* 45(14) (2007) 2717-2722.
- [62] A.B. Fuertes, D.M. Nevskaya, Control of mesoporous structure of carbons synthesised using a mesostructured silica as template, *Microporous and Mesoporous Materials* 62(3) (2003) 177-190.
- [63] K. Matsuoka, Y. Yamagishi, T. Yamazaki, N. Setoyama, A. Tomita, T. Kyotani, Extremely high microporosity and sharp pore size distribution of a large surface area carbon prepared in the nanochannels of zeolite Y, *Carbon* 43(4) (2005) 876-879.
- [64] J.J. Cai, M.L. Yang, Y.L. Xing, X.B. Zhao, Large surface area sucrose-based carbons via template-assisted routes: Preparation, microstructure, and hydrogen adsorption properties, *Colloids and Surfaces a-Physicochemical and Engineering Aspects* 444 (2014) 240-245.
- [65] T.J. Bandoz, J. Jagiello, K. Putyera, J.A. Schwarz, Sieving Properties of Carbons Obtained by Template Carbonization of Polyfurfuryl Alcohol within Mineral Matrices, *Langmuir* 11(10) (1995) 3964-3969.
- [66] L. Chen, R.K. Singh, P. Webley, Synthesis, characterization and hydrogen storage properties of microporous carbons templated by cation exchanged forms of zeolite Y with propylene and butylene as carbon precursors, *Microporous and Mesoporous Materials* 102(1-3) (2007) 159-170.
- [67] W.M. Qiao, Y. Song, S.H. Hong, S.Y. Lim, S.H. Yoon, Y. Korai, I. Mochida, Development

- of mesophase pitch derived mesoporous carbons through a commercially nanosized template, *Langmuir* 22(8) (2006) 3791-7.
- [68] R.R. Salunkhe, Y.H. Lee, K.H. Chang, J.M. Li, P. Simon, J. Tang, N.L. Torad, C.C. Hu, Y. Yamauchi, Nanoarchitected graphene-based supercapacitors for next-generation energy-storage applications, *Chemistry* 20(43) (2014) 13838-52.
- [69] M. Yi, Z.G. Shen, A review on mechanical exfoliation for the scalable production of graphene, *Journal of Materials Chemistry A* 3(22) (2015) 11700-11715.
- [70] H. Tan, D. Wang, Y. Guo, A Strategy to Synthesize Multilayer Graphene in Arc-Discharge Plasma in a Semi-Opened Environment, *Materials (Basel)* 12(14) (2019) 2279.
- [71] X. Li, L. Colombo, R.S. Ruoff, Graphene Films: Synthesis of Graphene Films on Copper Foils by Chemical Vapor Deposition (*Adv. Mater.* 29/2016), *Adv Mater* 28(29) (2016) 6264.
- [72] L. Qiu, X. Yang, X. Gou, W. Yang, Z.F. Ma, G.G. Wallace, D. Li, Dispersing carbon nanotubes with graphene oxide in water and synergistic effects between graphene derivatives, *Chemistry* 16(35) (2010) 10653-8.
- [73] R.H. Baughman, A.A. Zakhidov, W.A. de Heer, Carbon nanotubes--the route toward applications, *Science* 297(5582) (2002) 787-92.
- [74] K.H. Maria, T. Mieno, Synthesis of single-walled carbon nanotubes by low-frequency bipolar pulsed arc discharge method, *Vacuum* 113 (2015) 11-18.
- [75] C.D. Scott, S. Arepalli, P. Nikolaev, R.E. Smalley, Growth mechanisms for single-wall carbon nanotubes in a laser-ablation process, *Applied Physics a-Materials Science & Processing* 72(5) (2001) 573-580.
- [76] C.J. Lee, J. Park, J.A. Yu, Catalyst effect on carbon nanotubes synthesized by thermal chemical vapor deposition, *Chemical Physics Letters* 360(3-4) (2002) 250-255.
- [77] D.S. Bethune, C.H. Kiang, M.S. de Vries, G. Gorman, R. Savoy, J. Vazquez, R. Beyers, Cobalt-catalysed growth of carbon nanotubes with single-atomic-layer walls, *Nature* 363(6430) (1993) 605-607.
- [78] T. Yamada, T. Namai, K. Hata, D.N. Futaba, K. Mizuno, J. Fan, M. Yudasaka, M. Yumura, S. Iijima, Size-selective growth of double-walled carbon nanotube forests from engineered iron catalysts, *Nat Nanotechnol* 1(2) (2006) 131-6.
- [79] K.A. Wepasnick, B.A. Smith, K.E. Schrote, H.K. Wilson, S.R. Diegelmann, D.H. Fairbrother, Surface and structural characterization of multi-walled carbon nanotubes following different oxidative treatments, *Carbon* 49(1) (2011) 24-36.
- [80] M. Lu, G. Wang, B. Li, J. Chen, J. Zhang, Z. Li, B. Hou, Molecular interaction balanced one- and two-dimensional hybrid nanoarchitectures for high-performance supercapacitors, *Phys Chem Chem Phys* 21(40) (2019) 22283-22292.
- [81] H. Pan, J. Li, Y. Feng, Carbon nanotubes for supercapacitor, *Nanoscale Res Lett* 5(3) (2010) 654-68.
- [82] C. Zheng, W.Z. Qian, C.J. Cui, G.H. Xu, M.Q. Zhao, G.L. Tian, F. Wei, Carbon nanotubes for supercapacitors: Consideration of cost and chemical vapor deposition techniques, *Journal of Natural Gas Chemistry* 21(3) (2012) 233-240.
- [83] N.J. Coville, S.D. Mhlanga, E.N. Nxumalo, A. Shaikjee, A review of shaped carbon nanomaterials, *South African Journal of Science* 107(3-4) (2011) 44-58.
- [84] M.H. Al-Saleh, U. Sundararaj, Review of the mechanical properties of carbon nanofiber/polymer composites, *Composites Part a-Applied Science and Manufacturing* 42(12) (2011) 2126-2142.
- [85] T. Azami, D. Kasuya, R. Yuge, M. Yudasaka, S. Iijima, T. Yoshitake, Y. Kubo, Large-scale production of single-wall carbon nanohorns with high purity, *Journal of Physical Chemistry C* 112(5) (2008) 1330-1334.
- [86] K. Murata, K. Kaneko, F. Kokai, K. Takahashi, M. Yudasaka, S. Iijima, Pore structure of single-wall carbon nanohorn aggregates, *Chemical Physics Letters* 331(1) (2000) 14-20.
- [87] L. Benxuan, Z. Shijie, W. Haolan, H. Bo, A.J.A. Gehan, Asymmetric Carbon Nanohorn Enabled Soft Capacitors with High Power Density and Ultra-Low Cutoff Frequency, 2020.
- [88] C.M. Yang, H. Noguchi, K. Murata, M. Yudasaka, A. Hashimoto, S. Iijima, K. Kaneko, Highly ultramicroporous single-walled carbon nanohorn assemblies, *Advanced Materials* 17(7) (2005) 866-+.
- [89] S. Utsumi, J. Miyawaki, H. Tanaka, Y. Hattori, T. Itoi, N. Ichikuni, H. Kanoh, M. Yudasaka, S. Iijima, K. Kaneko, Opening mechanism of internal nanoporosity of single-wall carbon nanohorn, *J Phys Chem B* 109(30) (2005) 14319-24.

- [90] K. Ajima, M. Yudasaka, K. Suenaga, D. Kasuya, T. Azami, S. Iijima, Material storage mechanism in porous nanocarbon, *Advanced Materials* 16(5) (2004) 397-+.
- [91] S. Iijima, M. Yudasaka, R. Yamada, S. Bandow, K. Suenaga, F. Kokai, K. Takahashi, Nano-aggregates of single-walled graphitic carbon nano-horns, *Chemical Physics Letters* 309(3-4) (1999) 165-170.
- [92] A. Izadi-Najafabadi, T. Yamada, D.N. Futaba, M. Yudasaka, H. Takagi, H. Hatori, S. Iijima, K. Hata, High-power supercapacitor electrodes from single-walled carbon nanohorn/nanotube composite, *ACS Nano* 5(2) (2011) 811-9.
- [93] K.P. Annamalai, J.P. Gao, L.L. Liu, J. Mei, W.M. Lau, Y.S. Tao, Nanoporous graphene/single wall carbon nanohorn heterostructures with enhanced capacitance, *Journal of Materials Chemistry A* 3(22) (2015) 11740-11744.
- [94] R. Andrews, D. Jacques, D. Qian, T. Rantell, Multiwall carbon nanotubes: synthesis and application, *Acc Chem Res* 35(12) (2002) 1008-17.
- [95] C. Ruan, Y. Lian, Purification of Carbon Nano-Onions Fabricated by Arc Discharge, *Fullerenes Nanotubes and Carbon Nanostructures* 23(6) (2015) 488-493.
- [96] G. Radhakrishnan, P.M. Adams, L.S. Bernstein, Plasma characterization and room temperature growth of carbon nanotubes and nano-onions by excimer laser ablation, *Applied Surface Science* 253(19) (2007) 7651-7655.
- [97] T. Cabioch, M. Jaouen, E. Thune, P. Guérin, C. Fayoux, M.F. Denanot, Carbon onions formation by high-dose carbon ion implantation into copper and silver, *Surface and Coatings Technology* 128-129 (2000) 43-50.
- [98] X.H. Chen, F.M. Deng, J.X. Wang, H.S. Yang, G.T. Wu, X.B. Zhang, J.C. Peng, W.Z. Li, New method of carbon onion growth by radio-frequency plasma-enhanced chemical vapor deposition, *Chemical Physics Letters* 336(3-4) (2001) 201-204.
- [99] Y. Gao, Y.S. Zhou, M. Qian, X.N. He, J. Redepenning, P. Goodman, H.M. Li, L. Jiang, Y.F. Lu, Chemical activation of carbon nano-onions for high-rate supercapacitor electrodes, *Carbon* 51 (2013) 52-58.
- [100] M. Zhi, C. Xiang, J. Li, M. Li, N. Wu, Nanostructured carbon-metal oxide composite electrodes for supercapacitors: a review, *Nanoscale* 5(1) (2013) 72-88.
- [101] A. Borenstein, O. Hanna, R. Attias, S. Luski, T. Brousse, D. Aurbach, Carbon-based composite materials for supercapacitor electrodes: a review, *Journal of Materials Chemistry A* 5(25) (2017) 12653-12672.
- [102] S.J. He, W. Chen, High performance supercapacitors based on three-dimensional ultralight flexible manganese oxide nanosheets/carbon foam composites, *Journal of Power Sources* 262 (2014) 391-400.
- [103] R. Borgohain, J.C. Li, J.P. Selegue, Y.T. Cheng, Electrochemical Study of Functionalized Carbon Nano-Onions for High-Performance Supercapacitor Electrodes, *Journal of Physical Chemistry C* 116(28) (2012) 15068-15075.
- [104] R.B. Rakhi, D.H. Nagaraju, P. Beaujuge, H.N. Alshareef, Supercapacitors based on two dimensional VO₂ nanosheet electrodes in organic gel electrolyte, *Electrochimica Acta* 220 (2016) 601-608.
- [105] Q. Qu, S. Yang, X. Feng, 2D sandwich-like sheets of iron oxide grown on graphene as high energy anode material for supercapacitors, *Adv Mater* 23(46) (2011) 5574-80.
- [106] L. Manjakkal, C.G. Nunez, W.T. Dang, R. Dahiya, Flexible self-charging supercapacitor based on graphene-Ag-3D graphene foam electrodes, *Nano Energy* 51 (2018) 604-612.
- [107] D.W. Kim, K.Y. Rhee, S.J. Park, Synthesis of activated carbon nanotube/copper oxide composites and their electrochemical performance, *Journal of Alloys and Compounds* 530 (2012) 6-10.
- [108] Y.Y. Wang, X. Xiao, H.G. Xue, H. Pang, Zinc Oxide Based Composite Materials for Advanced Supercapacitors, *Chemistryselect* 3(2) (2018) 550-565.
- [109] G. Milczarek, A. Ciszewski, I. Stepniak, Oxygen-doped activated carbon fiber cloth as electrode material for electrochemical capacitor, *Journal of Power Sources* 196(18) (2011) 7882-7885.
- [110] D.S. Jeong, J.M. Yun, K.H. Kim, Highly porous nitrogen-doped carbon for superior electric double-layer capacitors, *Rsc Advances* 7(71) (2017) 44735-44742.
- [111] S. Umezawa, T. Douura, K. Yoshikawa, Y. Takashima, M. Yoneda, K. Gotoh, V. Stolojan, S.R.P. Silva, Y. Hayashi, D. Tanaka, Supercapacitor electrode with high charge density based on boron-doped porous carbon derived from covalent organic frameworks, *Carbon*

- 184 (2021) 418-425.
- [112] K. Jurewicz, K. Babel, A. Ziolkowski, H. Wachowska, Ammoxidation of active carbons for improvement of supercapacitor characteristics, *Electrochimica Acta* 48(11) (2003) 1491-1498.
- [113] X.Y. Chen, C. Chen, Z.J. Zhang, D.H. Xie, X. Deng, J.W. Liu, Nitrogen-doped porous carbon for supercapacitor with long-term electrochemical stability, *Journal of Power Sources* 230 (2013) 50-58.
- [114] J. Biemolt, I.M. Denekamp, T.K. Slot, G. Rothenberg, D. Eisenberg, Boosting the Supercapacitance of Nitrogen-Doped Carbon by Tuning Surface Functionalities, *ChemSusChem* 10(20) (2017) 4018-4024.
- [115] G.A. Ferrero, A.B. Fuertes, M. Sevilla, N-doped microporous carbon microspheres for high volumetric performance supercapacitors, *Electrochimica Acta* 168 (2015) 320-329.
- [116] M. Zhou, F. Pu, Z. Wang, S.Y. Guan, Nitrogen-doped porous carbons through KOH activation with superior performance in supercapacitors, *Carbon* 68 (2014) 185-194.
- [117] N.D. Kim, W. Kim, J.B. Joo, S. Oh, P. Kim, Y. Kim, J. Yi, Electrochemical capacitor performance of N-doped mesoporous carbons prepared by ammoxidation, *Journal of Power Sources* 180(1) (2008) 671-675.
- [118] M.B. Barbosa, J.P. Nascimento, P.B. Martelli, C.A. Furtado, N.D. Mohallem, H.F. Gorgulho, Electrochemical properties of carbon xerogel containing nitrogen in a carbon matrix, *Microporous and Mesoporous Materials* 162 (2012) 24-30.
- [119] S. Yu, D. Liu, S.Y. Zhao, B.F. Bao, C.D. Jin, W.J. Huang, H. Chen, Z.H. Shen, Synthesis of wood derived nitrogen-doped porous carbon-polyaniline composites for supercapacitor electrode materials, *Rsc Advances* 5(39) (2015) 30943-30949.
- [120] H.F. Gorgulho, F. Goncalves, M.F.R. Pereira, J.L. Figueiredo, Synthesis and characterization of nitrogen-doped carbon xerogels, *Carbon* 47(8) (2009) 2032-2039.
- [121] J.P.S. Sousa, M.F.R. Pereira, J.L. Figueiredo, NO oxidation over nitrogen doped carbon xerogels, *Applied Catalysis B-Environmental* 125 (2012) 398-408.
- [122] B. Xu, S. Hou, G. Cao, F. Wu, Y. Yang, Sustainable nitrogen-doped porous carbon with high surface areas prepared from gelatin for supercapacitors, *Journal of Materials Chemistry* 22(36) (2012) 19088-19093.
- [123] F. Gao, J.Y. Qu, Z.B. Zhao, Z.Y. Wang, J.S. Qiu, Nitrogen-doped activated carbon derived from prawn shells for high-performance supercapacitors, *Electrochimica Acta* 190 (2016) 1134-1141.
- [124] J. Wang, L.F. Shen, Y.L. Xu, H. Dou, X.G. Zhang, Lamellar-structured biomass-derived phosphorus- and nitrogen-co-doped porous carbon for high-performance supercapacitors, *New Journal of Chemistry* 39(12) (2015) 9497-9503.
- [125] S.N. Faisal, E. Haque, N. Noorbehesht, W.M. Zhang, A.T. Harris, T.L. Church, A.I. Minett, Pyridinic and graphitic nitrogen-rich graphene for high-performance supercapacitors and metal-free bifunctional electrocatalysts for ORR and OER, *Rsc Advances* 7(29) (2017) 17950-17958.
- [126] K. Tian, J. Wang, L. Cao, W. Yang, W. Guo, S. Liu, W. Li, F. Wang, X. Li, Z. Xu, Z. Wang, H. Wang, Y. Hou, Single-site pyrrolic-nitrogen-doped sp²-hybridized carbon materials and their pseudocapacitance, *Nat Commun* 11(1) (2020) 3884.
- [127] S. Uchida, T. Masese, Electric Double-Layer Capacitors Based on Non-Aqueous Electrolytes: A Comparative Study of Potassium and Quaternary Ammonium Salts, *Batteries & Supercaps* 3(5) (2020) 392-396.
- [128] B.J. Jiang, C.G. Tian, L. Wang, L. Sun, C. Chen, X.Z. Nong, Y.J. Qiao, H.G. Fu, Highly concentrated, stable nitrogen-doped graphene for supercapacitors: Simultaneous doping and reduction, *Applied Surface Science* 258(8) (2012) 3438-3443.
- [129] M. Seredych, D. Hulicova-Jurcakova, G.Q. Lu, T.J. Bandosz, Surface functional groups of carbons and the effects of their chemical character, density and accessibility to ions on electrochemical performance, *Carbon* 46(11) (2008) 1475-1488.
- [130] S.L. Candelaria, G.Z. Cao, Increased working voltage of hexamine-coated porous carbon for supercapacitors, *Science Bulletin* 60(18) (2015) 1587-1597.
- [131] P.J. Hall, M. Mirzaeian, S.I. Fletcher, F.B. Sillars, A.J.R. Rennie, G.O. Shitta-Bey, G. Wilson, A. Cruden, R. Carter, Energy storage in electrochemical capacitors: designing functional materials to improve performance, *Energy & Environmental Science* 3(9) (2010) 1238-1251.

- [132] E. Frackowiak, Carbon materials for supercapacitor application, *Phys Chem Chem Phys* 9(15) (2007) 1774-85.
- [133] G. Shul, D. Belanger, Self-discharge of electrochemical capacitors based on soluble or grafted quinone, *Phys Chem Chem Phys* 18(28) (2016) 19137-45.
- [134] K. Jurewicz, R. Pietrzak, P. Nowicki, H. Wachowski, Capacitance behaviour of brown coal based active carbon modified through chemical reaction with urea, *Electrochimica Acta* 53(16) (2008) 5469-5475.
- [135] M. Khademi, D.P.J. Barz, Structure of the Electrical Double Layer Revisited: Electrode Capacitance in Aqueous Solutions, *Langmuir* 36(16) (2020) 4250-4260.
- [136] H.Y. Lee, J.B. Goodenough, Supercapacitor behavior with KCl electrolyte, *Journal of Solid State Chemistry* 144(1) (1999) 220-223.
- [137] G. Lota, J. Tyczkowski, R. Kapica, K. Lota, E. Frackowiak, Carbon materials modified by plasma treatment as electrodes for supercapacitors, *Journal of Power Sources* 195(22) (2010) 7535-7539.
- [138] K. Fic, G. Lota, M. Meller, E. Frackowiak, Novel insight into neutral medium as electrolyte for high-voltage supercapacitors, *Energy & Environmental Science* 5(2) (2012) 5842-5850.
- [139] K. Fic, A. Platek, J. Piwek, J. Menzel, A. Slesinski, P. Bujewska, P. Galek, E. Frackowiak, Revisited insights into charge storage mechanisms in electrochemical capacitors with Li₂SO₄-based electrolyte, *Energy Storage Materials* 22 (2019) 1-14.
- [140] A. Gambou-Bosca, D. Belanger, Electrochemical characterization of MnO₂-based composite in the presence of salt-in-water and water-in-salt electrolytes as electrode for electrochemical capacitors, *Journal of Power Sources* 326 (2016) 595-603.
- [141] P. Lannelongue, R. Bouchal, E. Mourad, C. Bodin, M. Olarte, S. le Vot, F. Favier, O. Fontaine, "Water-in-Salt" for Supercapacitors: A Compromise between Voltage, Power Density and Stability, *Journal of the Electrochemical Society* 165(3) (2018) A657-A663.
- [142] Q. Dou, S. Lei, D.-W. Wang, Q. Zhang, D. Xiao, H. Guo, A. Wang, H. Yang, Y. Li, S. Shi, X. Yan, Safe and high-rate supercapacitors based on an "acetonitrile/water in salt" hybrid electrolyte, *Energy & Environmental Science* 11(11) (2018) 3212-3219.
- [143] J. Lee, P. Srimuk, S. Fleischmann, X. Su, T.A. Hatton, V. Presser, Redox-electrolytes for non-flow electrochemical energy storage: A critical review and best practice, *Progress in Materials Science* 101 (2019) 46-89.
- [144] N.R. Chodankar, D.P. Dubal, A.C. Lokhande, A.M. Patil, J.H. Kim, C.D. Lokhande, An innovative concept of use of redox-active electrolyte in asymmetric capacitor based on MWCNTs/MnO₂ and Fe₂O₃ thin films, *Sci Rep* 6(1) (2016) 39205.
- [145] A. Singh, A. Chandra, Enhancing Specific Energy and Power in Asymmetric Supercapacitors - A Synergetic Strategy based on the Use of Redox Additive Electrolytes, *Sci Rep* 6(1) (2016) 25793.
- [146] J. Lee, B. Kruner, A. Tolosa, S. Sathyamoorthi, D. Kim, S. Choudhury, K.H. Seo, V. Presser, Tin/vanadium redox electrolyte for battery-like energy storage capacity combined with supercapacitor-like power handling, *Energy & Environmental Science* 9(11) (2016) 3392-3398.
- [147] Y. Teng, E.H. Liu, R. Ding, K. Liu, R.H. Liu, L. Wang, Z. Yang, H.X. Jiang, Bean dregs-based activated carbon/copper ion supercapacitors, *Electrochimica Acta* 194 (2016) 394-404.
- [148] C. Zhong, Y. Deng, W. Hu, J. Qiao, L. Zhang, J. Zhang, A review of electrolyte materials and compositions for electrochemical supercapacitors, *Chem Soc Rev* 44(21) (2015) 7484-539.
- [149] R.R. Galimzyanov, S.V. Stakhanova, I.S. Krechetov, A.T. Kalashnik, M.V. Astakhov, A.V. Lisitsin, A.Y. Rychagov, T.R. Galimzyanov, F.S. Tabarov, Electrolyte mixture based on acetonitrile and ethyl acetate for a wide temperature range performance of the supercapacitors, *Journal of Power Sources* 495 (2021) 229442.
- [150] A. Jänes, T. Thomberg, J. Eskusson, E. Lust, Supercapacitors Based on Propylene Carbonate Solution Operating from -45 °C to 100 °C, *ECS Transactions* 64(20) (2015) 31-40.
- [151] K. Chiba, T. Ueda, H. Yamamoto, Highly conductive electrolytic solution for electric double-layer capacitor using dimethylcarbonate and spiro-type quaternary ammonium salt, *Electrochemistry* 75(8) (2007) 668-671.

- [152] A. Jänes, E. Lust, Use of organic esters as co-solvents for electrical double layer capacitors with low temperature performance, *Journal of Electroanalytical Chemistry* 588(2) (2006) 285-295.
- [153] A. Cappetto, W.J. Cao, J.F. Luo, M. Hagen, D. Adams, A. Shelikeri, K. Xu, J.P. Zheng, Performance of wide temperature range electrolytes for Li-Ion capacitor pouch cells, *Journal of Power Sources* 359(C) (2017) 205-214.
- [154] E.R. Logan, E.M. Tonita, K.L. Gering, J. Li, X.W. Ma, L.Y. Beaulieu, J.R. Dahn, A Study of the Physical Properties of Li-Ion Battery Electrolytes Containing Esters, *Journal of the Electrochemical Society* 165(2) (2018) A21-A30.
- [155] M. Morita, M. Goto, Y. Matsuda, Ethylene Carbonate-Based Organic Electrolytes for Electric Double-Layer Capacitors, *Journal of Applied Electrochemistry* 22(10) (1992) 901-908.
- [156] A. Laheäär, H. Kurig, A. Jänes, E. Lust, LiPF₆ based ethylene carbonate–dimethyl carbonate electrolyte for high power density electrical double layer capacitor, *Electrochimica Acta* 54(19) (2009) 4587-4594.
- [157] M.I. Chaudhari, A. Muralidharan, L.R. Pratt, S.B. Rempe, Assessment of Simple Models for Molecular Simulation of Ethylene Carbonate and Propylene Carbonate as Solvents for Electrolyte Solutions, Springer International Publishing, Cham, 2018, pp. 53-77.
- [158] M. Armand, F. Endres, D.R. MacFarlane, H. Ohno, B. Scrosati, Ionic-liquid materials for the electrochemical challenges of the future, *Nat Mater* 8(8) (2009) 621-9.
- [159] S. Guo, F. Chen, L. Liu, Y. Li, X.M. Liu, K. Jiang, R.X. Liu, S.J. Zhang, Effects of the Water Content on the Transport Properties of Ionic Liquids, *Industrial & Engineering Chemistry Research* 58(42) (2019) 19661-19669.
- [160] R. Palm, H. Kurig, K. Tõnurist, A. Jänes, E. Lust, Is the mixture of 1-ethyl-3-methylimidazolium tetrafluoroborate and 1-butyl-3-methylimidazolium tetrafluoroborate applicable as electrolyte in electrical double layer capacitors?, *Electrochemistry Communications* 22 (2012) 203-206.
- [161] M. Galiński, A. Lewandowski, I. Stepniak, Ionic liquids as electrolytes, *Electrochimica Acta* 51(26) (2006) 5567-5580.
- [162] A. Lewandowski, A. Olejniczak, M. Galinski, I. Stepniak, Performance of carbon-carbon supercapacitors based on organic, aqueous and ionic liquid electrolytes, *Journal of Power Sources* 195(17) (2010) 5814-5819.
- [163] W.W. Liu, X.B. Yan, J.W. Lang, Q.J. Xue, Effects of concentration and temperature of EMIMBF₄/acetonitrile electrolyte on the supercapacitive behavior of graphene nanosheets, *Journal of Materials Chemistry* 22(18) (2012) 8853-8861.
- [164] C. Arbizzani, M. Bisio, D. Cericola, M. Lazzari, F. Soavi, M. Mastragostino, Safe, high-energy supercapacitors based on solvent-free ionic liquid electrolytes, *Journal of Power Sources* 185(2) (2008) 1575-1579.
- [165] A. Balducci, R. Dugas, P.L. Taberna, P. Simon, D. Plee, M. Mastragostino, S. Passerini, High temperature carbon-carbon supercapacitor using ionic liquid as electrolyte, *Journal of Power Sources* 165(2) (2007) 922-927.
- [166] A. Krause, A. Balducci, High voltage electrochemical double layer capacitor containing mixtures of ionic liquids and organic carbonate as electrolytes, *Electrochemistry Communications* 13(8) (2011) 814-817.
- [167] J. Cho, W.K. Shin, D.W. Kim, Y.R. Kim, B.J. Lee, S.G. Kim, Electrochemical Characterization of Electric Double Layer Capacitors Assembled with Pyrrolidinium-Based Ionic Liquid Electrolytes, *Journal of Electrochemical Science and Technology* 7(3) (2016) 199-205.
- [168] M. Lazzari, M. Mastragostino, A.G. Pandolfo, V. Ruiz, F. Soavi, Role of Carbon Porosity and Ion Size in the Development of Ionic Liquid Based Supercapacitors, *Journal of the Electrochemical Society* 158(1) (2011) A22-A25.
- [169] M. Lazzari, F. Soavi, M. Mastragostino, High voltage, asymmetric EDLCs based on xerogel carbon and hydrophobic IL electrolytes, *Journal of Power Sources* 178(1) (2008) 490-496.
- [170] V. Ruiz, T. Huynh, S.R. Sivakumar, A.G. Pandolfo, Ionic liquid-solvent mixtures as supercapacitor electrolytes for extreme temperature operation, *Rsc Advances* 2(13) (2012) 5591-5598.
- [171] R.Y. Lin, P.L. Taberna, S. Fantini, V. Presser, C.R. Perez, F. Malbosc, N.L. Rupesinghe, K.B.K. Teo, Y. Gogotsi, P. Simon, Capacitive Energy Storage from -50 to 100 degrees C

- Using an Ionic Liquid Electrolyte, *Journal of Physical Chemistry Letters* 2(19) (2011) 2396-2401.
- [172] E. Frackowiak, G. Lota, J. Pernak, Room-temperature phosphonium ionic liquids for supercapacitor application, *Applied Physics Letters* 86(16) (2005) 1-3.
- [173] B. Pal, S.Y. Yang, S. Ramesh, V. Thangadurai, R. Jose, Electrolyte selection for supercapacitive devices: a critical review, *Nanoscale Advances* 1(10) (2019) 3807-3835.
- [174] T.N.T. Tran, M.P. Clark, H.J. Chung, D.G. Ivey, Effects of Crosslinker Concentration in Poly(Acrylic Acid)-KOH Gel Electrolyte on Performance of Zinc-Air Batteries, *Batteries & Supercaps* 3(5) (2020) 409-416.
- [175] S. Çavuş, E. Durgun, Poly(vinyl alcohol) Based Polymer Gel Electrolytes: Investigation on Their Conductivity and Characterization, *Acta Physica Polonica A* 129(4) (2016) 621-624.
- [176] Y. Aihara, G.B. Appetecchi, B. Scrosati, A new concept for the formation of homogeneous, poly(ethylene oxide) based, gel-type polymer electrolyte, *Journal of the Electrochemical Society* 149(7) (2002) A849-A854.
- [177] K.T. Lee, J.F. Lee, N.L. Wu, Electrochemical characterizations on MnO₂ supercapacitors with potassium polyacrylate and potassium polyacrylate-co-polyacrylamide gel polymer electrolytes, *Electrochimica Acta* 54(26) (2009) 6148-6153.
- [178] R. López –Mayo, A. Rico, L.G. Arriaga, M.P. Gurrola, J. Ledesma-García, Development of a flexible poly(ether ether ketone) supercapacitor as electrolyte and separator, *Journal of Physics: Conference Series* 1407(1) (2019) 12100.
- [179] F. Abdul Latif, Review of poly (methyl methacrylate) based polymer electrolytes in solid-state supercapacitors, *International Journal of Electrochemical Science* (2022) ArticleID:22013.
- [180] S. Janakiraman, A. Agrawal, R. Biswal, A. Venimadhav, An amorphous polyvinylidene fluoride-co-hexafluoropropylene based gel polymer electrolyte for sodium-ion cells, *Applied Surface Science Advances* 6 (2021) 100139.
- [181] C.W. Huang, C.A. Wu, S.S. Hou, P.L. Kuo, C.T. Hsieh, H.S. Teng, Gel Electrolyte Derived from Poly(ethylene glycol) Blending Poly(acrylonitrile) Applicable to Roll-to-Roll Assembly of Electric Double Layer Capacitors, *Advanced Functional Materials* 22(22) (2012) 4677-4685.
- [182] C. Fringant, A. Tranchant, R. Messina, Behavior of Lithium-Electrolyte Interface during Cycling in Some Ether-Carbonate and Carbonate Mixtures, *Electrochimica Acta* 40(4) (1995) 513-523.
- [183] E.H. Lahrar, A. Belhboub, P. Simon, C. Merlet, Ionic Liquids under Confinement: From Systematic Variations of the Ion and Pore Sizes toward an Understanding of the Structure and Dynamics in Complex Porous Carbons, *ACS Appl Mater Interfaces* 12(1) (2020) 1789-1798.
- [184] H. Moldenhauer, I. Diaz-Franulic, F. Gonzalez-Nilo, D. Naranjo, Effective pore size and radius of capture for K(+) ions in K-channels, *Sci Rep* 6(1) (2016) 19893.
- [185] Q. Abbas, D. Pajak, E. Frackowiak, F. Beguin, Effect of binder on the performance of carbon/carbon symmetric capacitors in salt aqueous electrolyte, *Electrochimica Acta* 140 (2014) 132-138.
- [186] N. Elgrishi, K.J. Rountree, B.D. McCarthy, E.S. Rountree, T.T. Eisenhart, J.L. Dempsey, A Practical Beginner's Guide to Cyclic Voltammetry, *Journal of Chemical Education* 95(2) (2018) 197-206.
- [187] D. Weingarh, A. Foelske-Schmitz, R. Kötz, Cycle versus voltage hold – Which is the better stability test for electrochemical double layer capacitors?, *Journal of Power Sources* 225 (2013) 84-88.
- [188] P.W. Ruch, D. Cericola, A. Foelske-Schmitz, R. Kotz, A. Wokaun, Aging of electrochemical double layer capacitors with acetonitrile-based electrolyte at elevated voltages, *Electrochimica Acta* 55(15) (2010) 4412-4420.
- [189] R. Kötz, P.W. Ruch, D. Cericola, Aging and failure mode of electrochemical double layer capacitors during accelerated constant load tests, *Journal of Power Sources* 195(3) (2010) 923-928.
- [190] S.D. Kang, W.C. Chueh, Galvanostatic Intermittent Titration Technique Reinvented: Part I. A Critical Review, *Journal of the Electrochemical Society* 168(12) (2021) 120504.
- [191] B.A. Mei, O. Munteshari, J. Lau, B. Dunn, L. Pilon, Physical Interpretations of Nyquist Plots for EDLC Electrodes and Devices, *Journal of Physical Chemistry C* 122(1) (2018) 194-206.

- [192] M.F. Dupont, S.W. Donne, A Step Potential Electrochemical Spectroscopy Analysis of Electrochemical Capacitor Electrode Performance, *Electrochimica Acta* 167 (2015) 268-277.
- [193] A.J. Gibson, S.W. Donne, A step potential electrochemical spectroscopy (SPECS) investigation of anodically electrodeposited thin films of manganese dioxide, *Journal of Power Sources* 359 (2017) 520-528.
- [194] M. Forghani, A.J. Roberts, Application of step potential electrochemical spectroscopy in pouch cell prototype capacitors, *Electrochimica Acta* 390 (2021) 138845.
- [195] M. Forghani, S.W. Donne, Modification of the Step Potential Electrochemical Spectroscopy Analysis Protocol to Improve Outcomes, *Journal of the Electrochemical Society* 166(13) (2019) A2727-A2735.
- [196] A.K. Shukla, A. Banerjee, M.K. Ravikumar, A. Jalajakshi, Electrochemical capacitors: Technical challenges and prognosis for future markets, *Electrochimica Acta* 84 (2012) 165-173.
- [197] J.R. Miller, A.F. Burke, Electrochemical Capacitors: Challenges and Opportunities for Real-World Applications, *Electrochemical Society Interface* 17(1) (2008) 53-57.
- [198] P. Simon, Y. Gogotsi, Perspectives for electrochemical capacitors and related devices, *Nat Mater* 19(11) (2020) 1151-1163.
- [199] R. Gonçalves, S. Lanceros-Méndez, C.M. Costa, Electrode fabrication process and its influence in lithium-ion battery performance: State of the art and future trends, *Electrochemistry Communications* 135 (2022) 107210.
- [200] H. Bockholt, M. Indrikova, A. Netz, F. Golks, A. Kwade, The interaction of consecutive process steps in the manufacturing of lithium-ion battery electrodes with regard to structural and electrochemical properties, *Journal of Power Sources* 325 (2016) 140-151.
- [201] J. Barthel, R. Neueder, H. Roch, Density, relative permittivity, and viscosity of propylene carbonate plus dimethoxyethane mixtures from 25 degrees C to 125 degrees C, *Journal of Chemical and Engineering Data* 45(6) (2000) 1007-1011.
- [202] A.B. McEwen, S.F. McDevitt, V.R. Koch, Nonaqueous electrolytes for electrochemical capacitors: Imidazolium cations and inorganic fluorides with organic carbonates, *Journal of the Electrochemical Society* 144(4) (1997) L84-L86.
- [203] Q. Zhang, J.P. Rong, D.S. Ma, B.Q. Wei, The governing self-discharge processes in activated carbon fabric-based supercapacitors with different organic electrolytes, *Energy & Environmental Science* 4(6) (2011) 2152-2159.
- [204] T. Abdallah, D. Lemordant, B. Claude-Montigny, Are room temperature ionic liquids able to improve the safety of supercapacitors organic electrolytes without degrading the performances?, *Journal of Power Sources* 201 (2012) 353-359.
- [205] J.M. Griffin, A.C. Forse, W.Y. Tsai, P.L. Taberna, P. Simon, C.P. Grey, In situ NMR and electrochemical quartz crystal microbalance techniques reveal the structure of the electrical double layer in supercapacitors, *Nat Mater* 14(8) (2015) 812-9.
- [206] W.Y. Tsai, P.L. Taberna, P. Simon, Electrochemical quartz crystal microbalance (EQCM) study of ion dynamics in nanoporous carbons, *J Am Chem Soc* 136(24) (2014) 8722-8.
- [207] N. Jäckel, S. Patrick Emge, B. Krüner, B. Roling, V. Presser, Quantitative Information about Electrosorption of Ionic Liquids in Carbon Nanopores from Electrochemical Dilatometry and Quartz Crystal Microbalance Measurements, *The Journal of Physical Chemistry C* 121(35) (2017) 19120-19128.
- [208] Y. Wang, D. Rochefort, Solid-State NMR and Electrochemical Dilatometry Study of Charge Storage in Supercapacitor with Redox Ionic Liquid Electrolyte, *ECS Meeting Abstracts* MA2020-01(1) (2020) 6-6.
- [209] J.W. Long, D. Belanger, T. Brousse, W. Sugimoto, M.B. Sassin, O. Crosnier, Asymmetric electrochemical capacitors-Stretching the limits of aqueous electrolytes, *Mrs Bulletin* 36(7) (2011) 513-522.
- [210] L. Demarconnay, E. Raymundo-Pinero, F. Beguin, A symmetric carbon/carbon supercapacitor operating at 1.6 V by using a neutral aqueous solution, *Electrochemistry Communications* 12(10) (2010) 1275-1278.
- [211] M.P. Bichat, E. Raymundo-Pinero, F. Beguin, High voltage supercapacitor built with seaweed carbons in neutral aqueous electrolyte, *Carbon* 48(15) (2010) 4351-4361.

Co-authorship statements



Przemysław Galek

March 31, 2022

Declaration of individual contribution in publications and computer software

As the co-author of the following papers and computer software, I hereby declare that my contribution to these works was:

Article A1 (contribution in unpublished article)

Authors:	Przemysław Galek (60%), Krzysztof Fic (40%)
Title:	<i>Rheological properties and optimal composition of electrode slurry: its determination based on activated carbon</i>
Journal:	-
DOI:	-
Contribution:	<ul style="list-style-type: none">- contributing to the research idea- performing the experiments- discussing the results- manuscript writing and drafting- figures preparation

Article A2

Authors:	Przemysław Galek (50%), Elżbieta Frąckowiak (15%), Krzysztof Fic (35%)
Title:	<i>Interfacial aspects induced by saturated aqueous electrolytes in electrochemical capacitor applications</i>
Journal:	Electrochimica Acta 334 (2020) 135572
DOI:	10.1016/j.electacta.2019.135572
Contribution:	<ul style="list-style-type: none">- performing the experiments- discussing the results- manuscript writing and drafting- figures preparation





Article A3

Authors:	Przemyslaw Galek (35%) , Adam Ślesięski (15%), Krzysztof Fic (10%), Jakub Menzel (40%)
Title:	<i>Peculiar role of the electrolyte viscosity in the electrochemical capacitor performance</i>
Journal:	Journal of Materials Chemistry A 9 (2021) 8644 – 8654
DOI:	10.1039/D0TA11230E
Contribution:	<ul style="list-style-type: none">– contributing to the research idea– performing the experiments– discussing the results– manuscript writing and drafting– figures preparation

Article A4

Authors:	Przemyslaw Galek (30%) , Paulina Bujewska (15%), Scott Donne (5%), Krzysztof Fic (10%), Jakub Menzel (40%)
Title:	<i>New insight into ion dynamics in nanoporous carbon materials: An application of the step potential electrochemical spectroscopy (SPECS) technique and electrochemical dilatometry</i>
Journal:	Electrochimica Acta 377 (2021) 138115
DOI:	10.1016/j.electacta.2021.138115
Contribution:	<ul style="list-style-type: none">– performing the SPECS calculations and experiments in Swagelok systems– manuscript writing– figures preparation

Article A5 (contribution in unpublished article)

Authors:	Paulina Bujewska (50%), Przemyslaw Galek (30%) , Krzysztof Fic (20%)
Title:	<i>Impact of electrolyte pH on the ion population at the electrode/electrolyte interface monitored by electrochemical dilatometry</i>
Journal:	-
DOI:	-
Contribution:	<ul style="list-style-type: none">– performing the SPECS calculations– figures preparation (graphical abstract, ions dimensions, SPECS)– discussing the SPECS results– manuscript drafting





Computer software (contribution in unpublished software)

Authors: Przemysław Galek (40%), Maciej Staszak (40%),
Krzysztof Fic (20%)

Title: *SPECSfit – computer software for data conversion from
Step Potential Electrochemical Spectroscopy technique*

Journal: -

DOI: -

Contribution: – providing experimental data and theoretical knowledge
about technique
– validation and calibration of the model
– testing software

Przemysław Galek
.....
(signature)



Krzysztof Fic
March 31, 2022

Declaration of individual contribution in publications and computer software

As the co-author of the following papers and computer software, I hereby declare that my contribution to these works was:

Article A1 (contribution in unpublished article)

Authors:	Przemyslaw Galek (60%), Krzysztof Fic (40%)
Title:	<i>Rheological properties and optimal composition of electrode slurry: its determination based on activated carbon</i>
Journal:	-
DOI:	-
Contribution:	<ul style="list-style-type: none">- contributing to the research idea- providing the access to the necessary equipment- supervising the research progress- knowledge support- manuscript reviewing and editing

Article A2

Authors:	Przemyslaw Galek (50%), Elżbieta Frąckowiak (15%), Krzysztof Fic (35%)
Title:	<i>Interfacial aspects induced by saturated aqueous electrolytes in electrochemical capacitor applications</i>
Journal:	Electrochimica Acta 334 (2020) 135572
DOI:	10.1016/j.electacta.2019.135572
Contribution:	<ul style="list-style-type: none">- contributing to the research idea- providing the access to the necessary equipment- supervising the research progress- knowledge support- manuscript reviewing and editing

KF





Article A3

Authors:	Przemyslaw Galek (35%), Adam Ślesiński (15%), Krzysztof Fic (10%) , Jakub Menzel (40%)
Title:	<i>Peculiar role of the electrolyte viscosity in the electrochemical capacitor performance</i>
Journal:	Journal of Materials Chemistry A 9 (2021) 8644 – 8654
DOI:	10.1039/D0TA11230E
Contribution:	– providing the access to the necessary equipment – supervising the research progress – knowledge support – manuscript reviewing and editing

Article A4

Authors:	Przemyslaw Galek (30%), Paulina Bujewska (15%), Scott Donne (5%), Krzysztof Fic (10%) , Jakub Menzel (40%)
Title:	<i>New insight into ion dynamics in nanoporous carbon materials: An application of the step potential electrochemical spectroscopy (SPECS) technique and electrochemical dilatometry</i>
Journal:	Electrochimica Acta 377 (2021) 138115
DOI:	10.1016/j.electacta.2021.138115
Contribution:	– providing the access to the necessary equipment – supervising the research progress – knowledge support – manuscript reviewing and editing

Article A5 (contribution in unpublished article)

Authors:	Paulina Bujewska (50%), Przemyslaw Galek (30%), Krzysztof Fic (20%)
Title:	<i>Impact of electrolyte pH on the ion population at the electrode/electrolyte interface monitored by electrochemical dilatometry</i>
Journal:	-
DOI:	-
Contribution:	– contributing to the research idea – providing the access to the necessary equipment – supervising the research progress – knowledge support – manuscript reviewing and editing

fu





Computer software (contribution in unpublished software)

Authors: Przemysław Galek (40%), Maciej Staszak (40%),
Krzysztof Fic (20%)

Title: *SPECSfit – computer software for data conversion
from Step Potential Electrochemical Spectroscopy technique*

Journal: -

DOI: -

Contribution: – providing theoretical knowledge about technique
– managing software development

Krzysztof Fic
.....
(signature)





Jakub Menzel
March 31, 2022

Declaration of individual contribution in publications

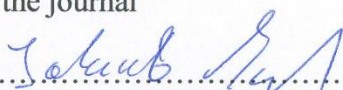
As the co-author of the following papers, I hereby declare that my contribution to these works was:

Article A3

Authors:	Przemyslaw Galek (35%), Adam Ślesiński (15%), Krzysztof Fic (10%), Jakub Menzel (40%)
Title:	<i>Peculiar role of the electrolyte viscosity in the electrochemical capacitor performance</i>
Journal:	Journal of Materials Chemistry A 9 (2021) 8644 – 8654
DOI:	10.1039/D0TA11230E
Contribution:	<ul style="list-style-type: none">– contributing to the research idea– performing the contact angle experiments– discussing the results– supervising the research progress– manuscript writing– handling the correspondence with the journal

Article A4

Authors:	Przemyslaw Galek (30%), Paulina Bujewska (15%), Scott Donne (5%), Krzysztof Fic (10%), Jakub Menzel (40%)
Title:	<i>New insight into ion dynamics in nanoporous carbon materials: An application of the step potential electrochemical spectroscopy (SPECS) technique and electrochemical dilatometry</i>
Journal:	Electrochimica Acta 377 (2021) 138115
DOI:	10.1016/j.electacta.2021.138115
Contribution:	<ul style="list-style-type: none">– contributing to the research idea– manuscript writing and drafting– supervising the research progress– handling the correspondence with the journal

.....

(signature)





Paulina Bujewska
March 31, 2022

Declaration of individual contribution in publications

As the co-author of the following papers, I hereby declare that my contribution to these works was:

Article A4

Authors: Przemyslaw Galek (30%), **Paulina Bujewska (15%)**, Scott Donne (5%), Krzysztof Fic (10%), Jakub Menzel (40%)

Title: *New insight into ion dynamics in nanoporous carbon materials: An application of the step potential electrochemical spectroscopy (SPECS) technique and electrochemical dilatometry*

Journal: Electrochimica Acta 377 (2021) 138115

DOI: 10.1016/j.electacta.2021.138115

Contribution: – performing the electrochemical dilatometry experiments
– manuscript drafting

Article A5 (contribution in unpublished article)

Authors: **Paulina Bujewska (50%)**, Przemyslaw Galek (30%), Krzysztof Fic (20%)

Title: *Impact of electrolyte pH on the ion population at the electrode/electrolyte interface monitored by electrochemical dilatometry*

Journal: -

DOI: -

Contribution: – contributing to the research idea
– performing the electrochemical dilatometry experiments
– writing “Introduction”, “Experimental” and “Conclusions” parts
– discussing the dilatometry results
– manuscript drafting
– figures preparation (ECD, Raman)

Paulina Bujewska
.....
(signature)





Maciej Staszak
March 31, 2022

Declaration of individual contribution in computer software

As the co-author of the following computer software, I hereby declare that my contribution to this work was:

Computer software (contribution in unpublished software)

Authors: Przemysław Galek (40%), **Maciej Staszak (40%)**,
Krzysztof Fic (20%)

Title: *SPECSfit – computer software for data conversion from
Step Potential Electrochemical Spectroscopy technique*

Journal: -

DOI: -

Contribution: – developing computer software

(signature)





Adam Ślesiński
March 31, 2022

Declaration of individual contribution in publication

As the co-author of the following paper, I hereby declare that my contribution to this work was:

Article A3

Authors:	Przemysław Galek (35%), Adam Ślesiński (15%) , Krzysztof Fic (10%), Jakub Menzel (40%)
Title:	<i>Peculiar role of the electrolyte viscosity in the electrochemical capacitor performance</i>
Journal:	Journal of Materials Chemistry A 9 (2021) 8644 – 8654
DOI:	10.1039/D0TA11230E
Contribution:	– performing the pressure and leakage current experiments and discussing the results

.....*Adam Ślesiński*.....
(signature)






Elżbieta Frąckowiak
March 31, 2022

Declaration of individual contribution in publication

As the co-author of the following paper, I hereby declare that my contribution to this work was:

Article A2

Authors:	Przemyslaw Galek (50%), Elżbieta Frąckowiak (15%) , Krzysztof Fic (35%)
Title:	<i>Interfacial aspects induced by saturated aqueous electrolytes in electrochemical capacitor applications</i>
Journal:	Electrochimica Acta 334 (2020) 135572
DOI:	10.1016/j.electacta.2019.135572
Contribution:	– knowledge support – manuscript reviewing and editing


.....
(signature)





THE UNIVERSITY OF
NEWCASTLE
AUSTRALIA

Professor Scott W. Donne
Discipline of Chemistry

March 22, 2022

Re: Declaration

To whom it may concern,

As the co-author of the following paper:

Przemyslaw Galek (30%), Paulina Bujewska (15%), **Scott Donne (5%)**, Krzysztof Fic (10%), Jakub Menzel (40%)

New insight into ion dynamics in nanoporous carbon materials: An application of the step potential electrochemical spectroscopy (SPECS) technique and electrochemical dilatometry

Electrochimica Acta 377 (2021) 138115

DOI: 10.1016/j.electacta.2021.138115

I hereby declare that my contribution to this work was:

5% - by providing the research support (verification of the calculation results, discussions) concerning the SPECS calculations.

Yours sincerely,

Scott W. Donne